Title
Engineering *Escherichia coli* for molecularly defined electron transfer to metal oxides and electrodes

Author
Jensen, Heather Marie

Publication Date
2013

Peer reviewed|Thesis/dissertation

Engineering *Escherichia coli* for molecularly defined electron transfer to metal oxides and electrodes

By

Heather Marie Jensen

A dissertation submitted in partial satisfaction of the requirements

for the degree of

Doctor of Philosophy

in

Chemistry

in the graduate division

of the

University of California, Berkeley

Committee in charge:
John T. Groves
Matthew Francis
Bryan Krantz
J. Christopher Anderson

Spring 2013

Abstract

Engineering *Escherichia coli* for molecularly defined electron transfer to electrodes

By

Heather Marie Jensen

Doctor of Philosophy in Chemistry

University of California, Berkeley

Professor John T. Groves, Chair

Both organisms and human-made technological devices use the flow of charge as the basic currency of information and energy. The soft materials properties and waxy cell membranes generally do not interface electrically with solid materials. Creating an interface that permits electrical communication between living and non-living systems would enable new opportunities in fields such as biosensing, bioenergy conversion, and biocomputing. Thus my dissertation focuses on creating a blueprint for the bidirectional flow of electrons between living and non-living systems that is transferrable to a multitude of cell lines. I take a biologically-focused approach to connect the living and non-living worlds: use synthetic biology to introduce a new electron transfer pathway into *E. coli*. This strategy takes advantage of the respiratory capability of the dissimilatory metal reducing bacterium *Shewanella oneidensis* MR-1. *Shewanella* uses a network of multiheme cytochromes that are able to transfer charge across the inner and outer membranes of the bacteria *via* the heme moiety in the cytochromes. This pathway enables *Shewanella* to route electrons along a well-defined path from the cell interior to an extracellular inorganic material acting as a terminal electron acceptor during anaerobic respiration. By genetically engineering the cell to build and maintain the bioelectronic connections, the cells can autonomously assemble and repair these connections. This work describes the first time the outer membrane spanning and double membrane spanning *Shewanella* electron transfer pathway was heterologously expressed in *Escherichia coli*. Additionally, these engineered *E. coli* strains are shown to reduce soluble iron, solid iron oxide, and anodes. This work not only serves as a landmark for the expression of complex membrane associated pathways, but it also demonstrates proof of concept that this pathway could be transferrable to other cell lines. This dissertation represents the first step towards engineering bidirectional communications with electrodes, and it opens up an array of opportunities for studying the biochemical and enzymatic properties of these unique proteins as well as the potential for novel hybrid technologies.

Dedication

I am honored to dedicate this work to all those who supported me and my growth as an individual and as a scientist: my family and my mentors.

Thank you to my parents, Frances and Gil, and sisters, Kim and Suz, for your constant support and love. I am blessed to have you as my family, and I can always count on you to be by my side. And thank you to Joe. Your love, support, and encouragement really helped me survive this whole process with my sanity intact.

A special thank you is due to Cynthia Chubbuck for inspiring me to pursue a career in science and for pushing me at a young age to strive for excellence.

I am extraordinarily grateful to my professors at Cal Poly, who both nurtured me and pushed me to endeavor for nothing less than my best. In particular, I'd like to dedicate this work to Dr. Gragson, Dr. Immoos, and Dr. Schoonover. I cannot express my level of gratitude for your support and encouragement, both as a student and as an alumna. I know how special my experience was with you at Cal Poly, and I have been truly blessed to have you as mentors.

Finally, I would like to dedicate this work to my advisors, Caroline and Jay. I am incredibly grateful for your faith in me and entrusting this project to me. Your thoughtful mentorship, support, and advice enabled me to succeed during my graduate career. I could not have had more inspiring advisors in graduate school, and I am particularly indebted to you both.

Table of Contents

Appendices.

List of Figures

List of Tables

List of symbols and abbreviations

δ-ALA:	Aminolevulinic acid:
ccm:	Cytochrome *c* maturation
DMRB:	Dissimilatory metal reducing bacteria
ET:	electron transfer
ETP:	electron transfer pathway
FMN:	Flavin mononucelotide
GFP:	Superfolding green fluorescent protein
gsp:	General secretory pathway
IPTG:	Isopropyl β-D-1-thiogalactopyranoside
ITO	Indium tin oxide
MFC:	Microbial fuel cell
mtr:	Metal reducing
PEEK	Polyether ether ketone
RBS:	Ribosome binding site
SDS-PAGE:	Sodium dodecyl sulfate polyacrylamide gel electrophoresis
SRP	Signal recognition particle
T2SS:	Type II secretion system
TMBZ:	3,3′,5,5′-tetramethylbenzidine

Acknowledgments

I would like to thank my committee members, who were generous with their expertise and time throughout my graduate career. Additionally, I would like to thank the Molecular Foundry Nanobio Facility, especially Ron Zuckermann, for creating a nurturing and friendly work environment.

This work would not have been possible without the fruitful collaboratorations that devolped in my time in graduate school. Yuri Londer and Peter Weigele of New England Biolabs were instrumental in helping us develop an expression strategy for the pathway. Ben Gross and Moh El-Naggar at the University of Southern California graciously shared their knowledge and experience with electrochemistry. Michaela TerAvest and Lars Angenent at Cornell University were especially .

I was fortunate to work with several extremely bright undergraduate researchers that both inspired and challenged me during their time here. I am particularly proud of Mark Kokish and his achievements in our lab and in other labs. Mark is an inspiration and an incredible friend. I look forward to see what his future holds as he moves on to graduate school.

I am extremely grateful the support of my labmates and friends. Their support and humor helped me stay motivated and sane, especially over the last few months. I would like to thank Cheryl Goldbeck, Behzad Rad, Jolene Lau, Rita Garcia, Andrea Bayles, Leah Witus, Jenny Cappuccio, David Hanifi, Andrew Cho, and Matt Hepler for keeping the laughter at full speed over the last few years. And I'd like to especially thank Rita, Cheryl, and David for always being there to listen. Finally, I would like to thank my ladies Susan Albinger, Trish Bailey, and Jeannette Osterloh. You keep me grounded and always know exactly how to make me smile. You are the pieces of me that I cannot live without. Thank you, everyone, for being my urban family.

Chapter 1

Requirements for rebuilding electron transport pathways in heterologous hosts

1.1. Building electronic communication between biological and inorganic materials.

1.1.1. Extracellular electron transfer pathways offer a molecularly defined route for electronic connections between living and non-living systems.

Both organisms and human-made technological devices use the flow of charge as the basic currency of information and energy. The soft materials properties and waxy membrane of cells generally do not interface electrically with solid materials. Creating an interface that permits electrical communication between living and non-living systems would enable new opportunities in fields such as biosensing, bioenergy, and cellular engineering (*1*, *2*). While most technological devices are electronic (i.e. rely on electron flow), a limited set of techniques is available to permit transfer of electrons from a variety of cell types to electrodes. Most approaches rely on the introduction of non-cellular redox species (*3*, *4*) to transport electrons from intracellular redox enzymes to extracellular electrodes in bacterial (*5*, *6*), fungal (*7*), and mammalian cells (*8*), but such mediators rely on diffusion to interact with multiple cellular substrates, thus obscuring a molecular-level understanding of the electron path. Other techniques, such as patchclamping, require physical means to abrogate the inherently electrically insulating character of cellular membranes (*9*).

In the absence of exogenous mediators, a limited set of bacterial species are able to directly transfer electrons to electrodes (*10–12*). However, a general strategy to create cell-electrode connections with a well-defined electron transfer path that is broadly applicable to many cell types has remained elusive. Creating a blueprint for the bidirectional flow of electrons between living and non-living systems that is transferrable to a multitude of cell lines would create new opportunities in energy conversion (*13–15*), biosensing (*16*), and biocomputing (*17*, *18*).

The work described in this dissertation explores a radically different, biologically-focused approach to connecting the living and non-living worlds. Most approaches focus upon engineering the materials; however, our approach uses synthetic biology to introduce a new electron transfer pathway into *E. coli*, a species that ordinarily lacks the ability to interface with electrodes. This pathway routes electrons along a well-defined path from the cell interior to an extracellular inorganic material. By genetically engineering the cell to build the bioelectronic connections, target cells can autonomously assemble and repair these connections. Additionally, this system has essentially unlimited material as cells are capable of self-replication.

1.1.2. Microorganisms have evolved electron transfer pathways to respire using extracellular electron acceptors.

Few bacterial species are capable of "breathing metals;" that is, utilizing solid metals and metal oxides as extracellular electron acceptors in anaerobic respiration. This class of microbes is called dissimilatory metal reducing bacteria (DMRB), and the most

studied DMRB genera are *Shewanella* and *Geobacter*. *Shewanella* uses a network of multiheme cytochromes that are able to transfer charge across the inner and outer membranes of the bacteria *via* the heme moiety in the cytochromes. These mechanisms enable *Shewanella* and *Geobacter* to use solid metal oxides as terminal electron acceptors during anaerobic respiration (*19–21*).

Bacterial metal oxide respiration was first termed dissimilatory metal reduction by Derek Lovley in 1988 in reference to the ability of strain GS-15, isolated from anaerobic freshwater sediments in the Potomac River, to reduce solid Fe_2O_3 (*22*); this strain was later named *Geobacter metallireducens* str. GS-15 (*23*). Lovley reported that the *Geobacter* strain was able to couple acetate oxidation to both Fe(III) and Mn(IV) respiration (*22*). Concurrently in the literature, Myers and Nealson published in *Science* that *Altermonas putrefaciens* MR-1 coupled oxidation of lactate to manganese oxide respiration (*21*). This strain was also published under the name *Shewanella putrefaciens* MR-1, and it has since been renamed *Shewanella oneidensis* MR-1. This *Shewanella* strain was isolated from anaerobic sediments from Lake Oneida, New York (*21*). Since then, 61 and 17 isolates in the *Shewanella* and *Geobacter* genera have been discovered.

The concept of bacterial anode reduction was first introduced in 1962 with the concept of the microbial fuel cell (MFC) (*24*). Microbial fuel cells are electrochemical cells in which microbes act as the electron donor to an anode and protons from microbial respiration react at the cathode to form water (Appendix F). It was not until 2003 that these metal-reducing *Shewanella* and *Geobacter* strains were implicated in anode reduction (*11*, *25*). More recently, Jeff Gralnick reported that *Shewanella* could utilize the same pathway to oxidize a cathode, representing the beginning of a new field: electrosynthesis (*26*). Additionally, the Lovley lab has shown the same injection of electrons into acetogens to convert carbon dioxide into water and complex carbon organic compounds (*27*, *28*).

There are important yet subtle differences that must be recognized between these two genera. *Shewanella* is a facultative anaerobe while *Geobacter* is an obligate anaerobe. The *Shewanella* strains are known to reduce metal oxides and anodes *via* direct contact to the material or through diffusible redox species (*5*, *29*); *Geobacter*, however, requires direct contact with electrodes (*11*, *30*). *Geobacter* forms biofilms up to 50 microns thick, while *Shewanella* typically forms biofilms that are a single monolayer thick. Finally, the *Shewanella* electron transport pathway has been well characterized, as discussed in the following section, while the exact *Geobacter* pathway has remained largely elusive.

Other genera are emerging in the DMRB field, such as *Geothrix fermentans* (*31*). As more microbes and pathways are characterized and add to our understanding of dissimilatory metal reduction, we may be able to utilize the different pathways to specifically tune the redox potentials necessary for different types of anode or cathode reactions.

1.1.3. The Mtr electron transfer pathway of *Shewanella oneidensis* MR-1 transports metabolic electrons across the double membrane.

The best understood electron transfer pathway (ETP) in the DMRB family belongs to *Shewanella oneidensis* MR-1. It is comprised of *c*-type cytochromes that shuttle electrons from cytoplasmic- and inner membrane-oxidizing enzymes toward the

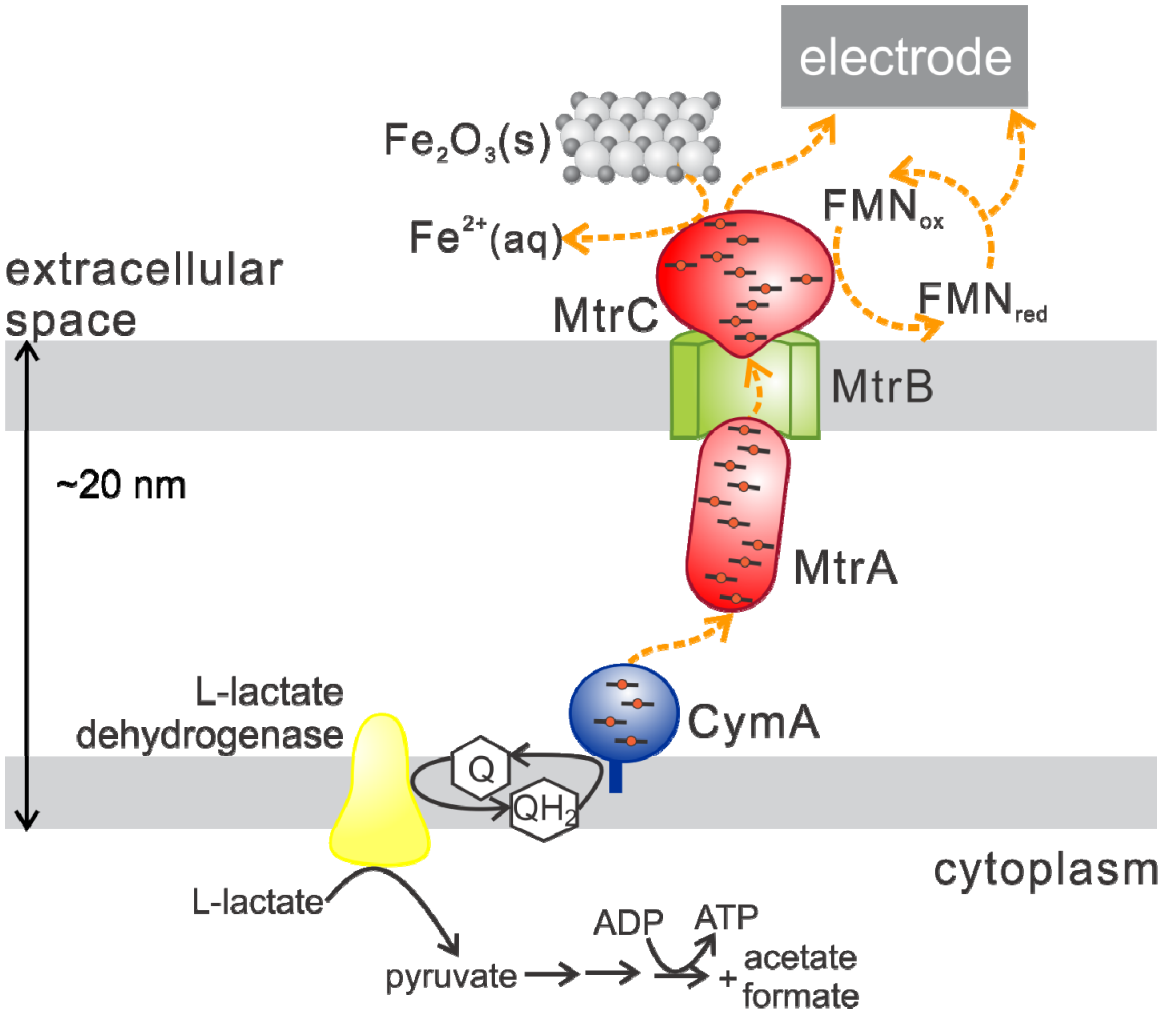

Figure 1-1. A schematic of the extracellular electron conduit in *Shewanella oneidensis* MR-1. Reducing equivalents resulting from L-lactate oxidation by lactate dehydrogenase are delivered to the periplasmic reductase CymA *via* menaquinol. Electrons are transferred from CymA to MtrA and from MtrA to MtrC within the MtrCAB complex. From MtrC, electrons can be transported to terminal electron acceptors through redox shuttles (FMN) or direct contact with either a metal oxide (silver and black spheres) or an electrode. A version of this cartoon is in Appendix D with spatial information of a typical gram negative bacterium membrane and dimensions of the electron conduit proteins.

Table 1-1. Properties of the *Shewanella oneidensis* MR-1 electron conduit proteins.

Property	Gene/Protein			
	cymA	***mtrC***	***mtrA***	***mtrB***
Locus No.	SO4591	SO1778	SO1777	SO1776
Other annotation	n/a	n/a	*omcB*	n/a
No. base pairs	564	2016	1002	2094
% GC of gene	44.5	44.7	44.7	46.3
Protein signal sequence cleavage site	Pos. 39 LHA-TS	Pos. 21 LTG-CG	Pos. 34 AYA-SK	Pos. 21 AVA-AD
No. amino acids, **(1) Unprocessed** **(2) Cleaved**	187 148	671 650	333 299	697 676
Protein size (kD) **(1) Unprocessed** **(2) Cleaved** **(3) Holoprotein**	20.8 16.6 19.0	71.2 68.8 74.8	36.1 32.4 38.6	77.7 75.5 n/a
pI	8.6	6.0	7.8	4.4
No. heme(s)	4	10	10	n/a
Spin state of heme(s)	3 low spin 1 high spin	10 low spin	10 low spin	n/a
Heme axial ligands	3 His/His 1 (His-Lys)/H_2O	10 His/His	10 His/His	n/a
Extinction coefficients (mM^{-1} cm^{-1})	$\varepsilon_{Soret}^{oxidized} = 380$ $\varepsilon_{Soret}^{reduced} \sim 550$ $\varepsilon_{552\ nm}^{reduced} = 104$ $\varepsilon_{552\ nm}^{oxidized} = 32$ $\varepsilon_{630\ nm}^{oxidized} \sim 3$	$\varepsilon_{Soret}^{oxidized} = 1260$	$\varepsilon_{Soret}^{oxidized} = 1320$ $\varepsilon_{Soret}^{reduced} \sim 1700$ $\varepsilon_{552\ nm}^{reduced} = 280$	n/a
Additional post-translation modification	n/a	Lipidation and extracellular secretion	n/a	Insertion into outer membrane
Function	Quinol dehydrogenase, ET to MtrA	ET from CymA to MtrC/OmcB	ET from MtrA to extracellular e^- acceptors	Required for assembly of MtrC/OmcA on OM
Homologues	NapC, TorC, TorY	None greater than 50%	NrfB (N-terminal), MtrD, DmsE, SO4360	None greater than 50%
Paralogues	NapC, SirCD	OmcA, MtrF	MtrD, DmsE, SO4360	MtrE, DmsF, SO4359
Structural information	α-helix inner membrane domain (GXXG) (NrfH structure)	Staggered-cross heme structure (MtrF structure)	Rod-shaped with aspect ratio 2.2-2.5 (SAXS)	Predicted 28-strand *β*-barrel (PRED-BB)
Approximate dimensions (nm)	~1.3nm along heme	8.5nm long; ~2 nm protrusion into MtrB	~8-10nm long; ~3 nm diameter	Pore: ~3-4nm

ET = electron transfer

outside of the cell during anaerobic respiration. Extensive genetic and biochemical data suggest that the major components of the *Shewanella* ETP are the inner membrane tetraheme cytochrome CymA, the periplasmic decaheme cytochrome MtrA, the outer membrane decaheme cytochrome MtrC, and the outer membrane β-barrel protein MtrB (Figure 1-1) (*32–36*). In *Shewanella*, lactate dehydrogenase oxidizes L-lactate to pyruvate (*37*), and then pyruvate is converted to formate and acetate (*38*, *39*). Reducing equivalents from these reactions are transferred to the menaquinol (MQ) pool, which acts as a store for electrons for inner membrane quinol dehydrogenases. Reducing equivalents resulting from L-lactate oxidation are delivered to the periplasmic reductase CymA *via* menaquinol (*40*). Electrons are transferred from CymA to MtrA (*41–43*) and from MtrA to MtrC within the MtrCAB complex (*35*, *44*). From MtrC, electrons can be transported to terminal electron acceptors through redox shuttles in the cell growth media (*5*, *29*, *45–48*), or through direct contact with electrodes (*49*, *50*) (Figure 1-1). This electron conduit is also reversible and can accept electrons from a cathode to drive intracellular reduction reactions (*26*).

The proteins involved in the electron transfer pathway were elucidated by biochemical and molecular biology techniques. MtrA is a 32-kD periplasmic decaheme cytochrome *c* (*51*), and MtrC is a 69-kD cell-surface-exposed (*52*), lipid-anchored decaheme cytochrome *c* (*53*). MtrC requires MtrB (*54*), a 72-kD putative twenty-eight strand β-barrel outer membrane protein (*55*), for correct assembly in the outer membrane (*54*). MtrA also appears to be necessary for MtrB stability (*44*, *56*). Details of these proteins and references can be found in Table 1-1. However, the crystal structures have not been solved for any of these proteins; at best, a homologue crystal structure has been solved (*45*, *55*, *57–60*). Thus it is currently unknown exactly what the overall structure of the electron conduit is in the cell.

The current most popular proposed arrangement of the conduit is based on homologue structures, biochemical analysis, and predictive modeling. When purified from *Shewanella*, MtrC:MtrA:MtrB co-purify in a 1:1:1 ratio (*35*), leading to the assertion that these proteins form a 1:1:1 complex. Recent advances in modeling and determination of the structures of homologues of these proteins support this ratio. The crystal structure of the MtrC homologue MtrF (e-value = 7×10^{-74}), was solved by Clarke and Richardson, revealing a unique staggered-cross heme structure (*45*) (Figure 1-2A). This paper also suggested the domain of MtrF near heme 10 would fit into the predicted pore size of MtrE (a MtrB homologue, e-value = 2×10^{-136}) and that this domain is predicted to be involved in protein-protein contact (PPI-PRED) (Figure 1-2D) (*45*). Clarke and Richardson propose this staggered-cross structure is the basis for electron transfer *via* direct contact and soluble redox carriers, like flavin. However, they were unable to crystallize MtrF in the presence of quinol. Additionally, Clarke and Richardson crystallized a *Shewanella* undecaheme cytochrome *c*, UndA, with a similar staggered-cross heme structure (*57*). This structure revealed an additional heme next to heme 7 in MtrF (Figure 1-2A). In this report, they were crystallized UndA with Fe(III) citrate chelated to the additional heme, claiming this supports their hypothesis that heme 2 and 7 in MtrF are specifically for soluble substrate reduction (*57*). Additionally, computational results have been reported on the theoretical redox potentials of the ten hemes in MtrF (~MtrC) (*61*). While there is not an available method to substantiate these calculations, they still provide an interesting redox profile for the protein (Figure 1-2B).

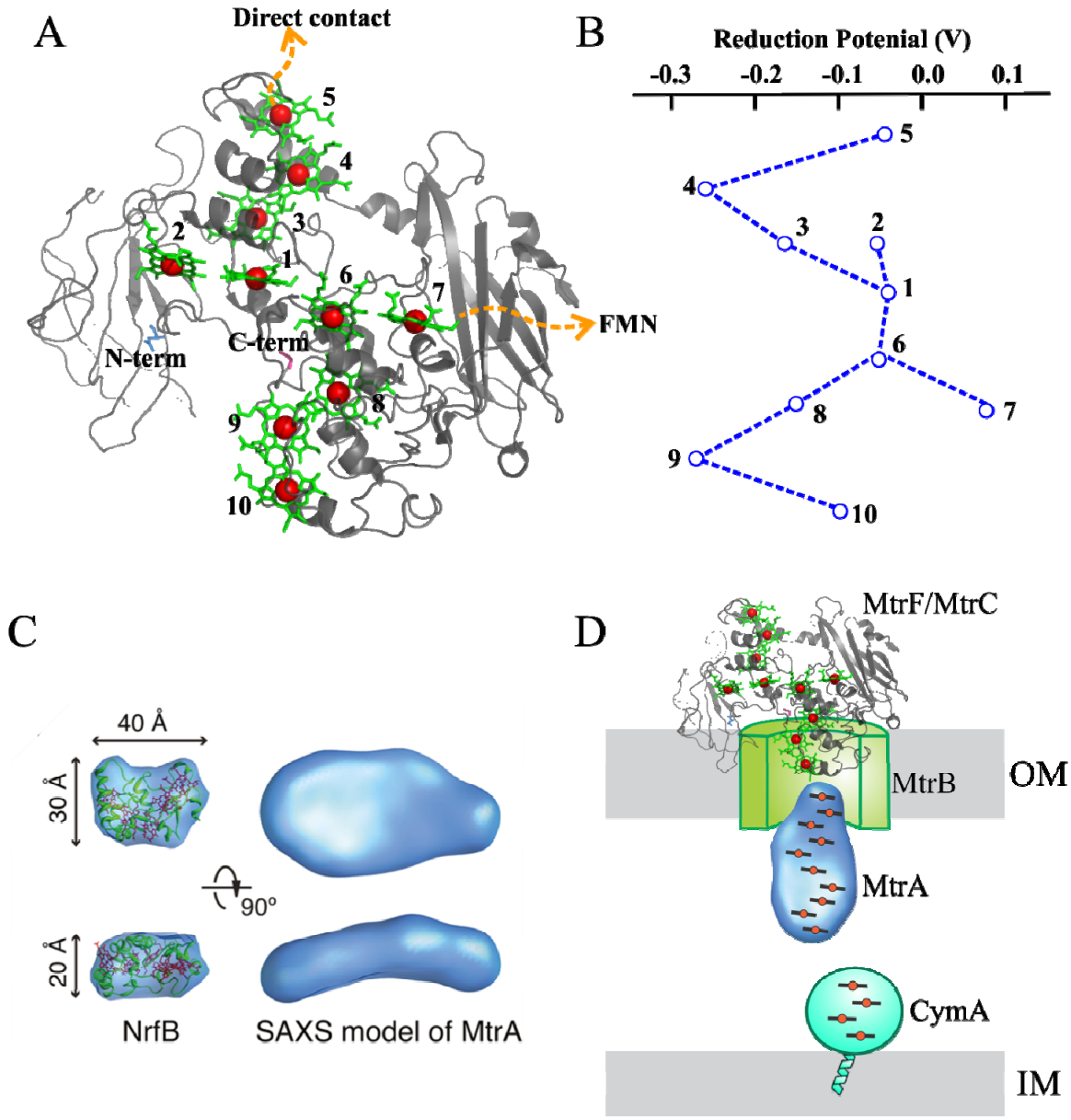

Figure 1-2. Proposed structural model of the electron conduit based on structural studies of MtrF and MtrA. (A) The crystal structure for the MtrC homologue, MtrF, was recently solved. This structure showed a novel jagged-cross heme structure. The porphyrin heme structure is shown in green while the iron redox center is represented by red spheres. The N-terminus is shown in blue; the C-terminus is shown in pink. Lastly, the hemes are labeled by order encoded in the primary sequence of MtrF. Heme 10 is proposed to face the membrane, and heme 5 is proposed to be the terminal reductase on solid surfaces. Heme 7 and heme 2 are proposed to reduce soluble iron or diffusible redox species. (B) The theoretical heme redox potentials of MtrF show a unique profile. Adapted with permission from reference (*61*). Copyright 2012 American Chemical

Society. (C) The limited structural information available for MtrA was obtained with SAXS. It is similar to half of NrfB, which shows high sequence homology to the first half of MtrA. Reprinted with permission from reference (*59*). Copyright 2011 American Chemical Society. (D) Based on the structural information available for these proteins, the accepted arrangement of MtrCAB in the literature fits MtrA and MtrC into the pore of the MtrB β-barrel.

Separately, small x-ray scattering data in combination with solution-based modeling by the Elliot research group predicts MtrA to be a "sausage shaped" protein with an approximate diameter similar to the predicted MtrB pore size (*59*). Together, this group has proposed a structural model in which both MtrA and MtrC fit inside the pore of MtrB, explaining how MtrB facilitates charge transfer between MtrA and MtrC across the outer membrane (Figure 1-2D) (*45*, *59*).

It is widely accepted that CymA acts as a central player in many routes of *Shewanella* respiration (*62*, *63*). CymA is a tetraheme menaquinol-7 dehydrogenase (*40*) involved in many pathways. CymA lends to respiratory flexibility and plays a role in the anaerobic respiration of fumarate, nitrite, DMSO, and soluble and insoluble forms of Fe(III) (*63*). Although little is known about the structure of CymA, crystal structures have been solved for proteins in the same family, the NapC/NirT family (*42*, *58*, *64*). Based on the homologue structural information available, it is believed that CymA has a transmembrane N-terminal α-helix and that the heme interacting with quinol is a high spin heme. Recently, Marritt and coworkers have shown that CymA indeed has one high-spin ($S = 5/2$) heme with (His or Lys)/H_2O axial ligands (*62*). The remaining three hemes of CymA are all low-spin His/His ligated hemes. See Appendix E for information on how the spins state and axial ligands change the visible spectra of the cytochrome *c*.

Although there has been significant work toward understanding the pathway, rebuilding a simpler version of the pathway in *E. coli* may help us learn more about the pathway. This may allow us to address the question of whether electrons come from CymA directly to MtrA or whether they require an intermediation, such as Stc. Thus by expressing the pathway in a modular way, we may add to the understanding of the ratio of the electron conduit components for proper function.

1.2. Previous advances in heterologous cytochrome *c* expression and functional analysis focused on conditions for the expression of single cytochromes.

Prior to our work in this field, there were many advances toward developing techniques for expression, purification, and classification of these cytochromes. The plasmid pEC86 is universally used for the constitutive expression of the cytochrome c maturation genes (*ccm*), and its development was a crucial component of aerobic synthesis of multiheme cytochromes in *E. coli* (*65*). Yuri Londer pioneered the expression of multiheme cytochromes in *E. coli* by developing growth conditions and plasmids that permitted high level heterologous expression of cytochromes *c* (*66–70*). Pitts and coworkers were the first to heterologously express MtrA in *E. coli*, and this paper represents the best characterization of MtrA in the literature (*51*). Pitts performed

experiments *in vitro* to determine which *E. coli* proteins transfer electrons to MtrA (*51*). However, Pitts did not do detailed analysis on how MtrA interacts with *E. coli in vivo* (*51*).

The Spormann lab also is a significant contributor to this field (*64*, *71*, *72*). The Spormann lab is primarily a *Shewanella* biofilm lab, but they have expressed a handful of the pertinent *Shewanella* proteins in *E. coli*. Among these proteins are CymA, MtrA, and FccA (*64*, *71*, *72*). In these papers, Spormann and coworkers performed *in vivo* assays of Fe(III) nitrilotriacetic acid (NTA) reduction. However, they neglected to include a wild type *E. coli* negative control, so it is unclear by how much their engineered strains have improved over the background. This is especially important when using Fe(III) NTA; in our experiments, we have seen that wild type *E. coli* is able to significantly reduce Fe(III) NTA.

Donald et al. were the first to express the outer membrane decaheme cytochrome *c* OmcA in *E. coli* (*73*). This report made an extremely important observation with respect to the expression of these complex proteins in *E. coli*. Donald tried to express OmcA in both an A-strain and a B-strain of *E. coli* and reported that only the B-strain was capable of localizing OmcA to the outer membrane. Donald suggests that this is because A-strains of *E. coli* lack the type II secretion system (T2SS), which has been shown necessary for localization of the *Shewanella* cytochromes *c* to the outer membrane (*73–75*).

This previous work set the precedence that the expression of single multi-heme cytochromes *c* in *E. coli* was possible. In this dissertation, I build upon this previous work by expressing several of these cytochromes *c* in one strain for the express purpose of rebuilding this pathway for *in vivo* function in a variety of microbes.

1.3. The blueprint for heterologous expression of membrane-associated cytochromes *c* involves several pathways required for post-translational modifications.

Unlike heterologous expression of cytosolic proteins, this particular pathway depends on many factors beyond transcriptional and translational controls. This section provides a blueprint of the steps that must be considered when engineering this particular pathway into another organism. The overall scheme for the expression of this pathway (Figure 1-3) is as follows: (1) transcription; (2) translation; (3) secretion across the inner membrane; (4) heme biosynthesis and localization to the periplasm; (5) covalent heme ligation; (6) lipidation; and (7) final localization. Thus, proper localization and folding of one copy of the CymAMtrCAB pathway involves 39 membrane-associated proteins and 33 post-translational medications. All of these steps are discussed in further detail below.

1.3.1. Membrane protein expression contributes to additional challenges for *in vivo* applications.

Maintaining a healthy membrane is essential to cell viability. Not only does the membrane provide a barrier to the external environment, but the membrane is the milieu for many energy reactions essential to viability. The real estate, so to speak, of the membrane for protein expression is significantly limited compared to the cytoplasm. During stationary phase, *E. coli* has 4 μm^2 of 2-dimensional area in the membrane (*76*) while the internal volume of the cell is 0.6 μm^3 (*77*). Considering a cross sectional area of $1.5x10^{-5}$ μm^2 in the cell, then there is space for about 30x more protein in the cytoplasm

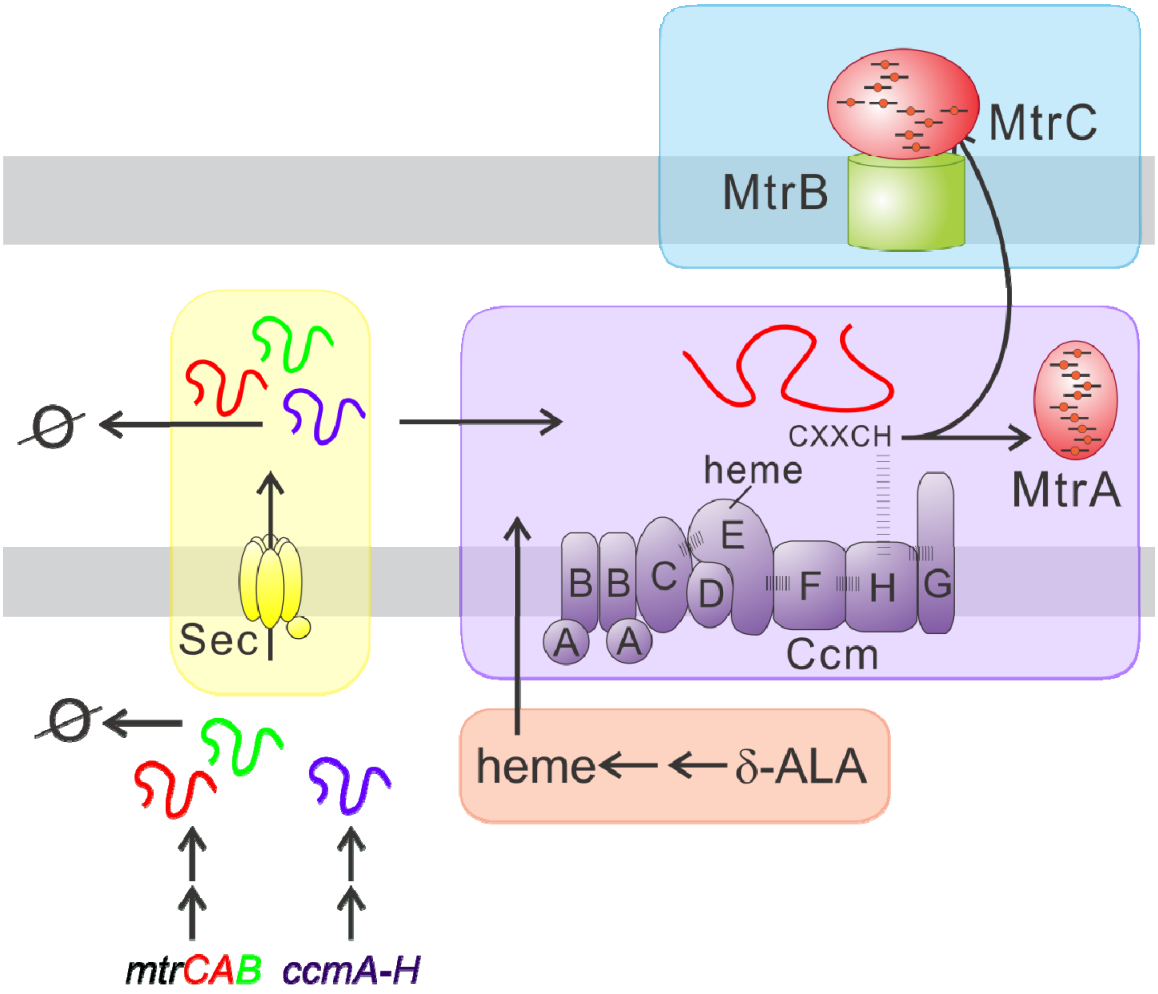

Figure 1-3. A streamlined blueprint of heterologous expression of cytochromes *c* in *E. coli*. The steps of cytochrome *c* expression in *E. coli* are as follows: (1-2) transcription and translation (green box; (3) secretion by type II secretion (yellow box); (4) heme biosynthesis and secretion to the periplasm (red box); (5) covalent heme attachment by CcmA-H (purple box); (6) final localization by either Bam or Gsp (blue box); and (7) lipidation (not shown).

than in the membrane. Despite the limited space in the membrane, about 30% of the proteome consists of membrane proteins (*78*). Thus, to express proteins in the membrane without damaging normal cellular processes requires a delicate balance. In addition, the protein:lipid ratio must remain below a certain level (~50%) to maintain membrane integrity (*79*), which makes engineering the membrane particularly challenging due to the fact that the membrane is already crowded by respiratory enzymes, ATP synthases, and transporters (*80*).

Both *E. coli* and *Shewanella* are gram negative bacteria. In gram negative bacteria the outer membrane, unlike the inner membrane, is asymmetric. The inner leaflet is comprised of phospholipids and separated from the outer membrane by the periplasmic space and peptidoglycan layer (*77*, *81*). The outer membrane is instead comprised of lipopolysaccharides (*77*).

It has generally been observed that overexpression of membrane proteins leads to decreased cell viability and damaged membranes. High levels of leader-sequence bearing polypeptides can saturate the signal recognition particle (SRP), leading to the misfolding of unsecreted polypeptides and accumulation of cytoplasmic aggregates (*82*). Additionally, depletion of SRP has been shown to repress ribosome biogenesis in *E. coli* due to upregulation of the ribosome-inactivating protein ribosome modulation factor (RMF) (*83*).

Wagner and coworkers did a thorough analysis of pleotropic changes in *E. coli* cells during the overexpression of three different membrane proteins (*84*). Flow cytometry was used to quantify changes in cell size and granularity. In this technique, forward scatter is generally interpreted as cell size while side scatter is interpreted as granularity or an increase in the number of inclusion bodies. Using microscopy, Wagner and coworkers observed that there was specifically an increase in the population of elongated or filamentous bacteria. This report also used 2-D gel electrophoresis to observe changes in different protein levels in whole cell lysates. To summarize their findings, they saw an increase in the expression of secretory proteins and heat shock proteins as well as cytoplasmic aggregates of their selected overexpressed membrane proteins (*84*). They also observed lower oxygen consumption by these strains (*85*).

In the previous examples, the proteins expressed were inner membrane proteins (*84*, *85*). However, the pathway discussed in this dissertation spans both the inner and outer membranes. Thus, in our system we may be additionally limited by the chaperones used specifically for periplasmic and outer membrane proteins.

1.3.2. Post-translational modifications required for the expression of membrane cytochromes *c*.

The function of the ETP relies upon functional expression of the proteins as well as localization. *C*-type cytochromes require a high degree of post-translational modification. In addition to the extra translocation step, these particular proteins require heme ligation and, in the case of MtrC, lipid attachment.

This series of post-translational modifications creates multiple points for misregulation of the synthesis and maturation of the MtrCAB complex in *E. coli*. Since L-lactate dehydrogenase is an inner membrane protein, secretion impairment has the potential to negatively impact the flux of electrons to menaquinone from lactate metabolism and hinder the synthesis of MtrCAB. Misregulation of cytochrome *c*

synthesis can also be caused by inadequate heme, which will result in degradation of apocytochromes c by periplasmic proteases, such as DegP. Thus *c*-type cytochrome biogenesis requires an appropriate balance between the rates and levels of polypeptide synthesis, heme biosynthesis, polypeptide secretion, and cytochrome *c* maturation.

1.3.2.1. Heme biosynthesis.

Heme plays a ubiquitous role in many respiratory enzymes in both aerobic and anaerobic respiration. There are many different types of heme present in *E. coli* proteins, including heme *b* (protoheme), heme *c*, heme *d*, and heme *o* (Figure 1-4). While this dissertation focuses on heme *c* in cytochromes *c*, the biosynthesis for these different hemes uses five common enzymes and only diverges at the last step.

Heme belongs to the tetrapyrrole family of biomolecules, and the biosynthesis generally begins at δ-aminolevunlinic acid (δ-ALA). δ-ALA biosynthesis is broken down into two routes. In eukaryotes and α-proteobacteria, such as photosynthetic bacteria, the synthesis of δ-ALA by δ-aminolevulinic acid synthase involves the condensation of glycine (Gly) and succinyl-coenzyme A (CoA) (*77*). The second route, which will be focused on below, is observed in plants, algae, archea and most bacteria, including *E. coli*. In *E. coli*, the five carbon "skeleton" of glutamine (Glu) is ligated to tRNA and reduced. Lastly, the N and oxo atoms are interchanged, forming δ-ALA (Figure 1-5). This process requires both ATP and divalent cations (*86*, *87*).

The remaining reactions for conversion from δ-ALA to protoporphyrin IX are highlighted in Figure 1-5 (*77*, *88–90*). Ferrochetalase inserts the iron center into porphyrin IX to form protoheme IX (heme *b*). Finally, protoheme IX may be converted to the other types of heme (Figure 1-4). However, heme *c* is unique in that it does not require any chemical conversion from protoheme; rather, heme *b* becomes a c-type heme once it is covalently linked by thioether bonds to conserved cysteine (Cys) residues in the apoprotein.

It was previously observed, and additionally observed in my experiments, that addition of δ-ALA in aerobic growth media leads to the accumulation and export of protoheme (heme *b*) (*91*, *92*). This suggests that δ-ALA biosynthesis is the rate limiting step towards heme *c* synthesis. Thus, in situations when maximal cytochrome *c* expression is desired, it is advised to add 1 mM δ-ALA to the media during growth. However, as addressed in Chapters 3 and 5, greater cytochrome *c* content per cell does not necessarily lead to increased reduction of extracellular electron acceptors (*92*).

1.3.2.2. Secretion of polypeptides to the periplasm *via* Type II Secretion.

After synthesis, the Ccm and Mtr polypeptides are secreted into the periplasm *via* the type II secretion system (T2SS). The T2SS is well-studied because of its role in pathogenesis, and extensive detail on the protein structures and interactions is found in many reviews (*93–97*). Generally, there are three ways that the T2SS targets peptides to the inner membrane: i) SecB-dependent, ii) signal recognition particle (SRP) dependent, and iii) twin-arginine translocation (TAT) (Figure 1-6). Irrespective of targeting route, the apoproteins are translocated by SecYEG. Here SecB-dependent and SRP-dependent methods of targeting the apoproteins to the inner membrane are highlighted.

SecB-dependent translocation: SecB dependent secretion is normally used for the

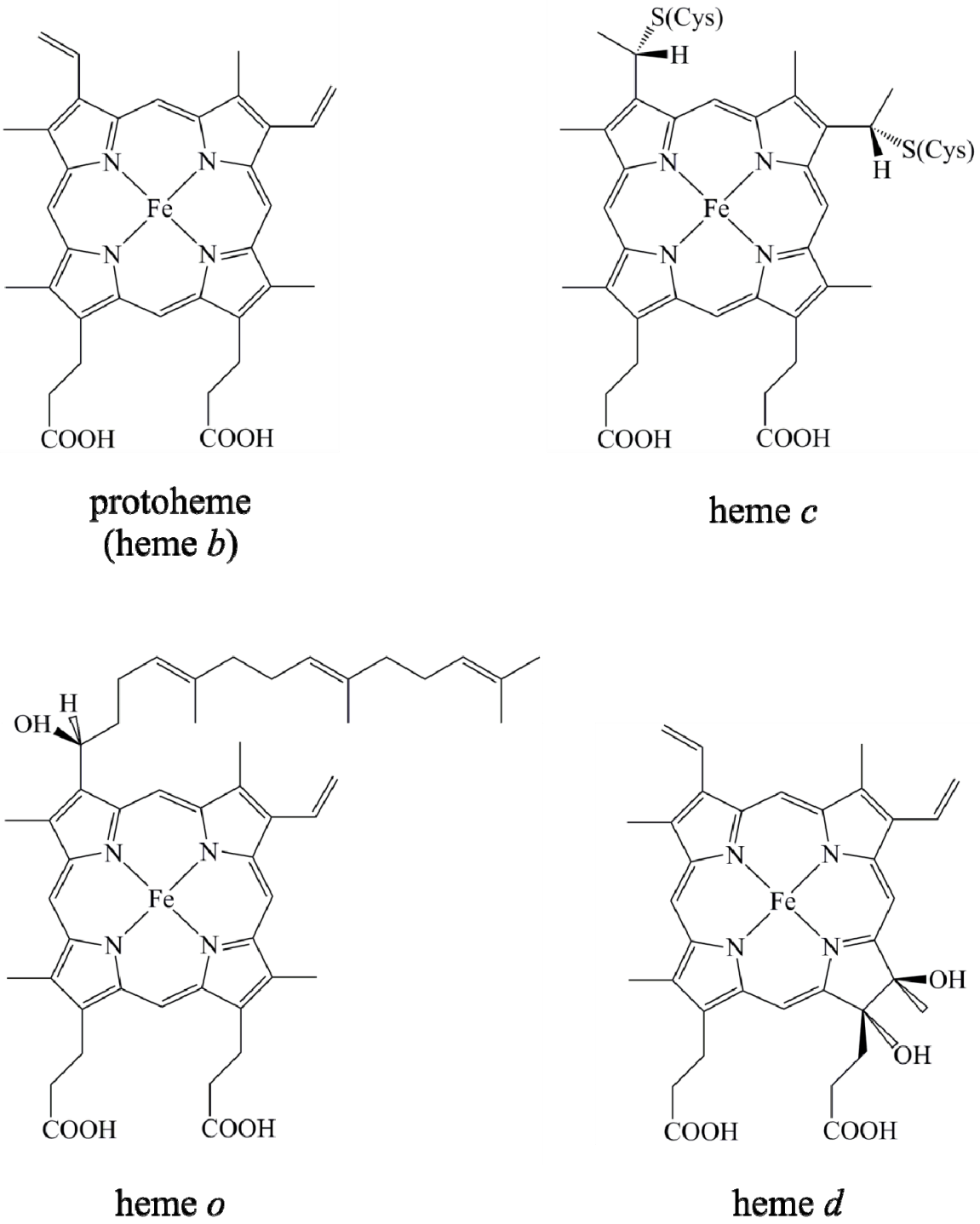

Figure 1-4. Heme structures found commonly in *E. coli* respiratory enzymes. The heme structures vary in their functional groups on the porphyrin ring. Heme *c* is the only one of these structures that covalently attaches to the apoprotein.

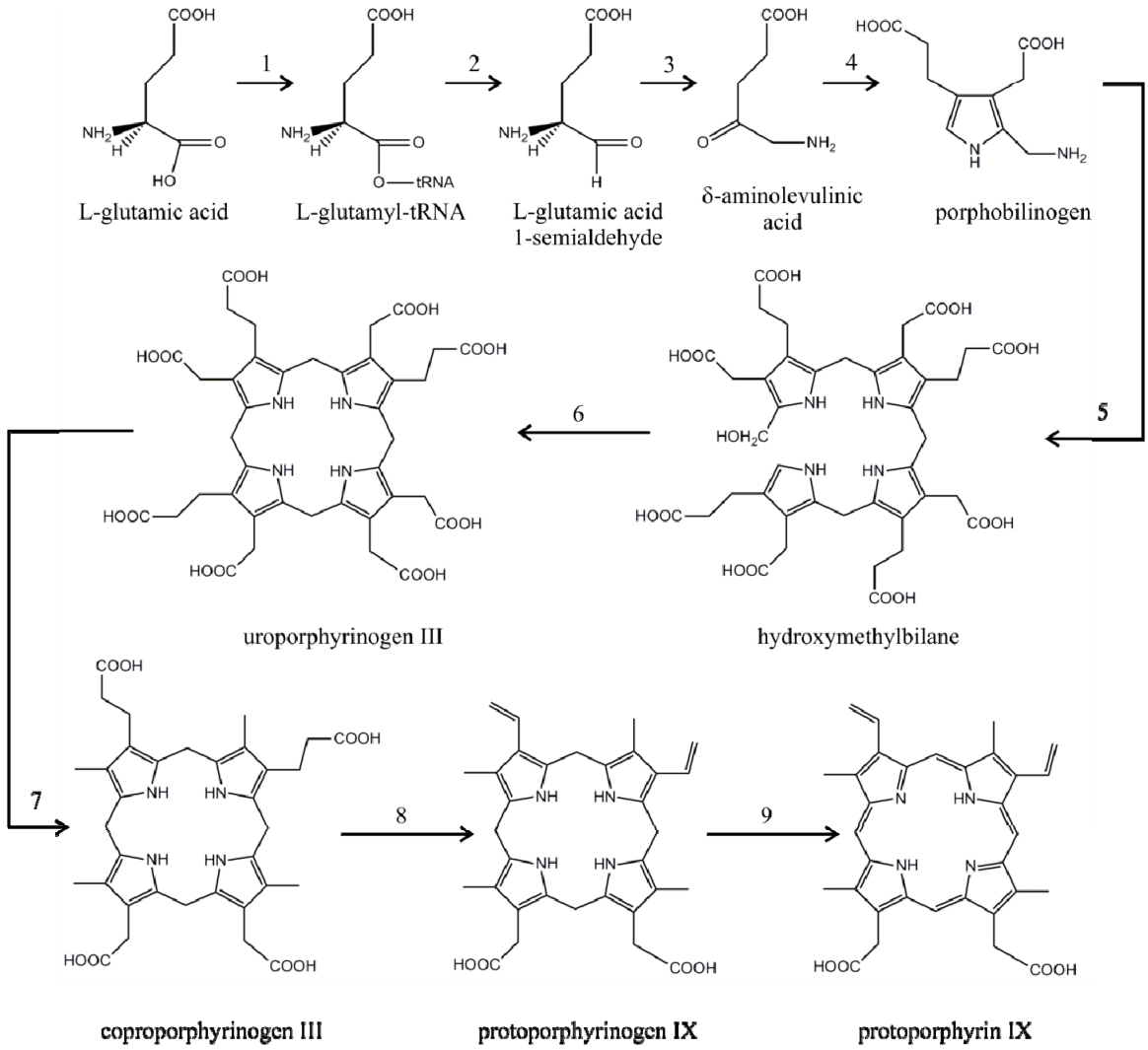

Figure 1-5. Heme biosynthesis scheme. The enzymes that perform this series of reactions are as follows: (1) Glu-tRNA synthetase; (2) Glu-tRNA reductase; (3) Glu 1-semialdehyde aminotransferase; (4) δ-ALA dehydratase; (5) hydroxymethylbilane synthase; (6) uroporphyrinogen III synthase; (7) uroporphyrinogen III decarboxylase; (8) coproporphyrinogen III oxidative decarboxylase; (9) protoporphyrinogen IX oxidase. The final step to protoheme synthesis is the addition of iron to the center of the porphyrin ring by ferrochetalase. Protoheme, or heme *b*, is covalently linked to the CXXCH motif in cytochromes *c* to form heme *c*. The limiting step in this synthesis is the synthesis of δ-aminolevulinic acid (δ-ALA) (*91*, *92*).

secretion of periplasmic and outer membrane proteins (*98*). In the SecB-dependent method, the secretion sequence is recognized by trigger factor (TF) on the ribosome (*99*, *100*) and then by chaperone SecB. The signal sequence is generally 20-30 amino acid residues located at the N-terminus. The general structure of this sequence (in the N to C direction) is a positive region followed by a hydrophobic region followed by a polar region (*93*, *101*, *102*); these are also known as the N-, H-, and C- regions, respectively. The signal sequence also has sequence specific effects on the translation rate (*102*). The positive region of the signal sequence is believed to be especially important because increasing the density of positive charge increases the translocation rate (*93*, *102*, *103*).

SecB acts as a chaperone to SecA and interacts with the apoprotein to prevent premature folding (*96*, *104–108*). SecA is bound to SecY, and SecYEG are important for sequence specificity of the signal sequence (*109*). SecA is an adenosine triphosphatase (ATPase) that uses chemical energy from ATP hydrolysis to power the motor function (*96*). SecYEG is the integral membrane protein complex that transports the unfolded apoprotein across the inner membrane. The apoproteins are translocated through SecYEG in a step-wise manner (*96*), using energy from the ATP hydrolysis of SecA as well as proton motive force to drive the translocation (Figure 1-6A) (*94*, *96*, *110*). After translocation, the signal peptide is cleaved by a periplasmic signal peptidase, releasing the apoprotein from SecYEG to be folded. There are about 300-500 copies of SecYEG per cell in *E. coli* (*111*).

Signal recognition particle: In the SRP-dependent targeting of apoproteins to the inner membrane, the nascent protein is transported to the inner membrane in a nascent state while still associated with the ribosome (Figure 1-6B) (*98*). It is believed that the SRP method is the primary chaperone for integral membrane proteins to SecYEG (*112*, *113*). SRP is a GTPase that docks to the ribosome near the peptide exit site; here it binds hydrophobic α-helices (i.e. transmembrane helices) with high affinity as the peptide is synthesized on the ribosome (*114*). SRP is chaperoned by FtsY (*112*), which targets the apoprotein to the inner membrane where it is translocated by SecYEG (as described above) or YidC (Figure 1-B) (*110*, *112*). It has been observed that trigger factor (TF) and SRP are competitive and that eliminating TF increases the number of integral membrane proteins by ~5 fold (*100*).

Twin arginine translocation (TAT): Unlike the SecYEG translocon, TAT exports folded proteins across the inner membrane. The signal sequence for TAT follows the same general positive/hydrophobic/polar region pattern, but the consensus motif for TAT is highly conserved and specific: S-R-R-x-F-L-K (*115*, *116*). For more information on TAT, see these reviews (*115–117*).

There have been significant advances toward the prediction of the signal sequence cleavage site. The Center for Biological Sequence Analysis (CBS) provides online calculators for the prediction of the signal sequence in gram negative bacterial protein sequence (http://www.cbs.dtu.dk/services/SignalP/) as well as prediction of lipoprotein sequence (http://www.cbs.dtu.dk/services/LipoP/) (*118*, *119*).

The next post-translational modification is heme ligation followed by final localization by T2SS. The translocation of the outer membrane proteins *via* the T2SS is

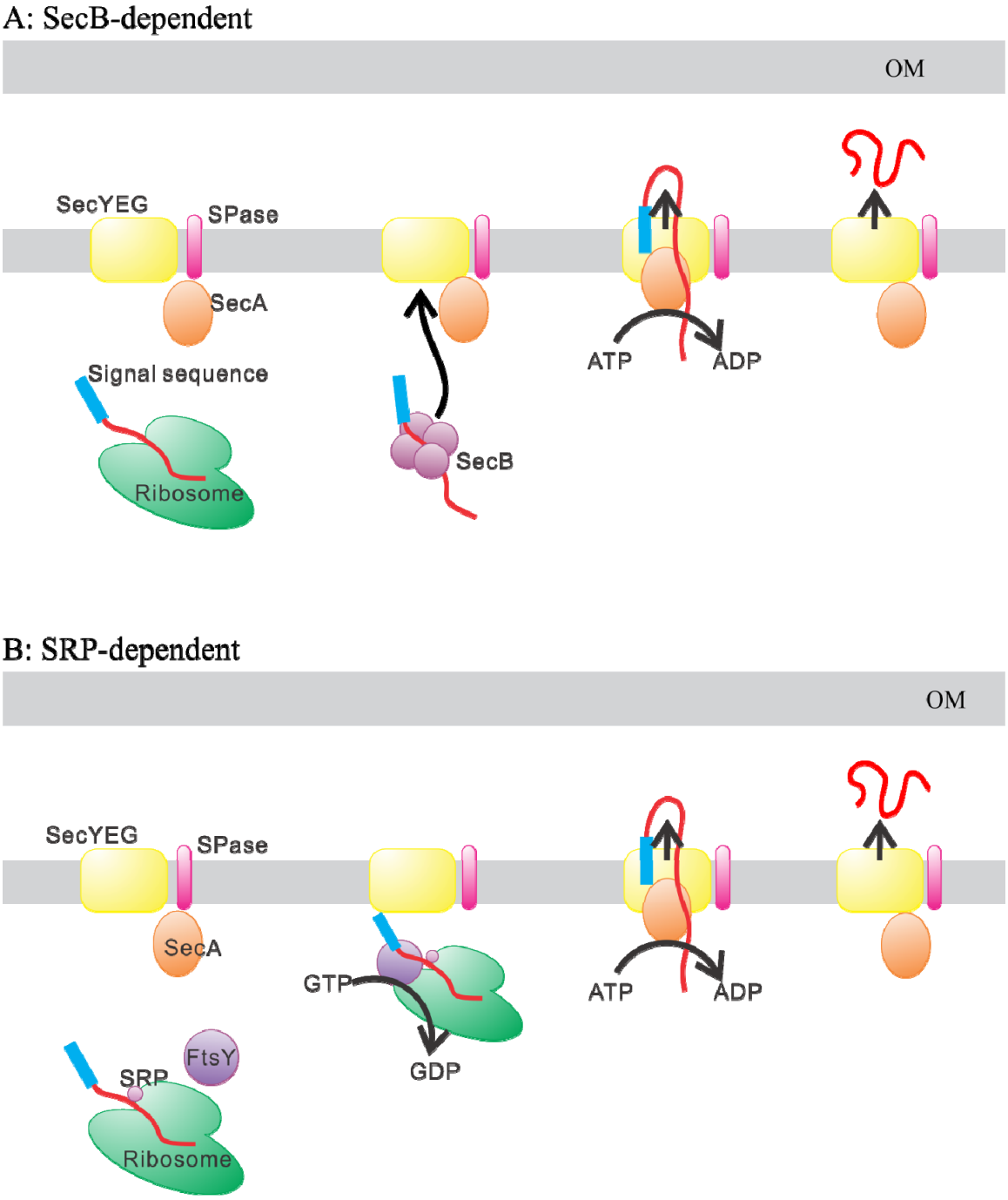

Figure 1-6. Schematic of the translocation of apoprotein across the inner membrane *via* the type II secretion system (T2SS). (A) The SecB-dependent mechanism uses SecB (purple) as a chaperone of the apoprotein to SecA (orange) at the inner membrane. Then SecA uses both ATP hydrolysis and proton motive force to translocate the protein across the inner membrane *via* SecYEG (yellow). The signal sequence (cyan) is cleaved by a signal peptidase (SPase). (B) The SRP-dependent mechanism differs from Sec-B dependent in that the entire ribosome is chaperoned to SecYEG by FtsY.

discussed in Section 1.3.2.5.

1.3.2.3. Cytochrome *c* maturation (*ccm*) in *E. coli*.

In cytochromes *c*, heme is covalently attached to the protein backbone *via* the cytochrome *c* maturation (CcmABCDEFGH) pathway which is located on the periplasmic face of the inner membrane (*77*, *120–122*). CymA, MtrC, and MtrA biogenesis requires the cytochrome *c* maturation (*ccm*) genes, which encode the eight membrane proteins CcmA-H. Together, this system acts as a heme lyase for covalent attachment of protoheme IX to the apoprotein. The conserved heme binding motif is CXXCH; the two cysteine thiols covalently bind the porphyrin, and the histidine acts as one of the axial ligands to the iron redox center (*120–122*). The second axial ligand of iron is typically another histidine located elsewhere in the protein sequence; this arrangement of heme binding results in low spin iron ($S = 1/2$). Occasionally other axial ligands such as methionine have been observed; this arrangement of heme binding results in high spin iron ($S = 5/2$); this is the case with one of the hemes of CymA (*62*).

It was long postulated that the ATP binding cassette (ABC) transporter CcmAB translocates heme across the inner membrane to the heme chaperone, CcmE. However, due to conflicting evidence in the literature (*123*, *124*), it is still debated how heme is translocated to the periplasm. CcmE, a heme chaperone, covalently binds heme at a conserved His residue (*125*, *126*). CcmF, CcmH, and CcmG have all been implicated in the role of heme lyase, and together they catalyze the formation of thioether bonds between the apoprotein heme binding motif cysteines and heme *b* (Figure 1-7) (*120*, *121*, *126*). Once these processes are complete, the axial ligands coordinate to the heme iron. It is as yet unclear if the Ccm machinery attaches the hemes in a single multiheme cytochrome *c* in a step-wise manner or if the apoprotein dissociates after each heme attachment.

Since transcription of the genomic *ccm* operon in *E. coli* is repressed under aerobic conditions (*127*), the *ccm* genes must be expressed from a plasmid to mature MtrC and MtrA. This is traditionally done with co-transformation of the helper plasmid, pEC86, which uses a constitutive *tet* promoter to express the *E. coli ccm* genes (*65*, *128*). After their synthesis, the Ccm and Mtr polypeptides are secreted into the periplasm. The Ccm system plays a role in translocating heme into the periplasm and then catalyzes the formation of thioether bonds that link heme to two cysteine residues (*120*). Once these processes are complete, the axial ligands (typically histidine) are coordinated to the heme iron and the holocytochrome *c* is folded (*120*).

1.3.2.4. Lipidation of lipoproteins.

Lipidation in *E. coli* is performed by the enzymes Lgt, LspA, and Lnt, and then the lipidated protein is localized to the outer membrane by the Lol pathway. These processes are well documented in reviews (*129–135*). It is unclear whether lipidation happens before, after, or in conjunction with heme *c* attachment. The consensus sequence for lipidation is LXXC; more specifically, the lipobox sequence is L-(A/S)-(G/A)-C and located within the N-terminal signal sequence of proteins exported through T2SS (Figure 1-8A). The cell differentiates inner membrane lipoproteins by an Asp residue after the lipobox Cys residue. An identifier for lipoprotein sorting between the inner leaflet and the outer leaflet of the outer membrane has not yet been discovered.

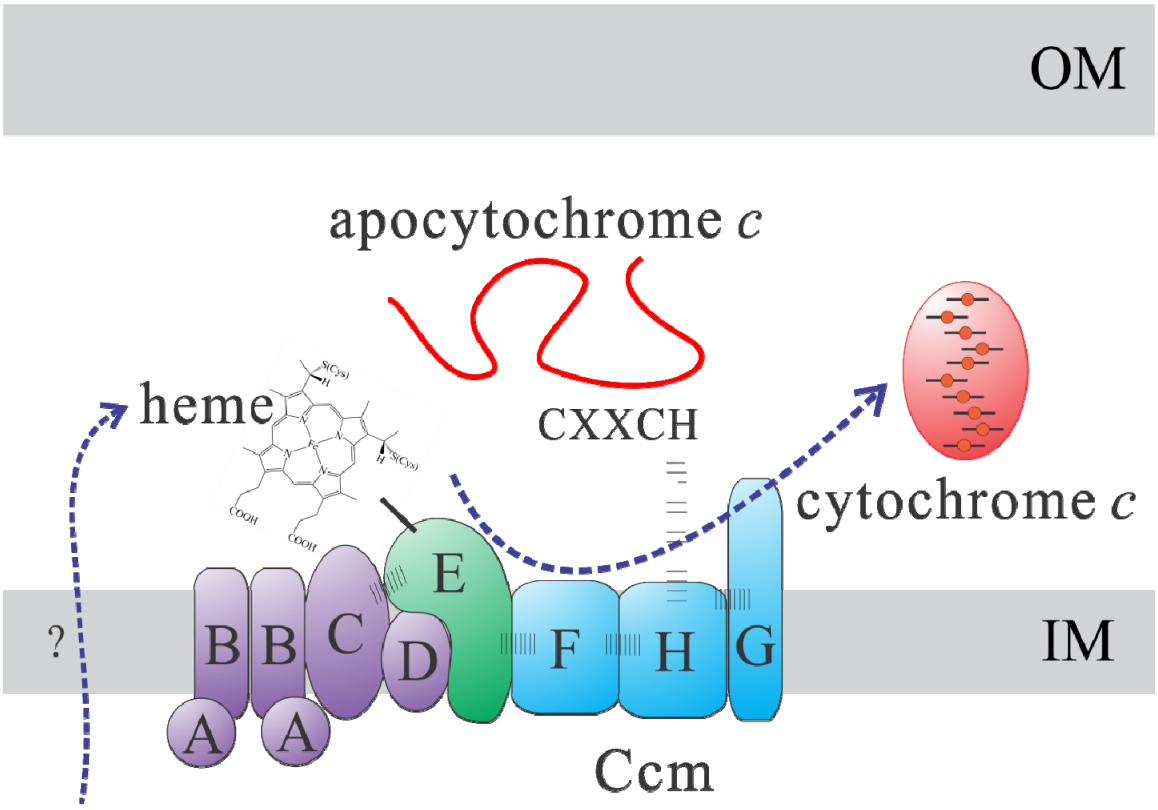

Figure 1-7. A schematic for the cytochrome *c* maturation (*ccm*) machinery. Heme is transported to the periplasm by an as yet unknown mechanism. Heme is chaperoned by CcmE (green) *via* covalent attachment to a histidine residue in the periplasmic domain of CcmE. Although the specific role of each protein is not yet well known, CcmF and CcmGH (cyan) have been implicated as the heme lyases.

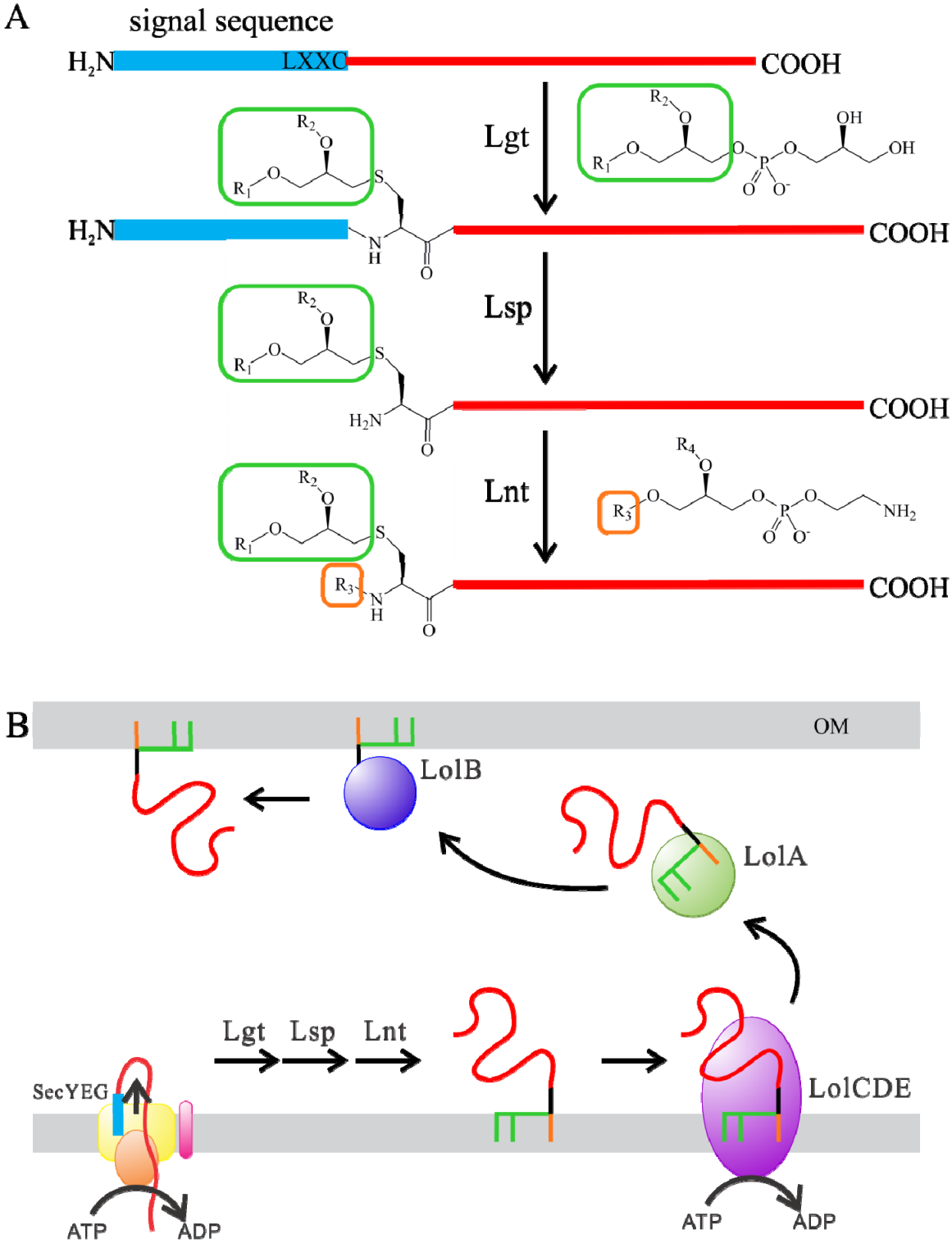

Figure 1-8. Schematic of lipidation by LolABCDE. (A) The lipidation of prelipoproteins by Lgt, LspA, and Lnt. (B) The Lol system in *E. coli* normally localizes lipoproteins to the inner leaflet of the outer membrane. Lipoproteins with a Cys residue after the lipobox (position 2 of the cleaved protein) remain in the inner membrane.

LolCDE (purple) hydrolyzes ATP to release the lipoprotein to the chaperone LolA. LolA (green) chaperones the lipoprotein across the periplasm to LolB. Lastly, LolB (blue) inserts the lipoprotein into the membrane.

Lipidation can be broken down into three stages as shown in the schematic in Figure 1-8A. (1) Phosphatidylglycerol: proliprotein diacylglycerol transferase (Lgt) forms a thioether linkage between Cys and diacylglycerol. (2) The lipoprotein specific signal peptidase, LspA, cleaves before the Cys residue in the lipobox. (3) Finally, apolipoprotein *N*-acyltransferase (Lnt) amino-acylates the Cys residue. Figure 1-8A depicts this reaction scheme.

After the lipidation, an ATP binding cassette (ABC) transporter at the inner membrane, LolCDE, sorts the proteins by the lipobox sequence. LolA acts as a periplasmic chaperone for the lipidated protein, essentially keeping the hydrophobic lipidated protein shielded from the aqueous periplasm. Finally, LolB, a lipoprotein on the inner leaflet of the outer membrane, accepts the lipoprotein from the chaperone LolA and incorporates it into the outer membrane. Figure 1-8B contains a pictorial representation of this mechanism (*129*, *130*).

In the *Shewanella* electron conduit we are expressing in *E. coli*, the only protein that is lipidated is MtrC (*33*). In the original organism, the majority of the outer membrane cytochromes *c* are lipidated, including OmcA and MtrF (*33*). In *E. coli*, most lipoproteins are localized to the inner leaflet of the outer membrane. In the following section, the implications of the lipidation of MtrC on localization to the outer leaflet of the outer membrane are described.

1.3.2.5. Localization to the outer membrane *via* the T2SS secretin (Gsp) and BAM.

Finally, MtrC and MtrB must be translocated to the outer membrane, presumably by type II secretion (*73–75*). Translocation of apoprotein across the inner membrane through T2SS was discussed in Section 1.3.2.2. The translocation of MtrC and MtrB occur through different mechanisms because MtrC is a surface displayed decaheme cytochrome *c* while MtrB is an integral membrane β–barrel.

The general secretory pathway (Gsp) is a subset of T2SS that secretes exoproteins to the extracellular space of the cell. It is believed that after secretion the lipoprotein MtrC associates with the outer leaflet of the cell due to the hydrophobic nature of the lipid. It is known that MtrB stabilizes MtrC in the outer membrane, but it is unknown if MtrB plays any role in the localization of MtrC. On the other hand, MtrB is inserted into the outer membrane by the β–barrel assembly machinery (BAM) complex. Below both pathways are summarized.

T2SS Secretin (Gsp): After secretion by SecYEG, proteins destined for the extracellular space are secreted by the general secretory pathway, or Gsp secretin (GspCDEFGHIJKLMO). This structure spans both the inner and outer membranes, forming a pseudopilin that is used to push the protein from the periplasmic space to outside the cell. The inner membrane component is comprised of GspFLM and uses ATP

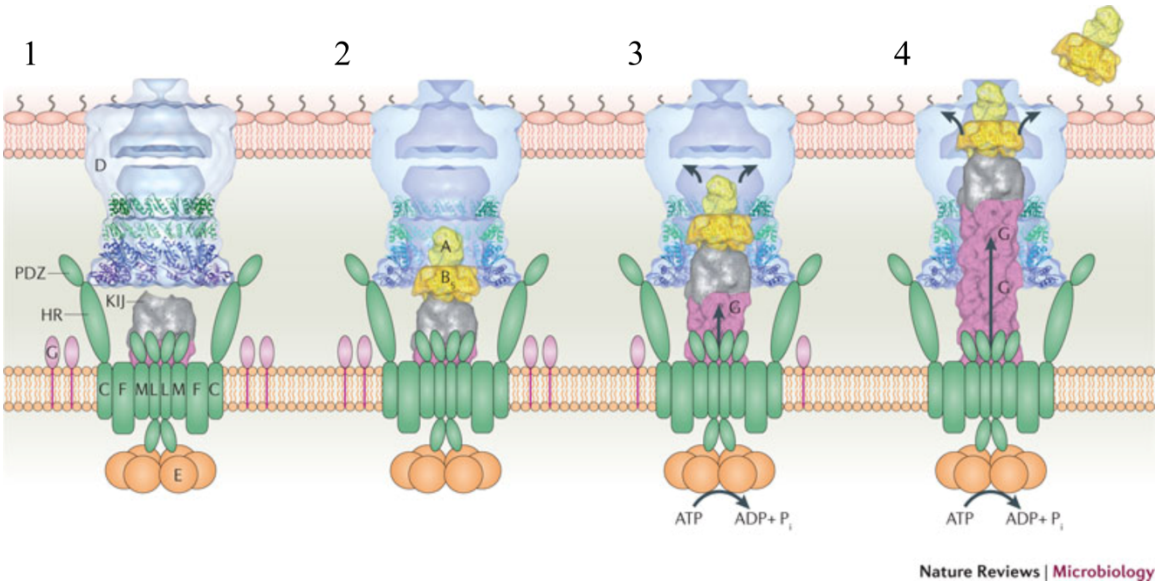

Figure 1-9. The hypothesized mode of secretion to the outer leaflet of the outer membrane by Gsp. Reprinted by permission from Macmillan Publishers Ltd: *Nature Reviews Microbiology* (*136*), copyright 2012. The Gsp General secretory pathway (Gsp) proteins are identified with capital letters. The possible architecture of Gsp is shown in panel 1. Panel 2 shows Gsp with an example of an exoprotein in the periplasmic vestibule (in this case, cholera toxin). How proteins are chaperoned or localized into the periplasmic vestibule is unknown, but it is currently attributed to the transient nature of this protein complex or some sort of affinity with GspC. Panel 3 shows the hydrolysis of ATP by GspE for which conformational changes are coupled with GspL, which may be involved in adding pseudopilins GspH and GspG. The addition of these pseudopilins, as shown in Panel 3, begins to move the exoprotein through the secretin GspD. Panel 4 shows the extension of pseudopilin GspG acting as a piston, pushing the exoprotein through the extracellular gate.

hydrolysis to power export *via* the GspE ATPase. The pseudopilin component is comprised of GspGHIJK; GspG is found in excess. The outer membrane complex is comprised of the secretin dodecamer GspD and lipoprotein GspS, also called pilotin. Recent reviews on the structure and composition of the Gsp complex are available for greater detail (*136*, *137*).

The actual secretion process by the pseudopilin is not well characterized. However, a model was proposed by Reichow, et al., based upon electron microscopy structural studies (*138*). The proposed architecture of Gsp is as shown in Figure 1-9, panel 1. The folded protein is recognized by either GspC or the secretin (GspD), and a signal is sent to the ATPase hexameric GspE to induce ATP hydrolysis. The protein is moved into the vestibule of Gsp, as suggested by the dynamic nature of the system. The protein settles onto the GspKIJ tip, and the psuedopilins GspG and GspH are moved into the vestibule to form a piston. The size of the GspKIJ tip is such that it cannot be exported during the piston-like action. The primarily GspG piston works to push the protein through the secretin. The overall process is shown pictorially in Figure 1-9. More details on the proposed mechanism of action may be found in several recent reviews (*136–138*).

It has been shown GspD and GspG are vital in *Shewanella* for dissimilatory metal reduction (*74*, *75*), and thus the T2SS has been implicated as essential in the expression of the cytochromes. It is currently unclear how the lipidation of MtrC and its localization to the inner leaflet of the outer membrane by Lol may feed into Gsp localization to the outer leaflet of the outer membrane. It is possible that there is a separate chaperone or even a separate unidentified localization mechanism that moves the lipoprotein MtrC to the extracellular surface of the cell. It is worth noting that the gene product of LP2086 in the spirochete *Borerelia burgdorferi* is a surface-exposed lipoprotein; however, *B. burgdorferi* does not have *lolB* encoded on the genome (*139*). The authors suggest that the absence of LolB causes the localization of LP2086 to the outer leaflet, but it is not clear if this is universally true. However, *Shewanella* has the *lolB* coding sequence on its genome and is still able to localize MtrC to the outer leaflet, contradicting this suggestion by Schulze (*134*, *139*, *140*). It is interesting to note that, out of the LolABCDE, *Shewanella* LolB is least homologous to B-strain *E. coli* Lol proteins (Appendix C). Thus further work must be performed in *Shewanella* to identify the mechanism of localization of lipoproteins to the outer leaflet of the outer membrane.

β*–barrel assembly machinery (BAM) complex*: Once secreted through the inner membrane *via* SecYEG, hydrophobic β–barrel proteins are chaperoned across the periplasm by either SurA or DegP/Skp to the BAM complex in the outer membrane. The interaction of these chaperones has been studied in detail (*141–143*). This complex is comprised of 5 gene products; these proteins were recently renamed BamA (YaeT), BamB (YfgL), BamC (NlpB), BamD (YfiO), and BamE (SmpA), with the original denominations in parentheses (*97*, *144*). The Bam denominations will be used in this dissertation for clarity. When β–barrel proteins are overexpressed, DegP will also degrade excess preprotein.

In BamA, regions known as POTRA (polypeptide transport associated) domains are believed to interact with immature hydrophobic β–barrel proteins (*145*, *146*). There are two proposed methods of β–barrel folding. The first is the pore folding model in

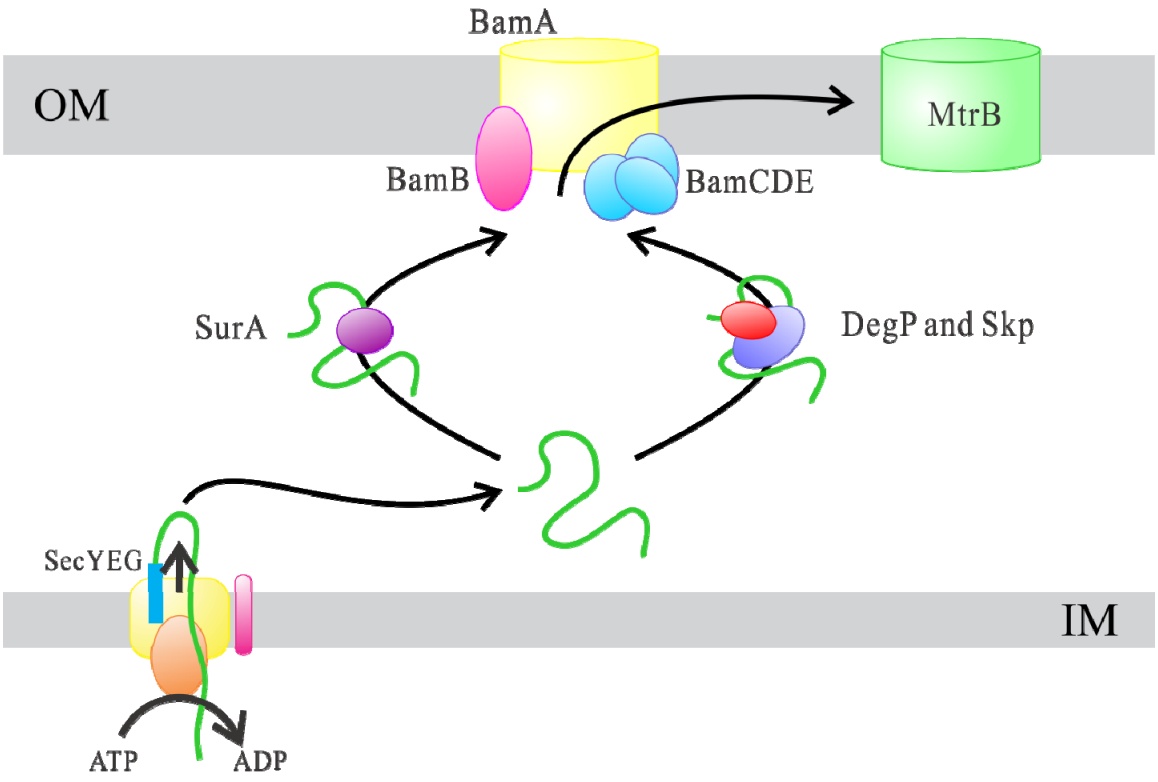

Figure 1-10. Schematic of secretion of integral membrane β-barrel proteins to the outer membrane by the BAM complex. After secretion by SecYEG, the unfolded β-barrel protein is chaperoned to the outer membrane by either SurA (purple) or DegP/Skp (blue and red). Then the β-barrel protein is folded and inserted into the membrane by the Bam compelx, BamABCDE. BamA (yellow) periplasmic exposed loops, known as POTRA, are known to interact with the immature hydrophobic regions of the β-barrel. The exact mechanism of the insertion into the outer membrane is unknown.

which the unfolded β–barrel is threaded into the pore of BamA where it uses the core of BamA as a template for folding. The second is the chaperone folding model in which the periplasmic chaperones fold the protein and chaperone the protected protein within the core of the chaperone, forming an overall hydrophilic complex. However, the mechanism for incorporating the β–barrel into the outer membrane is currently unknown. The overall process is shown pictorially in Figure 1-10. A comprehensive overview of this process may be found in several recent reviews (*97*, *98*, *144*).

1.3.3. Increasing the number of electron conduits does not necessarily increase current production.

It is generally unknown how the concentration of this pathway per cell will determine the function on a per-cell basis. Our assumption at the commencement of this project was that increasing the number of electron conduits would (a) increase the number of contact points of the engineered bacteria and the metal oxide surface and (b) increase the number of routes that the electron could take out of the cell, thus increasing overall reduction rate. However, as discussed in Chapters 3 and 5, we actually found that increasing the number of electron conduits seemed to be more damaging to the overall systematic functions of the cell. To date, increasing the number of conduits by transcriptionally upregulating *mtrCAB* has never increased iron oxide or electrode reduction in our hands, and we have not yet determined why. One possible explanation is that membrane damage from increasing membrane protein expression decreases cell viability. A second explanation is that lactate oxidation by lactate dehydrogenase is rate limiting, inherently limiting the number of electrons delivered to the conduit.

Regardless, when designing this type of system in another organism, it is important to consider how tightly transcription and translation are controlled. For instance, although a sufficient amount of the conduits must be displayed and localized correctly, excessive protein synthesis may become a drain on normal cellular resources, clog up the T2SS pathways, or place a significant burden on the cytochrome *c* maturation machinery. In other words, the processive rates of all the post-translational modifications discussed above must be matched such that there is not an excessive burden or rate limiting step on any particular step. In addition, the electron conduit may necessitate tuning of the relative protein ratios for proper function. Thus, the more control one has over the synthesis of the proteins, the more likely one will be able to find a sweet spot in both expression and function.

1.3.4. Strain selection in the future requires careful investigation of the pathways required for cytochrome *c* biogenesis.

It is important to note that some strains of *E. coli* have a silenced version of type II secretion, specifically K strains (*147*). It was observed by Donald, et al., that expression of OmcA in the K-12 strain was not possible, supposedly because of the silenced T2SS (*73*). Because of the dependence on T2SS for cytochrome *c* expression, *E. coli* B strains were exclusively used in this dissertation (*92*, *148*).

One downside to using *E. coli* B-strains is their inability to form biofilms (*149*, *150*), which are known to be important in *Geobacter* and *Shewanella* electrode reduction. There are artificial means to bypass natural biofilm formation such as the generation of synthetic biofilms (*151*) or chemical attachment *via* DNA (*152*), however both of these

techniques have their disadvantages. Synthetic biofilms managed by the cell are attractive, but production requires a third plasmid that must have a unique origin of replication (*ori*) and antibiotic resistance gene to other plasmids transformed into the cell. Additionally, this would provide even greater membrane stress on the cell without careful consideration of expression levels. Another attractive option developed by the Francis lab is chemical attachment to surfaces *via* DNA hybridization (*152*). In this method, complementary single stranded DNA is covalently linked to the surface and to sugars on the cell surface; once these two materials are in contact, DNA hybridization between the surface and the cell locks the cells in place, creating a microbial film (*152*). However, it is yet unknown how the DNA-attachment chemistry affects the viability of these strains. Additionally, these reactions were optimized to attach cells to glass-like surfaces. This effectively limits cell attachment to one type of electrode: indium tin oxide (ITO) coated glass slides. ITO is a unique electrode material that is generally used because of its transparency; however, ITO is not an ideal electrode material. For the use of DNA attachment, it would be ideal to reconfigure the reactions to a high surface area graphite electrode.

When moving into different organisms in the future, one should consider if the strain has the type II secretion pathway, performs aerobic and anaerobic expression of the *ccm* pathway, and the ability to form biofilms. The ideal strain will, obviously, contain all three of these elements. If a particular strain is lacking in one or more of these pathways, one must consider how to up-regulate or add this capability.

1.3.5. Other considerations when moving forward into other microbial systems.

From this work, we have learned much about the heterologous expression of cytochromes *c*. One of the overall goals of this work is to transfer this system into a strain with more complicated pathways, such as photosynthetic and carbon-fixing bacteria. When looking forward to engineering future strains, the following questions about how we adapt this system to a new strain must be addressed.

In addition to the strain criteria explained in section 1.3.4 above, it is worth continually asking ourselves if we are expressing "the right" cytochromes. In other words, is there another pathway in the dissimilatory metal reducing bacteria subset that will perform better than this particular *Shewanella* pathway? This is an open-ended question that does not have an easy answer. The *Geobacter* pathway is not well characterized, inherently making it difficult to reengineer in another strain. However, this pathway is unique from *Shewanella* in that it only performs electron transfer in direct contact with an electrode. So if an application cannot rely on soluble redox factors, perhaps the *Geobacter* pathway would be better suited than the *Shewanella* pathway. Furthermore, if we are already engineering a heterologous pathway *de novo*, we have the ability to "mix-and-match" cytochromes from different pathways or different organisms to find an optimal electron conduit cassette.

Another important concern is anaerobic metabolism. In my work, I have specifically avoided carbon sources that provide types of growth other than anaerobic respiration (i.e. anaerobic fermentation). Thus a new strain would need to have the dehydrogenases required for anaerobic respiration, such as lactate, acetate, formate, or glycerol dehydrogenases. These dehydrogenases perform the first step to generating both proton motive force and provide an electron source in the quinol pool. Thus the specific

activity of these enzymes should be closely analyzed to determine which carbon source(s) should be used. However, the assumption that fermentation will siphon electrons away from the electron conduit has not been proven; one could argue that a combination of fermentation and respiration could better support growth, and thus increase current out of the cell. Although I have done a series of experiments to determine what carbon source works best in our engineered *E. coli* strains, experiments using a mixture of these carbon sources with a fermentable sugar, such as glucose, may provide valuable insight into what impact fermentation has on anode reduction.

1.4. Closing remarks.

Engineering an efficient means of electronic communication between living and nonliving systems has the potential to create hybrid sensors and electronics capable of self-replication and self-repair. Although existing technologies can transfer electrons from a cell to an electrode, no single approach has achieved what the next generation applications require: molecularly defined electron flow across a variety of cell types. In the following chapters, I have demonstrated the feasibility of a wholly biological approach that meets this challenge and provides a novel blueprint for cellular-electronic connections. Through the addition of novel genetic information, we have engineered electronic communication between living cells and inorganic materials. The genetic nature of this approach makes it applicable to many cell types and specifies the route of electron transfer. To transfer the system to a different prokaryote would simply require the choice of an appropriate promoter and origin of replication, use of a host-specific signal sequence to ensure proper localization, and modification of the ccm genes to achieve their expression under aerobic conditions. Another unique advantage is that the cell directs the assembly of these bioelectronic connections such that they are self-repairing, requiring no experimenter assembly or intervention. Finally, based on the natural system's respiratory versatility, we anticipate that our engineered system should be able to reduce multiple types of inorganic electrodes.

Additionally, this provides a unique opportunity to understand the *Shewanella* electron transfer pathway. The *S. oneidensis* MR-1 genome encodes for 42 *c*-type cytochromes. Thus it is difficult to study a well-defined molecular route in the native system. Laborious one-by-one knockouts in the *S. oneidensis* MR-1 genome might lead to some basic understanding, but these genomic modifications may also lead to other mutations in the genome, potentially skewing results. By simultaneously expressing only select cytochromes, we have control over the route of the electron to an electrode.

Another unique advantage to creating a blueprint for extracellular electron transfer that may be transferrable across a diverse set of microbes is that it creates the potential to combine cellular-electronic connections with other unique microbial pathways. For example, by transferring this system to acetogens, it would be possible to inject electrons into a cell for the cell to fix carbon. Another exciting example would be transferring this pathway to photosynthetic bacteria, potentially allowing the cell to harvest electrons from light and then transfer those electrons to an electrode. These unnatural pathway combinations would drastically expand the applications in energy conversion.

Chapter 2

Engineering a synthetic electron conduit in living cells

2.1. Introduction

Engineering efficient, directional electronic communication between living and non-living systems has the potential to combine the unique characteristics of both materials for advanced biotechnological applications. However, the cell membrane is designed by nature to be an insulator, restricting the flow of charged species; therefore introducing a biocompatible pathway for transferring electrons across the membrane without disrupting the cell is a significant challenge. Here we describe a genetic strategy to move intracellular electrons to an inorganic extracellular acceptor along a molecularly-defined route. To do so, we reconstitute a portion of the extracellular electron transfer chain of *Shewanella oneidensis* MR-1 into the model microbe *Escherichia coli.* This engineered *E. coli* can reduce metal ions and solid metal oxides ~8x and ~4x faster than its parental strain. We also find that metal oxide reduction is more efficient when the extracellular electron acceptor has nanoscale dimensions. This work demonstrates that a genetic cassette can create a conduit for electronic communication from living cells to inorganic materials, and it highlights the importance of matching the size scale of the protein donors to inorganic acceptors.

This approach specifically takes advantage of a natural electron pathway that has evolved to utilize a variety of solid metals and metal oxides as terminal electron acceptors. Since such an extracellular electron transfer pathway is absent in most cell types, we have the ability to create a well-defined electron path with precise and flexible control over the combination and localization of the electron-carrying proteins. This approach is now tractable in part because the advent of genome sequencing has greatly added to the molecular level understanding of diverse organisms (*153*, *154*). Also key to this approach, the growing field of synthetic biology offers more sophisticated tools available to create and modify genetic systems (*155–160*). Now armed with greater control over translation and transcription of synthetic genes and pathways (*161*, *162*), it is possible to engineer the living cell as a material for advanced biological systems and applications.

In this chapter, we set out to determine whether we could convert a bacterial strain that is incapable of reducing solid metal oxides to one that can by installing a synthetic electron conduit that bridges the cytosol to the extracellular space. To do so, we expressed the MtrC, MtrA, and MtrB proteins from *S. oneidensis* MR-1 in *Escherichia coli*. In this heterologous system, we find that the mature proteins are functionally expressed, and MtrC and MtrA are redox active. We present evidence that MtrA interacts with at least one native *E. coli* redox protein and that it has a direct role in accelerating the rate of soluble Fe(III) reduction. Most importantly, we show that expression of *mtrCAB* can 'wire up' *E. coli* to inorganic solids, i.e. it confers the ability to reduce solid δ-Fe_2O_3 and that the rate of electron flow is increased when the solid has nanometer dimensions.

2.2. Design of the synthetic electron conduit using *S. oneidensis* MR-1 *mtrCAB*.

2.2.1. *Escherichia coli* chosen as an optimal heterologous platform.

Because it is a genetically tractable, gram-negative bacterium with readily available tools for heterologous expression of cytochromes c, *E. coli* was chosen as a testbed to determine whether we could genetically introduce a molecularly-defined electron conduit modeled on the extracellular electron transfer pathway of *S. oneidensis* MR-1. The physical arrangement of *S. oneidensis* MR-1 cytochromes (Figure 2-1a) suggests that an inner membrane, a periplasmic, and an outer membrane cytochrome are required to achieve extracellular electron transfer in *E. coli*. In support of this hypothesis, while CymA (*64*, *72*), MtrA (*51*, *72*), OmcA (*73*), and the combination of MtrA and CymA (*72*) have been expressed in *E. coli*, none of these systems has been shown sufficient to reduce solid Fe(III) oxides to Fe(II). Additionally, published reports suggest that the outer membrane 28 strand β-barrel protein MtrB is required for correct folding and localization of MtrC and OmcA (*54*) and may be involved in interactions between MtrC and MtrA (*163*). Yet, since extensive post-translational processing is required to correctly incorporate the multiple hemes, fold, and localize each of these cytochromes c, heterologous expression of even a single multi-heme cytochrome c is a significant technical challenge. To our knowledge, multiple decaheme cytochromes have not been simultaneously expressed in *E. coli*, so we sought to select a minimal number of proteins to heterologously express. The work of both Pitts and Gescher suggest that the native *E. coli* inner membrane tetraheme cytochrome NapC, which is 52% sequence similar to CymA, can reduce heterologously expressed MtrA (*51*, *64*). Therefore, we selected the *mtrCAB* genes as a potentially minimal set required to create a synthetic electron conduit that would allow *E. coli* to reduce insoluble metal oxides. To allow us to dissect the electron transfer paths of this heterologous pathway and to separately investigate the role of MtrA and MtrC in Fe(III) reduction, we also chose to express MtrA by itself (Figure 2-1c).

2.2.2. Plasmid design and construction.

We created two plasmids containing *mtrA* and *mtrCAB* under the control of a *T7 lac* promoter (Figure 2-1b) (*164*, *165*). Primers containing EcoRI and XbaI restriction sites (Table 2-1, primers 1 and 2 for *mtrA*; primers 3 and 4 for *mtrCAB*), and Platinum Pfx Polymerase (Invitrogen) were used to amplify the respective sequences. After digestion with EcoRI and XbaI, these DNA fragments were ligated into the modified pET30a+ vector using T4 DNA Ligase (Roche). The modified pET30a+ vector had an NdeI site (CATATG) directly upstream of the EcoRI site used for insertion. The ATG in the NdeI site was used as the start codon, and the forward primers for PCR were designed to clone from the second codon of *mtrA* and *mtrC* in the *Shewanella* genome. This design adds the two codons from the EcoRI site coding Glu-Phe; however, the extra amino acids will be cleaved by the Sec system in the process signal sequence cleavage of MtrA and MtrC in plasmids *mtrA* and *mtrCAB*, respectively.

Since the *E. coli* cytochrome c maturation (*ccmABCDEFGH*) genes are required for heme insertion but are not transcribed under aerobic conditions (*122*), the *mtrA* and *mtrCAB* plasmids were co-transformed with pEC86, a cytochrome c maturation (*ccm*)

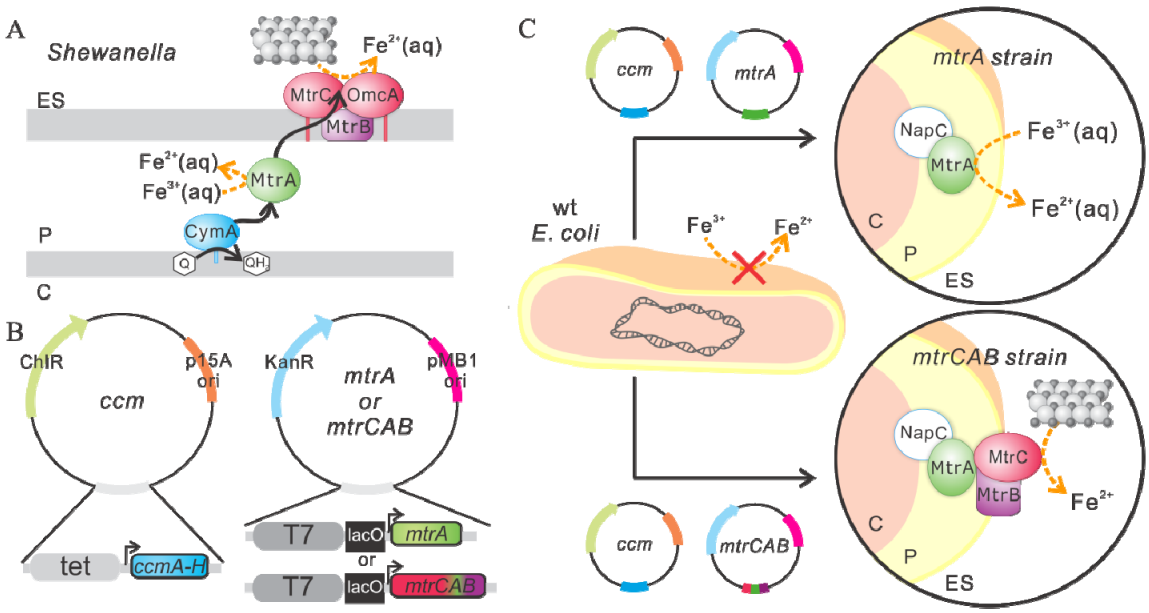

Figure 2-1. An overview of the strategy to rebuild electron conduits in a heterologous organism. (A) Schematic of proposed extracellular electron transfer pathway in *Shewanella oneidensis* MR-1 where ES denotes the extracellular space, P denotes the periplasm, and C denotes the cytoplasm. The silver and black spheres represent extracellular iron oxide. (B) Schematic of plasmids used to create the *ccm*, *mtrA*, and *mtrCAB* strains in *E. coli*. (C) Schematic of the engineered *mtrA* and *mtrCAB* strains for soluble and extracellular metal reduction.

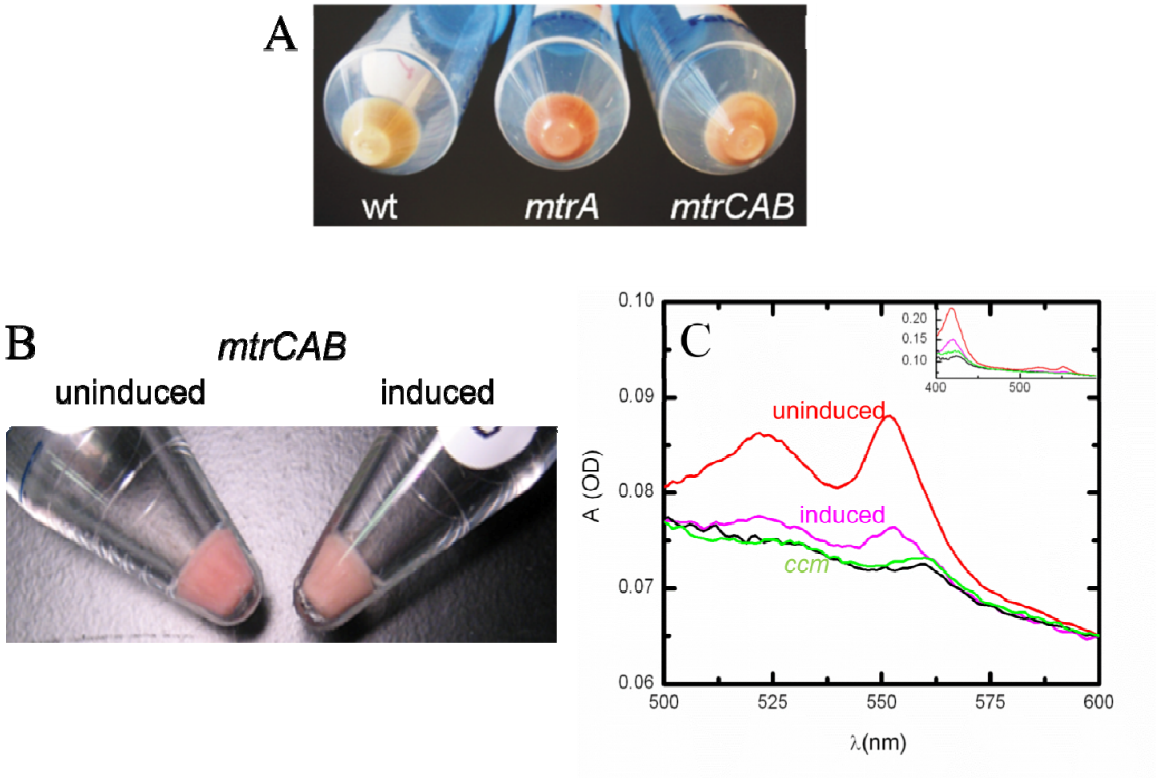

Figure 2-2. The red color of cell pellets serves as a visual indication of the amount of holocytochrome *c* expressed per cell. (A) The cell pellets of uninduced wt, *mtrA,* and *mtrCAB* strains show different red intensities. The red color is caused by the hemes within the cytochromes *c*. (B) Interestingly, addition of as little as 10 μM IPTG to the *mtrCAB* culture resulted in a less intense red color of the cell pellets compared to cultures growth without IPTG. (C) Additionally, this decrease in holocytochrome *c* was confirmed by decreased peaks in spectroscopy. Thus, basal expression of the *mtrA* and *mtrCAB* plasmids yields a higher concentration of correctly folded cytochrome c than induced expression.

plasmid. The *ccm* plasmid, pEC86, encodes the genes *ccmA-H* under a constitutive tet promoter and carries a chloramphenicol resistance marker (Figure 2-1b) (*65*).

2.3. Functional expression of *mtrC, mtrA* and *mtrB* in *E. coli*.

2.3.1. Induction of the *T7 lac* promoter synthesized less functional Mtr than no induction.

BL21(DE3) cells (wt strain) and cells carrying only the *ccm* plasmid (*ccm* strain) were pale-yellow in color; conversely, cells containing both the *ccm* and *mtrA* (*mtrA* strain) or *mtrCAB* (*mtrCAB* strain) plasmids were red (Figure 2-2), indicating that the cytochromes were expressed. Addition of isopropyl β-D-1-thiogalactopyranoside (IPTG), which derepresses the *T7 lac* promoter, would be expected to increase expression of MtrA and MtrCAB in the *mtrA* and *mtrCAB* strains, respectively. However, even low concentrations of IPTG (10 μM) resulted in cell pellets with a less intense red color as compared to the same strain uninduced, suggesting more protein was expressed under non-inducing conditions; therefore we performed all subsequent growth of the BL21(DE3) strains in the absence of IPTG.

2.3.2. Localization of MtrCAB

In *S. oneidensis* MR-1, the periplasmic and outer membrane localization of MtrA and MtrC are believed to be crucial for extracellular electron transfer (*32*). To probe the localization of heterologously expressed MtrA and MtrC, aerobically-grown wt, *ccm*, *mtrA*, and *mtrCAB* strains were fractionated into periplasmic and membrane fractions. These fractions were analyzed by SDS-PAGE followed by 3,3′,5,5′-tetramethylbenzidine (TMBZ) staining, which stains proteins with covalently bound heme (*166*). The periplasmic and membrane fractions of wt and *ccm* strains had no visible bands in the TMBZ stain, suggesting that no or little native c-type cytochrome is present (Figure 2-3a,b). The periplasmic fractions of both *mtrA* and *mtrCAB* strains had a band at 32 kD, the expected molecular mass of MtrA, indicating that MtrA is correctly targeted to the periplasm (Figure 2-3a). MtrA is present to a lesser degree in the membrane fractions of both strains, while a band at the expected molecular mass of MtrC, 71 kD, is present only in the membrane fraction of the *mtrCAB* strain (Figure 2-3b). Finally, only the membrane fraction of the *mtrCAB* strain produced a band at the expected molecular mass of MtrB, 77 kD, in an immunoblot with an MtrB-specific antibody (Figure 2-3c). This pattern of localization for MtrA, MtrB, and MtrC in *E. coli* is identical to that reported for *S. oneidensis* MR-1, indicating that heterologous expression preserved these proteins' native localizations (*33*, *51*, *167*).

2.3.3. Redox activity of MtrCAB

The MtrCAB proteins must also be redox active for functional electron transport. We probed the redox activity of heterologously expressed MtrA and MtrC using UV-Vis absorption spectroscopy. The visible spectra of the periplasm and membrane fractions of *mtrA* and *mtrCAB* strains were obtained under oxidizing (air) and reducing conditions (sodium dithionite). The most prominent features of oxidized c-type cytochromes are the Soret band at 410 nm and a broad second peak at 530 nm. After chemical reduction with sodium dithionite, the Soret band shifts to 420 nm and the β- and α- bands are seen at 525

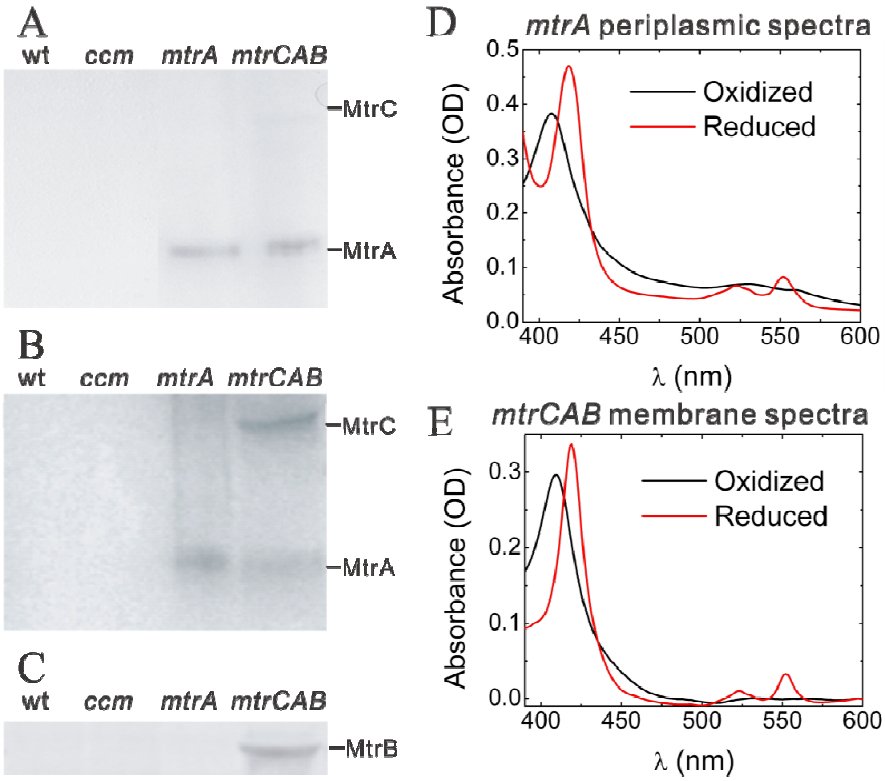

Figure 2-3. Expression of full-length redox-active MtrA and MtrC in *E. coli*. Heme-stained SDS-PAGE gels of (A) periplasmic fractions and (B) membrane fractions of the WT, *ccm*, *mtrA*, and *mtrCAB* strains. (C) Anti-MtrB immunoblot of membrane fractions of the WT, *ccm*, *mtrA*, and *mtrCAB* strains. (D) Absorption spectra of the periplasmic fraction of the *mtrA* strain under oxidizing and reducing conditions. (E) Absorption spectra of the membrane fraction of the *mtrCAB* strain under oxidizing and reducing conditions.

nm and 552 nm. The periplasmic fractions of *mtrA and mtrCAB* strains and the membrane fraction of *mtrCAB* all exhibited signature absorption spectra typical of oxidized and reduced c-type cytochrome (Figure 2-3d,e). Additionally, using $A_{552\ nm}$ of the periplasmic fractions and the extinction coefficient of purified MtrA ($\varepsilon_{552} = 28\ mM^{-1}\ cm^{-1}\ heme^{-1}$) (*51*), we estimate that there are 4000 and 2100 redox active MtrA present per cell in the *mtrA* and *mtrCAB* strains, respectively. Assuming the same extinction coefficient for MtrC, we estimate there are 75 redox active MtrC per cell. Taken together, these data demonstrate that redox active, full length MtrA and MtrC were heterologously expressed in *E. coli* with their native localization.

2.4. Expression of *S. oneidensis* MR-1 cytochromes in *E. coli* increases soluble Fe(III) citrate reduction rates.

We next sought to determine whether heterologous expression of MtrA and MtrC in *E. coli* enabled *in vivo* reduction of soluble chelated iron species, which diffuse into the periplasm. To test iron reduction in live cultures, we added 10 mM Fe(III) citrate separately to sterile media or a fixed concentration ($OD_{600\ nm} = 0.5$) of heat-killed, wt, *ccm*, *mtrA*, and *mtrCAB* cells under anaerobic conditions and measured the Fe(II) concentration of the resulting cultures as a function of time using the ferrozine assay (*168*). For each time point, the Fe(II) concentration at that time was subtracted by the corresponding Fe(II) concentration in media-only sample, representing abiotic Fe(III) reduction, and normalized by the ratio of the original $OD_{600\ nm}$ to the current $OD_{600\ nm}$ to account for the relative number of cells at each time point.

As shown in Figure 2-4, metabolically-inactive heat killed *E. coli* showed a small amount of Fe(III) reduction over the 10 day period that is most likely caused by non-metabolic processes that have remained unidentified to date (*169*). Living strains reduce Fe(III) citrate at a rate above the metabolically inactive *E. coli* that is nearly identically for the first two days. After two days, the rate of Fe(III) reduction in the wt strain levels off ($10 \pm 2\ \mu M\ day^{-1}$). The *ccm* strain reduces Fe(III) at a slightly faster rate ($33 \pm 3\ \mu M\ day^{-1}$). Since increased expression of native *E. coli* c-type cytochromes slightly increases iron reduction (*72*), we tentatively assign this rate increase to *E. coli* c-type cytochromes resulting from the over-expression of the *ccm* operon. In striking contrast, the average rates of reduction in the *mtrA* ($83 \pm 3\ \mu M\ day^{-1}$) and *mtrCAB* ($59 \pm 11\ \mu M\ day^{-1}$) strains are ~8 and ~6 times greater, respectively, than the rate of wt reduction. We attribute the dramatic changes in Fe(III) reduction rate in the *mtrA* and *mtrCAB* strains to the presence of the heterologous cytochromes c expressed in each strain. Surprisingly, the *mtrCAB* strain reduced Fe(III) at a lesser rate than the *mtrA* strain. We suggest that this could be due to decreased expression of MtrA in the *mtrCAB* strain and its preferential ability over MtrC to reduce Fe(III) citrate.

2.5. The redox state of MtrA is kinetically linked to Fe(III) citrate reduction in *E. coli*.

The increase in Fe(III) citrate reduction in the *mtrA* strains relative to the *ccm* strain suggests that MtrA directly reduces Fe(III) citrate. To confirm this, we simultaneously measured Fe(II) concentration and monitored the α-band absorption at 552 nm in high-density anaerobic cell suspensions of the *mtrA* strain before and after adding 50 μM Fe(III) citrate. In order to clearly detect the α-band of MtrA over cell

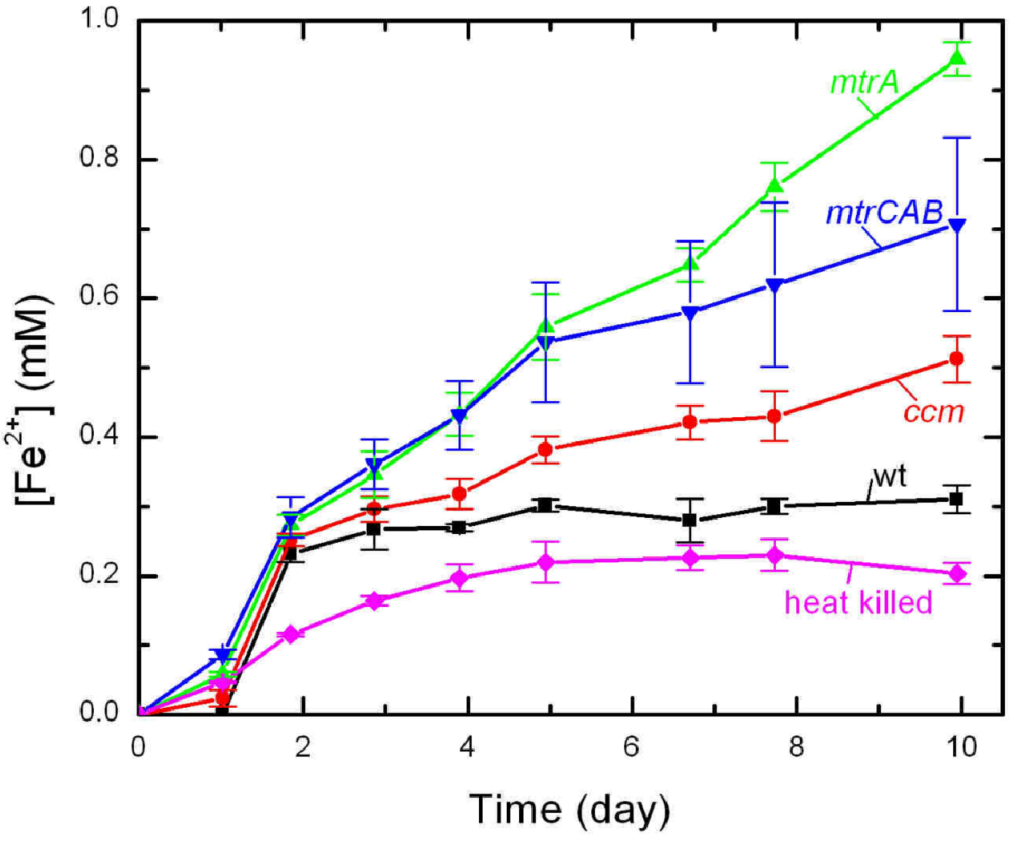

Figure 2-4. Reduction of Fe(III) citrate to Fe(II) as a function of time by the engineered *E. coli* strains. Reduction of 10 mM Fe(III) citrate to Fe(II) as a function of time for the WT, *ccm*, *mtrA*, and *mtrCAB E. coli* strains. Error bars represent the standard deviation between triplicates from individual biological cultures. The average rates of reduction in the *mtrA* (83 ± 3 μM day^{-1}) and *mtrCAB* (59 ± 11 μM day^{-1}) strains are ~8 and ~6 times greater, respectively, than the rate of wt reduction.

scatter and to observe Fe(II) formation over a shorter timescale, these experiments required unusually high cell densities and much lower concentrations of Fe(III) citrate; however, changes in the α-band absorption could be unambiguously detected even with an $OD_{600\ nm}$ around 3.0 (Figure 2-5a). Before the addition of Fe(III) citrate, the UV-Vis spectrum showed that MtrA is in a reduced state (black line). Upon Fe(III) addition, the α-band absorption immediately decreased (red line), indicating MtrA is rapidly oxidized. As time elapsed, the α-band absorption increased (dashed lines), indicating that MtrA is re-reduced, presumably by cellular species.

Closer analysis can be undertaken by plotting $\Delta A_{552\ nm}$ and Fe(II) concentration as a function of time relative to Fe(III) citrate addition (Figure 2-5b). Immediately following Fe(III) citrate addition, the A_{552nm} decreases by ~0.15 OD and dwells in this oxidized state for 12 minutes. Over the same time period, ~30 μM is reduced to Fe(II). These observations provide for the first time a direct link between the timescales of MtrA oxidation and Fe(III) reduction in a heterologous host and strongly suggest that MtrA directly reduces Fe(III). They also suggest that movement of Fe(III) and Fe(II) in and out of the periplasm is extremely fast. Interestingly, after these fast initial events, the remaining Fe(III) is gradually converted to Fe(II) while MtrA is slowly re-reduced to its initial redox state. The instantaneous rate of Fe(III) reduction decreasing as a function of time indicates that the reduction rate depends on the concentration of remaining Fe(III). This would be expected for any non-zeroth order chemical reaction. The slow re-reduction of MtrA indicates that native *E. coli* proteins (ex: NapC) are capable of reducing MtrA, but that this process is quite slow relative to the oxidation of MtrA by Fe(III).

2.6. NapC is not the only electron donor to MtrA in *E. coli*.

While the data in Figure 2-5 show that MtrA is capable of being re-reduced, it does not indicate which *E. coli* native protein(s) pass electrons from the quinol pool to MtrA in the periplasm. Previous work has suggested that NapC, a native *E. coli* inner membrane tetraheme cytochrome c, could functionally replace CymA, *S. oneidensis* MR-1's inner membrane tetraheme cytochrome c, because of the 52% sequence similarity (31). If NapC is the sole electron donor to MtrA, then we expect that an *E. coli* strain expressing *ccmA-H* and *mtrA* but lacking *napC* would reduce soluble Fe(III) at the same rate as the *ccm* strain. To explore this hypothesis, a *napC* knockout was made in BL21(DE3) using the λ-red gene disruption method (*170*). This new strain, Δ*napC*, was co-transformed with *ccm* and/or *mtrA* to create the Δ*napC ccm* and Δ*napC mtrA* strains which were analyzed for their ability to reduce soluble Fe(III) citrate. As shown in Figure 2-6, the Δ*napC ccm* strain reduces Fe(III) more slowly than the *ccm* strain (21 ± 1 vs. 33 ± 3 μM day^{-1}, respectively) which is in accord with previous reports that suggested increased expression of NapC could enable soluble iron reduction in *E. coli* (*64*). Interestingly, the *ΔnapC mtrA* strain reduces Fe(III) more slowly than the *mtrA* strain (51 ± 6 vs. 83 ± 3 μM day^{-1}, respectively). If NapC were the only protein transferring electrons from *E. coli* inner membrane to MtrA, it would be expected that the Δ*napC mtrA* strain reduction rate would be similar to that of the Δ*napC ccm* strain. However, destroying NapC expression does not completely diminish the reduction rate to that of the Δ*napC ccm* strain, suggesting that there are other electron donors to MtrA.

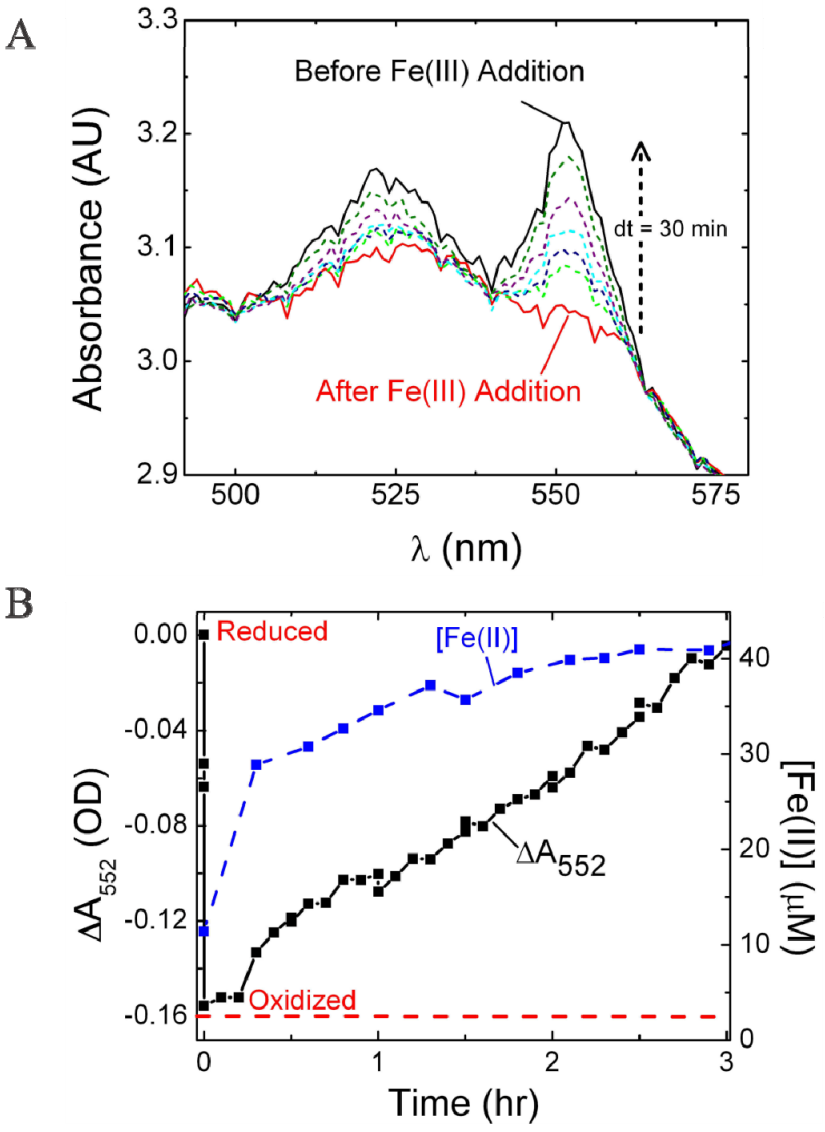

Figure 2-5. Direct link of MtrA redox state to Fe(III) citrate reduction. (A) Absorption spectra showing the α-band of MtrA in high-density, anaerobic cell suspensions of the *mtrA* strain before and after the addition of Fe(III) citrate. MtrA begins reduced (black line, strong α-band absorption), but is oxidized upon the addition of 50 μM Fe(III) citrate (red line). Over time, the α-band absorbance recovers (colored dotted lines). (B) $\Delta A_{552\ nm}$ and Fe(II) concentration immediately before and after Fe(III) citrate addition as measured by the ferrozine assay.

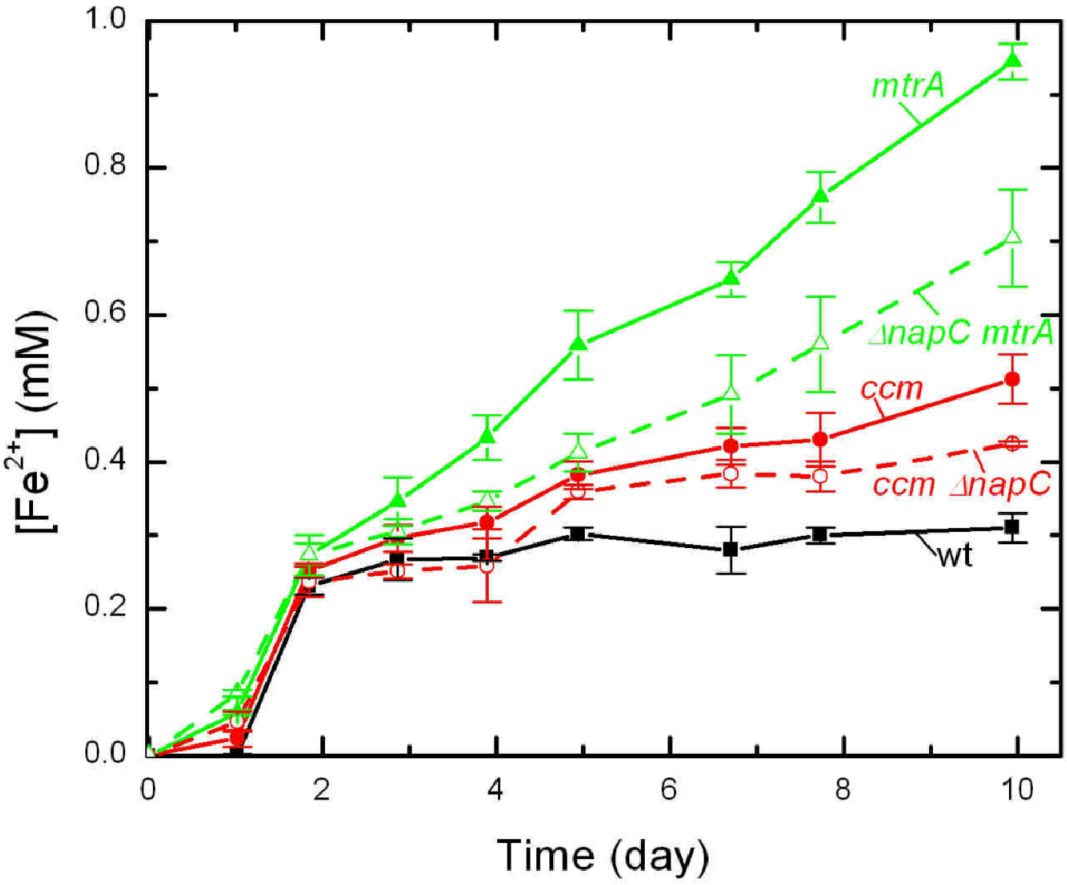

Figure 2-6. NapC is not the sole electron donor to MtrA. Reduction of 10 mM Fe (III) citrate to Fe(II) by WT, *ccm*, Δ*napC ccm*, *mtrA*, and Δ*napC mtrA* strains. The Δ*napC ccm* strain reduces Fe(III) more slowly than the *ccm* strain (21 ± 1 vs. 33 ± 3 μM day^{-1}, respectively). The *ΔnapC mtrA* strain reduces Fe(III) more slowly than the *mtrA* strain (51 ± 6 vs. 83 ± 3 μM day^{-1}, respectively).

2.7. MtrCAB in *E. coli* Reduces Solid δ-Fe_2O_3.

Since our primary interest is in exploring a new approach to electronically connect living cells and inorganic materials, we sought to determine whether the *mtrCAB* cluster is capable of reducing extracellular metal oxides. To test if heterologous expression of *mtrCAB* would reduce solid Fe_2O_3, we added δ-Fe_2O_3 (Figure 2-7a, $d \sim 5$ μm) to a final concentration of 2.5 mg mL^{-1} separately to sterile media or a fixed concentration ($OD_{600\ nm} = 1.0$) of wt, *ccm*, *mtrA*, and *mtrCAB* cells under anaerobic conditions, and measured the Fe(II) concentration and colony forming units (CFU) of the resulting cultures as a function of time. The Fe(II) concentrations were normalized by CFU mL^{-1} at each time point. Figure 2-7b shows a representative time point (t =24 days) of bulk δ-Fe_2O_3 reduction for all strains. Very little solid Fe(III) is reduced by the wt, *ccm*, and *mtrA* strains; no solid δ-Fe_2O_3 reduction is expected from the *E. coli* strains unless there is a complete electron transfer pathway that crosses both membranes because the *E. coli* genome does not encode for any proteins capable of transferring electrons from the periplasm to the extracellular space. Interestingly, the *mtrCAB* strain reduces significant amounts of δ-Fe_2O_3 per live cell ($11 \pm 5 \times 10^{-6}$ μM/CFU mL^{-1}) in comparison to the wt strain ($2.6 \pm 0.4 \times 10^{-6}$ μM/CFU mL^{-1}). Thus by expressing only three proteins from *S. oneidensis* MR-1, we are able to create a new electron transfer pathway in *E. coli* which transfers cytosolic electrons to the surface of extracellular δ-Fe_2O_3. Additionally, these *in vivo* data provide further evidence to existing *in vitro* data that MtrA, MtrB, and MtrC are necessary and sufficient to reduce extracellular metal oxides.

Electron transfer theory predicts that in order for the *mtrCAB* strain to reduce δ-Fe_2O_3, the MtrC-containing outer membrane must come into physical contact with the solid surface (*171*). This suggests that the rate of extracellular iron reduction by the *mtrCAB* strain would increase with increased Fe_2O_3 surface area. To test this prediction, we synthesized crystalline δ-Fe_2O_3 nanoparticles (Figure 2-7c, d = 13 nm), added these particles to a final concentration of 0.25 mg mL^{-1} to the wt, *ccm*, *mtrA*, and *mtrCAB* strains, and measured the formation of Fe(II) as described above. As in the bulk Fe_2O_3 experiments, wt, *ccm*, and *mtrA* strains show very little reduction of δ-Fe_2O_3 in comparison to the *mtrCAB* strain ($27 \pm 1 \times 10^{-6}$ μM/CFU mL^{-1}) (Figure 2-7d). Moreover, the amount of Fe(III) reduced was ~2.5 fold greater for δ-Fe_2O_3 nanoparticles than micron-sized δ-Fe_2O_3 over the same time period despite the fact that Fe_2O_3 concentration was 10 fold lower.

2.8. Discussion.

Engineering an efficient means of electronic communication between living and non-living systems has the potential to create hybrid sensors and electronics capable of self-replication and -repair. While existing technologies can transfer electrons from a cell to an electrode, no single approach has achieved what the next generation applications require: molecularly-defined electron flow across a variety of cell types. Here we have demonstrated the feasibility of a wholly biological approach that meets this challenge and provides a new blueprint for cellular-electronic connections. By the addition of new genetic information, we have engineered electronic communication between living cells and inorganic materials. The genetic nature of this approach makes it applicable to many cell types and specifies the route for electron transfer. To transfer the system to a different prokaryote would simply require the choice of an appropriate promoter and

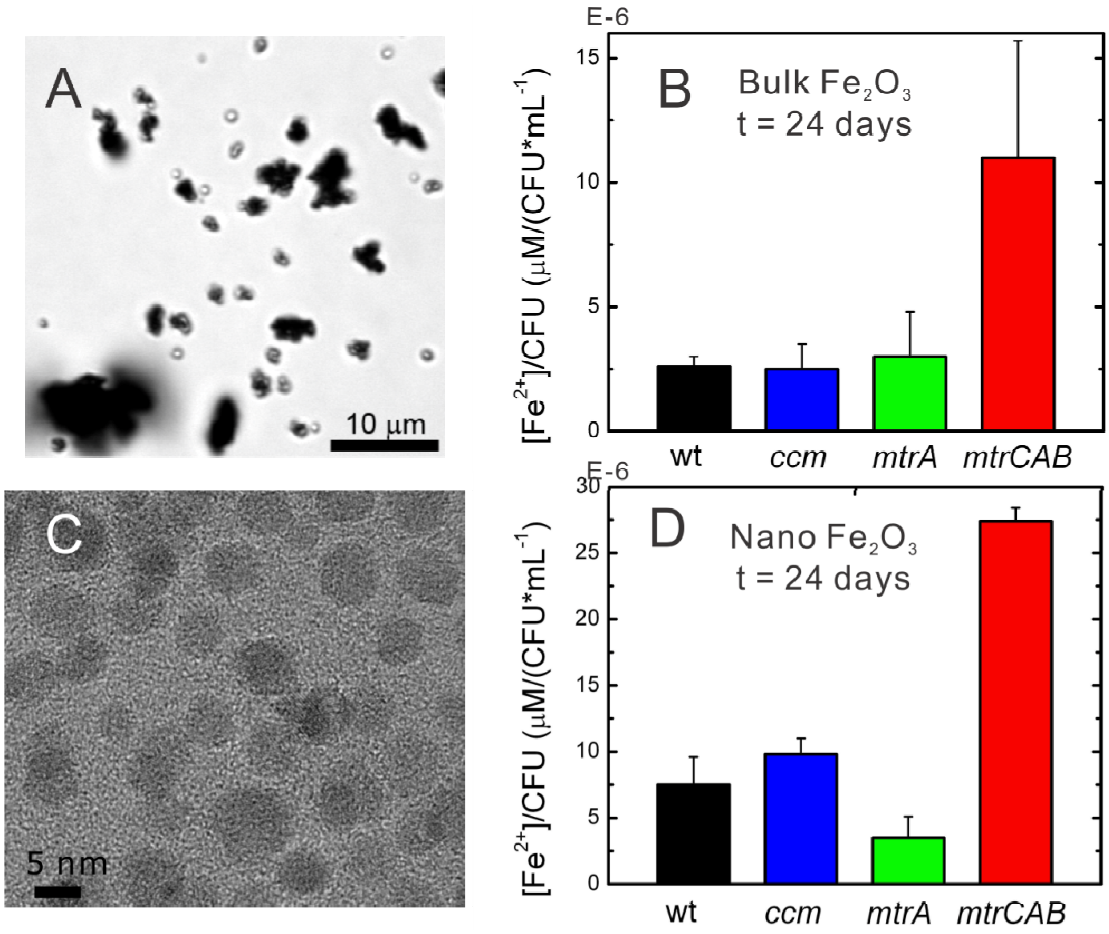

Figure 2-7. MtrCAB reduces solid α-Fe_2O_3. (A) Brightfield optical image of bulk α-Fe2O3, *d* ~ 5 μm. (B) The concentration of bulk α-Fe_2O_3 reduced by WT, *cmm*, *mtrA*, *mtrCAB* strains normalized by colony forming units after 24 d. The *mtrCAB* strain reduces significant amounts of δ-Fe_2O_3 per live cell (11 ± 5 x 10^{-6} μM/CFU mL^{-1}) in comparison to the wt strain (2.6 ± 0.4 x 10^{-6} μM/CFU mL^{-1}). (C) Transmission electron microscopy of crystalline α-Fe_2O_3 nanoparticles, *d* = 13 nm. (D) The concentration of α-Fe2O3 nanoparticles reduced by WT, *ccm*, *mtrA*, *mtrCAB* strains normalized by colony forming units after 24 d. As in the bulk Fe_2O_3 experiments, wt, *ccm*, and *mtrA* strains show very little reduction of δ-Fe_2O_3 in comparison to the *mtrCAB* strain (27 ± 1 x 10^{-6} μM/CFU mL^{-1}).

origin of replication, use of a host-specific signal sequence to ensure proper localization, and modification of the *ccm* genes to achieve their expression under aerobic conditions. Another unique advantage is that the cell directs the assembly of these bioelectronic connections such that they are self-repairing, requiring no experimenter assembly or intervention. Lastly, based on the natural system's respiratory versatility, we anticipate that our engineered system should be able to reduce multiple types of inorganic electrodes.

While this work achieves a molecularly defined electron conduit that may be introduced into other cell types, it is useful to compare the rate at which our engineered strains reduce Fe(III) to both wt *E. coli* and *S. oneidensis* MR-1 as a means of determining its relative efficiency. The *mtrCAB* strain reduces soluble and insoluble Fe(III) ~6-fold and ~4-fold faster, respectively, than wt *E. coli*; however, compared to *S. oneidensis* MR-1, the *mtrCAB* strain reduces soluble and insoluble Fe(III) ~100-fold and ~1000-fold more slowly (*172*, *173*). This rate difference suggests there is still room to optimize the efficiency and speed of the electron transfer pathway in our engineered strain.

In the case of soluble Fe(III) reduction, the transfer of electrons from native proteins of *E. coli* to MtrA is very likely the rate limiting step. The observation that no native *E. coli* cytochromes are detectable by TMBZ staining while MtrA is readily detectable (Figure 2-2) indicates there is a relatively low ratio of electron donors to electron acceptors. The slow re-reduction of MtrA in the high cell density experiments (Figure 2-5) also supports this hypothesis. The rate of this initial electron transfer step may potentially be enhanced either by increasing the expression of native *E. coli* inner membrane cytochromes that donate electrons to MtrA (such as NapC) or by additionally expressing the native electron donor of MtrA, the *S. oneidensis* MR-1 inner membrane cytochrome CymA. These approaches could potentially translate into an increase in soluble Fe(III) reduction rate.

For solid Fe_2O_3 reduction, it is likely that the last step in the electron transport chain, reduction of Fe(III) by MtrC, is the rate limiting step. Since our data, as well as other studies (*34*, *174*, *175*), indicate that MtrC is the only significant donor of electrons to Fe_2O_3 (Figure 2-7), the relatively low abundance of MtrC relative to MtrA (75 vs. 2100 per cell, respectively) is a plausible explanation of why the *mtrCAB* strain does not reduce solid Fe(III) at the rates of *S. oneidensis* MR-1. Given the relative simplicity of our genetic device, future work will focus on optimizing expression of MtrC to improve overall electron transfer rates to extracellular metal oxides.

The increase in reduction rate for nanocrystalline δ-Fe_2O_3 also suggests that materials engineering as well as synthetic biology will play a substantial role in optimizing electron transfer between engineered cells and inorganic materials. The *mtrCAB* strain generated 2.5-fold more Fe(II) from the δ-Fe_2O_3 nanoparticles than bulk δ-Fe_2O_3 over the same time period, even though the Fe_2O_3 concentration was 10-fold less. While this is a significant rate enhancement, the surface area of the nanoparticles (d = 13 nm) is about 4 million times greater than the bulk δ-Fe_2O_3 ($d \sim 5$ μm), indicating that the reduction rate does not scale linearly with the surface area. The nanocrystalline Fe_2O_3 is coated with citric acid to make the nanoparticles water-dispersible, and we speculate that this organic layer may modulate electron transfer from MtrC to the solid Fe_2O_3.

In summary, we have installed a novel electron transfer pathway in *E. coli* that allows intracellular electrons to be shuttled to the outer membrane where extracellular solid metal oxides can be reduced. These experiments demonstrate that *mtrCAB* is a genetic cassette which creates a molecularly defined pathway for electrons to move between living cells and inorganic materials. We envision that by installing this electronic pathway into organisms that evolve intracellular electrons in response to light, we could create extremely cheap, self-replicating photocatalysts that directly store energy in batteries. Additionally by combining our platform with organisms that modulate gene expression in response to small molecules, we could create living biosensors that provide electrical read-outs. More broadly, our approach demonstrates that synthetic biology can be used to radically alter the materials properties of living cells much in the way that materials engineering can be used to alter physical properties of materials. Because this is an effective method to functionally interface cells with inorganic nanomaterials, we anticipate that this synthetic biology approach will find application in a host of new nanobiotechnologies and bioelectronics.

2.9. Materials and Methods

2.9.1. Strains and Plasmids.

A table of primers, plasmids, and strains can be viewed in Table 2-1,2,3, respectively.

Table 2-1. Primers used in the construction of *mtrA* and *mtrCAB* plasmids.

Primer No.	Sequence (5'–3')
1	GGCCGAATTCAAGAACTGCCTAAAAATGAA
2	AACCTCTAGATTAGCGCTGTAATAGCTTGCCA
3	CCGCGAATTCATGAACGCACAAAAATCAAAAATCGC
4	CCGGTCTAGATTAGAGTTTGTAACTCATGCTC
5	CGCTCACAAAGTAACTCTCTGGCTTCAAGCATACCCACGCAATAACCCTG GTGTAGGCTGGAGCTGCTTC
6	TGGGGAATACCTTTACCCCATCAAAAGGTTACGGGAAATAAGAGGTTATT ATGGGAATTAGCCATGGTCC
7	CGCTCACAAAGTAACTCTCTGGCTT
8	TGGGGAATACCTTTACCCCATCAAA

Table 2-2. Plasmids used in Chapter 2.

Plasmid	Promoter	Protein Coding Regions(s)	Antibiotic Resistance	Source
pSB1ET2 (pET)	T7 lac	n/a	Kan	(this dissertation)
I5023	T7 lac	*mtrA*	Kan	(this dissertation)
I5024	T7 lac	*mtrCAB*	Kan	(this dissertation)
pEC86	Tet	*ccmA-H*	Chl	Dr. Steve Singer
pKD46	P_{araB}	λ-red recombinase	Amp	Coli Genetic Stock
pKD3	n/a	n/a	Amp, Chl	Coli Genetic Stock
pKD4	n/a	n/a	Amp, Kan	Coli Genetic Stock
pCP20	n/a	FLP	Amp	Coli Genetic Stock

Table 2-3. Strains used in Chapter 2.

Strain	Cell Line	Plasmids	Gene(s)
wt	BL21(DE3)	pSB1ET2 empty vector	None
ccm	BL21(DE3)	pSB1ET2_empty + pEC86	*ccmA-H*
mtrA	BL21(DE3)	pSB1ET2_MtrA + pEC86	*mtrA, ccmA-H*
mtrCAB	BL21(DE3)	pSB1ET2_MtrCAB + pEC86	*mtrCAB, ccmA-H*
Δ*napC*	BL21(DE3)Δ*napC*	pSB1ET2 empty vector	None
Δ*napC ccm*	BL21(DE3)Δ*napC*	pSB1ET2_empty + pEC86	*ccmA-H*
Δ*napC mtrA*	BL21(DE3)Δ*napC*	pSB1ET2_MtrA + pEC86	*mtrA, ccmA-H*
Δ*napC mtrCAB*	BL21(DE3)Δ*napC*	pSB1ET2_MtrCAB + pEC86	*mtrCAB, ccmA-H*

2.9.1.1. Construction of *mtrA* and *mtrCAB* plasmids.

We created two plasmids containing *mtrA* and *mtrCAB* under the control of a *T7 lac* promoter (*164*, *165*). Primers containing EcoRI and XbaI restriction sites (Table 2-1, primers 1 and 2 for *mtrA*; primers 3 and 4 for *mtrCAB*), and Platinum Pfx Polymerase (Invitrogen) were used to amplify the respective sequences. After digestion with EcoRI and XbaI, these DNA fragments were ligated into the modified pET30a+ vector using T4 DNA Ligase (Roche). The modified pET30a+ vector had an NdeI site (CATATG) directly upstream of the EcoRI site used for insertion. The ATG in the NdeI site was used as the start codon, and the forward primers for PCR were designed to clone from the second codon of *mtrA* and *mtrC* in the *Shewanella* genome. This design adds the two codons from the EcoRI site coding Glu-Phe; however, the extra amino acids will be cleaved by the Sec system in the process signal sequence cleavage of MtrA and MtrC in plasmids *mtrA* and *mtrCAB*, respectively.

Since the *E. coli* cytochrome c maturation (*ccmABCDEFGH*) genes are required for heme insertion but are not transcribed under aerobic conditions (*122*), the *mtrA* and *mtrCAB* plasmids were co-transformed with pEC86, a cytochrome c maturation (*ccm*) plasmid. The *ccm* plasmid, pEC86, encodes the genes *ccmA-H* under a constitutive tet promoter and carries a chloramphenicol resistance marker (Figure 2-1b) (*65*).

2.9.1.2. Construction of BL21(DE3)Δ*napC* deletion strain.

The Δ*napC* deletion strain was made using the λ-red strategy as described by Datsenko and Wanner (*170*). The plasmids used in the gene disruption process, pKD46, pKD3, pKD4, and pCP20, were obtained from the Coli Genetic Stock Center at Yale University. Primers 5 and 6 (Table 2-1) contain regions homologous to the region directly upstream and downstream, respectively. These primers were used to amplify a cassette containing kanamaycin resistance flanked by FRT sites off of pKD4 using Platinum Pfx Polymerase (Invitrogen, Carlsbad, CA). This PCR product was electroporated with BL21(DE3) expressing pKD46, induced with 10mM L-arabinose, to replace *napC* in the *E. coli* BL21(DE3) genome. Cells were grown with antibiotic selection on kanamycin LB plates grown at 37˚C. Colony PCR using primers 7 and 8 (Table 2-1) was performed to verify the replacement in the genome. Kanamycin resistance was removed by electroporating the new strain with pCP20, which removes the sequence between the FRT sites. After pCP20 inactivation, colony PCR was performed using primers 7 and 8 to verify removal of the kanamycin resistance gene. The resulting strain is BL21(DE3)Δ*napC*.

2.9.2. Aerobic cell growth for cytochrome c expression.

All strains, unless otherwise specified, were grown in 2xYT media at 30ºC with 50 μg mL^{-1} kanamycin; strains containing the *ccm* plasmid were grown with an additional 30 μg mL^{-1} chloramphenicol. Glycerol stocks were used to inoculate 5 mL media and cultures were grown overnight at 37ºC with 250 rpm shaking. Then 50 μL of overnight cultures were back-diluted into 5 mL media and grown with 250 rpm shaking for 12 hours. For Fe(III) reduction assays, 50 mL of fresh 2xYT in 250 mL Erlynmeyer flasks was inoculated with 500 μL of the previous culture and then grown 16 hours with 200 rpm shaking. For periplasmic and membrane fractionations, 5 mL of overnight culture were used to inoculate 1L media and were grown for 16 hours.

2.9.3. Subcellular fractionation and analysis of fractions by SDS-PAGE and visible spectroscopy.

The periplasmic and membrane fractionation was performed as described by Y. Y. Londer (*67*) and Nikaido (*176*), respectively.

2.9.3.1. Periplasmic Fractionation.

The cells from a 1 L culture were pelleted by centrifugation for 15 minutes at 4000 rcf and 4ºC. The resulting cell pellet was slowly resuspended to homogeneity in 30 mL of ice-cold TES, pH 8.0, by pressing the cells with a rubber policeman on the side of the flask. Chicken egg white lysozyme (Sigma, St. Louis, MO) was added to the resuspended pellet to a final concentration 0.5 mg mL^{-1} and incubated at room temperature for 15 minutes. After addition of 30 mL of ice-cold water, the suspension was shaken horizontally on ice for 15 minutes at 100 rpm then centrifuged at 12,000 rcf for 20 min at 4ºC. The supernatant was collected as the periplasmic fraction while the outer membrane and intact cytoplasm was in the pellet. The periplasmic fraction was analyzed by SDS-PAGE heme-stained gels and by UV-Vis for redox spectral properties.

2.9.3.2. Membrane Fractionation.

The cells from a 1L culture were pelleted by centrifugation for 15 minutes at 4000 rcf and 4ºC and then washed in 1L 10 mM HEPES, pH 7.4. The washed pellet was then resuspended in 120 mL ice-cold 10 mM HEPES, pH 7.4. Chicken egg white lysozyme was added to the cell suspension to a final concentration of 20 μg mL^{-1} and incubated at room temperature for 30 minutes. The protease inhibitor phenylmethylsulfonyl fluoride (PMSF) (Thermo Scientific, Rockford, IL 61105) was added to a final concentration of 1 mM. The cells were disrupted *via* ultrasonication (power level 5, 9 min. total duty in cycles of 30s on, 30s off, Misonix 3000, Misonix Inc. Farmingdale, NY) in an ice bath. Unbroken cells were removed by centrifugation at 1000 rcf for 15 minutes, and the resulting supernatant was removed and centrifuged at 100,000 rcf for 2 hours at 4 ºC to yield a pellet corresponding to the crude cell envelope, containing both the outer and inner membrane. This membrane fraction was solubilized in a solution of 5% (w/v) Triton X-100, 50 mM HEPES pH 7.4, 200 mM NaCl before analysis by SDS-PAGE, western blotting, and UV-Vis spectroscopy. The supernatant of this spin was saved for analysis by SDS-PAGE.

2.9.3.3. TMBZ Peroxidase Stain of SDS-PAGE.

The 3,3′,5,5′-tetramethylbenzidene (TMBZ) peroxidase stain method was adapted from Thomas (48) to identify cytochromes c. Protein samples were suspended in LDS without β-mercaptoethanol. The samples were run in 12.5% Tris HCl polyacrylamide gel (Bio-Rad, Hercules, CA) at 16ºC at 200 V for 60 minutes. TMBZ was dissolved in methanol to 6.3 mM and mixed 3:7 TMBZ solution:0.25 M Sodium acetate, pH 5. The gel was immersed in this mixture in the dark with occasional mixing for 2 hours. Hydrogen peroxide was added to a final concentration of 30 mM and bands were visualized 30 minutes after peroxide addition.

2.9.3.4. MtrB Western.

Denatured membrane protein samples were electrophoresed in 12.5% polyacrylamide gel, and transferred to nitrocellulose membranes. The primary antibody for MtrB (Rabbit Anti-MtrB) was kindly provided by Prof. Daad Saffarini (University of Wisconsin-Madison) and used at 1:10,000 dilution. The Immun-Star Goat Anti-Rabbit (GAR)-HRP Conjugate kit was used as the secondary antibody at 1:60,000 dilution. The western and visualization of bands was done as per the Immun-Star WesternC Chemiluminescent Kit (BioRad).

2.9.3.5. Visible Spectra of Cytochrome Samples.

Samples from the periplasmic fraction and membrane fractionation were diluted such the absorbance was within the linear range. Visible spectra of air-exposed samples were considered as fully oxidized protein samples. The protein was chemically reduced by adding sodium dithionite crystals (Sigma, St. Louis, MO), and the spectrum was taken again. Membrane fractions were baseline subtracted to consider the scattering of light caused by Triton X-100 micelles.

2.9.4. Iron reduction assay using ferrozine.

Cells from 50 mL cultures were pelleted, washed, and resuspended to an $OD_{600\ nm}$ of 0.5 in anaerobic M9 minimal media (12.8 g L^{-1} Na_2HPO_4-$7H_2O$, 3.0 g L^{-1} KH_2PO_4, 0.50 g L^{-1} NaCl, 1.0 g L^{-1} NH_4Cl) (Difco, Franklin Lakes, NJ) supplemented with 0.4% lactate (Alfa Aesar, Ward Hill, MA), 1 mM thiamine HCl (Sigma, St. Louis, MO), 0.2% casamino acids (Merck, Gibbstown, NJ), 2.0 mM $MgSO_4$ (Aldrich, St. Louis, MO), and 0.1 mM $CaCl_2$ (Aldrich, St. Louis, MO). All subsequent steps were performed in an anaerobic chamber (Coy Laboratory Products, Grass Lake, MI) with an environment of 2% H_2 balanced in N_2. Fe(III) citrate (Sigma, St. Louis, MO) was added to a final concentration of 10 mM, and at the time of addition and subsequent time points, aliquots were removed to determine the optical density at 600 nm and Fe(II) concentration.

The Fe(II) concentration was determined with the ferrozine assay, adapted from L. Stookey (43). One aliquot of each culture was centrifuged at 4000 rcf for 5 minutes at room temperature in the anaerobic chamber to pellet the cells, and the supernatant was acid extracted in 0.5 M HCl for 1 hour. The total iron concentration was determined by a separate acid extraction with 10% hydroxylamine hydrochloride (HAHC) (Aldrich) in 0.5 M HCl for 1 hour. An aliquot of each acid extracted sample was then added to the dye, ferrozine (Acros Organics) buffered in 100 mM HEPES, pH 8.0, which absorbs at 563 nm ($\varepsilon_{563\ nm}$ =27.9 mM^{-1} cm^{-1}) when chelating Fe(II). The absorbance of all samples was

recorded at 563 nm with a UV-Vis spectrophotometer (Perkin Elmer Lambda 35) and was used to determine the change of Fe(II) concentration over time as well as monitor total iron concentration available in the media. The concentration of Fe(II) in each culture was subtracted by any abiotic iron reduction observed in media controls at each time point and was normalized to the relative number of cells by multiplying by the factor $\frac{0.5}{OD_{600\ nm}^{t=n}}$. Error bars represent standard deviation by triplicate cultures.

2.9.5. Cytochrome *c* redox assay in intact cells.

Dense cell suspensions in anaerobic M9 minimal media supplemented with 0.4% lactate were transferred into sealable quartz cuvettes in an anaerobic chamber. The absorption spectrum of each culture was measured before iron addition, immediately after addition of 50 μM Fe(III) citrate, and at regular intervals afterwards to observe changes in the redox state of the cytochromes. The concentration of Fe(II) was simultaneously monitored *via* the ferrozine assay.

After apparent recovery of the redox state of the cytochrome, an additional 25 μM of Fe(III) citrate was added. The spectrum was monitored again with similar results. All spectra were normalized to the average absorbance at 561 nm, an approximate isobestic point. $\Delta A_{552\ nm}$ was calculated by subtracting the initial $A_{552\ nm}$ from all time points.

2.9.6. Synthesis of δ-Fe_2O_3(citrate)$_n$ Nanoparticles.

δ-Fe_2O_3 (citrate) nanoparticles were synthesized using a two step approach. Oleate passivated nanocrystals were prepared according to a modified, previously published literature procedure (*177*)**.** The oleate shell was subsequently displaced with citric acid before aqueous transfer into buffer.

Iron(III) chloride hexahydrate (544 mg, 2.01 mmol), sodium oleate (1.826 g, 6.00 mmol), oleic acid (1.0 mL, 3.14 mmol), absolute ethanol (5.0 mL), and H_2O (8.0 mL) were combined in in a 20 mL microwave reaction vial and stirred for 1 h at 25 °C, giving an opaque, dark reddish brown organic top layer and a clear, pale yellow aqueous bottom layer in the microwave vial. The reaction vessel was transferred to a microwave synthesizer (Biotage Initiator 8), and heated at 80 °C for 8 h, then at 180 °C for 15 min. The contents of the vessel were transferred to a 50 mL conical tube and centrifuged at 4400 rpm for 30 min, affording a dark, reddish brown pellet of nanocrystals. The liquid portion was decanted off and the pellet washed sequentially with H_2O (5.0 mL) and absolute ethanol (5.0 mL). The pellet was resuspended in hexanes (50 mL) and the tube centrifuged at 4400 rpm for 5 min., giving a clear, dark reddish brown hexanes solution containing smaller, soluble Fe_2O_3 nanoparticles, and a reddish brown pellet containing larger, insoluble Fe_2O_3 nanoparticles and Fe_2O_3 nanoparticle aggregates. The hexanes solution was filtered through an Acrodisc Syringe Filter (0.22 μm, Pall Corporation), giving a clear, dark reddish brown solution containing oleic acid-coated Fe_2O_3 nanoparticles. Dynamic Light Scattering (DLS) measurements (Malvern Instruments) performed in hexanes at 20 °C showed that the particles were narrowly distributed, with a mean diameter of 13 nm.

Fe_2O_3 nanoparticles were heated with citric acid (480 mg) in anhydrous DMSO (2.5 mL) at 100 °C for 24 h with stirring. The resulting solution was added slowly to 100 mL of 100 mM sodium tetraborate buffer, pH 10.0, with periodic adjustment of pH to 10

with NaOH (1.0 M), giving a clear, reddish brown aqueous solution. The nanoparticles were concentrated by spin dialysis (Amicon Ultra-15 10K MWCO, Millipore Corporation), and dialyzed with 5 × 15 mL of 10 mM sodium tetraborate buffer, pH 8.3. Dynamic Light Scattering (DLS) measurements (Malvern Instruments) performed in buffer at 20 °C showed that the citrate coated Fe_2O_3 particles were narrowly distributed, with a mean diameter of 13 nm.

2.9.7. Reduction of bulk and nano Fe_2O_3.

Cells from 50 mL cultures were pelleted, washed, and re-suspended in anaerobic M9 minimal media to a final $OD_{600\ nm}$ of 1.0. All subsequent steps were performed in an anaerobic chamber. For the bulk Fe_2O_3 assay, 50 mg particulate Fe_2O_3 (Sigma, St. Louis, MO) and 20 mL of anaerobic culture was added to a sterile bottle, yielding a final Fe_2O_3 concentration of 2.5 mg mL^{-1}. For nanoparticle cultures, the anaerobic nanoparticle solution (4 mg mL^{-1}) was added to a final concentration of 0.25 mg mL^{-1}.

At each time point, the colony forming units and Fe(II) concentration for each culture. To determine colony forming units, dilutions of each cultures were plated on LB plates supplemented with Kanamycin (to test for the presence of the *mtrA* or *mtrCAB* plasmids). Plates were grown at 30˚C for 24 hours. The concentration of Fe(II) was determined by the ferrozine assay, as described above, and was normalized for each culture by CFU. Error bars represent standard deviation by triplicate cultures.

Chapter 3

Tuning Promoter Strengths for Improved Synthesis and Function of Electron Conduits in *Escherichia coli.*

3.1. Introduction

Introduction of the electron transfer complex MtrCAB from *Shewanella oneidensis* MR-1 into a heterologous host provides a modular and molecularly defined route for electrons to be transferred to an extracellular inorganic solid. However, an *Escherichia coli* strain expressing this pathway displayed limited control of MtrCAB expression and impaired cell growth. To overcome these limitations and to improve heterologous extracellular electron transfer, we used an *E. coli* host with a more tunable induction system and a panel of constitutive promoters to generate a library of strains that separately transcribe the *mtr* and cytochrome *c* maturation (*ccm*) operons over 3 orders of magnitude. From this library, we identified strains that show 2.2 times higher levels of MtrC and MtrA and that have improved cell growth. We find that a ~300-fold decrease in the efficiency of MtrC and MtrA synthesis with increasing *mtr* promoter activity critically limits the maximum expression level of MtrC and MtrA. We also tested the extracellular electron transfer capabilities of a subset of the strains using a three-electrode microbial electrochemical system. Interestingly, the strain with improved cell growth and fewer morphological changes generated the largest maximal current per cfu, rather than the strain with more MtrC and MtrA. This strain also showed ~30-fold greater maximal current per cfu than its *ccm*-only control strain. Thus, the conditions for optimal MtrCAB expression and anode reduction are distinct, and minimal perturbations to cell morphology are correlated with improved extracellular electron transfer in *E. coli*.

In Chapter 2, we transferred the MtrCAB electron transfer pathway (Figure 3-1a) into the model microbe *E. coli* and demonstrated that the resultant strain could reduce inorganic solids (*148*). In *E. coli*, NapC and other unidentified proteins partially substituted for the function of CymA in *S. oneidensis* MR-1 (*148*). However, close examination of this strain, referred to here as the BL21(DE3) *mtrCAB* strain, reveals two key shortcomings: (i) this strain has dramatically slowed growth relative to its parent strain, and (ii) inducing transcription of the *mtr* operon with isopropyl β-d-1-thiogalactopyranoside (IPTG) caused the cell pellet to appear less red (*148*), suggesting that fewer *c*-type cytochromes were produced at higher transcription rates.

These challenges likely arise from the high degree of post-translational modifications required to make *c*-type cytochromes described in the introduction chapter (Figure 3-1b). This series of post-translational modifications creates multiple points for misregulation of the synthesis and maturation of the MtrCAB complex in *E. coli*. High levels of leader-sequence bearing polypeptides can saturate the signal recognition particle, leading to the misfolding of the unsecreted polypeptides and accumulation of cytoplasmic aggregates (*84*). This results in pleiotropic cellular impairments including an increase in the size and granularity of *E. coli* cells, decreased growth, and decreased expression of the inner membrane proteome (*82*). Since L-lactate dehydrogenase is an inner membrane protein, secretion impairment has the potential to negatively impact the

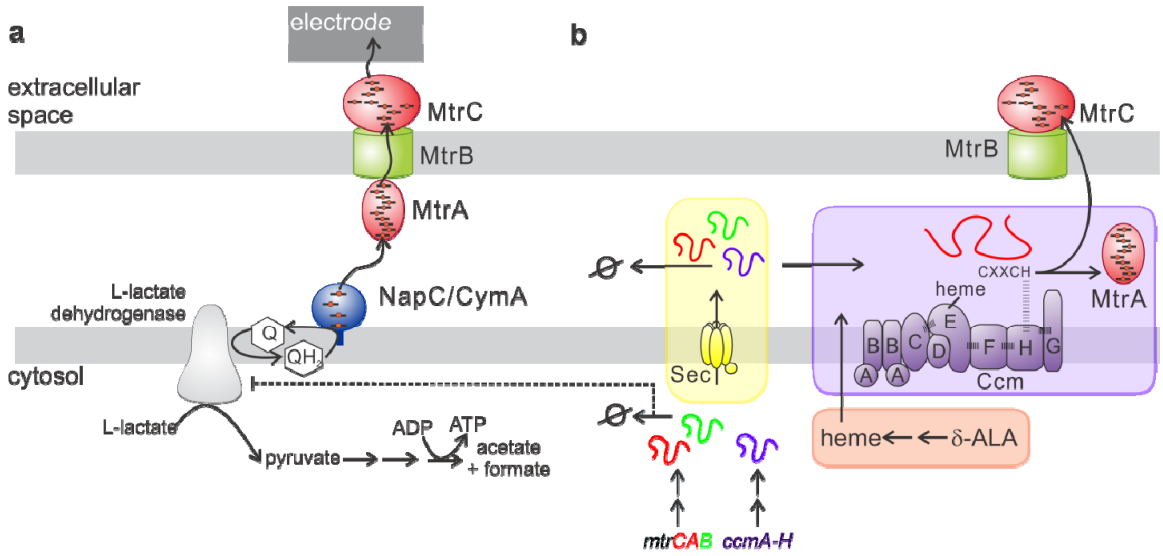

Figure 3-1. Multiple post-translational modifications are required to synthesize the components of the Mtr electron conduit, and misregulation of these processes has the potential to negatively impact extracellular respiration. (a) Route for electrons from lactate to an anode *via* the Mtr pathway. L-Lactate is oxidized into pyruvate, and the resulting reducing equivalents are used to reduce menaquinone (MQ) to menaquinol (MQH2). In *S. onedensis* MR-1, CymA is the inner membrane cytochrome *c* that accepts electrons from menaquinol; in *E. coli*, this function is achieved by NapC, as well as yet unidentified proteins. From the inner membrane protein, electrons are passed through the periplasm and outer membrane to extracellular electron acceptions *via* the MtrCAB complex. (b) After transcription and translation, the Mtr and Ccm polypeptides are secreted into the periplasm by the Sec secretion system. Excessive production of signal sequence-containing polypeptides can overload the Sec translocon, resulting in aggregation and/or retention of the polypeptides in the cytoplasm. The Ccm machinery then loads heme into the apocytochromes *c* to form mature MtrC and MtrA. Low production of heme or inadequate concentrations of Ccm biogenesis machinery relative to the steady-state apocytochrome c concentration can trigger degradation of the apocytochrome *c* by periplasmic proteases such as DegP.

flux of electrons to menaquinone from lactate metabolism as well as the synthesis of MtrCAB (Figure 3-1b). Misregulation of cytochrome *c* synthesis can also be caused by inadequate heme, which will result in degradation of apocytochromes *c* by the periplasmic proteases, such as DegP (*178*) (Figure 3-1b). Thu *c*-type cytochrome biogenesis requires an appropriate balance between the rates and levels of polypeptide synthesis, heme biosynthesis, polypeptide secretion, and cytochrome *c* maturation. Reflecting this, other groups have found that heterologous multiheme cytochrome *c* expression in *E. coli* can be increased in two ways: (i) by enhancing heme biosynthesis with heme precursors, such as δ-aminolevulinic acid (δ-ALA) (*66*) or rich media (*68*) and (ii) by lowering apopolypeptide synthesis through weaker transcriptional promoters (*69*, *70*), different *E. coli* hosts, and lower copy number of the cytochrome *c* genes (*64*).

The slow growth of BL21(DE3) *mtrCAB* and decrease in cytochrome *c* expression upon induction suggests that the basal transcription rate of *mtr* and the constitutive expression of *ccm* outpace the rates of heme synthesis, polypeptide secretion, and/or cytochrome *c* maturation. In this chapter, we hypothesize that by balancing the *ccm* and *mtr* transcription to avoid misregulation of post-transcriptional modifications, we can improve cytochrome *c* expression, cell growth, and/or extracellular electron transfer relative to the BL21(DE3) *mtrCAB* strain. Through the use of a more tightly regulated and tunable induction system and a panel of constitutive promoters, we created strains with varying expression of the *ccm* and *mtr* operons. We show that cytochrome *c* expression and cell growth are strongly affected by the *mtr* promoter activity. Surprisingly, we also find that the *ccm* and *mtr* promoter strengths for optimal cytochrome *c* expression are distinct from those for improved anode reduction.

3.2. Design of strains with variable levels of transcription of the *ccm* and *mtr* operons.

The overall goal of this work is to provide controllable and improved synthesis and function of the MtrCAB pathway in *E. coli*. The BL21(DE3) *mtrCAB* strain contains a pET30a+-derived plasmid containing *mtrCAB* under the control of a *T7 lac* promoter and a cytochrome *c* maturation plasmid containing the *ccm* operon regulated by the constitutive *tet* promoter (pEC86) (*148*). Designed as a control for the *ccm* operon, the BL21(DE3) *ccm* strain only carries the pEC86 plasmid. Interestingly, the BL21(DE3) *mtrCAB* and BL21(DE3) *ccm* strains grew 27 ± 8% and 7 ± 1% more slowly than the BL21(DE3) WT strain, respectively (Figure 3-2a). Moreover, the BL21(DE3) *mtrCAB* strain shows 2-fold greater forward scatter relative to BL21(DE3) WT strain (Figure 3-2b), indicating that MtrCAB expression causes an increase in cell size. Additionally, induced BL21(DE3) *mtrCAB* appear less red than uninduced cell pellets (*148*), indicating that increased transcription of *mtrCAB* led to decreased production of holocytochrome *c*.

Because expression of multiheme *c*-type cytochromes and membrane proteins have previously been improved by lowering transcriptional levels (*85*, *179*), we hypothesized that a similar strategy would improve control or levels of cytochrome *c* expression or both. To achieve controlled expression, we changed the host strain to C43(DE3), which has lower basal and induced levels of T7 RNA polymerase relative to BL21(DE3) due to mutations in the lacUV5 promoter region (*85*). Using the methodology of Kelly et al. (*180*), we calibrated the relative promoter activity by varying the concentration of IPTG. We found that induction of the *T7 lac* promoter can modulate

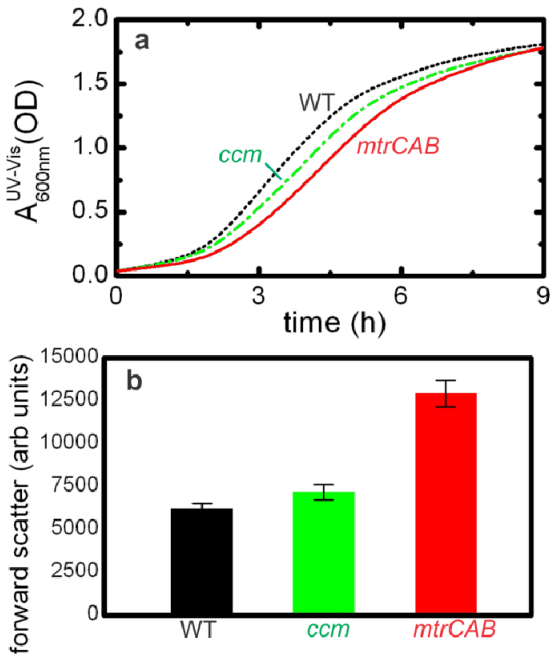

Figure 3-2. The BL21(DE3) *ccm* and *mtrCAB* strains show slowed growth and altered phenotypes relative to the BL21(DE3) WT strain. (a) The absorbance at 600 nm as measured by UV-Vis spectroscopy as a function of time shows that the BL21(DE3) *ccm* (green dot-dashed line) and BL21(DE3) *mtrCAB* (red solid line) strains grow 7 ± 1% and 27 ± 8% more slowly than the BL21(DE3) WT strain (black dashed line). (b) The forward scatter (solid bars, left y-axis) from cells of the BL21(DE3) wt strain (black bars) is significantly lower (p-value = 3.5x10-4, Student's T-test, 1-tailed distribution, equal variance) than BL21(DE3) *mtrCAB* (red bars), indicating that expression of *mtrCAB* impacts cellular morphology.

transcription over ~3 orders of magnitude in the C43(DE3) strain (Figure 3-3a,b,c and Table 3-1). We used this promoter (in the previously described *mtrCAB* plasmid (*148*)) in the C43(DE3) strain to control transcriptional levels of *mtrCAB*.

Since the BL21(DE3) *ccm* strain showed slower cell growth, which has been correlated with misregulation of membrane protein expression (*84*), we hypothesized that decreasing the level of *ccm* expression could improve cell growth and possibly functional expression of the MtrCAB pathway. Thus, we calibrated a series of constitutive promoters of varying strength generated by the BioFAB (Emeryville, CA; Mutalik et al., unpublished data), again using the methodology of Kelly et al. (*180*). This library spanned 3.5 orders of magnitude in promoter strength (Figure 3-3d,e,f and Table 3-2), providing a wide window over which to tune *ccm* transcription. Golden Gate cloning (*181*) was used to introduce the BioFAB promoters in front of the *ccm* operon, creating a library of plasmids with variable *ccm* transcription.

Table 3-1. Normalized GFP expression per cell in the C43(DE3) strain as a function of IPTG concentration.

[IPTG] (μM)	**norm. GFP intensity (arb. units cell^{-1})**
0.0	1.3 (± 0.6) x10^{-3}
0.5	4.4 (± 0.9) x10^{-3}
1.0	1.1 (± 0. 8) x10^{-2}
2.0	3.6 (± 3.6) x10^{-2}
4.0	6.8 (± 3.1) x10^{-2}
8.0	1.5 (± 0.2) x10^{-1}
16.0	2.4 (± 0.6) x10^{-1}
32.0	2.9 (± 0.7) x10^{-1}
62.5	4.0 (± 0.4) x10^{-1}
125	4.7 (± 1.5) x10^{-1}
250	7.2 (± 1.9) x10^{-1}
500	1.0

Table 3-2. Normalized GFP expression per cell in the C43(DE3) strain for the pFAB promoters.

BioFab ID	**Sequence**	**Norm. GFP intensity (arb. units cell^{-1})**
pFAB656	TTCCTGGTTAATCATCCGGCTCATAAAA TTTGTGGA	2.6 (± 0.3) x10^{-4}
pFAB550	TTATTCCTTAATCATCGGCTCGTATAAT GTGTGGA	1.0 (± 0.2) x10^{-3}
pFAB554	TTAGCCCTTAATCATCCGGCTCGTATAA TGTGTGGA	2.2 (± 0.5) x10^{-3}
pFAB577	TTTCAGGTTAATCATCGGCTCGTATAAT GTGTGGA	2.4 (± 0.1) x10^{-3}
pFAB698	TTATAAATTAATATCCGGCTCGTATAAT GTGTGGA	3.2 (± 0.3) x10^{-3}
pFAB589	TTCCTCCTTAATCATCCGGCTCGTATAA TGTGTGGA	5.9 (±1.0) x10^{-3}
pFAB586	TTGTGCTTTAATCATCCGGCTCGTAGAG TGTGTGGA	1.5 (±0.1) x10^{-2}
pFAB611	TTGACAATTAATCATCGGCTCGTAGATT	2.7 (±0.4) x10^{-2}

	TTGTGGA	
pFAB613	TTGACAATTAATCATCCGGCTCTTAGGT TCTGTGGA	2.8 (±0.5) x10^{-2}
pFAB640	TTTGCGGTTAATCATCCGGCTCGTATAA TGTGTGGA	3.3 (±0.5) x10^{-2}
pFAB635	TTCAAATTTAATCATCCGGCTCGTATAA TGTGTGGA	9.9 (±1.9) x10^{-2}
pFAB661	TTTCAATTTAATCATCCGGCTCGTATAA TGTGTGGA	2.1 (±0.1) x10^{-1}
pFAB662	TTGCCGCTTAATCATCCGGCTCGTATAA TGTGTGGA	2.4 (±0.1) x10^{-1}
pFAB669	TTGACAATTAATCATCCGGCTCATATCG TTTGTGGA	3.4(±0.1) x10^{-1}
pFAB670	TTGACAATTAATCATCCGGCTCGTAGGT TATGTGGA	4.4 (±0.5) x10^{-1}
pFAB668	TTGACAATTAATCATCCGGCTCGTAGTG TTTGTGGA	5.4 (±0.1) x10^{-1}
pFAB708	TTGACAATTAATCATCCGGCTCGTAATG TTTGTGGA	7.5 (±1.0) x10^{-1}
pFAB704	TTGACAATTAATCATCCGGCTCATAAAA TTTGTGGA	1.0

3.3. High transcriptional levels of *ccm* and *mtr* decrease cytochrome *c* expression and cell growth.

The *ccm* plasmids were co-transformed with the previously described *mtrCAB* plasmid (*148*) into C43(DE3) cells to generate a series of *mtrCAB*-expressing strains (Table 3-3). We notate the different transcriptional levels of *ccm* and *mtr* operons in these cultures as $ccm^{\#}mtrCAB^{\#}$ where the superscripts indicate the *ccm* promoter strength and *mtr* promoter activity based on our calibrated scale in Tables 3-2 and 3-1, respectively. As a control, the C43(DE3) WT strain was generated by co-transformation of the empty pET30a+ and pACYC184 plasmids.

To screen the effects of simultaneously tuning the *ccm* promoter strength and the *mtr* promoter activity on cytochrome *c* expression, the $ccm^{\#}mtrCAB^{\#}$ strains were grown in 96-well plates with varying IPTG concentrations to generate 192 different transcriptional combinations. This number of combinations precluded direct analysis of cytochrome *c* content. Instead, because *c*-type cytochromes are red in color, we quantified the relative red intensity of the cell pellets (calculated as described in Methods 3.10.3) and used this value as a metric for cytochrome *c* production. To measure the relative red intensity, equal volumes of each culture were centrifuged, and images of the resulting cell pellets were acquired using a scanner. The heatmap shown in Figure 3-4b summarizes the results of varying the transcriptional levels of both the *ccm* and *mtr* operons on the relative red intensity of the cell pellet. Unlike the BL21(DE3) *mtrCAB* strain, the $ccm^{\#}mtrCAB^{\#}$ cultures show little or no relative red intensity in the absence of induction (Figure 3-4b, leftmost column). This increased control reflects the lower basal transcription of T7 RNA polymerase in the C43(DE3) strain. The pellets with the greatest relative red intensities were localized in the narrow range of *mtr* promoter activities between ~0.1 to 0.3 arb. units and *ccm* promoter strengths between ~0.01 to 0.2 arb. units (Figure 3-4b). At *ccm* or *mtr* transcription levels outside this optimal range, the relative

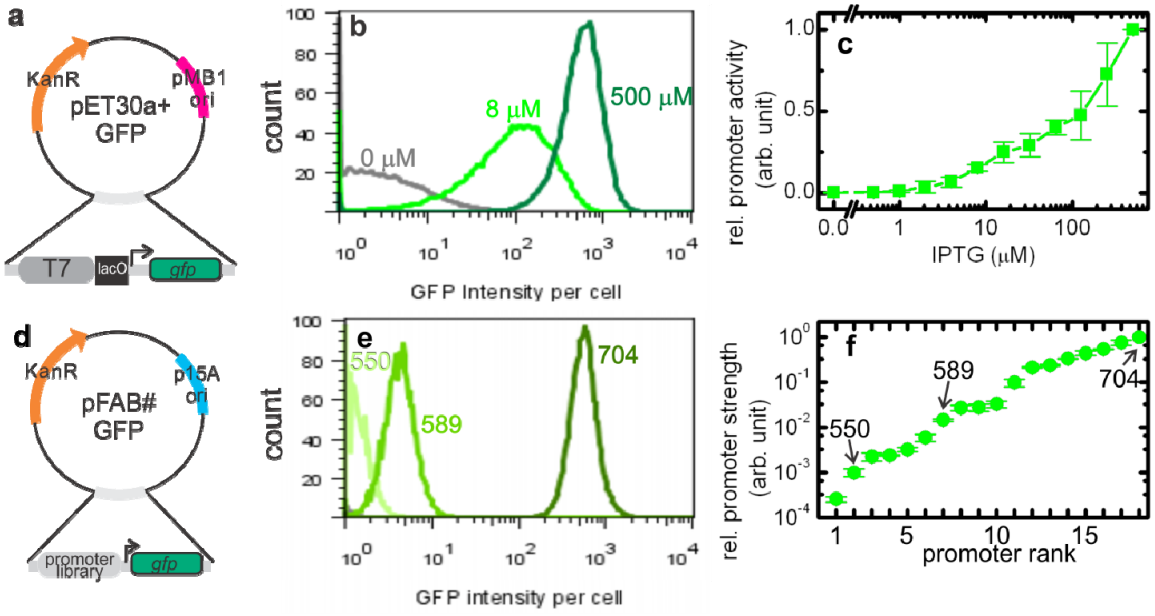

Figure 3-3. GFP expression was used to quantitatively assess *ccm* promoter strength and *mtr* promoter activity in C43(DE3) cells. (a) Schematic of plasmid used to express superfolder GFP from pET30a+ backbone. (b) Histograms of GFP intensity per cell from the C43(DE3) strain containing the pET30a+ GFP plasmid in the presence of 0, 8, and 500 μM IPTG.(c) The relative promoter activity for this range of IPTG concentration spans ~3 orders of magnitude. (d) Schematic of plasmids containing pFAB# promoter library driving expression of superfolder GFP. (e) Histograms of GFP intensity per cell from C43(DE3) strains harboring the pFAB550, pFAB589, and pFAB704 promoters upstream of GFP show that expression is homogeneous across the population. (f) The relative promoter strengths for this promoter panel spans ~3.5 orders of magnitude.

Table 3-3. Strains used in Chapter 3.

Strain #	Strain name	Strain Background	Description	Plasmids (ori, resistance marker)
MFe207	BL21(DE3) WT	BL21(DE3)	T7 lacO with no coding sequence	pSB1ET2(pMB1, Kan)
MFe540	C43(DE3) WT	C43(DE3)	no coding sequence in either plasmid	pACYC184(p15A, Chl), pSB1ET2(pMB1, Kan)
GFP-expressing strains				
MFe513		C43(DE3)	BioFAB promoter 550 regulating GFP	G550 (p15A, Kan)
MFe514		C43(DE3)	BioFAB promoter 554 regulating GFP	G554 (p15A, Kan)
MFe515		C43(DE3)	BioFAB promoter 577 regulating GFP	G577 (p15A, Kan)
MFe516		C43(DE3)	BioFAB promoter 586 regulating GFP	G586 (p15A, Kan)
MFe517		C43(DE3)	BioFAB promoter 589 regulating GFP	G589 (p15A, Kan)
MFe518		C43(DE3)	BioFAB promoter 598 regulating GFP	G598 (p15A, Kan)
MFe519		C43(DE3)	BioFAB promoter 611 regulating GFP	G611 (p15A, Kan)
MFe520		C43(DE3)	BioFAB promoter 613 regulating GFP	G613 (p15A, Kan)
MFe521		C43(DE3)	BioFAB promoter 635 regulating GFP	G635 (p15A, Kan)
MFe522		C43(DE3)	BioFAB promoter 640 regulating GFP	G640 (p15A, Kan)
MFe523		C43(DE3)	BioFAB promoter 656 regulating GFP	G656 (p15A, Kan)
MFe524		C43(DE3)	BioFAB promoter 661 regulating GFP	G661 (p15A, Kan)
MFe525		C43(DE3)	BioFAB promoter 668 regulating GFP	G668 (p15A, Kan)
MFe526		C43(DE3)	BioFAB promoter 704 regulating GFP	G704 (p15A, Kan)
MFe527		C43(DE3)	BioFAB promoter 708 regulating GFP	G708 (p15A, Kan)
MFe504	pET30a GFP	C43(DE3)	T7 lac promoter regulating GFP	**pET30a+ GFP (pMB1, Kan)**
Cytochrome C maturation gene-containing strains				
MFe447		Mach1	BioFAB promoter 635 regulating ccmA-H	M635(p15A, Chl)
MFe448		Mach1	BioFAB promoter 613 regulating ccmA-H	M613(p15A, Chl)
MFe449		Mach1	BioFAB promoter 611 regulating ccmA-H	M611(p15A, Chl)
MFe450		Mach1	BioFAB promoter 586 regulating ccmA-H	M586(p15A, Chl)
MFe451		Mach1	BioFAB promoter 589 regulating ccmA-H	M589(p15A, Chl)
MFe452		Mach1	BioFAB promoter 554 regulating ccmA-H	M554(p15A, Chl)
MFe453		Mach1	BioFAB promoter 656 regulating ccmA-H	M656(p15A, Chl)
MFe454		Mach1	BioFAB promoter 640 regulating ccmA-H	M640(p15A, Chl)
MFe455		Mach1	BioFAB promoter 698 regulating ccmA-H	M698(p15A, Chl)
MFe456		Mach1	BioFAB promoter 597 regulating ccmA-H	M597(p15A, Chl)
MFe457		Mach1	BioFAB promoter 550 regulating ccmA-H	M550(p15A, Chl)
MFe458		Mach1	BioFAB promoter 661 regulating ccmA-H	M661(p15A, Chl)
MFe459		Mach1	BioFAB promoter 704 regulating ccmA-H	M704(p15A, Chl)
MFe208	BL21(DE3) *ccm*	BL21(DE3)	tet promoter regulating ccmA-H	pEC86 (p15A, Chl)
MFe543	least perturbed *ccm*	C43(DE3)	BioFAB promoter 640 regulating ccmA-H	M640(p15A, Chl)
MFe499	most cytochrome c *ccm*	C43(DE3)	BioFAB promoter 635 regulating ccmA-H	M635(p15A, Chl)
MtrCAB expressing strains				
MFe290	BL21(DE3) *mtrCAB*	BL21(DE3)	tet promoter regulating ccmA-H, T7 lacO regulating mtrCAB	
MFe464	most cytochrome c	C43(DE3)	BioFAB promoter 635 regulating ccmA-H, T7 lacO regulating mtrCAB	C635(p15A, Chl), I5023 (pMB1, Kan)
MFe465		C43(DE3)	BioFAB promoter 613 regulating ccmA-H, T7 lacO regulating mtrCAB	C613(p15A, Chl), I5023 (pMB1, Kan)
MFe466		C43(DE3)	BioFAB promoter 611 regulating ccmA-H, T7 lacO regulating mtrCAB	C611(p15A, Chl), I5023 (pMB1, Kan)
MFe467		C43(DE3)	BioFAB promoter 586 regulating ccmA-H, T7 lacO regulating mtrCAB	C586(p15A, Chl), I5023 (pMB1, Kan)
MFe468		C43(DE3)	BioFAB promoter 589 regulating ccmA-H, T7 lacO regulating mtrCAB	C589(p15A, Chl), I5023 (pMB1, Kan)
MFe469		C43(DE3)	BioFAB promoter 554 regulating ccmA-H, T7 lacO regulating mtrCAB	C554(p15A, Chl), I5023 (pMB1, Kan)
MFe470		C43(DE3)	BioFAB promoter 656 regulating ccmA-H, T7 lacO regulating mtrCAB	C656(p15A, Chl), I5023 (pMB1, Kan)
MFe471	least perturbed	C43(DE3)	BioFAB promoter 640 regulating ccmA-H, T7 lacO regulating mtrCAB	C640(p15A, Chl), I5023 (pMB1, Kan)
MFe472		C43(DE3)	BioFAB promoter 698 regulating ccmA-H, T7 lacO regulating mtrCAB	C698(p15A, Chl), I5023 (pMB1, Kan)
MFe473		C43(DE3)	BioFAB promoter 597 regulating ccmA-H, T7 lacO regulating mtrCAB	C597(p15A, Chl), I5023 (pMB1, Kan)
MFe474		C43(DE3)	BioFAB promoter 550 regulating ccmA-H, T7 lacO regulating mtrCAB	C550(p15A, Chl), I5023 (pMB1, Kan)
MFe477		C43(DE3)	BioFAB promoter 661 regulating ccmA-H, T7 lacO regulating mtrCAB	C661(p15A, Chl), I5023 (pMB1, Kan)
MFe477		C43(DE3)	BioFAB promoter 704 regulating ccmA-H, T7 lacO regulating mtrCAB	C704(p15A, Chl), I5023 (pMB1, Kan)
MFe409		C43(DE3)	tet promoter regulating ccmA-H, T7 lacO regulating mtrCAB	pEC86 (p15A, Chl), I5023 (pMB1, Kan)

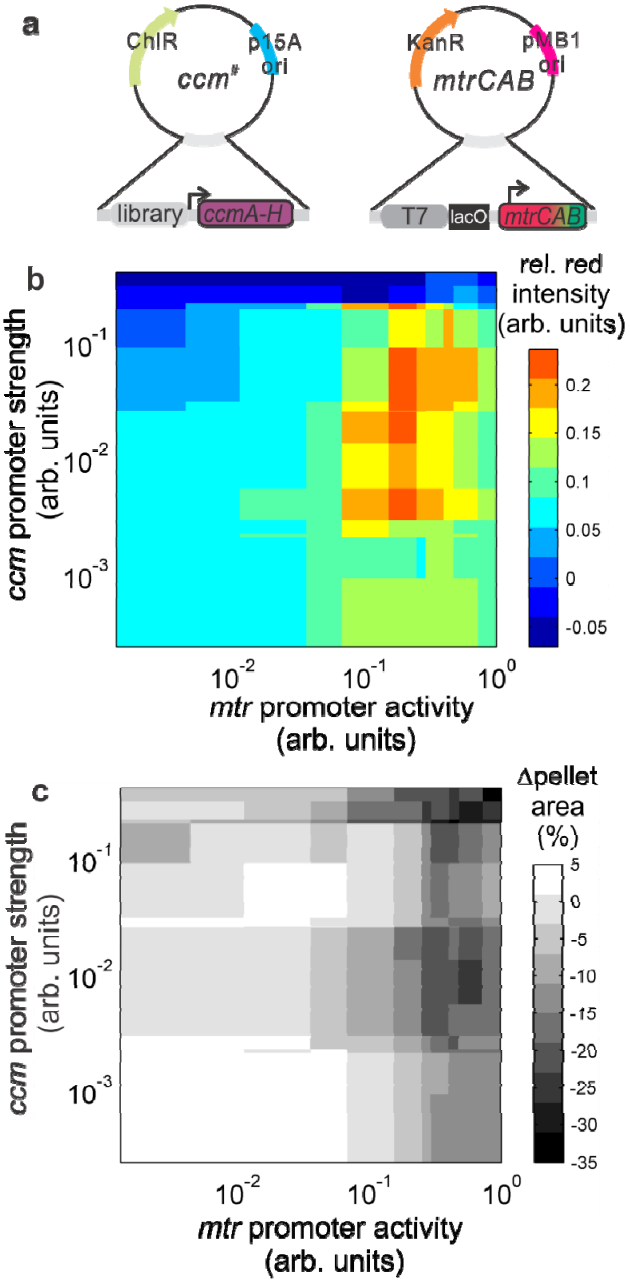

Figure 3-4. Cytochrome *c* expression and cell growth are optimal in localized ranges of *mtr* promoter activity and *ccm* promoter strength. (a) Schematic of the *ccm* plasmid library and the *mtrCAB* plasmid used to create *ccm# mtrCAB* strains. (b) A heat map displaying the relative red intensity of the cell pellet of these strains as a function of the *mtr* promoter activity and ccm promoter strength. On this scale, *E. coli* cells expressing no cytochrome *c* and a purely red *E. coli* cell pellet would have relative red intensities of 0 and 2.1, respectively. This map reveals a localized region of maximal relative red intensity at intermediate ccm promoter strength and mtr promoter activity. (c) A heat map displaying the change in apparent cell pellet size as a function of the *mtr* promoter activity and *ccm* promoter strength shows sharply decreasing pellet size with increasing

mtr promoter activity. In both panels b and c, the values plotted are the mean of at least three measurements, and granularity of each heatmap was set to the average of the standard deviation across all the measurements.

---

red intensity of the cell pellets decreased sharply. This decrease suggests that there is misregulation in the post-transcriptional processes. The *ccm*$^{\#}$*mtrCAB*$^{\#}$ culture with the greatest relative red intensity (0.22 ± 0.02) was more intensely red than the BL21(DE3) *mtrCAB* cells (0.11 ± 0.03), indicating that our screen produced a strain with higher expression levels of cytochrome *c* than the original strain.

To assess the impact of *mtr* and *ccm* transcriptional levels on cell growth, we calculated (as described in Methods 3.10.3) the change in apparent cell pellet area relative to the C43(DE3) WT strain. This area is proportional to the pellet volume and thus the total cell biomass. As shown in the heatmap in Figure 3-4c, the apparent cell pellet area was unchanged in strains with both very low *mtr* and *ccm* transcriptional levels. The pellet area slightly decreased with increasing *ccm* promoter strength and steeply decreased with increasing *mtr* promoter activity, such that the apparent pellet area decreased by up to 35% (Figure 3-4c). Thus, transcription of the *mtr* operon negatively impacts the maximal cell density. Moreover, cytochromes *c* expression and cell growth were impacted in distinct manners by the transcriptional levels of the *ccm* and *mtr* operons.

3.4. Diffuse reflectance spectroscopy is a sensitive technique to quantitatively measure cytochrome c in intact cells.

Because heme-containing proteins other than c-type cytochromes can contribute to the redness of cell pellets, we next sought to quantify the trends observed in the high-throughput screen by measuring the cytochrome abundance per cell. A distinct advantage of c-type cytochromes is their unique absorption at 552 nm. However, the cell densities required to detect A_{552nm} above the scattering baseline typically push the A_{552nm} into a regime in which Beer's law cannot be used quantitatively to determine the cytochrome c concentration. This can be circumvented by fractionating the cells and analyzing the periplasmic and membrane fractions for the cytochrome c concentration by UV-Vis spectroscopy (*148*). However, fractionation is time-consuming and requires large volumes of culture. To overcome these issues, we used diffuse reflectance spectroscopy to quantitatively measure the concentration of c-type cytochromes in intact cells. Figure 3-5a shows the spectra, normalized to $A_{600\ nm}$, of intact *ccm*$^{0.099}$ *mtrCAB*$^{0.154}$ cells in a reducing environment as measured by dual-beam UV-Vis spectroscopy and diffuse reflectance spectroscopy. The Soret band at ~420 nm is barely detectable by UV-Vis, but the c-type cytochrome α-band at 552 nm is obscured by the cell scatter (Figure 3-5a, blue trace). In contrast, when the same sample was measured by diffuse reflectance spectroscopy, the Soret band and the α-band are detectable against the scattering background (Figure 3-5a, orange trace). Diffuse reflectance thus provides a sensitive measurement of cytochromes in whole cells.

Next, we sought to determine whether diffuse reflectance spectroscopy could serve as a stand-alone method to quantitatively assess the concentration of c-type cytochromes per unit of *E. coli* cell density. To do this, the spectra must provide

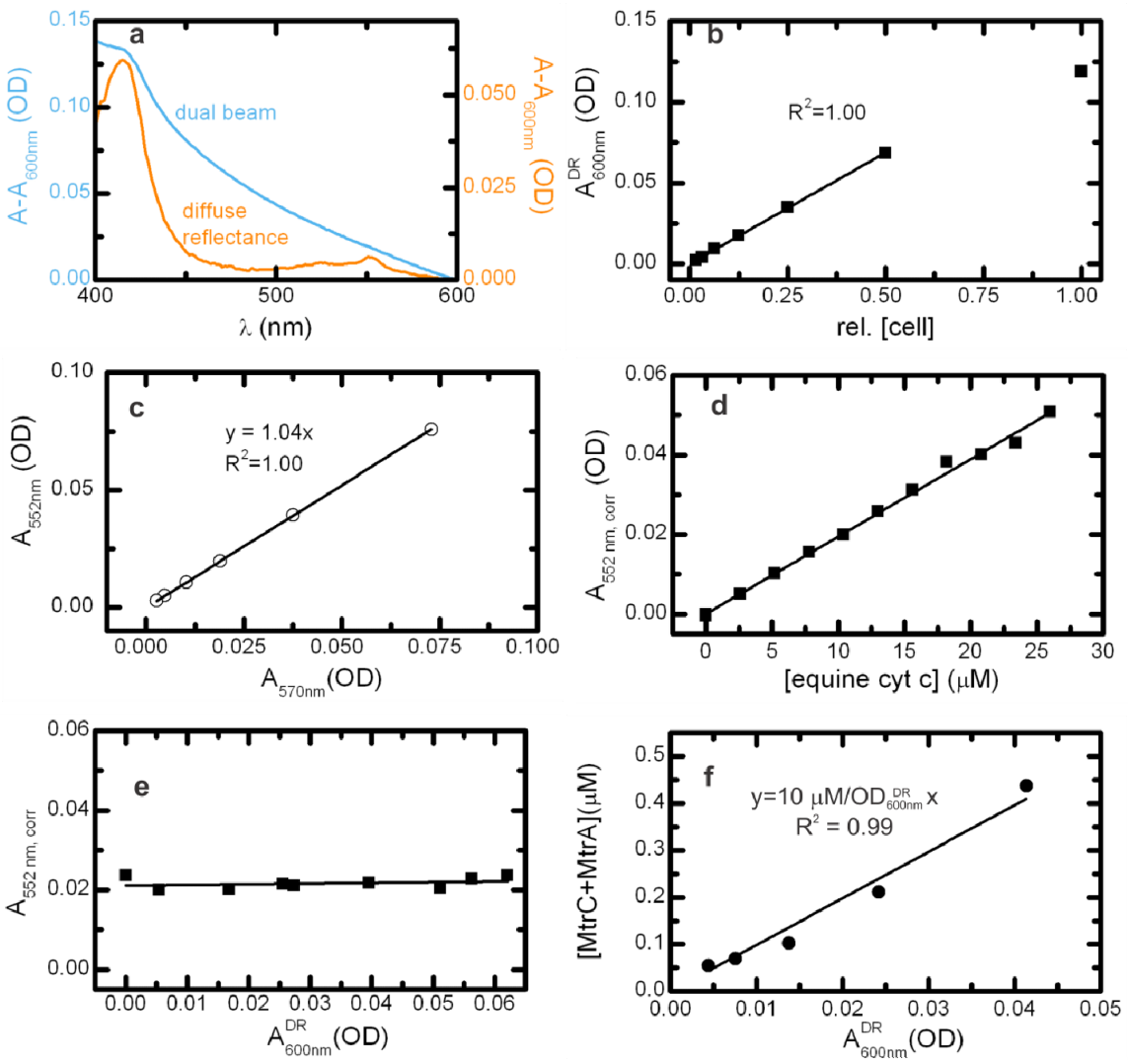

Figure 3-5. Diffuse reflectance can be used to assess the absolute concentration of *c*-type cytochromes per unit cell density. (a) The absorbance spectrum of the same sample of cells from a *ccm*$^{0.099}$*mtrCAB*$^{0.15}$ culture measured under reducing conditions in a dual-beam UV-Vis spectrophometer (light blue, left y-axis) and in a diffuse reflectance spectrophometer (orange, right y-axis). The Soret and α-band of reduced *c* *c*-type cytochromes peaks at 418 nm and 552 nm, respectively, are obscured by cell scattering in the dual beam spectrum, yet are clearly visible in the diffuse reflectance spectrum. (b) The $A_{600\ nm}$ due to cell scatter as a function of the relative concentration cells of the BL21(DE3) WT strain. At $A \leq 0.07$, A_{600nm} is linearly related to the relative cell density (R^2 =1.00). (c) The relationship between $A_{552\ nm}$ and A_{570nm} solely due to cell scatter from cells of the non-cytochrome *c* expressing BL21(DE3) WT strain. The slope of this line, 1.04 (R^2 =1.00), provides the background correction factor. (d) The background corrected A_{552nm} of suspensions of non-cytochrome *c* expressing cells mixed with different concentrations of purified equine cytochrome *c* measured under reducing conditions. The average slope relating the $A_{552nm,\ corr}$ and the equine cytochrome *c* concentration across

three measurements is $1.93 \times 10^3 \pm 0.09$ M^{-1} $OD^{DR}_{600\,nm}$. Using the extinction coefficient for equine cytochrome *c*, this provides an effective pathlength of 0.0792±0.003 cm. (e) The $A_{552nm,\,corr}$ as a function of $A^{DR}_{600\,nm}$ for suspensions of 10.4 μM equine cytochrome *c* mixed with varying concentrations of cells BL21(DE3) WT strain. The invariance of $A_{552nm,corr}$ over this range of concentrations demonstrates that the effective pathlength does not change with cell density. (f) [MtrC+MtrA] as a function of $A^{DR}_{600\,nm}$ for the BL21(DE3) *mtrCAB* strain. The slope of the line between $A^{DR}_{600\,nm}$ and [MtrC+MtrA] is a quantitative measure of the concentration of cytochrome *c* per cell in the BL21(DE3) *mtrCAB* strain.

---

independent measurements of the cell density and the cytochrome *c* concentration. For the former value, the cell concentration is linearly proportional to the absorbance at 600 nm measured by diffuse reflectance ($A^{DR}_{600\,nm}$) for $A^{DR}_{600\,nm}$ <0.065 OD (roughly equivalent to $A^{UV-Vis}_{600\,nm}$~7 OD, Figure 3-5b). For the cytochrome *c* concentrations, we required a simple means to isolate the cytochrome *c* specific absorption at 552 nm from the background absorption arising from cell scatter. Thus, we used non-cytochrome *c* expressing cells to relate the scattering contributions at A_{570nm} to those at A_{552nm} (Figure 3-5c) and used this relationship to derive the background corrected value of $A_{552\,nm}$ ($A_{552\,nm,corr}$): $A_{552\,nm,corr} = A_{552\,nm} - 1.04*A_{570\,nm}$.

To test whether Beer's law holds under our diffuse reflectance conditions, we mixed varying amounts of purified equine cytochrome *c* with C43(DE3) WT cells and measured the peak at 552 nm using diffuse reflectance. The $A_{552\,nm,\,corr}$ of this suspension is linearly proportional ($R^2 = 0.994$) to the equine cytochrome *c* concentration (Figure 3-5d); three replicates of this measurement yield an average slope of $1.93 \times 10^3 \pm 0.09$ OD M^{-1}. Since the extinction coefficient of equine cytochrome is 24,300 OD M^{-1} cm^{-1} at 552 nm, a Beer's law relationship yields an effective pathlength (*b'*) of 0.0792 ± 0.004 cm. This value is reasonable given that the cuvette used in these measurements is 0.08 cm wide. We also measured the diffuse reflectance spectra of solutions of 10 μM equine cytochrome *c* mixed with varying numbers of C43(DE3) WT cells. The resulting $A_{552nm,corr}$ is independent of the cell density (Figure 3-5e), indicating that the effective pathlength is valid for the entire range of cell densities.

Lastly, to confirm that this measurement of cytochrome *c* abundance was independent of the cell density, the diffuse reflectance spectra of different cell densities of the BL21(DE3) *mtrCAB* strain was measured under reducing conditions. The total decaheme cytochrome *c* concentration, [MtrC+MtrA], was then calculated using the effective pathlength of 0.08 cm and the extinction coefficients for MtrA and MtrC ($\varepsilon^{MtrA,MtrC}_{552nm}$ = 280,000 M^{-1} cm^{-1}) (*44*, *51*). As shown in Figure 3-5f, the [MtrC+MtrA] is linearly related to $A^{DR}_{600\,nm}$, indicating the cytochrome *c* abundance per cell density in this strain is 10 ± 1 μM/$OD^{DR}_{600\,nm}$. Thus the use of calibrated diffuse reflectance provides a straightforward, comparatively rapid means to measure the absolute cytochrome *c* concentration on a per cell basis.

3.5. Increasing the *ccm* promoter activity results in decreased levels of CcmE and cytochrome *c* maturation.

The initial screen (Figure 3-4) suggested that *ccm* and *mtr* transcription levels impact cytochrome *c* expression and total cell biomass, both of which are likely to be important for extracellular electron transfer in *E. coli*. To confirm these trends and to understand their molecular underpinnings, we determined the cytochrome *c* abundance and cell density for a subset of cultures that showed high relative red intensities in the initial screen. These strains were grown as 50 mL cultures in flasks, and the final cell density was measured using traditional UV–vis spectroscopy. Diffuse reflectance spectroscopy was performed on intact cells to quantitatively determine [MtrC+MtrA] per unit cell density using the unique absorption of *c*-type cytochromes at 552 nm (see Sections 3.4, Methods 30.10.4, and Figure 3-5 for description). Spectroscopic measurements (Figure 3-6a) and heme-staining of whole-cell lysates (Figure 3-6b) show that only MtrC and MtrA, rather than endogenous cytochromes *c*, contribute to the absorption at 552 nm.

Measurements of relative red intensity and [MtrC+MtrA] from the same culture are highly correlated (r = 0.9, Pearson's correlation coefficient, Figure 3-7a,b), confirming that relative red intensity is an effective screen for high cytochrome *c* production per cell. As in the initial screening experiments, all the $ccm^{\#}mtrCAB^{\#}$ strains measured have a low [MtrC+MtrA] (2.5 $\mu M/OD_{600\,nm}{}^{DR}$) in the absence of induction by IPTG. The [MtrC+MtrA] increased to the 10–20 $\mu M/OD_{600\,nm}{}^{DR}$ range in the $ccm^{\#}mtr^{0.15}$ cultures (Figure 3-8a). These observations confirm that the new C43(DE3)-derived strains offer enhanced control of decaheme cytochrome *c* expression compared to the BL21(DE3) *mtrCAB* strain. The [MtrC+MtrA] gradually increased by 3.5 times as the *ccm* promoter activity increased 67-fold to 0.21 arb. units, but the [MtrC+MtrA] abruptly decreased with *ccm* promoter strengths above 0.34 arb. units (Figure 3-8a). These observed trends in the cytochrome *c* abundance mimic the dependence of relative red intensity on *ccm* promoter strength found in the initial screen (Figure 3-7c) and confirm that the decaheme cytochrome *c* concentration per cell is nonmonotonically dependent on the *ccm* promoter activity. Also mirroring observations from our initial screen, the final cell density for $ccm^{\#}mtrCAB^{0.15}$ cultures was high and independent of the *ccm* promoter strength (Figure 3-8b). These observations indicate that increasing the *ccm* promoter strength up to 0.21 arb. units modestly improves cytochrome *c* expression without affecting cell growth.

We sought to explain the decrease in holocytochrome *c* with high *ccm* promoter strengths (≥0.34 arb. units) to develop a deeper mechanistic understanding of the controls on decaheme cytochrome *c* production. We hypothesized that high *ccm* promoter strengths could reduce the translation (*182*) or secretion efficiency (*84*), which would decrease functional Ccm machinery present in the inner membrane and decrease cytochrome *c* maturation. To quantitatively compare the membrane-associated CcmE levels across different strains (Figure 3-8c, inset), we normalized the CcmE band intensity of each strain by the band intensity arising from an equal mass of $ccm^{0.21}mtrCAB^{0.15}$ culture lysate. This normalized CcmE intensity was linear with CcmE abundance over the range of our measurements (Figure 3-9). The membrane-associated CcmE levels dramatically decreased with *ccm* promoter strengths ≥0.34 arb. units, the same *ccm* promoter strengths that showed a sharp decline in [MtrC+MtrA]. Thus, this trend is consistent with a translation or secretion defect at high *ccm* promoter strengths, which decreases Ccm protein levels in the membrane. In turn, the low level of

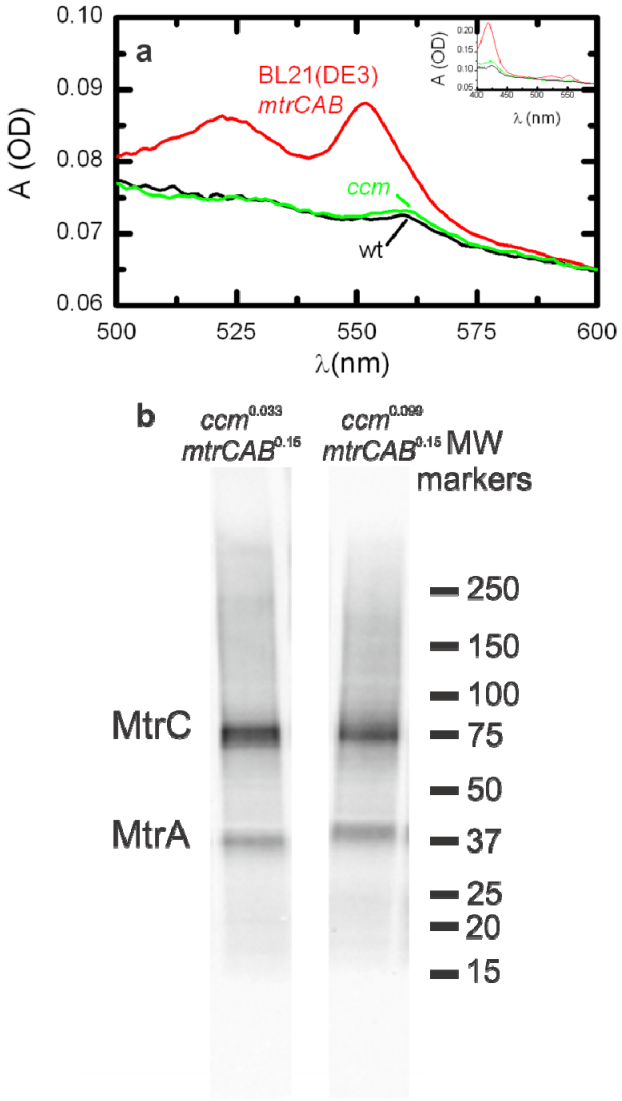

Figure 3-6. MtrC and MtrA are the predominant *c*-type cytochromes present in *mtrCAB* strains. (a) The absorbance spectrum of the BL21(DE3) WT, BL21(DE3) *ccm*, and BL21(DE3) *mtrCAB* strains. The BL21(DE3) *mtrCAB* strain has a strong absorption at 552 nm, which is characteristic of *c*-type cytochromes. In contrast, the BL21(DE3) WT and BL21(DE3) *ccm* strains do not have absorption peaks at ~550 nm, indicating endogenous cytochromes *c* are not present at significant levels relative to MtrC and MtrA in *mtrCAB* strains. The 560 nm absorption peak arises from endogenous cytochromes *b*. (b) Heme staining of the whole cell lysates from $ccm^{0.033}$ $mtrCAB^{0.15}$ and $ccm^{0.099}$ $mtrCAB^{0.15}$ cultures separated by SDS–PAGE. Staining was performed with enhanced chemiluminence, as described in the text. The numbers on the right with horizontal lines represent the molecular weight standards (in kDa).

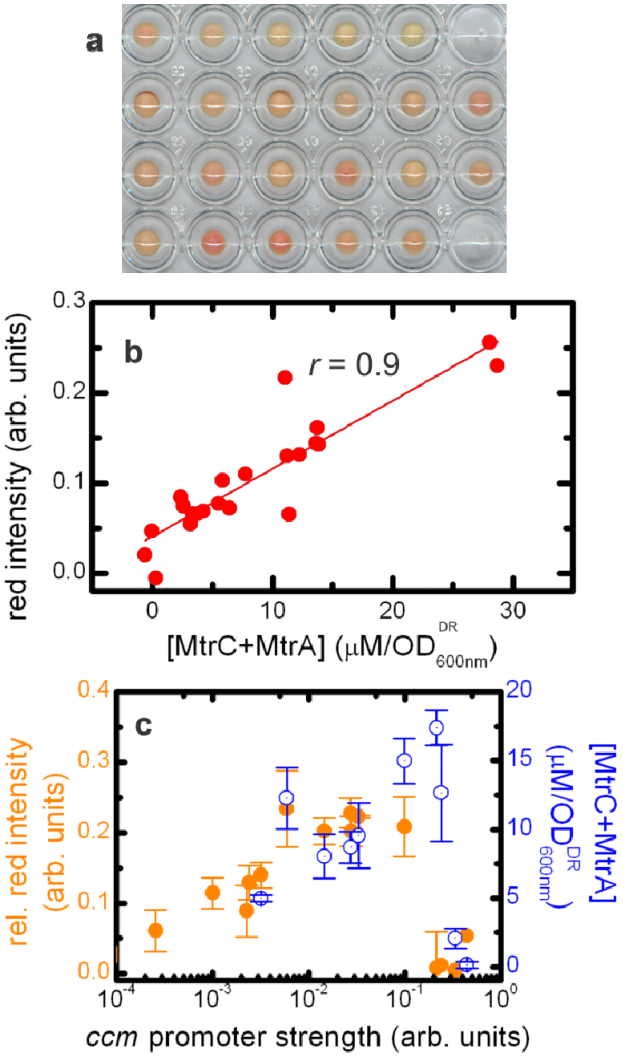

Figure 3-7. The red intensity of cell pellets is strongly correlated with MtrC+MtrA concentration. (a) An image of cell pellets from 22 different *mtrCAB* containing strains and growth conditions. (b) The red intensity of the cell pellets compared to [MtrC+MtrA] for these 22 different strains and growth conditions. The Pearson's correlation coefficient between the red intensity and the cytochrome *c* concentration is 0.9. (c) The relative red intensity (solid orange circles, left hand axis) and [MtrC+MtrA] (dotted blue circles, right hand axis) for $ccm^{\#}$ $mtrCAB^{0.15}$ cultures show very similar trends as a function of *ccm* promoter strength.

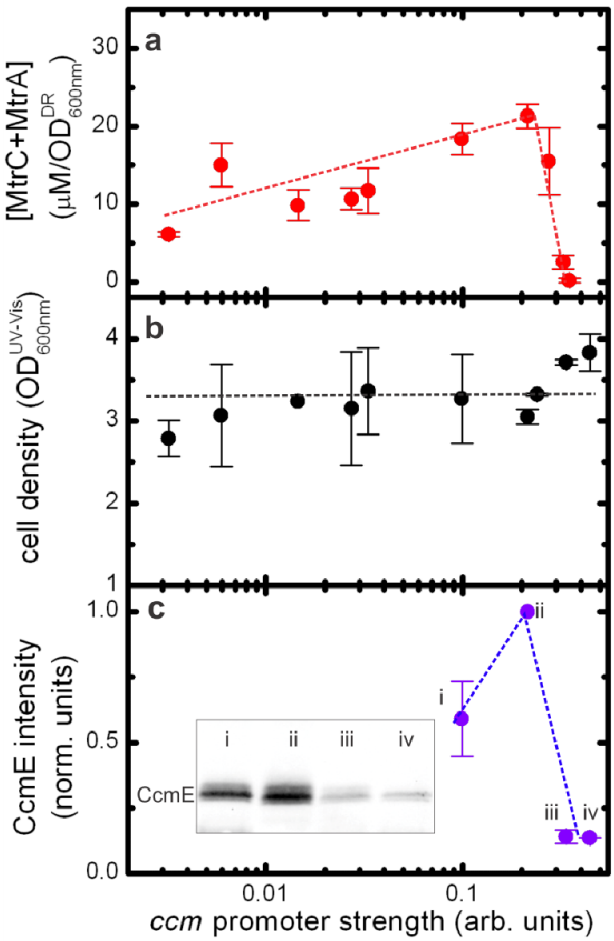

Figure 3-8. *ccm* promoter strength modestly affects MtrC + MtrA concentration without affecting final cell density. (a) The total concentration of MtrA and MtrC per unit of $ccm^{\#}$ $mtrCAB^{0.15}$ cultures as a function of *ccm* promoter strength. [MtrC+MtrA] reaches a maximum with *ccm* promoter strength of ~0.1 but is near background levels with *ccm* promoter strengths ≥0.34 arb. units. (b) The normalized CcmE intensity as a function of *ccm* promoter strength. The abundance of membrane-associated CcmE decreases with *ccm* promoter strengths ≥0.34 arb. units. The inset gel is the immunoblot of CcmE present in the membrane fraction of cell lysates from (i) $ccm^{0.099}mtrCAB^{0.15}$, (ii) $ccm^{0.21}mtrCAB^{0.15}$, (iii) $ccm^{0.34}mtrCAB^{0.15}$, and (iv) $ccm^{0.44}mtrCAB^{0.15}$ cultures. (c) The final cell density of $ccm^{\#}mtrCAB^{0.15}$ cultures as a function of *ccm* promoter strength shows that *ccm* promoter strength does not significantly affect the cell density.

Ccm biogenesis machinery decreases the maturation of apo-proteins into holo-MtrC and holo-MtrA.

3.6. Efficiency of MtrC and MtrA maturation and cell growth decrease strongly with increasing *mtr* promoter activity.

We next investigated the effect of modulating the *mtr* promoter activity on decaheme cytochrome *c* expression and cell growth. We probed these trends as described above in the$ccm^{0.099}mtrCAB^{\#}$ cultures because these cultures showed a robust expression of *c*-type cytochromes across a wide range of *mtr* promoter activities in our initial screen (Figure 3-4). As shown in Figure 3-10a, the [MtrC+MtrA] in this strain sharply increased with increasing *mtr* transcriptional levels, reaching a maximum when the *mtr* promoter activity was 0.29 arb. units. Notably, the MtrC and MtrA abundance in the $ccm^{0.099}mtrCAB^{0.29}$ culture is the highest that we have measured (22 ± 3 μM/$OD_{600\ nm}^{DR}$) and is 2.2 times higher than in the previously reported BL21(DE3) *mtrCAB* strain. After this optimum, the cytochrome *c* concentration decreased to approximately half its maximal value.

We sought to understand the origin of this decrease to improve our mechanistic understanding of the controls on decaheme cytochrome *c* production. We calculated the efficiency of cytochrome *c* synthesis to assess how transcriptional levels of *mtr* are translated into holo-MtrC and holo-MtrA levels. The efficiency synthesis was calculated by dividing the [MtrC+MtrA] by the *mtr* promoter activity and normalized such that the maximum efficiency was 1. Strikingly, the efficiency of decaheme cytochrome *c* synthesis in the $ccm^{0.099}mtrCAB$ strain (solid black squares) drops by ~300-fold as the *mtr* promoter activity is increased (Figure 3-10b). The same analysis of the $ccm^{\#}mtrCAB^{0.001}$ and $ccm^{\#}mtrCAB^{0.15}$ cultures show that different *ccm* transcriptional levels (empty magenta circles) have a minor impact on the efficiency of cytochrome *c* synthesis, as long as the transcriptional levels are below those that result in secretion impairment. Thus, at high *mtr* promoter activities, the increase in *mtr* transcripts is negated by the lower efficiency of synthesis from these transcripts, leading to a decreased yield of decaheme cytochrome *c*.

Two known mechanisms could result in decreased efficiency of cytochrome *c* synthesis with increasing cytochrome *c* transcript levels: (i) saturation of translation or secretion (*84*) by high *mtr* expression (*182*) could decrease Ccm and thus decreased ability to mature protein (*178*), or (ii) inadequate heme production (*178*) could lead to increased degradation of partially matured decaheme cytochrome *c*. We first probed membrane-associated CcmE abundance as a function of *mtr* promoter activity (Figure 3-10c). The membrane-associated CcmE levels were within 1 standard deviation of each while the *mtr* promoter activity was varied by ~5-fold, indicating that there is no significant decrease in the Ccm biogenesis machinery of the strain (Figure 3-10c). Next, spent media from highly induced $ccm^{0.099}mtrCAB^{0.72}$ cultures supplemented with the heme biosynthesis precursor δ-ALA was analyzed spectroscopically for heme. The visibly red media contained ~0.3 μM heme b (not shown), ruling out heme limitation as a cause of the decrease in cytochrome *c* synthesis efficiency. Further supporting this idea, we measured the [MtrC+MtrA] in $ccm^{0.099}mtrCAB$ cultures lacking δ-ALA (dotted red squares, Figure 3-10a). While diminished bioavailability of heme decreases the efficiency of holocytochrome *c* synthesis by ~30% across all *mtr* promoter activities, it does not

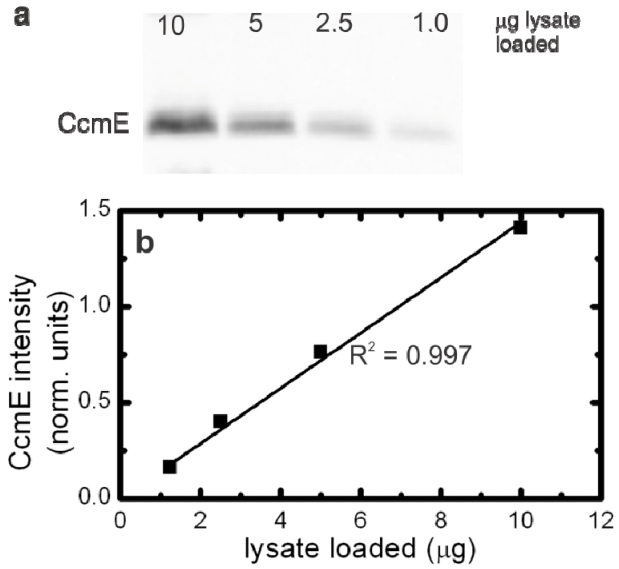

Figure 3-9. CcmE chemiluminescence is linearly related to CcmE abundance under immunoblotting conditions used. (a) Immunoblot of CcmE from 10 µg, 5 µg, 2.5 µg, and 1 µg total protein of membrane fraction of the *ccm*$^{0.099}$ *mtrCAB*$^{0.29}$ culture. (b) The normalized intensity of CcmE band is linearly related to the amount of membrane fraction loaded.

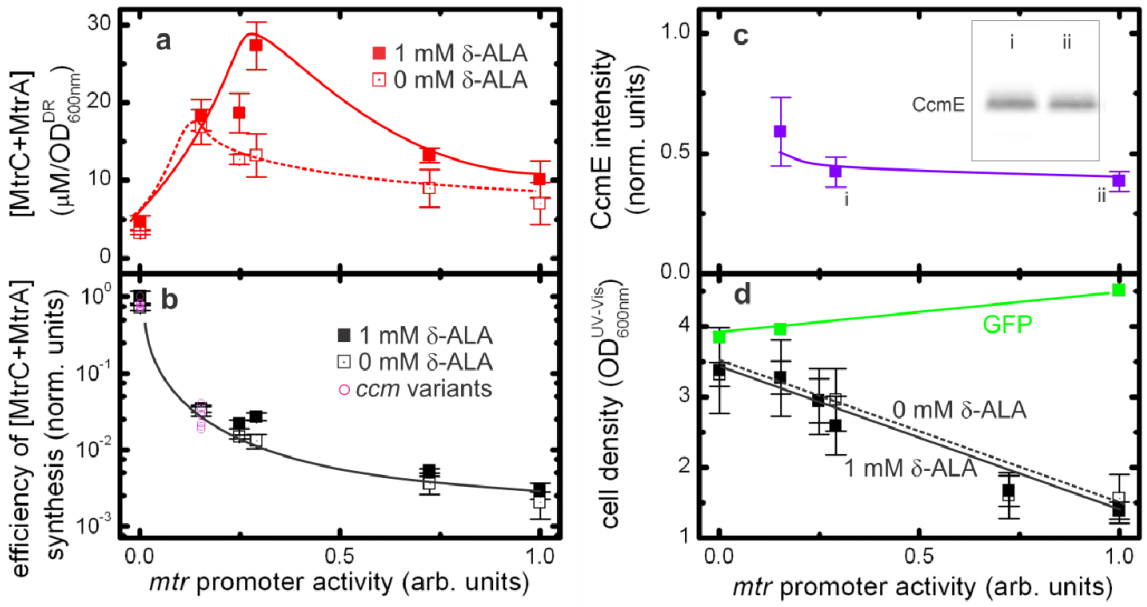

Figure 3-10. *mtr* promoter activity sharply affects the efficiency of MtrC + MtrA synthesis and final cell density. (a) The total concentration of MtrA and MtrC per $OD_{600\ nm}$ DR of cells in $ccm^{0.099}mtrCAB^{\#}$ cultures as a function of mtr promoter activity in the presence of 0 mM δ-ALA (filled squares) and 1 mM δ-ALA (empty squares). The [MtrC + MtrA] reaches a maximum with *mtr* promoter activities of ~0.2−0.25 arb. units and sharply declines at higher promoter activities. (b) Efficiency of MtrC + MtrA synthesis as a function of mtr promoter activity for the ccm0.099 mtrCAB strain in the presence of 0 mM δ-ALA (black filled squares) and 1 mM δ-ALA (black empty squares) and the $ccm^{\#}mtrCAB$ strains in the presence of 1 mM δ-ALA (empty magenta circles). All cultures experience a dramatic decrease in the efficiency of cytochrome *c* production with increasing mtr promoter strength. (c) The normalized CcmE intensity as a function of *mtr* promoter activities, showing that there is no significant decrease in the membrane associated CcmE levels with increasing *mtr* promoter activity. The inset gel is the immunoblot of CcmE present in the membrane fraction in (i) $ccm^{0.099}mtrCAB^{0.29}$ and (ii) $ccm^{0.099}mtrCAB^{1.0}$ cultures. (d) The final cell density as a function of *mtr* promoter strength in the presence of 1 mM δ-ALA (black filled circles) and absence of δ-ALA (dotted black circles), showing a strong decrease in cell density with *mtr* promoter activity (r = −0.97, Pearson's correlation coefficient). In contrast, the final cell density of a C43(DE3) strain harboring the pET30a+ GFP plasmid (filled green squares) increases slightly with IPTG induction.

significantly alter the relationship between efficiency of cytochrome *c* synthesis and mtr promoter activity (Figure 3-10b). Thus, our data rule out decreased Ccm biogenesis machinery and inadequate heme production as causes for the stark decrease in efficiency of cytochrome *c* synthesis with increasing *mtr* promoter activity.

To probe the impact of the *mtr* promoter on cell growth, we measured the final cell density in the $ccm^{0.099}mtrCAB^{\#}$ cultures. We observed that the cell density is negatively correlated with increasing *mtr* promoter activity in the presence (solid black squares) or absence (hollow black squares) of δ-ALA ($r = -0.97$, Pearson's correlation coefficient, Figure 3-10d). As described above, neither polypeptide synthesis nor heme bioavailability are limited in this strain. Therefore, the decrease in growth could be caused by toxicity of IPTG, MtrC, MtrA, or MtrB. To determine whether the decrease in cell density was caused by IPTG, we measured the final cell density of a C43(DE3) strain expressing GFP from the *T7 lac* promoter induced with varying [IPTG]. The final cell density of these cultures increased slightly with IPTG (solid green squares, Figure 3-10d), indicating that IPTG does not negatively influence growth. Additionally, comparison of the cytochrome *c* abundance data in Figure 3-10a and Figure 3-10d shows that [MtrC+MtrA] is not strongly correlated with cell density ($r = -0.28$, Pearson's correlation coefficient). For example, the $ccm^{0.099}mtrCAB^{0.24}$ and $ccm^{0.099}mtrCAB^{1.0}$ cultures have similar [MtrC+MtrA] (Figure 3-10a), yet the $ccm^{0.099}mtrCAB^{1.0}$ cultures have a final cell density that is 50% of the $ccm^{0.099}mtrCAB^{0.24}$cultures (Figure 3-10d). Therefore, our data suggest that the decrease in cell density with *mtr* promoter activity is not due to toxicity of IPTG, MtrA, or MtrC.

3.7. Anode-reduction correlates with minimal alterations in cell morphology and moderate MtrC and MtrA expression.

Our central hypothesis is that the number of MtrCAB electron conduits as well as minimal perturbations to cell growth and physiology may be important to achieve extracellular electron transfer in *E. coli*. From the assays and screens above, we selected several $ccm^{\#}mtrCAB^{\#}$cultures with high cytochrome *c* levels ([MtrC+MtrA] ≥ 10 $\mu M/OD_{600\ nm}^{DR}$) and high final cell density (cell density ≥2 $OD_{600\ nm}^{UV-vis}$). To provide an additional metric of overall cell morphology, we examined the forward scatter of these strains by flow cytometry (Figure 3-11a). Just as cells from the BL21(DE3) *mtrCAB* strain (Figure 3-11a, red filled triangle) showed increased scatter relative to the BL21(DE3) WT strain (Figure 3-11a, black filled triangle), cells from all of the $ccm^{\#}mtrCAB^{\#}$ cultures (Figure 3-11a, circles) also showed increased forward scatter compared to the C43(DE3) WT strain (Figure 3-11a, black filled circle). These measurements indicate expression of MtrCAB causes significant morphological changes without substantially altering the final cell density.

We sought to understand the correlation of cellular cytochrome *c* levels and cellular morphology to the ability of cells to transfer electrons to an electrode. Using a comparison of forward scatter versus [MtrC+MtrA] (Figure 3-11a), we selected a culture that shows less morphological perturbations (solid blue circle, $ccm^{0.033}mtrCAB^{0.15}$, henceforth referred to as the "least perturbed" culture) and a culture that shows higher [MtrC+MtrA] (solid magneta circle,$ccm^{0.099}mtrCAB^{0.29}$, henceforth referred to as the "most cytochrome *c*" culture), relative to the original BL21(DE3) strain. These strains and their respective *ccm*-only controls were inoculated at a high cell density into a three-

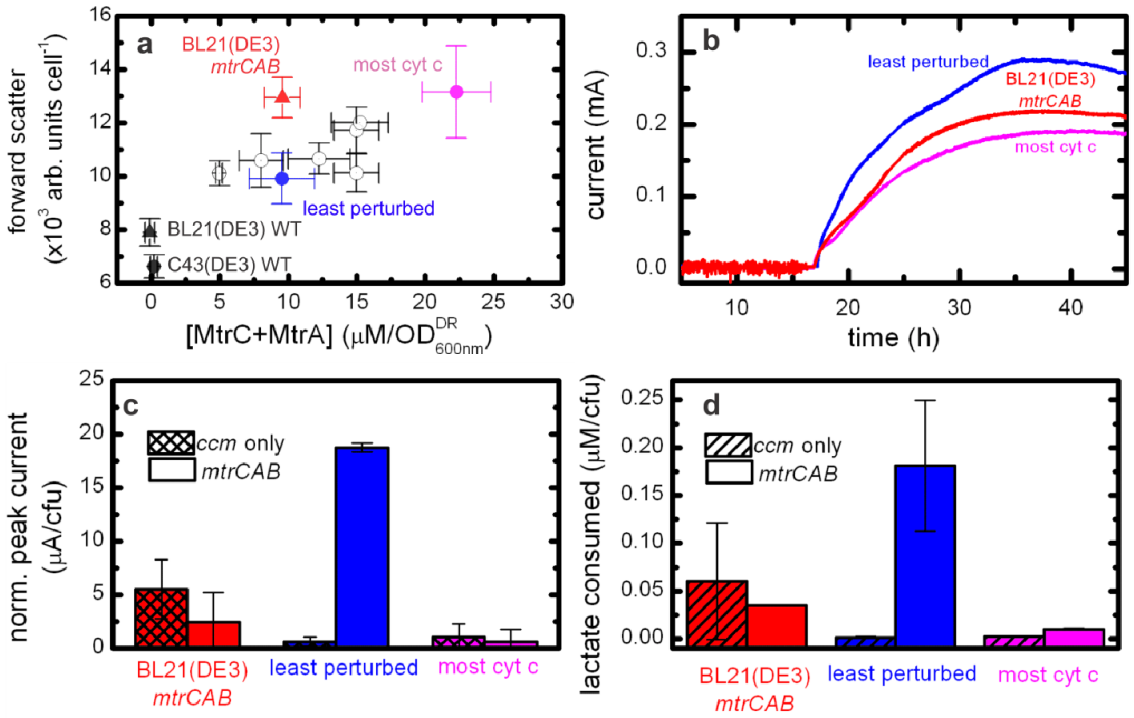

Figure 3-11. A C43-derived *mtrCAB* strain with a less perturbed cellular morphology can transfer electrons to an anode. (a) Forward scatter versus [MtrC+MtrA] for *ccm*$^{\#}$*mtrCAB*$^{\#}$ cultures. Highlighted are the BL21(DE3) WT (black triangle), C43(DE3) WT (black circle), BL21(DE3) *mtrCAB* (red triangle), least perturbed (blue circle), and most cytochrome c (magenta circle) strains. (b) Representative electrochemical measurements of BL21(DE3) *mtrCAB* culture (red line), the least perturbed culture (blue line), and most cytochrome *c* culture (magenta line). (c) Maximal current per cfu for the BL21(DE3) *mtrCAB* cells (solid red bar), the least perturbed culture (solid blue bar), and most cytochrome *c* culture (solid magenta bar) and their respective *ccm*-only strains: the BL21(DE3) *ccm* (cross-hashed red bar), least perturbed *ccm* (cross-hashed blue bar), and most cytochrome *c ccm* (cross-hashed magenta bar). There is a significant difference in maximal current per cfu between the least perturbed culture and its control, the least perturbed *ccm* strain (p-value = 0.01, Student's one-tailed t test with equal variances). (d) Lactate consumption per cfu for the BL21(DE3) *mtrCAB* cells (solid red bar), the least perturbed (solid blue bar), and most cytochrome *c* (solid magenta bar) cultures and their respective *ccm*-only strains BL21(DE3) *ccm* (hashed red bar), least perturbed *ccm* (hashed blue bar), and most cytochrome *c ccm* (hashed magenta bar). There is a significant difference in lactate consumed per cfu between the least perturbed and least perturbed *ccm* strains (p-value = 0.03, Student's one-tailed t test with equal variances).

electrode microbial electrochemical system (*183*). The working electrode was poised at 0.2 V versus Ag/AgCl (satd KCl), L-lactate was supplied as the electron donor, and the electric current production was recorded over several days (Figure 3-11b). Interestingly, the least perturbed strain achieved higher current than either the BL21(DE3) *mtrCAB* strain or most cytochrome *c* strain. Additionally, the least perturbed strain also produced ~30-fold greater maximum current per cfu than its counterpart *ccm*-only strain (significantly different with a *p*-value = 0.01, Figure 3-11c), indicating that reduction of the electrode in the least perturbed strain is enhanced by the presence of the MtrCAB electron conduit. In contrast, both the BL21(DE3) *mtrCAB* and most cytochrome *c* strains showed low maximal current per cfu, which were not statistically significant from their respective *ccm*-only strains (*p*-value = 0.25, Figure 3-11c). Although *S. oneidensis* MR-1 typically produces ~1000 times higher current than the least perturbed strain in these three-electrode electrochemical systems, the difference in current per cfu between the least perturbed strain in comparison to the other *E. coli* strains indicates it is possible to engineer anode reduction into new organisms using the MtrCAB electron conduit.

Additionally, HPLC analysis of the spent media (Figure 3-11d) shows that the most lactate per cfu was consumed by the least perturbed culture, supporting the hypothesis that electrons delivered to the electrode originate from *E. coli* metabolism of L-lactate. These observations indicate that heterologous expression of MtrCAB allows *E. coli* to transfer metabolic electrons to an electrode and that phenotypic features and [MtrC+MtrA] are correlated with the efficiency and rate of extracellular electron transfer.

3.8. Transcriptional balance is critical for optimal *in vivo* synthesis and function of electron conduits.

Using our library of transcriptional variants, we are able to quantitatively define regimes in which different mechanisms limit further synthesis of MtrC and MtrA (Figure 3-12). Below a threshold level of *ccm* transcription, decaheme cytochrome *c* is not produced because insufficient Ccm complexes are available to mature the apoproteins (Figure 3-12a). Above a certain limit, increasing the *ccm* transcriptional level actually decreases the membrane-associated Ccm biogenesis machinery (Figure 3-12b), setting a maximum level of Ccm biogenesis machinery available to mature apocytochrome *c*. Most critically, holocytochrome *c* synthesis was sharply dependent on the *mtr* promoter activity. Increased *mtr* transcription (Figure 3-12a) is outweighed by the decreased efficiency of MtrC and MtrA synthesis, resulting in decreased decaheme cytochrome *c* abundance.

To our knowledge, this is the first report systematically documenting a decrease in multiheme cytochrome *c* production efficiency, although other groups have shown that low induction levels are optimal for heterologous expression of multiheme cytochrome *c* in *E. coli* (*64*, *69*, *70*). Neither low heme abundance nor impairment in secretion account for this drop in efficiency of cytochrome *c* production. While it is possible that increasing levels of MtrC inhibit its correct localization into the outer membrane, previous work in *E. coli* (*73*) suggests that mislocalization of MtrC is unlikely to affect the overall levels of decaheme cytochrome *c*. We hypothesize that the low efficiency is due to an as-yet uncharacterized mechanism. One possible scenario is that the Ccm complex is insufficiently processive to rapidly mature decaheme cytochromes *c* (Figure 3-12c). Thus, the apoprotein level increases, CXXCH motifs from different polypeptides

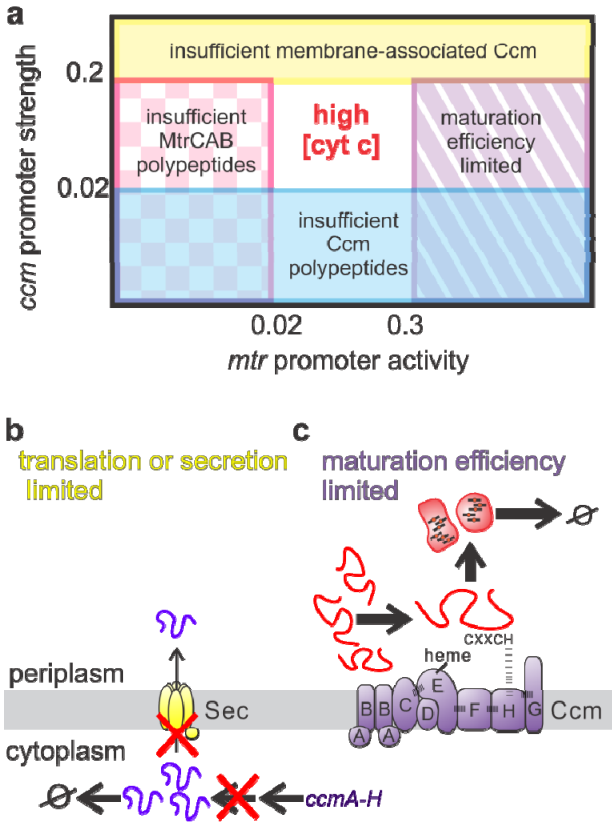

Figure 3-12. Constraints on decaheme cytochrome *c* production. (a) Phase diagram showing regions of limited and maximal MtrC and MtrA expression in relation to *ccm* promoter strength and *mtr* promoter activity. (b) Schematic illustrating that lowered cytochrome *c* expression at high *ccm* promoter strength is due to a decrease in the Ccm complex abundance, which prevents maturation of cytochromes *c*. (c) One proposed mechanism that would account for decreased cytochrome maturation at high mtr promoter activity. Poor processivity of the *E. coli* Ccm machinery coupled with a high concentration of apocytochromes *c* results in incompletely matured MtrC and MtrA, which are subsequently degraded by periplasmic proteases.

compete for binding to Ccm complex, resulting in a greater fraction of apoproteins being only partially matured and degraded. Three observations lend support to this idea: (i) heterologous expression of single heme cytochromes *c* does not show the same dramatic dependence on transcriptional levels (*184*), (ii) the modest 3.5-fold improvement of cytochrome *c* production with 67-fold increase in *ccm* transcriptional levels suggests that the Ccm complex is an inefficient enzyme for decaheme cytochrome *c* maturation (Figure 3-12a), and (iii) in *S. oneidensis* MR-1 40% of MtrC polypeptides never mature, suggesting that decaheme cytochrome *c* maturation is intrinsically inefficient (*185*).

In addition to the complexity of decaheme cytochrome *c* synthesis, the function of MtrCAB electron conduits in *E. coli* is not straightforward. Extracellular electron transfer in *E. coli* not only is governed by the cellular concentration of decaheme cytochrome *c* but also is correlated with minimal perturbations to cellular growth and morphology. Both MtrCAB subsystem-specific and more cellular-wide properties could underlie this observation. For example, a difference in ratio of MtrA:MtrB:MtrC or a change in percentage of properly localized MtrC, MtrB, or MtrA could negatively impact extracellular respiration without changing the decaheme content per cell. Alternatively, more cell-wide perturbations may be at root of this. For example, under aerobic growth conditions, the membrane stress response has been shown to decrease the rate of O_2 (g) consumption and impact the inner membrane proteome (*84*, *85*). Since reducing equivalents from L-lactate must pass through the inner membrane proteins L-lactate dehydrogenase and NapC, these alterations could critically affect the availability of electrons to enter the MtrCAB electron conduit. Thus, future investigations will attempt to untangle these many possibilities to more firmly understand the factors critical for extracellular respiration in *E. coli*. Indeed, given the degree to which this system interfaces with host machinery, we anticipate that additional systems-level analysis will improve heterologous extracellular respiration to levels practical for biosensing and bioenergy applications.

3.9. Conclusions

Here we report the impact of tuning *ccm* and *mtr* transcription on the synthesis and function of the MtrCAB electron conduit in *E. coli*. The use of the C43(DE3) strain enables the synthesis of MtrCAB to be controlled and improves MtrC and MtrA expression by 2.2-fold. Surprisingly, the strain that produces the greatest current at the anode does not have the greatest abundance of MtrA and MtrC. Instead, it has a moderate amount of decaheme cytochromes *c* and minimal perturbations in its cellular morphology. This strain delivers metabolic electrons to an electrode at a rate ~30-fold faster than *ccm*-only controls. While the efficiency of this process is modest in comparison to naturally occurring dissimilatory metal-reducing bacteria, this work indicates that it is possible to genetically engineer molecularly defined extracellular electron transfer into an organism.

3.10. Materials and Methods

3.10.1. Plasmids, strains, and growth conditions.

The strains used in this study are listed in Table 3-3. The BL21(DE3) WT, BL21(DE3) *ccm*, and BL21(DE3) *mtrCAB* strains were described previously (11). To

generate a strain that expressed GFP from the *T7 lac* promoter, the coding sequence for superfolder GFP (59) was amplified by PCR with primers that contained EcoRI and SpeI sites immediately upstream of the start codon and downstream of stop codon, respectively. This PCR product and the I5023 plasmid (previously described in Chapter 2) were separately digested with EcoRI and SpeI, and the resulting fragments were ligated together using T4 ligase. Finally, this plasmid was transformed into chemically competent C43(DE3) cells.

The pFAB#-GFP plasmids were obtained from the BioFAB (Emeryville, CA). To create a library of plasmids containing different promoters in front of the *ccm* coding sequence, the fragment between +66 and -225 relative to the *tet* transcriptional start site in pEC86 was replaced with a fragment containing two BsaI sites using site-directed mutagenesis to generate pCcm2. Golden Gate cloning (*181*) was used to insert BioFAB-derived promoter sequences into pCcm2. pCcm2 was digested with BsaI, dephosphorylated with Antarctic phosphatase (NEB, Ipswich, MA) followed by heat inactivation at 65 °C for 20 minutes. Forward and reverse strand oligonucleotides were mixed in a 1:1 molar ratio, and phosphorylated using polynucleotide kinase (NEB, Ipswich, MA). The phosphorylase was heat inactivated for 20 min at 65°C, and the DNA was hybridized in the presence of 60 mM NaCl. These oligonucleotide inserts were ligated into cut and dephosphorylated plasmid pCcm2 using T4 DNA ligase (NEB, Ipswich, MA). The resulting plasmids were sequenced and then co-transformed with plasmid I5203 into C43(DE3).

All strains, unless otherwise specified, were grown in 2xYT media with 50 μg mL^{-1} kanamycin and 30 μg mL^{-1} chloramphenicol. Glycerol stocks were used to inoculate 5 mL media, and cultures were grown overnight at 37° C with 275-rpm shaking. To grow strains in 96-deep well plates, overnight cultures were diluted 1:100 in 1.1 mL media containing 5-aminolevulinic acid (Sigma-Aldrich, St. Louis, MO), covered with foil, and grown at 37 °C with 275-rpm shaking. For growth in flasks, overnight cultures were diluted 1:100 into 50 mL media containing 5-aminolevulinic acid (δ-ALA) (Sigma-Aldrich, St. Louis, MO), and grown at 30°C in 250 mL flasks with 250-rpm shaking. For growth in plates or flask, transcription of *mtrCAB* was induced by addition of IPTG when the cultures reached an $OD_{600\ nm}^{UV-Vis}$ of 0.5 (typically ~2-3 h after inoculation). Cultures were grown for a total of 20 h after inoculation.

3.10.2. Quantitative measurement of relative promoter strength and activity.

We used the methodology of Kelly, *et al.,* (*180*) to indirectly measure the activity of promoters. In this approach, the mRNA transcriptional rate is encoded in the synthesis of green fluorescent protein (GFP), which is measured by GFP fluorescence. To calibrate the *T7 lacO* promoter in C43(DE3) cells, the MtrCAB coding region in the I5023 plasmid was replaced with the coding region for superfolder GFP (Figure 3-3a). GFP expression from a C43(DE3) strain harboring this plasmid was induced with increasing concentrations of IPTG, and after overnight growth in flasks, the fluorescence was measured at the single cell level using flow cytometry (Figure 3-3b). Specifically, a 5 μL aliquot of each culture was diluted into 1 mL of 0.22-μm sterile-filtered phosphate buffered saline (pH 7.4) and loaded into the flow cytometer. At least 50,000 events were captured for each sample using a FACS Aria Flow Cytometer and Cell Sorter (BD Biosciences, San Jose, CA). The average and standard deviation of the geometric means

measured from at least three biological replicates are reported. From these measurements, we calculated the relative *T7 lacO* promoter activity as a function of IPTG by normalizing to the maximum background corrected GFP fluorescence intensity measured when inducing with 500 μM IPTG (Figure 3-3c, Table 2-1). Likewise, GFP expression from the C43(DE3) strains harboring pFAB#-GFP plasmids (Figure 3-3d) was measured to calibrate these constitutive promoters. The GFP intensity was measured by flow cytometry as described above (Figure 3-3e). Amongst the pFAB#-GFP strains, the strain carrying pFAB704-GFP exhibited the greatest fluorescence intensity per cell, so we normalized the background corrected GFP intensity of all other pFAB#-GFP strains to the background corrected pFAB704 GFP intensity (Figure 3-3f, Table 3-2).

3.10.3. Analysis of cell pellets for assessment of cytochrome c expression and cell growth.

After growth in 96-well plates, 150 μL of culture was pelleted in clear, V-bottom 96-well polystyrene plates (ThermoScientific, Waltham, MA). The plates containing the cell pellets were scanned using a Scanjet G4050 scanner (HP, Palo Alto, CA). Regions of interest from each pellet were identified using the Matlab (R2009b) Image Processing Toolbox (MathWorks, Natick, MA). The relative red intensity was calculated by taking the ratio intensity in the red channel (I_{red}) to the grayscale intensity $\left(I_{gray}\right)$ and subtracting the red to gray ratio of C43(DE3) WT cells: relative red intensity = $(I_{red})/\left(I_{gray}\right) - \left(I_{red}^{C43(DE3)WT}\right)/\left(I_{gray}^{C43(DE3)WT}\right)$.

To calculate the change in cell pellet area, the difference in area between C43(DE3) WT cell pellet and the area of the cell pellet of interest was divided by the C43(DE3) WT cell pellet area.

The average of the relative red intensity from at least three biological replicates is reported, and the granularity of the heat map was set to one half the typical relative red intensity standard deviations (~0.03 arb. units).

3.10.4. Quantitative assessment of cytochrome c per cell by diffuse reflectance spectroscopy.

The cells from a 10 mL aliquot of culture were pelleted by centrifugation at 4,000 rcf for 10 min at 4°C. These cells were re-suspended in 10 mM HEPES buffer, (pH 7.4) to give a working cell suspension with $\mathrm{OD}_{600\,\mathrm{nm}}^{\mathrm{UV-Vis}}$ ~3-4 OD. In calibration experiments using purified cytochrome c, the appropriate volume of a 1.2 mg/mL solution of equine cytochrome c was added to the cells. This cell suspension was reduced by addition of sodium dithionite to a final concentration of 10 mM, and ~400 uL was loaded into a transparent chamber consisting of 0.08 mm deep, 22 mm square Secure-Seal™ hybridization gaskets (Life Technologies, Eugene, OR) adhered to 25 mm wide square glass coverslip. The access ports on the gaskets were sealed with an adhesive seal tab to form a fluid-tight homemade cuvette. The absorbance spectrum of the cell suspension was measured using Quality Spec Pro UV-Vis Spectrometer equipped with a Muglight diffuse reflectance attachment (ASD Inc, Boulder, CO).

In order for diffuse reflectance spectroscopy to serve as a stand-alone method to quantitatively assess the concentration of c-type cytochromes for *E. coli* cell density, the spectra must provide independent measurements of the cell density and the cytochrome c

concentration. For the former value, the cell concentration is linearly proportional to the absorbance at 600 nm ($A^{DR}_{600\ nm}$) for $A^{DR}_{600\ nm}$ <0.07 OD (roughly equivalent to $A^{UV-Vis}_{600\ nm}$~7 OD, Figure 3-5b). For the cytochrome c concentrations, we required a simple means to isolate the cytochrome c specific absorption at 552 nm from the background absorption arising from cell scatter. Thus, we used non-cytochrome c expressing cells to relate the scattering contributions at $A_{570\ nm}$ to those at $A_{552\ nm}$ (Figure 3-5c) and used this relationship to derive the background corrected value of $A_{552\ nm}$ ($A_{552\ nm,corr}$): $A_{552\ nm,\ corr} = A_{552\ nm} - 1.04*A_{570\ nm}$.

To test whether Beer's law holds in our system, we mixed varying amounts of purified equine cytochrome c with C43(DE3) WT cells and measured the peak at 552 nm using diffuse reflectance. The $A_{552\ nm,\ corr}$ of this suspension is linearly proportional (R = 0.994) to the equine cytochrome c concentration (Figure 3-5d); three replicates of this measurement yield an average slope of 1.93 $x10^3$ ± 0.09 OD M^{-1}. Since the extinction coefficient of equine cytochrome is 24,300 OD M^{-1} cm^{-1} at 552 nm, a Beer's law relationship yields an effective pathlength (*b'*) of 0.0792 ± 0.004 cm. This value is reasonable given that the cuvette used in these measurements is 0.08 cm wide. We also measured the diffuse reflectance spectra of solutions of 10 μM equine cytochrome c mixed with varying numbers of C43(DE3) WT cells. The resulting $A_{552nm,corr}$ is independent of the cell density (Figure 3-5e), indicating that the effective pathlength is valid for the entire range of cell densities.

The efficiency of [MtrC + MtrA] synthesis was calculated by dividing the [MtrC+MtrA] by the *mtr* promoter activity. To provide a relative scale, the efficiencies were normalized so that the maximal efficiency was 1.

3.10.5. Immunoblotting to detect CcmE.

Overnight cultures (45 ml) were centrifuged at 4000 rcf for 15 min at 4°C. The supernatant was removed and the pellets were frozen for later use. Pellets were thawed and resuspended in 10 mM HEPES (pH 7.4), 1 mM phenylmethylsulfonyl fluoride, 4.2 mM $MgSO_4$ and 0.02 U/μl DNase. Cells were lysed using EmulsiFlex-C3 cell homogenizer (Avastin, Ottawa, ON, Canada). Cells were processed at 18,000 psi, and non-lysed cells were removed by centrifugation at 1,000 rcf 15 min at 4°C. Crude membrane fractions were isolated by centrifugation at 100,000 rcf for 2 h at 4°C. Cell pellets were washed with 35 ml 10 mM HEPES (pH 7.4) and re-centrifuged as above, and the resulting pellet was solubilized in 1 ml B-Per (Thermo Scientific, Rockford, IL). Total protein content was determined using a Pierce BCA Protein Assay Kit (Thermo Scientific, Rockford, IL) and 2-5 ug of protein was mixed with Laemmili Sample Buffer, heated for 5 min at 95°C, and resolved by SDS-PAGE. The proteins were then transferred to a nitrocellulose membrane (*Bio-Rad*, Richmond, CA). Blocking and antibody dilutions were performed using 100 mM Tris, 140 mM sodium chloride (pH 8), 5% (w/v) non-fat powdered milk, and 0.3% (w/v) Tween-20. The primary antibody, a rabbit antisera to *E. coli* CcmE (gift from Stuart Ferguson) and the secondary antibody, Goat-anti rabbit-Peroxidase (Sigma, St. Louis, MO), were diluted 1/10,000 and 1/20,000, respectively. Development was performed using SuperSignal West Dura Substrate (Pierce, Rockford, IL). Blots were quantified using the ChemiDoc™ XRS+ System and software (*Bio-Rad*, Richmond, CA).

3.10.6. Electrochemistry.

Cultures were grown in flasks as described above. From each 50 mL culture, 40 mL was centrifuged at 7,000 rcf for 8 min at 4°C. The pellets were washed twice with 40 mL of sterile minimal M4 medium consisting of per L: 0.221 g K_2HPO_4, 0.099 g KH_2PO_4, 0.168 g $NaHCO_3$, 1.189 g NH_4SO_4, 7.305 g NaCl, 1.192 g HEPES, 10 mL $CaCl_2$ stock solution and 10 mL trace mineral solution. The trace mineral solution consisted of, per liter deionized water: 2.26 g Na_2EDTA; 24.89 g $MgSO_4 \cdot 7H_2O$; 0.029 g $MnSO_4 \cdot 4H_2O$; 0.058 g NaCl; 0.068 g $FeCl_2$; 0.065g $CoCl_2$; 0.029 g $ZnSO_4 \cdot 7H_2O$; 0.005 g $CuSO_4 \cdot 5H_2O$; 0.35 g H_3BO_3; 0.08 g Na_2MoO_4; 0.119 $NiCl_2 \cdot 6H_2O$; 0.028 Na_2SeO_4. The $CaCl_2$ stock consisted of 7.13 g $CaCl_2 \cdot 2H_2O$ dissolved in 1 L deionized water. Pellets were resuspended in 10 mL of minimal M4 medium. The OD_{600} was measured for each resuspension, and an equivalent of 10 mL of OD_{600} = 1.3 was inoculated into sterile bioreactors containing 350 mL minimal M4 medium with 40 mM L-lactate.

The bioreactors contained a three-electrode electrochemical system with a working electrode maintained at 0.2 V vs Ag/AgCl (sat' KCl) using a potentiostat (VSP, BioLogic USA, Knoxville, TN). The working electrode consisted of a 9 cm square piece of graphite cloth (PANEX ® 30 - PW06, Zoltek Corp, St Louis, MO) attached to a graphite rod with carbon cement. The counter electrode consisted of a graphite rod, and an in-house made Ag/AgCl (sat'd KCl) reference electrode was used. The bioreactors were maintained anaerobically by constant sparging with sterile N_2 gas, stirred at ~250 rpm with magnetic stirbars and maintained at 30°C using a recirculating water heater (VWR Scientific, Radnor, PA) connected to bioreactor water jackets. Current production was measured over several days, and lactate consumption was measured by HPLC at the end of the experiment. A Waters HPLC system was used with an Aminex HPX-87H column and 5 mM H_2SO_4 as the eluent. Analytes were detected using a refractive index detector.

Chapter 4

Electron transfer across the inner membrane is a key determinant of function and fitness in metal-reducing *Escherichia coli.*

4.1. Introduction

We seek to reconstitute efficient extracellular electron transfer in *E. coli* such that the vast majority of electrons traverse a single pathway. Previously, we have shown that expressing the partial pathway, MtrCAB, in *E. coli* gives the cells the ability to reduce iron and anodes in anaerobic conditions (*92*, *148*), albeit ~100x slower than *S. oneidensis* MR-1. We also identified that NapC, an inner membrane tetraheme cytochrome *c*, is capable of reducing MtrA in the native system (*148*). However, when NapC was absent, other proteins native to *E. coli* were able to donate electrons to MtrA (Figure 2-6, Pg 36). Here we used knockouts in the *E. coli* strain BL21(DE3) to further investigate what additional native inner membrane electron transfer proteins are capable of donating electrons to MtrA. Specifically, we investigated the effect of inner membrane pentaheme cytochromes *c* TorC and TorY; we additionally investigated iron-sulfur protein, NrfCD, due to the sequence homology to SirCD, which were found to functionally replace CymA in *Shewanella* (*71*). These knockouts were tested for iron reducing ability and changes in biomass with and without the expression of MtrA.

Proteins that have coevolved to interact with each other have specific structural features that allow them to dock with each other with high affinity. Thus, replacing one of the proteins, even with a close homologue, is likely to disrupt their ability to bind each other. We postulated that by expressing CymA with MtrA would greatly enhance Fe(III) citrate reduction rate and fitness under DMR conditions. Thus we engineered a strain expressing both CymA and MtrA. CymA is an inner membrane tetraheme cytochrome *c* that confers respiratory flexibility in *Shewanella* (*63*). Recently, more information has become available on the structure (*186*) and function (*40*, *62*) of CymA as a menaquinol dehydrogenase. It had been previously observed that CymA alone gave *E. coli* the ability to respire iron (*64*). Additionally, it was reported that CymAMtrA expressing *E. coli* strains reduce Fe(III) NTA slightly better than CymA strains alone (*72*). However, here we carefully assess relative CymA concentrations in a *cymA* and a *cymAmtrA* strain to better decipher what the role is of each protein in iron reduction and cell growth.

In this chapter, I investigate the ability of both *E. coli* and *S. oneidensis* inner membrane proteins to donate electrons to MtrA. The absence of select *E. coli* inner membrane electron transfer proteins results in different phenotypes, demonstrating different affects on strain fitness and iron reduction rate. Specifically, we found that CymA homologues TorC and TorY are not significant donors to MtrA, but that a completely different class of electron transfer proteins, NrfBCD, does significantly contribute both to iron reduction rate and cell survival. I have also shown that CymA is a critical addition to alleviate the previously observed electron rate limiting step at the inner membrane (Section 2.5). Additionally, a strong positive correlation between cell biomass and the iron reduction rate was apparent. These findings demonstrate the

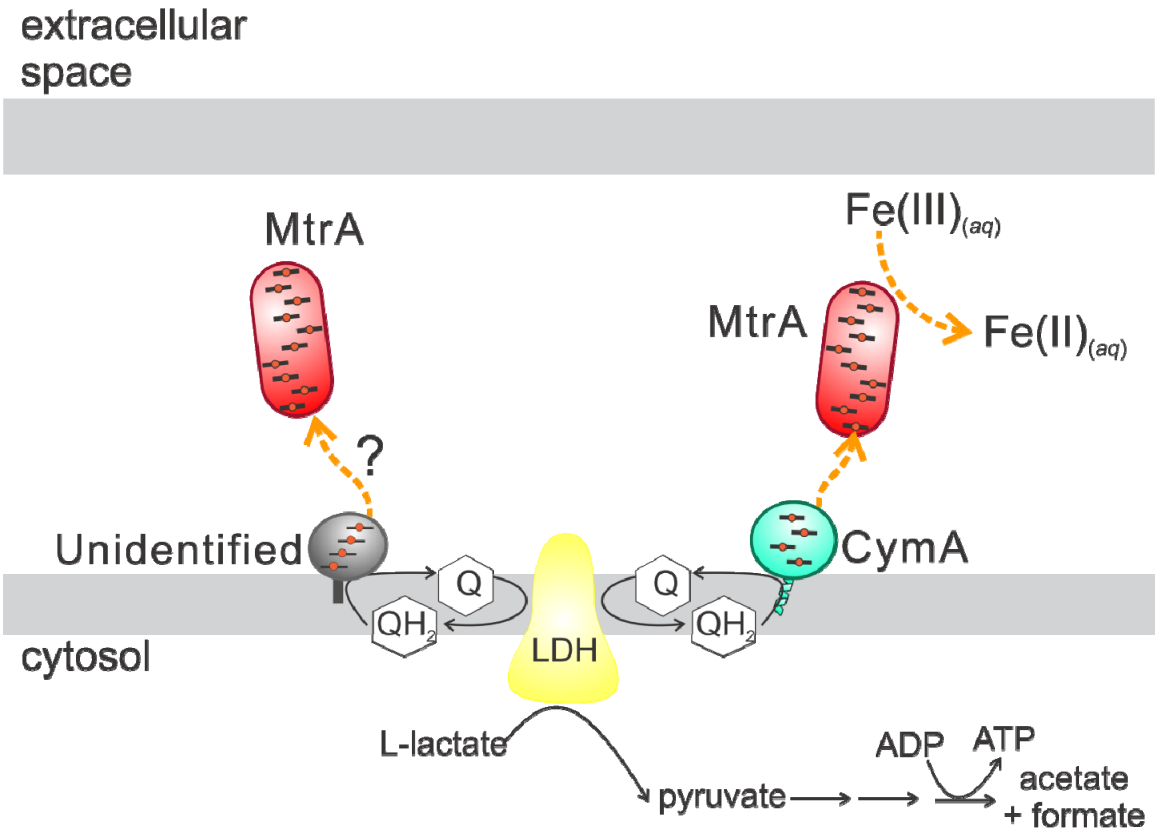

Figure 4-1. Transferring electrons from the inner membrane proteins to MtrA is the rate limiting step in the BL21(DE3) *mtrA* strain. In this chapter, I seek identify native *E. coli* proteins (grey) which functionally substitute for CymA by reducing MtrA in an *mtrA* strain. This is a vital step in donating reducing equivalents from the quinol pool (QH_2) to MtrA (red). This chapter also highlights the importance of adding CymA (cyan) to the engineered strain for increasing both function and biomass in soluble iron reducing conditions.

importance of matching coevolved protein interactions when designing an extracellular electron transfer pathway in a heterologous host, and it highlights the importance of cell health in the function of the electron conduit. This work further contributes to the potential of electrical communication between different cell types and inorganic materials.

4.2. Elucidating how *E. coli* splices electron transfer from the quinol pool to MtrA in the absence of CymA.

We seek to reconstitute efficient extracellular electron transfer in *E. coli* such that the electrons traverse a single pathway. In wild type *S. oneidensis*, CymA is the primary electron donor to MtrA (*43*), but Cordova and co-workers have recently demonstrated SirCD can functionally substitute for CymA in a Δ*cymA* strain (*71*). In *E. coli*, we previously found that the CymA homologue, NapC, is capable of reducing MtrA (Section 2.6) (*148*). However, since knocking out NapC does not completely arrest reduction of MtrA, other redox-active inner membrane proteins native to *E. coli* must also be able to donate electrons to MtrA (Figure 4-1). Knowing the partners of MtrA in the heterologous host is important for future work in streamlining the pathway. In order to build a molecularly defined route in another organism, one must know all the possible avenues of the electrons. Additionally, there are certain applications when other such routes must be eliminated, such as engineering an on/off toggle switch for anode reduction. In this section, additional inner membrane redox proteins are investigated for their ability to transfer electrons to MtrA.

4.2.1. Candidates for electron transfer to MtrA in engineered *E. coli*.

We reasoned that *E. coli* inner membrane proteins that are homologous to CymA or SirCD were most likely to serve as electron donors to MtrA in *E. coli*. The primary sequences of CymA and SirCD were analysed for sequence similarity across the *E. coli* genome; the summary of BLAST homology is shown below in Table 4-1 and complete detail is shown in Appendix C. TorY and TorC, pentaheme quinol dehydrogenases involved in anaerobic trimethylamine *N*-oxide (TMAO) respiration (*187–190*), have high sequence homologous to CymA. Likewise, NrfCD is homologous to SirCD (locus numbers SO0483 and SO0484, respectfully), which has been shown to functionally replace CymA in *Shewanella* (*71*) (Table 4-1). Thus, we selected TorC, TorY, and NrfCD as inner membrane electron transfer proteins that might also be capable of donating electrons to MtrA (Figure 4-2). It is also worth noting that NrfD/SirD are unique sequences in both genomes, whereas NrfC/SirC display high homology to many other [Fe-S] proteins.

To determine if NrfCD, TorC, or TorY donate electrons to MtrA, we deleted the corresponding genes in strains carrying *mtrA* and compared their rate of Fe(III) reduction to the original *mtrA* strain. We separately deleted the *nrfCD*, *torY,* and *torC* genes in the BL21(DE3) *E. coli* strain using the Datsenko and Wanner λ-red method (*170*). Because the coding sequence for NrfC overlaps with that of NrfB, *nrfB* was included in the knockout for *nrfCD,* resulting in a *nrfBCD* knockout strain. These knockout strains were then co-transformed with the pEC86 plasmid (*65*) and the previously described *mtrA* plasmid (*148*). We notate these strains as the Δ*gene mtrA* strains. To measure any changes in basal Fe(III) reduction in *ccm*-expressing *E. coli*, we also co-transformed the

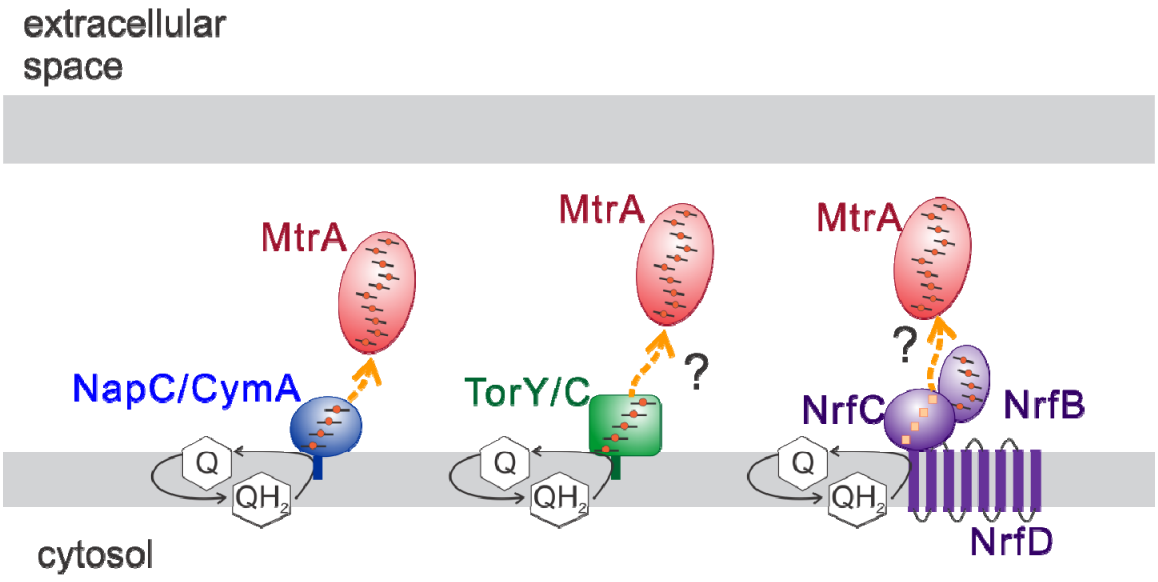

Figure 4-2. TorC, TorY, and NrfCD were identified as potential electron donors to MtrA in *E. coli*. It was discussed in Chapter 2 how NapC (blue) is able to functionally replace CymA in the engineered strain and reduce MtrA (red). In this chapter, I use this same experimental procedure with other deletion strains to identify other *E. coli* proteins capable of reducing MtrA. The pentaheme cytochromes *c* TorY and TorC show high sequence homology to CymA, but have an additional heme that may act as a specific binding site for their respective partners in TMAO respiration. NrfCD (purple) shows high sequence homology to SirCD, which was shown to functionally replace CymA in *Shewanella*.

knockout strains with pEC86 and an empty pET vector, and we refer to these as the Δ*gene ccm* strains.

Table 4-1: Homology of native BL21(DE3) inner membrane cytochromes *c* to CymA, SirC (SO0483), or SirD (SO0484).

Gene	Description	Positives	e-value
napC[1]	Tetraheme inner membrane cytochrome *c*; nitrate respiration	52%	5×10^{-21}
torY[1]	Pentaheme inner membrane cytochrome *c*; TMAO respiration	51%	3×10^{-22}
torC[1]	Pentaheme inner membrane cytochrome *c*; TMAO respiration	46%	7×10^{-20}
nrfC[2]	Predicted 4 [4Fe-4S] inner membrane protein; formate dependent nitrite reductase	58%	8×10^{-47}
nrfD[2]	Predicted inner membrane protein with 8 conserved hydrophobic segments	54%	4×10^{-47}

[1]BLAST performed using EcoGene (http://www.ecogene.org/old/blast.php) with mature protein sequences, i.e. with signal sequence cleaved as predicted by SignalP4.1 (http://www.cbs.dtu.dk/services/SignalP/)
[2]BLAST performed using EcoGene (http://www.ecogene.org/old/blast.php) with full protein sequence.

4.2.2. Fe(III) citrate reduction and biomass are used to measure the impact of native *E. coli* inner membrane electron transfer proteins.

In MtrA-containing *E. coli*, the re-reduction of MtrA is the rate-limiting step in Fe(III) citrate reduction (Section 2.5 and Ref (*148*)). Thus, strains which are impaired in their ability to donate electrons to MtrA also have lower rates of Fe(III) reduction (*148*). To test the iron reduction, we added 40 mM D,L-lactate as the carbon source and 10 mM Fe(III) citrate as the sole terminal electron acceptor to cells under anaerobic conditions at a fixed cell density ($OD_{600\ nm} = 0.5$). The Fe(II) concentration was measured as a function of time using the ferrozine assay (*168*). We anticipate that respiration of Fe(III) citrate should be the only means of energy generation available to *E. coli* under these experimental conditions. Therefore, we probed survival of these strains by monitoring the cell density of these cultures *via* their optical density at 600 nm ($OD_{600\ nm}$).

As shown in Figure 4-3A, both the *ccm* (hollow black circles) and *mtrA* (filled black circles) strains gradually reduced Fe(III) citrate. The *mtrA* strain produced Fe(II) 1.8x more rapidly than the *ccm* strain (Table 4-3A). These rates are higher than previously discussed in Chapter 2 for the *ccm* and *mtrA* strains (~2.5x and ~2x, respectively, Figure 2-4 (*148*)), which we suggest is due to using a more highly supplemented media in these assays. The cell density of the *ccm* and *mtrA* cultures also steadily decreased over the course of the experiment (Figure 4-3B), which suggests that the strains are respiring with Fe(III) citrate too slowly to generate enough energy to survive. However, the cell density of the *mtrA* culture decreased ~80% more slowly the *ccm* strain (Figure 4-3B and Table 4-2), indicating that expressing MtrA slightly improves *E. coli* survival when Fe(III) is the sole terminal electron acceptor.

A condition of interpreting the iron respiration in the knockout strains is that the knockout expressing *ccm* must not significantly differ from the BL21(DE3) *ccm* strain. Only if this is true can we interpret changes in the MtrA-containing strains as a result

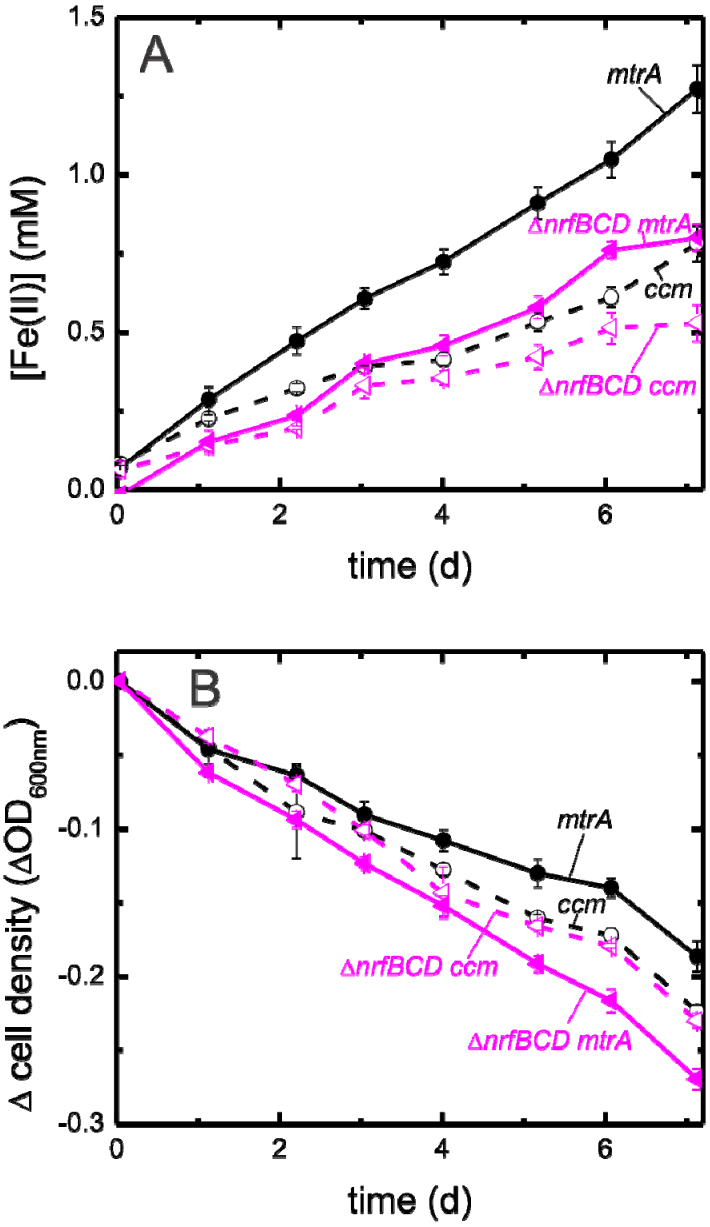

Figure 4-3. Deletion of NrfBCD slows Fe(III) reduction and reduces cell survival in MtrA-expressing *E. coli*. (A) Fe(II) concentration as a function of time for the *ccm* (open black circles), *mtrA* (filled black circles), Δ*nrfBCD ccm* (open magenta triangles), and Δ*nrfBCD mtrA* (filled magenta triangles) strains. Fe(III) reduction in the Δ*nrfBCD mtrA* strain occurs at a rate similar to Δ*nrfBCD ccm*, indicating that NrfBCD is a significant electron donor to MtrA. (B) Change in cell density over time for the *ccm*, *mtrA*, Δ*nrfBCD ccm*, and Δ*nrfBCD mtrA* strains. The cell density of the Δ*nrfBCD mtrA* decreases more sharply over time than the *mtrA* strain, demonstrating that NrfBCD is necessary for MtrA to improve cell survival.

from the MtrA-inner membrane interaction, as opposed to inner membrane protein Fe(III) reduction or unintentional/unexpected genomic changes from the knockout procedure. Thus, it can be inferred that if the difference between knockout-*ccm* and knockout-*mtrA* is less than that the difference between *ccm* and *mtrA*, that the knocked out protein is a donor of electrons to MtrA in the WT heterologous system. However, if there is a shift in the knockout-*ccm* relative to WT-*ccm*, then you must also consider how that knocked out protein is directly interacting with Fe(III) citrate and other normal cellular processes.

4.2.3. NrfBCD, but not TorC or TorY, is a substantial electron donor to MtrA in *E. coli* and is necessary for MtrA-dependent cell survival.

Interestingly, Δ*nrfBCD mtrA* strain (filled magenta triangles, Figure 4-3A) showed a significantly decreased Fe(III) reduction rate relative to the *mtrA* strain. Indeed, the Δ*nrfBCD mtrA* and Δ*nrfBCD ccm* (hollow magenta triangles), and *ccm* strains reduced Fe(III) at very similar rates (Table 4-2). These observations demonstrate that NrfCD can reduce MtrA, much like its *S. oneidensis* homologue SirCD (*71*). The change in cell density of the Δ*nrfBCD mtrA* strain is approximately the same as Δ*nrfBCD ccm* (Figure 4-3B and Table 4-2), indicating that the survival benefit conferred by MtrA in *E. coli* is eliminated when NrfBCD are absent. All together, this data suggests that the NrfBCD complex is the predominant electron donor to MtrA and is requisite for an MtrA-conferred improvement in survival in *E. coli.*

Table 4-2: Rates of iron reduction and fitness.

Strain	Function ($\mu M\ day^{-1}$)	Growth/Death Rate ($\Delta A_{600\ nm}\ day^{-1}$)
ccm	89 ± 7	-0.029 ± 0.003
mtrA	162 ± 8	-0.024 ± 0.003
Δ*torY ccm*	94 ± 2	-0.031 ± 0.002
Δ*torY mtrA*	157 ± 22	-0.032 ± 0.002
Δ*torC ccm*	139 ± 17	-0.033 ± 0.002
Δ*torC mtrA*	150 ± 14	-0.021 ± 0.003
Δ*nrfBCD ccm*	69 ± 8	-0.031 ± 0.003
Δ*nrfBCD mtrA*	117 ± 9	-0.035 ± 0.002
cymA	512 ± 23	-0.008 ± 0.004
cymAmtrA	627 ± 62	0.023 ± 0.005

The trends in Fe(III) reduction and cell density the Δ*torY* and Δ*torC* strains were strikingly different from the Δ*nrfBCD* strains. The Δ*torY ccm* and Δ*torY mtrA* strains demonstrated very similar trends in iron reduction (Figure 4-4A), and their overall iron reduction rates were extremely similar to the *ccm* and *mtrA* strains (Table 4-2). These observations indicate that the presence of TorY does not increase electron transfer to MtrA. The cell density of Δ*torY mtrA* culture decreased somewhat more rapidly than the *mtrA* strain (Figure 4-4B), suggesting that TorY somehow contributes to cell survival in the presence of MtrA. The Δ*torC* strains showed subtle, but complex, changes in Fe(III) reduction. The Δ*torC ccm* strain (hollow blue squares, Figure 4-4C) reduced Fe(III) more rapidly than the *ccm* strain (hollow black circles, Figure 4-4C). This difference

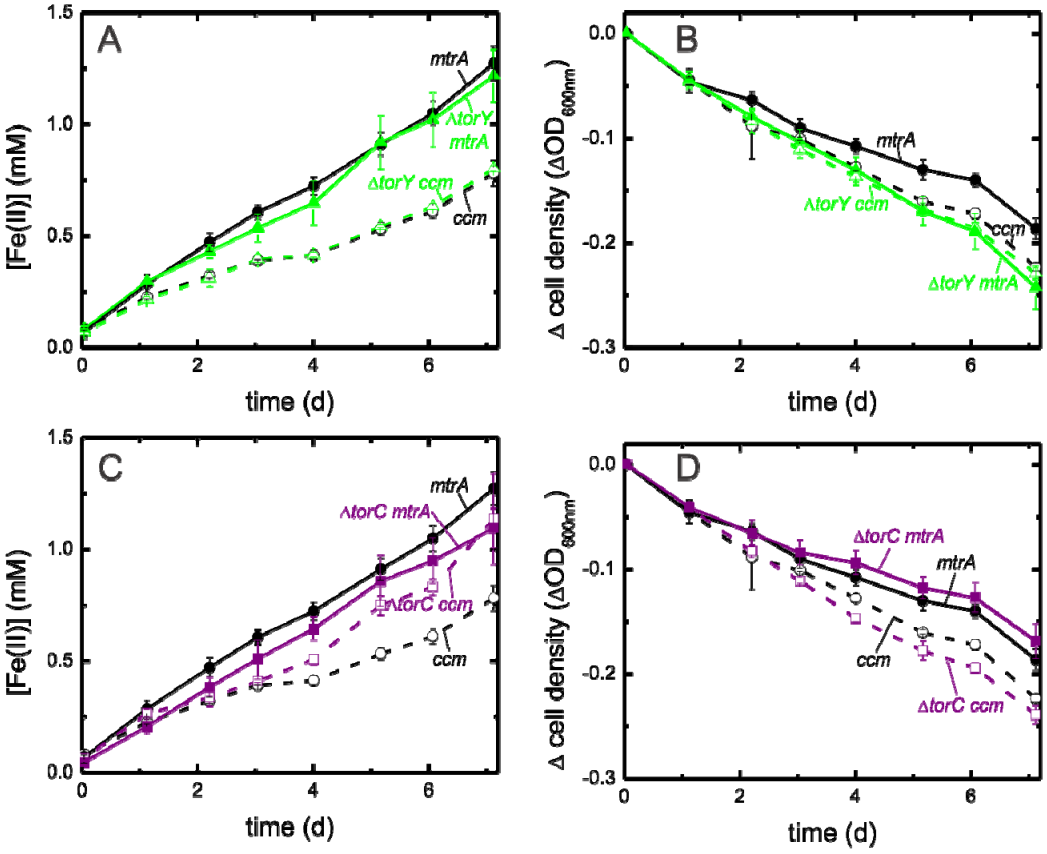

Figure 4-4. Deletion of TorY and TorC does not significantly affect Fe(III) reduction and cell survival in MtrA-expressing *E. coli*. (A) Fe(II) concentration as a function of time for the *ccm* (open black circles), *mtrA* (filled black circles), Δ*torY ccm* (open green triangles), and Δ*torY mtrA* (filled green triangles) strains. Fe(III)citrate is reduced at the same rate in the Δ*torY mtrA* and *mtrA* strains, indicating that TorY is not a significant electron donor to MtrA. (B) Change in cell density over time for the *ccm* (open black circles), *mtrA* (filled black circles), Δ*torY ccm* (open green triangles), and Δ*torY mtrA* (filled green triangles) strains. The cell density of the Δ*torY mtrA* strain decreases more sharply than the *mtrA* strain. (C) Fe(II) concentration as a function of time for the *ccm* (open black circles), *mtrA* (filled black circles), Δ*torC ccm* (open purple squares), and Δ*torC mtrA* (filled purple squares) strains. Fe(III)citrate is reduced more rapidly in the Δ*torY ccm* strain than the *ccm* strain, suggesting that TorY suppresses basal Fe(III) reduction by *E. coli* and limiting further interpretation. (D) Change in cell density over time for the *ccm* (open black circles), *mtrA* (filled black circles), Δ*torC ccm* (open purple squares), and Δ*torC mtrA* (filled purple squares) strains.

suggests that TorC actually reduces the basal Fe(III) reduction, and more critically, indicates that changes in Fe(III) reduction rates in the Δ*torC* strain background will not be solely reflective of changes in MtrA re-reduction. While we do observe changes in Fe(III) reduction and cell density (Figure 4-4D) in the Δ*torC mtrA* and Δ*torC ccm* strains, these differences are not dramatic (Table 4-2) and they are difficult to interpret in light of the significant changes in the basal Fe(III) reduction rate. In the context of our aims, we therefore suggest only that deletion of TorC is unlikely to simplify the route of extracellular electron transfer in MtrA-*E. coli*.

4.3. Expressing CymA improves electron transfer from the quinol pool to the terminal reductase, MtrA.

4.3.1. Design of the *cymA* and *cymAmtrA* strains.

Our previous work showed our MtrA-containing *E. coli* reduced Fe(III) citrate ~30 fold more slowly than *S. oneidensis* MR-1 (*148*) and that re-reduction of MtrA by native *E. coli* proteins was rate-limiting compared to reduction of Fe(III) citrate by MtrA (*148*). Since the inner membrane redox proteins in *E. coli* are present in relatively low abundance under aerobic conditions and have not co-evolved with MtrA, we hypothesized that co-expressing CymA with MtrA would improve extracellular ET rates. In order to better express both cytochromes *c* in *E. coli*, we used the Salis ribosome binding site (RBS) calculator (https://salis.psu.edu/software/) to design the RBS sequences close to native RBS strengths in *Shewanella* (Table 4-3) (*191*). Plasmids were constructed carrying the *cymA* only and *cymAmtrA* genes (Figure 4-5A) (see Methods for additional details). These plasmids were co-transformed the *cymA* and *cymAmtrA* plasmids with the pEC86 plasmid into BL21(DE3) cells to create the *cymA* and *cymAmtrA* strains.

The Salis ribosome binding site (RBS) calculator (*191*) predicted the translational initiation rate with two 16S rRNA sequences for *E. coli* strain BL21(DE3) (Table 4-3). It is as yet difficult to determine which 16S rRNA is the correct predictor in *E. coli* (personal communication, Dr. Salis). Interestingly, the two RNA options gave different ratios of translational strength the RBS sequences used.

4.3.2. The *cymA* and *cymAmtrA* strains express the full-length and redox active cytochromes *c*.

To confirm that full length CymA and MtrA were expressed and are redox active, we analyzed whole cell lysates of the *cymA*, *mtrA*, and *cymAmtrA* strains *via* PAGE and heme staining using enhanced chemiluminescence (Figure 4-5B). The CymA expressing strains (*cymA* and *cymAmtrA*) show a band at the molecular weight of CymA, 18.5 kD. Likewise, the MtrA expressing strains (*cymAmtrA* and *mtrA*) show a band at the molecular weight of MtrA, 35 kD. Thus, CymA and MtrA are both the correct molecular weight and redox active, as the peroxidase stain itself demonstrates redox activity.

The physical arrangement of these proteins is vital to the function of the pathway in *E. coli.* Thus, to confirm that CymA and MtrA were properly localized in *E. coli*, we isolated the periplasmic and membrane fractions of *cymAmtrA* cells and probed these fractions for cytochromes *c*. Heme-c detection with enhanced chemiluminescence showed bands for CymA and MtrA at 21.5 kD and 34 kD, respectively. CymA was only

present in the membrane fraction, whereas MtrA is present in both the periplasmic and membrane fractions (Figure 4-5C), which is consistent with the localization pattern reported for *Shewanella* (*33*, *51*, *62*, *167*). The periplasmic fraction is composed mostly of MtrA while the membrane fraction is a mixture of CymA and MtrA (Figure 4-5C). To determine whether the recombinant CymA and MtrA were redox active, we spectroscopically probed the periplasmic and membrane fractions under oxidizing and reducing conditions. In both samples, the oxidized spectra demonstrate the characteristic

Table 4-3: Calculated RBS strengths using the Salis Lab RBS Calculator (*191*)**.**

Gene (Plasmid)	Sequence[1-4]	16S rRNA[5]	Translation Initiation Rate (*AU*)	ΔG_{total} (*kcal/mol*)
cymA (I5040)	Atcccgcgaaattaatacgactcactatagggga attgtgagcggataacAatccccctcaagaaata attttgttaactttaagaaggagatatacatAt gaactggcgtgcactatttaaacccagcgcgaaa tattccatcctagcgctactggttgttggtatcg tgattggtgttgtgggctattttgcaactc	a	4.0E2	4.1
		b	1.1E4	-3.3
cymA (I5039)	ATCCCGCGAAATTAATACGACTCACTATAGGGGA ATTGTGAGCGGATAACAATTCCCCTCAAGAAATA ATTTTGTTTAACTTTAAGAAGGAGATATACATAT GTTGGAGATAGAGTAATGAACTGGCGTGCACTAT TTAAACCCAGCGCGAAATATTCCATCCTAGCGCT ACTGGTTGTTGGTATCGTGATTGGTGTTGTGGGC TATTTTGCAACTC	a	7.8E2, 1.2E2	2.6, 6.6
		b	2.2E4, 7.7E2	2.6, 6.6
cymA (I5052)	CGACTCACTATAGGGGAATTGTGAGCGGATAACA ATTCCCCTCAAGAAATAATTTTGTTTAACTTTAA GAAGGAGATATACATATTTTGGAGATAGAGTAAT GAACTGGCGTGCACTATTTAAACCCAGCGCGAAA TATTCCATCCTAGCGCTACTGGTTGTTGGTATCG TGATTGGTGTTGTGGGCTATTTTGCAACTC	a	6.8E2	2.9
		b	4.1E3	-1.1
cymA, Shewie	AATCGGCATTTTTAGGCTTGAAATCAAACTTCTA ATAAATAAAAAAACATAAAATAGTCTTATAAAAA CTGACTTTGACAATATTTTTGGAGATAGAGTAAT GAACTGGCGTGCACTATTTAAACCCAGCGCGAAA TATTCCATCCTAGCGCTACTGGTTGTTGGTATCG TGATTGGTGTTGTGGGCTATTTTGCAACTC	b	3.5E3	-0.75
mtrA (I5023)	ATCCCGCGAAATTAATACGACTCACTATAGGGGA ATTGTGAGCGGATAACAATTCCCCTCAAGAAATA ATTTTGTTTAACTTTAAGAAGGAGATATACATATT GGAACTCAAGAACTGCCTAAAAATGAAAAACCTA CTGCCGCACTTACCATCACAATGGCAATGTCTGC AGTTAATGGCATTAGTCGTCACACCAAACGTTATG	a	3.8E3	-0.9
		b	1.0E5	-8.3
mtrA (I5052)	CAAAAGGATAAGGTTTAACGCTGCAAGAATTCTT TGCCCAAGCAGGGGGAGCTCGCTCCCCCTTTCTT GAATTTTGTTGGGACAAATTGGGAAGCCTATTTAT GAAGAACTGCCTAAAAATGAAAAACCTACTGCCG GCACTTACCATCACAATGGCAATGTCTGCAGTTA TGGCATTAGTCGTCACACCAAACGTTATG	a	1.5E3	1.1
		b	6.7E3	-2.2
mtrA, Shewie	CAGTTGCAGATCACACTAAAGTGAAAATGTAATT TGCCCAAGCAGGGGGAGCTCGCTCCCCCTTTCTT GAATTTTGTTGGGACAAATTGGGAAGCCTATTTAT GAAGAACTGCCTAAAAATGAAAAACCTACTGCCG GCACTTACCATCACAATGGCAATGTCTGCAGTTA TGGCATTAGTCGTCACACCAAACGTTATG	b	6.7E3	-2.2

[1]Underlined sequence annotates an NdeI restriction site containing an ATG start codon, shown in red.
[2]Orange sequence annotates the RBS of the pET vector
[3]Blue sequence annotates the RBS of the respective *Shewanella* genes in the genome
[4]The original ATG start codons of *cymA* and *mtrA* are shown in green and purple respectively
[5]The code for the 16S rRNA are as follows, where (a) and (b) are for *E. coli* and (b) is for *Shewanella*: (a) TAACCGTAG and (b) ACCTCCTTA.

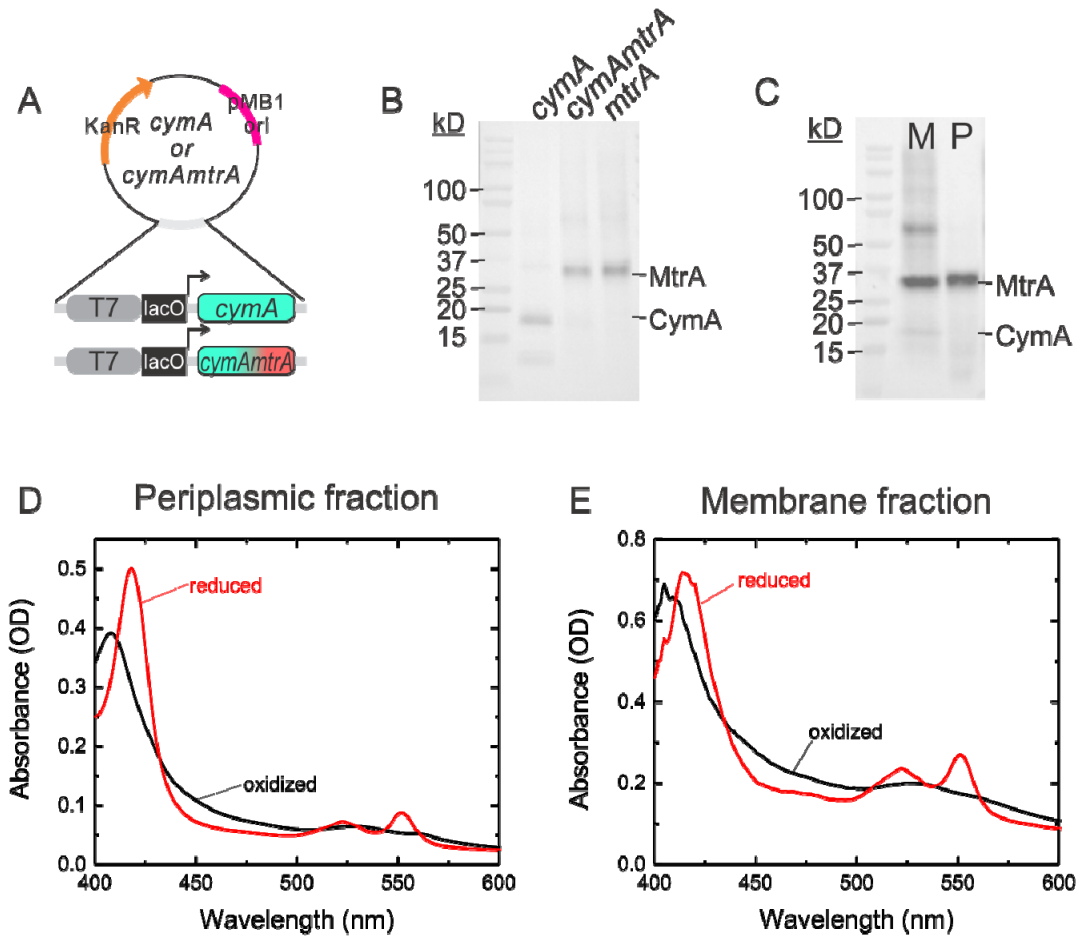

Figure 4-5. Co-expression of full length, redox active CymA MtrA in *E. coli*. (A) The plasmid schematic of the *cymA* and *cymAmtrA* plasmids. (B) Heme staining of whole cell lysates of the *cymA*, *cymAmtrA*, and *mtrA* strains. Samples were loaded normalized to total protein loaded (8 µg). Staining was performed with enhanced chemiluminescence, as described in the text. (C) Heme staining of the periplasmic fraction (P) and membrane fraction (M) of the *cymAmtrA* strain after separation by SDS–PAGE. Consistent with their localization in *S. oneidensis*, CymA is abundant in the membrane fraction, while MtrA is abundant in the periplasmic fraction. (C-D) The absorbance spectra of the periplasmic fraction (D) and membrane fraction (E) of the *cymAmtrA* strains show the characteristic peaks of low spin hemes in cytochromes *c*. The air oxidized samples are shown in black while the sodium dithionite reduced samples are shown in red. The membrane fraction spectra were taken with a 1 cm pathlength cuvette by diffuse reflectance, decreasing the scattering from the Triton X-100 in the sample.

Soret peak at 408 nm and broad α/β peak at 520-570 nm (black line, Figure 4-5D,E). When reduced, the spectra of the periplasmic and membrane fractions (red line, Figure 4-6D,E) showed the characteristic shift of the Soret peak to 418 nm and the distinct α and β peaks at 523 nm and 552 nm, respectively, indicating that both CymA and MtrA are redox active. The 630 nm band typical of high spin hemes, which is expected from CymA (*62*), was not observable; we attribute this to the fact that the extinction coefficient is very low (3 mM^{-1} cm^{-1}) and the relatively low concentration of CymA in the sample.

To determine the role of each CymA and MtrA in Fe(III) citrate reduction, we sought to determine the relative concentration of CymA in the *cymA* and *cymAmtrA* strains. A combination of diffuse reflectance to measure overall heme *c* concentration per cell and the ratio of the protein band intensities as observed by peroxidase staining was used to estimate the concentrations of CymA and MtrA per cell in the *cymAmtrA* strain. Diffuse reflectance of whole cells was used to quantify the total amount of heme *c* in the *cymA* and *cymAmtrA* strains using the extinction coefficient of 28 mM^{-1} cm^{-1} (*51*); over 3 measurements, the total cellular heme content was calculated to be 101 ± 4, 202 ± 1, and 190 ± 75 $\mu M/OD_{600\ nm}$ in the *cymA*, *cymAmtrA*, and *mtrA* strains, respectively (Table 4-4). Equal total protein (8 μg) of whole cell lysate of the *cymA*, *cymAmtrA*, and *mtrA* strains was analyzed on SDS-PAGE by enhanced chemiluminescence (Figure 4-5B). The CymA band intensity shows that the *cymA* only strain expresses more CymA per cell than the *cymAmtrA* strain. Because both CymA and MtrA contribute to the 552 nm α-band, it is necessary to know the ratio of MtrA to CymA to determine the concentration of CymA in the *cymAmtrA* strain. ImageJ was used to quantify the band intensity, and the densitometric volumes of the CymA and MtrA bands. Assuming that each heme contributes equally to the staining, the ratio of MtrA to CymA in the *cymAmtrA* strain is 3.8. Using this ratio and the total heme *c* concentration, the concentration of MtrA and CymA was calculated with the extinction coefficients at 552 nm of 104 mM^{-1} cm^{-1} (personal communication, Dr. Julea Butt) and 280 mM^{-1} cm^{-1} (*51*) for CymA and MtrA, respectively (Table 4-4). Overall, because there is a greater concentration of CymA per cell in the *cymA* only strain, any affect that CymA has on its own in cell growth or iron reducing rate will be slightly stronger in the *cymA* only strain.

Table 4-4: Concentrations of heme *c*, CymA, and MtrA determined by diffuse reflectance and densitometry analysis of SDS-PAGE ECL staining.

Strain	[heme *c*]* ($\mu M/OD_{600\ nm}$)	Band Volume		[CymA]* ($\mu M/OD_{600\ nm}$)	[MtrA]* ($\mu M/OD_{600\ nm}$)
		CymA	MtrA		
cymA	101 ± 4	6573	n/a	27 ± 1	n/a
cymAmtrA	202 ± 1	850	8048	~5	~18
mtrA	190 ± 75	n/a	11483	n/a	19 ± 8

*The [heme *c*] was calculated as previously described from diffuse reflectance with ε_{552nm} of 28 $mM^{-1}cm^{-1}$. The [CymA] and [MtrA] was calculated with ε_{552nm} of 104 $mM^{-1}cm^{-1}$ and 280 $mM^{-1}cm^{-1}$, respectively, using the total heme content and per-heme band volume.

4.3.3. Expressing CymA with MtrA dramatically increases iron reduction rates and cell fitness in *E coli*.

We next tested the *cymA* and *cymAmtrA* strains for their iron reducing ability and survival (biomass) under anaerobic conditions as described above. By comparing the

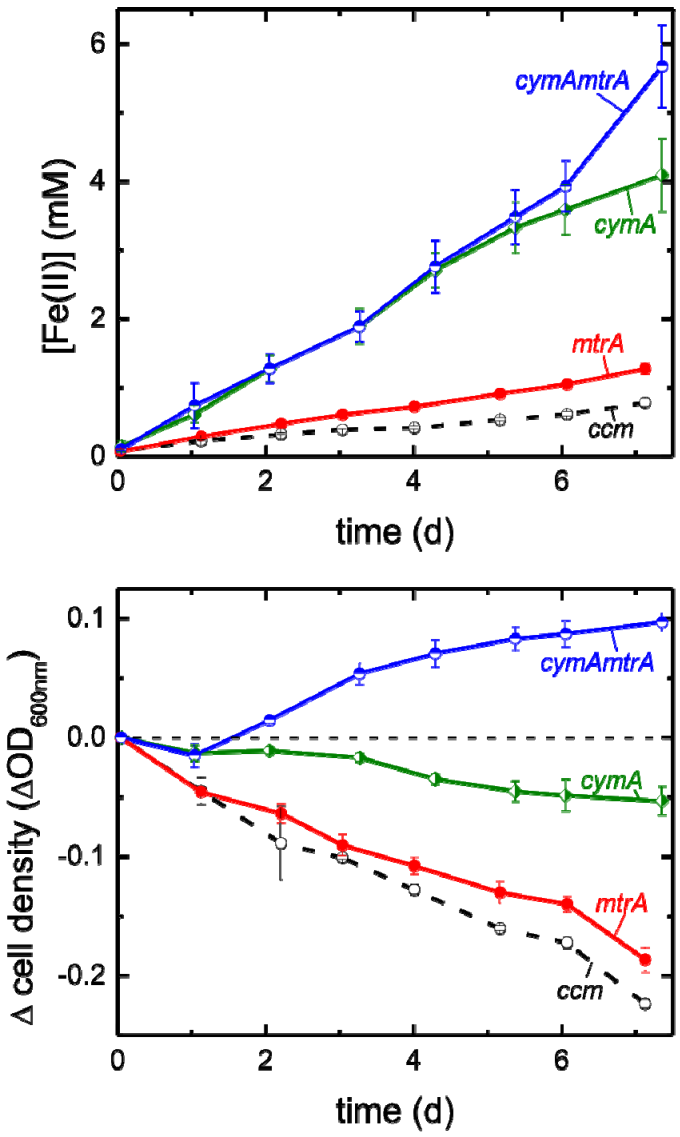

Figure 4-6. Expression of CymA in *E. coli* dramatically improves iron reduction and fitness in Fe(III) citrate reducing conditions. (A) Fe(II) concentration as a function of time for the *ccm* (open black circles), *mtrA* (closed red circles), *cymA* (half filled green circles), and *cymAmtrA* (half filled blue circles) strains. The *cymA* and *cymAmtrA* strains reduce Fe(III) citrate ~6x and ~7x faster than the *ccm* strain. (B) Change in cell density over time for the *ccm* (open black circles), *mtrA* (closed red circles), *cymA* (half filled green circles), and *cymAmtrA* (half filled blue circles) strains. The *cymAmtrA* strain is the only strain to grow under Fe(III) reducing conditions.

Figure 4-7. *cymAmtrA* was able to completely clear the Fe(III) citrate from the media. Clearing of Fe(III) citrate by the *cymAmtrA* culture (left) versus heat killed sample (right). None of the other strains described previously have ever shown complete clearing of Fe(III) citrate from the media.

cymA and *cymAmtrA* strains, we may differentiate the effects of CymA as an Fe(III) reductase versus the ability of CymA to reduce MtrA (Figure 4-8). Ideally, the two strains would have equal concentrations of CymA per cell; however, the *cymA* only strain has about 5x more holo-CymA than the *cymAmtrA* strain. Thus any behavior observed in the *cymA* strain would be inherently more pronounced than in the *cymAmtrA* strain.

The *cymA* strain increased the iron reduction rate over the *ccm* and *mtrA* strains by ~6x and ~3x, respectively (half filled green diamond, Figure 4-6A). However, the cell density of the *cymA* culture decreased ~30% more slowly the *ccm* strain (half filled green diamond, Figure 4-6B). The *cymAmtrA* strain increased the iron reduction rate over the *ccm* and *mtrA* strains by ~7x and ~4x, respectively (half filled blue circles, Figure 4-6A); the iron reduction rates of the *cymA* and *cymAmtrA* strains are statistically similar (two-sided t- test, $p = 0.059$). Moreover, the *cymAmtrA* strain increases in biomass (half filled blue circles, Figure 4-6B), whereas the *cymA* strain (half filled green circles, Figure 4-6B) biomass slowly decreases over time. Additionally, the *cymAmtrA* strain cleared the Fe(III) citrate from the culture completely, which to date had not been observed in any other cytochrome expressing strain in our lab (Figure 4-7).

Taken together, this data shows that less CymA is necessary for the same amount of iron reduction in the presence of MtrA, and the expression of CymA improves iron reducing capabilities in *E. coli*. Thus we found that expressing the native *Shewanella* inner membrane cytochrome *c* CymA in addition to MtrA is helps to alleviate the rate limiting step of electron transfer at the inner membrane.

4.4. Discussion.

4.4.1. NrfCD is a significant electron donor to MtrA in the engineered *E. coli* strain, while the cytochromes TorY and TorC are not.

NrfCD, an integral membrane protein complex with each protein predicted to contain four [4Fe-4S] clusters (*192*, *193*), is homologous to SirCD (*71*). NrfD, a predicted integral membrane protein with 8 transmembrane domains, is complexed with NrfC, predicted to contain four [4Fe-4S] clusters (*192*, *193*). The *nrfBCD* knockout was the only knockout strain in this study to show significant impact on iron reduction (Table 4-2 and Figure 4-3A). Additionally, the Δ*nrfBCD mtrA* strain cell density declined the fastest (Table 4-2 and Figure 4-3B), indicating the increased fitness advantage conferred by MtrA is eliminated when NrfBCD are absent. Taken together, our data indicates that NrfBCD is a significant electron donor to MtrA. This observation substantiates claims made by Cordova et al. that the NrfCD homologues in *Shewanella*, SirCD, functionally replace CymA in certain respiration pathways (*71*).

On the other hand, TorY and TorC were found to not significantly donate electrons to MtrA (Figure 4-4). TorY and TorC are pentaheme cytochromes *c* which function as quinol dehydrogenases in trimethylamine *N*-oxide respiration (*187–190*). Although in the NirT/NapC family, these proteins are structurally distinct from CymA and NapC in that they have a tetraheme N-terminus and a monoheme C-terminus (*194*). The N-terminus region interacts with the quinol pool and is the region homologous to CymA (Table 4-1); the C-terminus region binds and transfers electrons to the TMAO reductase TorA (*188*, *194*). I speculate that this conserved difference between NapC/NirT family proteins and TorY/TorC blocks the interaction between TorY/TorC and MtrA due

to specific binding affinity to the periplasmic partner TorA. We found that, unlike NapC, TorC and TorY do not improve the rate of re-reduction of MtrA, and are thus not important in the context of simplifying expression of an electron conduit.

4.4.2. CymA is a critical component for efficient electron transfer in heterologous extracellular electron conduits.

CymA was previously shown to act on its own as an Fe(III) reductase when overexpressed in *E. coli* (*64*). Thus to specifically investigate the interaction between CymA and MtrA, we designed both a *cymA* and a *cymAmtrA* strain. In the iron citrate respiration experiment, the *cymA* strain would reduce Fe(III) *via* CymA (Figure 4-8). The *cymAmtrA* strain could reduce Fe(III) by either CymA or by MtrA (Figure 4-8). Thus by the changes between these two strains, we may deduce what role CymA and MtrA have in the electron transfer pathway and whether the expression of CymA alleviates the rate limiting electron transfer to MtrA discussed in Section 2.5 (*148*).

The expression of CymA clearly highlights the importance of including the versatile *S. oneidensis* MR-1 quinol dehydrogenase in the heterologous system. The *cymA* strain and *cymAmtrA* strain reduce Fe(III) citrate at similar rates (512 ± 23 and 627 ± 62 μM day^{-1} respectively, Figure 4-6A). The *cymAmtrA* strain increased the Fe(III) citrate reduction rate over the *ccm* and *mtrA* strains by ~8x and ~5x, respectively (Figure 4-6A and Table 4-2). Additionally, the *cymAmtrA* strain cleared the Fe(III) citrate from the culture completely, which to date had not been observed in any other cytochrome expressing strain in our lab (Figure 4-7). The ability of the *cymA* strain to reduce Fe(III) ctirate confirms previous observations in the literature (*64*). The slight increase in iron reduction rate from the *cymA* strain to the *cymAmtrA* strain (~20% increase) suggests that there is a slight advantage to expressing both CymA and MtrA. Additionally, the *cymAmtrA* strain expresses about 2.5x less CymA per cell (Table 4-4), thus one can speculate that the iron reduced by CymA alone would be less pronounced in the *cymA* strain.

Expressing CymA alone increases the fitness of the strain over the *ccm* strain, but does not sustain growth in these conditions (half filled green circles, Figure 4-6B). The *cymAmtrA* strain supported anaerobic DMR growth in the engineered strains for the first time in our lab (half filled blue circles, Figure 4-6B). We speculate that the growth of the *cymAmtrA* strain suggests that MtrA stimulates quinol recycling by CymA; however, this claim is difficult to state definitively from these observations because the two strains do not have equal concentrations of CymA per cell. In the future, I suggest repeating these experiments in the more tunable C43(DE3) *E. coli* strain. In this chapter, I chose to use the "leaky" expression of the BL21(DE3) *E. coli* strain for direct comparison to the knockout strains, which were made in the BL21(DE3) genome. To better elucidate the role of CymA and its interaction with MtrA, one could tune the expression of the *cymA* and *cymAmtrA* plasmids in C43(DE3) to find a set of growth conditions in which the concentration of CymA is equal in the two strains. By repeating these experiments with *cymA* and *cymAmtrA* strains with equal CymA concentrations, one could directly infer the role of CymA in these conditions: if CymA is responsible for the majority of Fe(III) citrate reduction or the interaction between CymA and MtrA increases electron flux to the soluble terminal electron acceptor (Figure 4-8). Additionally, one could perform a series of experiments with increasing concentrations of CymA per cell, which would

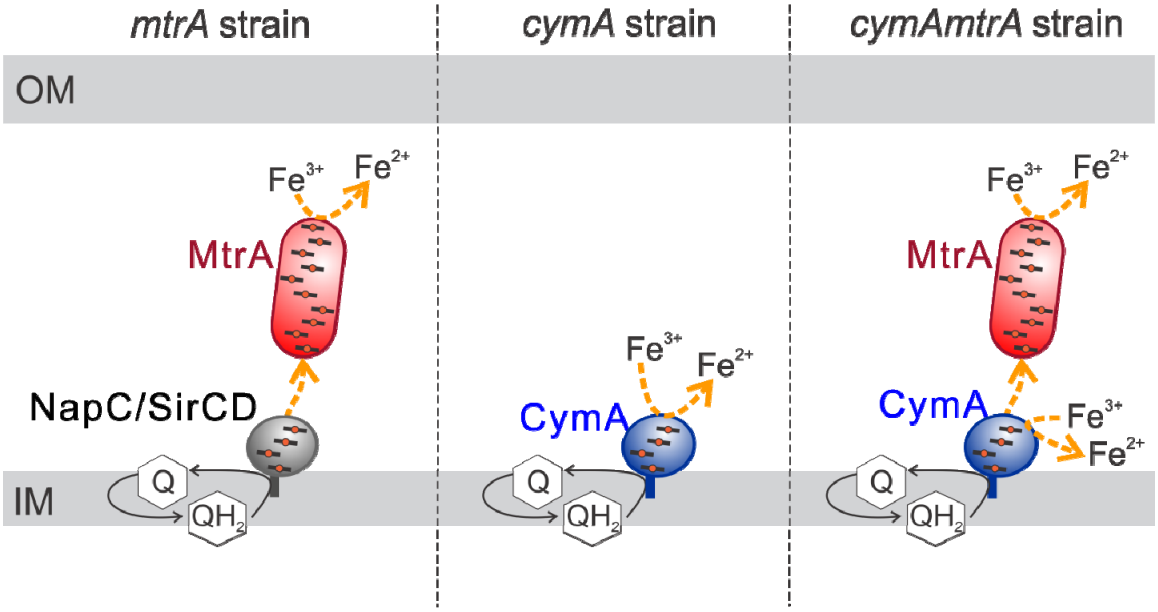

Figure 4-8. Possible terminal iron reductases and protein interactions in the *mtrA*, *cymA*, and *cymAmtrA* strains. To specifically investigate the interaction between CymA and MtrA, we designed both a *cymA* and a *cymAmtrA* strain. In the iron citrate respiration experiment, the *cymA* strain would reduce Fe(III) *via* CymA. The *mtrA* strain (left) relies upon native *E. coli* proteins to donate electrons to MtrA, acting as the terminal Fe(III) reductase. The *cymA* strain (middle) has no periplasmic partner and thus respires Fe(III) with CymA being the terminal reductase. The *cymAmtrA* strain has two potential iron reducates: CymA at the inner membrane and MtrA in the periplasm. The roles of CymA and MtrA and the interaction between these proteins may be deduced by comparing the iron reducing ability of these strains.

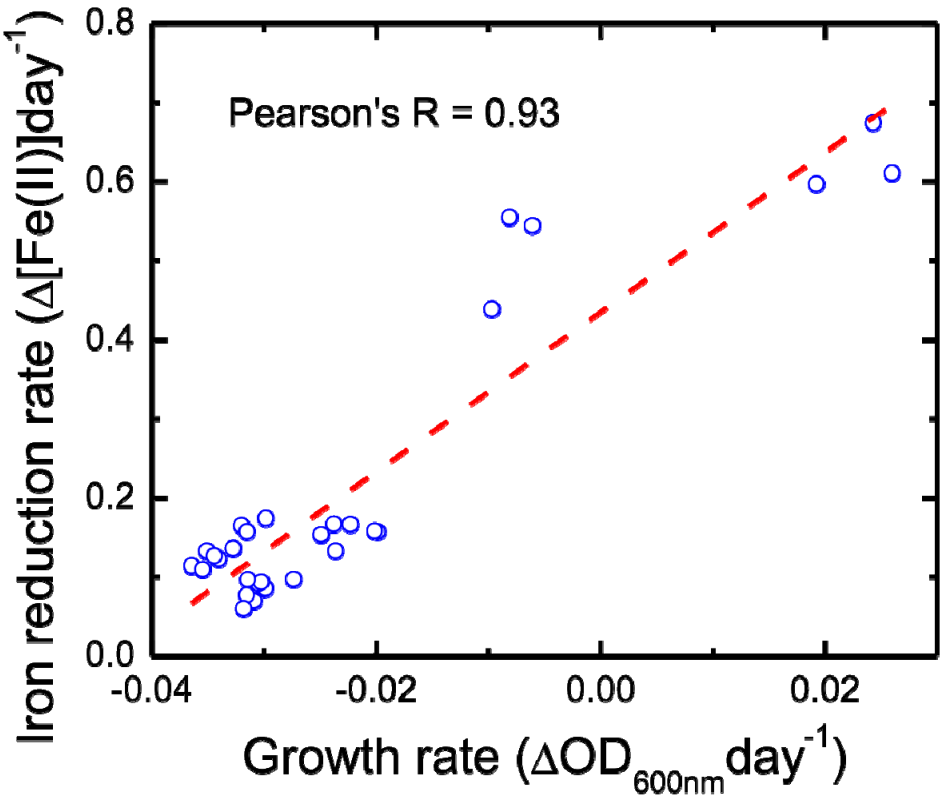

Figure 4-9. Fitness is strongly correlated to iron reduction rate. Iron reduction rates and growth rates of all samples (empty blue circles) were calculated over the linear portion of each experiment. There is a strong correlation (red dashed line, Pearson's r = 0.93) between growth rate and iron reduction rate. The slope of this correlation is 10.1 ± 0.8 Δ[Fe(II)] $\Delta A_{600\ nm}^{-1}$. This correlation highlights that optimizing the connection between the electron conduits and normal cellular metabolism will improve strain fitness, and thus strain function

provide a critical concentration of CymA necessary to perform maximal Fe(III) respiration. Although additional experiments are required to more precisely define the exact role of CymA in the engineered strains, the next chapter will provide additional evidence that the addition of CymA increases electron flux in the electron conduit (Sections 5.4 and 5.7.1). Thus our data finds that expressing the native *Shewanella* inner membrane cytochrome *c* CymA in addition to MtrA is critical to alleviate the rate limiting step of re-reducing MtrA in the engineered *E. coli* strains.

4.4.3. Cell function is strongly, positively correlated to cell fitness in metal-reducing *E. coli* strains.

We designed our experiments such that the only metabolism available to *E. coli* is anaerobic respiration of lactate with Fe(III) citrate as the terminal electron acceptor. Thus we hypothesized that Fe(III) citrate reduction should be correlated with cell survival. To determine quantitatively if function and fitness during Fe(III) citrate respiration are correlated, the linear iron reduction rate was plotted against the linear rate of change in optical density of all cultures reported in Figures 4-3,4,6 and Table 4-2 (open blue circles, Figure 4-9). We find that function and fitness are strongly, positively correlated (dashed red line, Figure 4-9, Pearson correlation coefficient, $p = 0.93$) with a slope of 10.1 ± 0.8 $\Delta[\text{Fe(II)}]\ \Delta A_{600\ \text{nm}}^{-1}$. In previous work, we suggest that expressing too many copies of the *mtrCAB* electron conduits damage the cell membranes (Appendix G), thus inhibiting the anode reducing function (Figure 3-11). However, this work highlights another factor important to electron transfer pathway function: cell health is closely correlated with the function of the Fe(III) reductase. Here, expressing CymA is an example of improving the recycling of the quinol pool, increasing the number of electrons available to reduce iron. Other cellular processes may also be optimized to stimulate more efficient electron transfer, such as increasing the function of the lactate dehydrogenase. Overall this work emphasizes the importance of using the proteins co-evolved in *Shewanella oneidensis* in a heterologous system for efficient electron transfer.

4.5. Materials and Methods.

4.5.1. Plasmids and strains.

The plasmids and strains used in this study are listed in Table 4-5 and Table 4-6, respectively. The *ccm* (pEC86) and *mtrA* (I5023) plasmids were described previously (*148*) and co-transformed into the *E. coli* strain BL21(DE3) (Invitrogen).

The knockout strains BL21(DE3)Δ*torY*, BL21(DE3)Δ*torC*, and BL21(DE3) Δ*nrfBCD* were constructed using the lambda-red knockout system as described by Datsenko and Wanner (*170*). The plasmids used in the gene disruption process, pKD46, pKD3, pKD4, and pCP20, were obtained from the Coli Genetic Stock Center at Yale University. Primers were designed with homology to the regions directly upstream and downstream of *torY* (primers 1, 4), *torC* (primers 2, 5), and *nrfBCD* (primers 3, 6) (Table 4-7). The sequence of *nrfB* was included in the *nrfCD* knockout because the coding sequence of *nrfB* overlaps with that of *nrfC*. These primers were used to amplify a cassette containing either chloramphenicol or kanamycin resistance flanked by FLP recombinase recognition target (FRT) sites off of pKD3 or pKD4, respectively, using Platinum Pfx Polymerase (Invitrogen). The resulting PCR product, containing antibiotic

resistance and FRT sites flanked by regions homologous to the gene locus of interest, was electroporated into BL21(DE3) expressing the λ-red recombinase from pKD46 (induced with 10 mM L-arabinose) to replace *torY*, *torC*, and *nrfBCD*, separately, in the *E. coli* BL21(DE3) genome. Cells were spread on LB-agar plates with the appropriate antibiotic selection and grown at 37 °C. Colony PCR was performed to verify the replacement of each gene with the chloramphenicol or kanamycin resistance gene in the BL21(DE3) genome (Table 4-7; Primers 7 and 10 for *torY*, 8 and 11 for *torC*, and 9 and 12 for *nrfBCD*). Antibiotic resistance was removed by electroporating the new strain with pCP20, which removes the sequence between the FRT sites. After pCP20 inactivation, colony PCR was performed using primers 7-12 (Table 4-7) to verify removal of the chloramphenicol or kanamycin resistance gene. The resulting strains are BL21(DE3)Δ*torY*, BL21(DE3)Δ*torC*, and BL21(DE3)Δ*nrfBCD*. Strains co-transformed the empty modified pET30a+ vector and the *ccm* plasmid, pEC86, are notated as *ccm* strains (e.g. Δ*torY ccm*). The strains expressing both the *ccm* and *mtrA* plasmids are notated as *mtrA* strains (e.g. Δ*torY mtrA*).

Table 4-5: Plasmids used in Chapter 4.

Plasmid	Promoter	Protein coding region	Antibiotic resistance	Source
pSB1ET2 (pET30a+)	T7 lac	none	Kan	Jensen 2010
pEC86	tet	*ccmA-H*	Chl	Arslan 1998
I5024	T7 lac	*mtrA*	Kan	Jensen 2010
I5040	T7 lac	*cymA*	Kan	This chapter
I5052	T7 lac	*cymAmtrA*	Kan	This chapter
pKD46	P_{araB}	λ-red recombinase	Amp	Coli genetic stock
pKD3	NA	NA	Amp, Chl	Coli genetic stock
pKD4	NA	NA	Amp, Kan	Coli genetic stock
pCP20	NA	FLP	Amp	Coli genetic stock

Table 4-6: Strains used in Chapter 4.

Strain	Cell Line	Plasmid(s)	Gene(s)
ccm	BL21(DE3)	pEC86	*ccmA-H*
mtrA	BL21(DE3)	pEC86, I5024	*ccmA-H, mtrA*
cymA	BL21(DE3)	pEC86, I5040	*ccmA-H, cymA*
cymAmtrA	BL21(DE3)	pEC86, I5052	*ccmA-H, cymAmtrA*
Δ*torY-ccm*	BL21(DE3)Δ*torY*	pEC86	*ccmA-H*
Δ*torY-mtrA*	BL21(DE3)Δ*torY*	pEC86, I5023	*ccmA-H, mtrA*
Δ*torC-ccm*	BL21(DE3)Δ*torC*	pEC86	*ccmA-H*
Δ*torC-mtrA*	BL21(DE3)Δ*torC*	pEC86, I5023	*ccmA-H, mtrA*
Δ*nrfBCD-ccm*	BL21(DE3)Δ*nrfBCD*	pEC86	*ccmA-H*
Δ*nrfBCD-mtrA*	BL21(DE3)Δ*nrfBCD*	pEC86, I5023	*ccmA-H, mtrA*

Because of overlapping primary sequence of *nrfB* and *nrfC* in the BL21(DE3) genome, *nrfB* was included in the knockout for *nrfCD,* resulting in a *nrfBCD* knockout

strain. NrfB is a periplasmic pentaheme cytochrome *c* that bridges the inner membrane quinol hydrogenase to NrfA, a periplasmic nitrite reductase (*60*). NrfB is also homologous to the N-terminus half of MtrA (e-value = 6 x10^{-14}).

The *cymA* and *cymAmtrA* plasmids were constructed separately. The *cymA* plasmid was made by amplifying *cymA* from the second codon to the stop codon with primers 13 and 15 (Table 4-7) from the *Shewanella oneidensis* MR-1 genome with Pfx Platinum polymerase (Invitrogen). After digestion with NdeI and EcoRI, the DNA fragment was ligated into the modified pET30a+ vector, pSB1ET2, using T4 DNA ligase (Roche). The start codon for *cymA* in this plasmid is within by the NdeI sequence.

Table 4-7: Primers used in Chapter 4.

Primer	Description	Primer Sequence (5'-3')[1-3]
1	Sense primer, *torY* homology PCR	ATTTAATTATACAATGATTTCGGTGTCCAGTAATT TAATTAGAGGAATCT**GTGTAGGCTGGAGCTGCTTC**
2	Sense primer, *torC* homology PCR	ATTTGCTCATTAAGATCGCTTCACTAAACCATAAT TCTACAGGGGTTATT**GTGTAGGCTGGAGCTGCTTC**
3	Sense primer, *nrfBCD* homology PCR	CAATAACCCCGTTCCGCCTCGCAAGGGGCGGAAAA CACAATGGAGTGAAT**GTGTAGGCTGGAGCTGCTTC**
4	Antisense primer, *torY* homology PCR	ATAAATTCACGTCTTGTTAATGTCATAACTTCCTC CCTGATCAACGAGGA**ATGGGAATTAGCCATGGTCC**
5	Antisense primer, *torC* homology PCR	TTGTGCCAGAAAACGCCGACGTGATGCCTGAAAGA GATCGTTATTGTTCA**ATGGGAATTAGCCATGGTCC**
6	Antisense primer, *nrfBCD* homology PCR	GAAAACCGACTTCAGGAAGGAATACGTCCAGAAAC CACCTCTTTTCTGGC**ATGGGAATTAGCCATGGTCC**
7	Sense primer, *torY* colony PCR	ATTTAATTATACAATGATTTCGGTG
8	Sense primer, *torC* colony PCR	ATTTGCTCATTAAGATCGCTTCACT
9	Sense primer, *nrfBCD* colony PCR	CAATAACCCCGTTCCGCCTCGCAAG
10	Antisense primer, *torY* colony PCR	ATAAATTCACGTCTTGTTAATGTCA
11	Antisense primer, *torC* colony PCR	TTGTGCCAGAAAACGCCGACGTGAT
12	Antisense primer, *nrfBCD* colony PCR	GAAAACCGACTTCAGGAAGGAATAC
13	Sense primer, PCR of *cymA* from *S. oneidensis* MR-1, 2nd-end	CCGCCAT**ATG**AACTGGCGTGCACTATTTAAACCCA G
14	Sense primer, PCR of *cymA* from *S. oneidensis* MR-1, w/ 14 bp upstream	CCGCCATATGTTGGAGATAGAGTA**ATG**AAC
15	Antisense primer, PCR of *cymA* from *Shewanella oneidensis* MR-1	CCGGGAATTCTTGCAGCGTTAAACCTTATCCTTTT GG
16	Sense primer, mutagenesis of NdeI site	AATAATTTTGTTTAACTTTAAGAAGGAGATATACA T***ATT***TTGGAGATAGAGTAATGAAC
17	Antisense primer, mutagenesis of NdeI site	GTTCATTACTCTATCTCCAA***AAT***ATGTATATCTCC TTCTTAAAGTTAAACAAAATTATT
18	Sense primer, PCR of *mtrA* from *S. oneidensis* MR-1, w/ 68 bp upstream	ATATGAATTCTTTGCCCAAGCAGGGGGAGCTCGCT CC
19	Antisense primer, PCR of *mtrA* from *S. oneidensis* MR-1, w/ 68 bp upstream	CCGGTCTAGATTAGCGCTGTAATAGCTTGC

[1]**Bold font**: homologous region to BL21(DE3) genome flanking gene to be knocked out
[2]Underlined: region upstream of *cymA* start codon
[3]***Bold-Italics***: mutation site
[4]**Bold-Underline**: Start codon of *cymA*

For construction of the *cymAmtrA* plasmid, primers containing an NdeI site and an EcoRI site (Table 4-7, Primers 14 and 15) and Pfx Platinum polymerase (Invitrogen) were used to amplify *cymA* from the *Shewanella oneidensis* MR-1 genome, including 14 base pairs upstream from the start codon. After digestion with NdeI and EcoRI (New England Biolabs), the DNA fragment was ligated into the modified pET30a+ vector, pSB1ET2, using T4 DNA Ligase (Roche). The ATG located in the NdeI site was removed to avoid premature transcription of *cymA* by site directed mutagenesis (QuikChange II, Agilent Technologies) using primers 16 and 17 (Table 4-7). Primers containing an EcoRI site and an XbaI site (Table 4-7, Primers 18 and 19) and Pfx Platinum polymerase (Invitrogen) were used to amplify *mtrA* from the *Shewanella oneidensis* MR-1 genome, including 68 base pairs upstream. The EcoRI site in the sense primer is a natural restriction site in the *Shewanella* genome. After digestion with EcoRI and XbaI (New England Biolabs), the *mtrA* DNA fragment was ligated into the pET-*cymA* vector using T4 DNA Ligase (Roche).

The resulting plasmids, *cymA* plasmid (I5040) and *cymAmtrA* (I5052), were co-transformed with pEC86 into BL21(DE3) to make the *cymA* and *cymAmtrA* strains, respectively.

4.5.2. Growth conditions and media composition.

All strains, unless otherwise specified, were grown in 2xYT media at 30 °C with 50 μg mL^{-1} kanamycin; strains containing the ccm plasmid were grown with an additional 30 μg mL^{-1} chloramphenicol. Glycerol stocks were used to inoculate 5 mL media, and cultures were grown overnight at 37 °C with 250-rpm shaking. Then 500 μL of overnight cultures were back-diluted into 50 mL 2xYT media and grown with 200-rpm shaking for 16 h at 30 °C. For periplasmic and membrane fractionations, 5 mL of overnight culture were used to inoculate 1 L media and were grown for 16 h.

Cell suspensions used for Fe(III) citrate reduction assays were resuspended in anaerobic defined M1 media supplemented with 40 mM D,L-Lactate and 0.2% casamino acids. The M1 media consists of 50 mM PIPES (piperazine-*N,N′*-bis(2-ethanesulfonic acid)), 7.5 mM NaOH (final pH 7.4), 28 mM NH_4Cl, 1.3 mM KCl, 4.3 mM $NaH_2PO_4 \cdot H_2O$, 100 mM NaCl, and 10 mL/L each of vitamin, amino acid, and trace mineral 100x stock solutions. The 100x vitamin stock solution contained: 2 mg/L D-biotin (B7), 2 mg/L folic acid (B9), 10 mg/L pyridoxine HCl (B6), 5 mg/L thiamine HCl (B1), 5 mg/L nicotinic acid (B3), 5 mg/mL D-panthothenic acid, hemicalcium salt (B5), 0.1 mg/L cobalamin (B12), 5 mg/L *p*-aminobenzoic acid (PABA), and 5 mg/L α-lipoic acid. The 100x amino acid stock solution (pH 7.0) contained: 2 g/L L-glutamic acid, 2 g/L L-arginine, and 2 g/L D,L-serine. The 100x trace mineral stock solution (pH 7.0) contained: 7.85 mM $C_6H_9NO_3Na_3$, 12.17 mM $MgSO_4 \cdot 7H_2O$, 2.96 mM $MnSO_4 \cdot H_2O$, 17.11 mM NaCl, 0.36 mM $FeSO_4 \cdot 7H_2O$, 0.68 mM $CaCl_2 \cdot 2H_2O$, 0.42 mM $CoCl_2 \cdot 6H_2O$, 0.95 mM $ZnCl_2$, 0.040 mM $CuSO_4 \cdot 5H_2O$, 0.021 mM $AlK(SO_4)_2 \cdot 12H_2O$, 0.016 mM H_3BO_3, 0.010 mM $Na_2MoO_4 \cdot 2H_2O$, 0.010 mM $NiCl_2 \cdot 6H_2O$, and 0.076 mM $Na_2WO_4 \cdot 2H_2O$.

4.5.3. Assaying soluble Fe(III) citrate reduction of live cells.

Cells from 50-mL cultures were pelleted, washed, and resuspended to an $OD_{600\ nm}$ of 0.5 in anaerobic M1 media supplemented with lactate as the carbon source. All

subsequent steps were performed in an anaerobic chamber (Coy Laboratory Products) with an environment of 2% H_2 balanced in N_2. Fe(III) citrate (Sigma) was added to a final concentration of 10 mM, and at the time of addition and subsequent time points, aliquots were removed to determine the optical density at 600 nm and Fe(II) concentration. The Fe(II) concentration was determined with the ferrozine assay, adapted from Stookey (*168*). One aliquot of each culture was acid extracted in 0.5 M HCl for 1 h. An aliquot of each acid extracted sample was then added to the dye, ferrozine (Acros Organics) buffered in 100 mM Hepes, pH 8.0, which absorbs at 563 nm ($\varepsilon_{563\ nm}$ = 27.9 mM^{-1} cm^{-1}) when bound to Fe (II). The absorbance of all samples was recorded at 563 nm with a UV-Vis spectrophotometer (Perkin–Elmer Lambda 35) and was used to determine the change of Fe(II) concentration over time. The concentration of Fe(II) in each culture was subtracted by any abiotic iron reduction observed in sterile media-only controls at each time point. Error bars represent standard deviation by triplicate cultures.

4.5.4. Subcellular fractionation.

Periplasmic and membrane preparations of the BL21(DE3) *cymAmtrA* strain were done as previously described (*148*) in Section 2.9.3. Membrane samples were solubilized in a solution of 5% (w/v) Triton X-100, 50 mM HEPES pH 7.4, and 200 mM NaCl.

4.5.5. Enhanced chemiluminescence (ECL) to detect *c*-type cytochromes in whole cell lysates.

A cell pellet from 1.5 mL of culture was resuspended in 0.1 mL Bacterial Protein Extraction Reagent (B-Per, ThermoScientific). The cells were frozen at -20 ºC immediately after growth and then thawed immediately before analysis. Cells were lysed for 30 minutes at room temperature with lysozyme and DNAse, along with salts necessary for optimal function, to the following final concentrations: 6 μg mL^{-1} chicken egg white lysozyme (Sigma), 1 μg mL^{-1} DNAase, 3.9 mM $MgSO_4$, 0.96 mM EDTA, and 0.98 mM phenylmethylsulfonyl fluoride (PMSF). Total protein of the cell lysates was determined by BCA Protein Assay Kit (ThermoScientific). The appropriate dilution of cells in 100 mM HEPES, pH 7.4, to load a total of 8 μg of protein of whole cell lysate was added to NuPAGE 4x Sample Buffer (Bio-Rad). Samples were heated at 95 °C for 5 minutes and run in a 4-20% Tris-HCl polyacrylamide gel (Bio-Rad) at 200 V for 1 hour. The gel was rinsed twice in water and then equilibrated in cold Pierce Western Transfer buffer (ThermoScientific) for 15 minutes. The proteins were transferred to a 0.45 μm nitrocellulose membrane (Bio-Rad) in Pierce Western Transfer buffer at 30 V for 100 minutes. Ponceau S staining was used to confirm uniform transfer across all lanes.

For the enhanced chemiluminescence staining, the blot was incubated for 5 minutes in 10 mL of Pierce Pico West Enhanced Chemiluminescence substrate (ThermoScientific), a 1: 1 mixture of Pico West Peroxide Solution and Luminol Enhancer solution. The chemiluminescent signal was detected using the ChemiDoc™ XRS system. The chemiluminescent signal and molecular weights were quantified using ImageJ.

4.5.6. Visible spectra of cytochrome samples by dual beam UV-Vis spectroscopy and diffuse reflectance.

Visible spectra of air-exposed periplasmic fraction and membrane fractionation were recorded by dual-beam UV-vis spectroscopy. The membrane fraction spectra were taken with a 1 cm pathlength cuvette by diffuse reflectance, decreasing the scattering from the Triton X-100 in the sample and making background subtraction unnecessary. The oxidized samples were air oxidized. The reduced samples were chemically reduced by adding sodium dithionite crystals (Sigma).

The concentration of cytochromes in live cells was determined by diffuse reflectance as previously described in Goldbeck et. al. (*92*).

Chapter 5

Enhanced entry and exit of electrons through the MtrCAB electron conduit improves survival in metal-oxide reducing *E. coli.*

5.1. Introduction.

The expression and function of the electron transfer pathway spanning the outer membrane, MtrCAB, in *E. coli* has been the focus of the previous chapters (*148*). The previous experiments demonstrated that engineering electron transfer to an extracellular terminal electron acceptor in *E. coli* is possible. This work focuses on techniques to improve the electron transfer rate by optimizing electron entry and exit *via* the heterologous *Shewanella oneidensis* MR-1 pathway. Overall, this chapter focuses on how three separate domains in the electron transfer pathway affect reduction of solid iron oxide: (1) quinol pool recycling by CymA; (2) the number of electron conduits per cell; and (3) soluble redox carriers (Figure 5-1). The first aspect is studied by adding the *cymA* coding sequence to the *mtrCAB* plasmid. The effect of the number of conduits per cell is probed by induction of the T7 *lac* operon by IPTG in the *mtrCAB* only strain as well as the *cymAmtrCAB* strain. Finally, the effect of redox carriers was studied by supplementing cultures with riboflavin.

The outer membrane spanning electron transfer pathway in the *mtrCAB* strain relied upon native *E. coli* proteins at the inner membrane to initiate electron transfer to MtrA. Chapter 4 demonstrated that the addition of CymA to the metal reducing *E. coli* strain improved both soluble iron reducing capability as well as *E. coli* viability in soluble iron reducing conditions. This crucial addition alleviated the electron transfer rate limiting step from the inner membrane to MtrA identified in Chapter 2. Thus, I hypothesized that expressing CymA in *mtrCAB* expressing strains during solid Fe_2O_3 reducing conditions would increase metal oxide respiration and viability. If the limiting step in solid metal oxide respiration is quinol recycling at the inner membrane, then the additional expression of CymA will dramatically increase the electron flux to the solid. Here, I set out to express the complete, double-membrane spanning *Shewanella* pathway, CymA MtrCAB, in *E. coli*.

There are additional potential rate limiting steps in solid metal oxide reduction. Direct contact of the terminal reductase, MtrC, could be limiting the terminal reductase activity. In the native organism, *Shewanella oneidensis* MR-1 reduces anodes and solid inorganic oxides both by direct contact and with diffusible redox species, such as riboflavin or flavin mononucleotide (FMN) (*5*, *29*, *47*). It is estimated that ~20% of the overall reduction of extracellular inorganic material is specifically due to direct contact with the surface while about ~80% is due to diffusible redox species (*48*, *195*). Thus it is plausible that electron flux to solid iron oxide in the engineered strains would increase with the supplementation of diffusible electron carriers.

The work described in this chapter explores factors that we predict could increase electron flux to extracellular metal oxides. Enhancing electron flux is vital to increase the maximal current that these engineered strains can deliver to an anode. We found that changing the concentration of the electron conduit, MtrCAB, in the present strains does

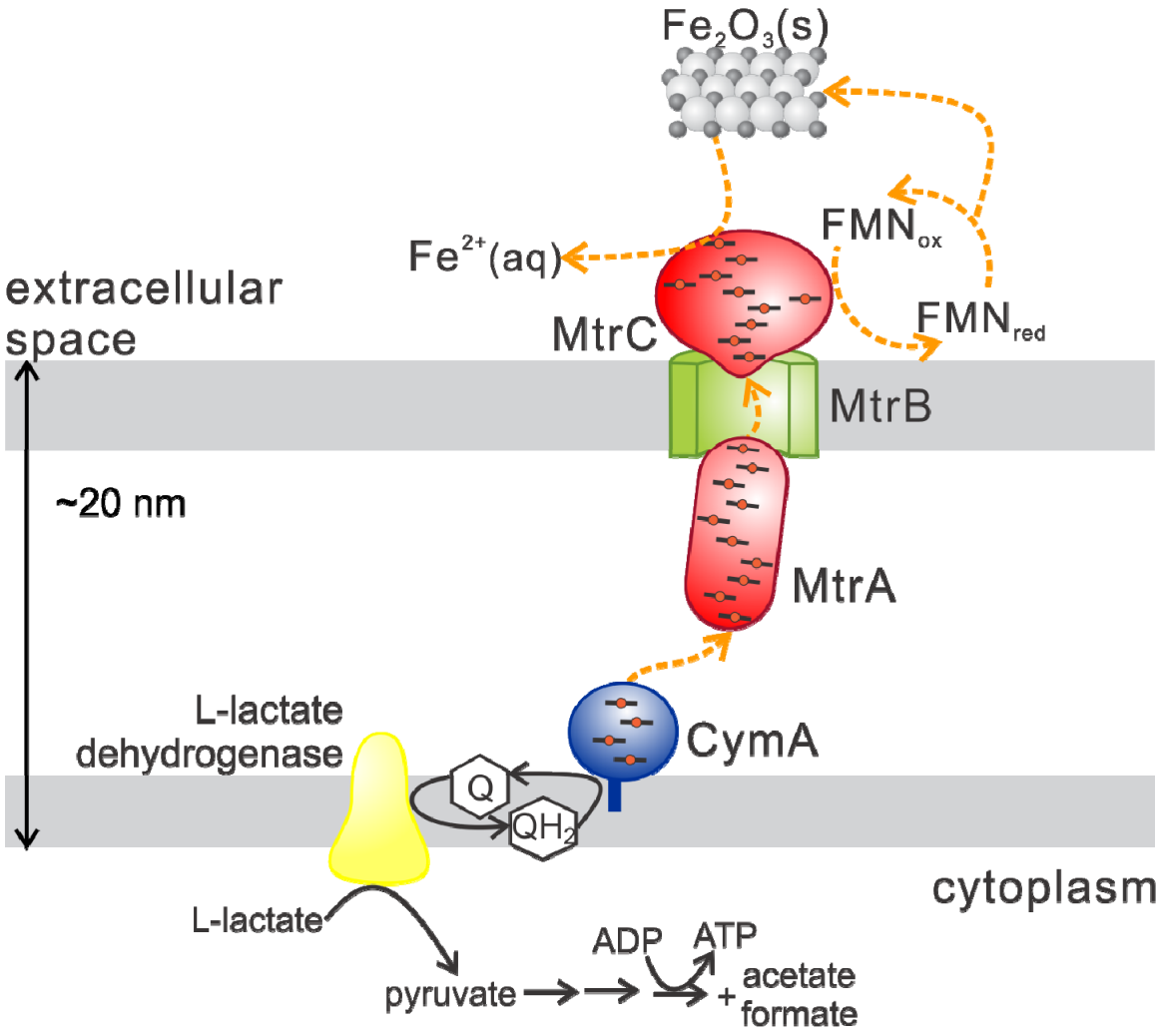

Figure 5-1. Routes for electrons from lactate to $Fe_2O_3(s)$ through the Mtr electron transfer pathway of *Shewanella oneidensis* MR-1. L-Lactate is oxidized into pyruvate, and the resulting reducing equivalents are used to reduce menaquinone (Q) to menaquinol (QH_2). CymA is the inner membrane cytochrome *c* that accepts electrons from menaquinol; in *E. coli*, this function is achieved by NapC and NrfBCD. From the inner membrane protein, electrons are passed through the periplasm and outer membrane to extracellular electron acceptors *via* the MtrCAB complex. From MtrC, electrons are transferred to $Fe_2O_3(s)$ through flavin mediators or by direct transfer to $Fe_2O_3(s)$ by MtrC.

Table 5-1: Calculated RBS strengths using the Salis Lab RBS Calculator (*191*).

Gene (Plasmid)	Sequence[1-2]	16S rRNA[3]	Translation Initiation Rate (*AU*)	ΔG_{total} (*kcal/mol*)
cymA (I5049)	CGACTCACTATAGGGGAATTGTGAGCGGATAACA ATTCCCCTCAAGAAATAATTTTGTTTAACTTTAA GAAGGAGATATACATATTTTGGAGATAGAGTAAT GAACTGGCGTGCACTATTTAAACCCAGCGCGAAA TATTCCATCCTAGCGCTACTGGTTGTTGGTATCG TGATTGGTGTTGTGGGCTATTTTGCAACTC	a	0.7×10^3	2.9
		b	4.1×10^3	-1.1
cymA, Shewie	AATCGGCATTTTTAGGCTTGAAATCAAACTTCTA ATAAATAAAAAAACATAAAATAGTCTTATAAAAA CTGATTTTGACAATATTTTTGGAGATAGAGTAAT GAACTGGCGTGCACTATTTAAACCCAGCGCGAAA TATTCCATCCTAGCGCTACTGGTTGTTGGTATCG TGATTGGTGTTGTGGGCTATTTTGCAACTC	b	3.5×10^3	-0.75
mtrA (I5023, I5049)	CAAAAGGATAAGGTTTAACGCTGCAAGAATTCTT TGCCCAAGCAGGGGGAGCTCGCTCCCCCTTTCTT GAATTTTGTTGGGACAAATTGGGAAGCCTATTAT GAAGAACTGCCTAAAAATGAAAAACCTACTGCCG GCACTTACCATCACAATGGCAATGTCTGCAGTTA TGGCATTAGTCGTCACACCAAACGCTTATG	a	1.5×10^3	1.1
		b	6.7×10^3	-2.2
mtrA, Shewie	CAGTTGCAGATCACACTAAAGTGAAAATGTAATT TGCCCAAGCAGGGGGAGCTCGCTCCCCCTTTCTT GAATTTTGTTGGGACAAATTGGGAAGCCTATTAT GAAGAACTGCCTAAAAATGAAAAACCTACTGCCG GCACTTACCATCACAATGGCAATGTCTGCAGTTA TGGCATTAGTCGTCACACCAAACGCTTATG	b	6.7×10^3	-2.2
mtrC (I5049)	ATCCACTTAAGTCGCTTCTAGTGATCAAATACAC AGACATAGAATCTGTTGGCGCTAGAGCATAGCGG TTAAGCAATGCCAAACCTATGCAGGGAAAAAAAT GATGAACGCACAAAAATCAAAAATCGCACTGCTG CTCGCAGCAAGTGCCGTCACAATGGCCTTAACCG GCTGTGGTGGAAGCGATGGTAATAACGGCA	a	1.4×10^3	1.27
		b	1.8E3	0.7
mtrC (I5023)	AAATTAATACGACTCACTATAGGGGAATTGTGAG CGGATAACAATTCCCCTCAAGAAATAATTTTGTT TAACTTTAAGAAGGAGATATACATATGGAATTCA TGAACGCACAAAAATCAAAAATCGCACTGCTGCT CGCAGCAAGTGCCGTCACAATGGCCTTAACCGGC TGTGGTGGAAGCGATGGTAATAACGGCAAT	a	3.1×10^3, 8.3×10^3	-0.5, -2.67
		b	87×10^3, 9.1×10^3	-7.89, -2.87
mtrC, Shewie	ATCCACTTAAGTCGCTTCTAGTGATCAAATACAC AGACATAGAATCTGTTGGCGCTAGAGCATAGCGG TTAAGCAATGCCAAACCTATGCAGGGAAAAAAAT GATGAACGCACAAAAATCAAAAATCGCACTGCTG CTCGCAGCAAGTGCCGTCACAATGGCCTTAACCG GCTGTGGTGGAAGCGATGGTAATAACGGCA	b	1.8×10^3	0.7
mtrB (I5049, I5023)	TGCCTTTACTGGTGGAAGAAGCTGCTTAAATTGC CATAGTCAGGTTCATGGTTCTAACCATCCATCTG GCAAGCTATTACAGCGCTAAGGAGACGAGAAAAAT GAAATTTAAACTCAATTTGATCACTCTAGCGTTA TTAGCCAACACAGGCTTGGCCGTCGCTGCTGATG GTTATGGTCTAGCGAATGCCAATACTGAAA	a	0.2×10^3	6.2
		b	2.7×10^3	-0.19
mtrB, Shewie	TGCCTTTACTGGTGGAAGAAGCTGCTTAAATTGC CATAGTCAGGTTCATGGTTCTAACCATCCATCTG GCAAGCTATTACAGCGCTAAGGAGACGAGAAAAAT GAAATTTAAACTCAATTTGATCACTCTAGCGTTA TTAGCCAACACAGGCTTGGCCGTCGCTGCTGATG GTTATGGTCTAGCGAATGCCAATACTGAAA	b	2.7×10^3	-0.19

[1]Blue sequence annotates the RBS of the respective *Shewanella* genes in the genome

[2]The ATG start codons are shown in purple. The underlined ATG in MtrC is from the NdeI restriction site. This adds an extra Glu-Phe sequence that will be cleaved off after signal sequence processing.

[3]The code for the 16S rRNA are as follows, where (a) and (b) are for *E. coli* and (b) is for *Shewanella*: (a) TAACCGTAG and (b) ACCTCCTTA.

not statistically increase electron flux to solid metal oxides. This suggests that the function of the pathway is currently not limited by the number of conduits. The additional expression of CymA was shown to increase total iron oxide reduced as well as strain fitness. Supplementing the media with exogenous redox carriers, like riboflavin, increased the total metal oxide reduced further, matching the behavior seen in *Shewanella*. Thus, we find that the addition of CymA and riboflavin are important factors in solid metal oxide reduction by our present strains. In total, the *mtrCAB* and *cymAmtrCAB* strains described below demonstrate iron oxide reduction rates 1.6x and 2.8x faster, respectively, than the initial strain described in chapter 2. Additionally, the supplementation with riboflavin increased the rates of the *mtrCAB* and *cymAmtrCAB* strains by 2.4x and 3.8x, respectively, over the original strain. Overall, by carefully optimizing the electron transfer pathway in *E. coli*, we were able to increase the electron transfer rate significantly over the original strains.

5.2. Designing an *E. coli* strain for the expression of the complete, double membrane spanning pathway, CymA MtrCAB.

This dissertation represents the first time the double membrane spanning pathway, CymA MtrCAB, was expressed in a heterologous organism. We had previously described a plasmid for the expression of the outer membrane spanning pathway, *mtrCAB* (*92*, *148*). Here we have developed a plasmid with encoding for *cymA* and *mtrCAB*. In the construction of this plasmid, 116 base pairs of non-coding region upstream of *mtrC* were used as a spacer between *cymA* and *mtrC*. Both plasmids are under the control of the inducible T7 *lac* promoter. The RBS translation initiation rates, as calculated by the Salis RBS calculator (*191*), for all genes in both plasmids are reported in Table 5-1. These calculations predict the translation initiation rate. These calculations show that the largest difference between the *Shewanella* RBS strength and the plasmid RBS strength is with *mtrC* on the *mtrCAB* plasmid. The *mtrCAB* and *cymAmtrCAB* plasmids were co-transformed with the *ccm* plasmid, pEC86, into the *E. coli* strain C43(DE3) to make the *mtrCAB* and *cymAmtrCAB* strains, respectively.

To confirm that CymA, MtrA, and MtrC are full length and are redox active, whole cell lysates were analyzed by SDS-PAGE and stained for peroxidase activity with enhanced chemiluminescence. Heme staining of whole cell lysates by SDS-PAGE by enhanced chemiluminescence shows that CymA, MtrA, and MtrC are the correct molecular weight and redox active (Figure 5-2A; 19, 35, and 76 kD, respectively). MtrB was previously shown to be localized in the membrane fraction in *E .coli* (Figure 2-3), thus we assume that it is localized correctly again; however, another immunoblot should be performed for complete characterization of the *cymAmtrCAB* strain. Membrane and periplasmic fractions also show that these proteins have a similar localization pattern as observed in *Shewanella oneidensis* MR-1 (Figure 5-2B) (*33*, *51*, *62*, *167*). Thus, the *cymAmtrCAB* strain expresses redox active and correctly localized CymA MtrCAB in *E. coli*.

Diffuse reflectance was used to probe the number of electron conduits per cell such that we could determine the effect of increasing the number of conduits on iron oxide respiration. Using the diffuse reflectance technique described in Chapter 3 (*92*), we quantitatively measured the concentration of total cytochrome content per cell under a range of inducing conditions. Because the extinction coefficients of MtrA, MtrC, and

CymA are different at 552 nm due to different numbers of low spin heme per protein, we used an extinction coefficient of 28 mM^{-1} cm^{-1} per heme (*51*, *62*). The concentration of heme *c* per $OD_{600\ nm}$ as a function of promoter activity, as measured in Goldbeck et al., is shown in Figure 5-2C (Table 5-2). These values are used to annotate the induction of the electron transfer genes within a strain from now on in superscript. For example, *mtrCAB* induced with 10 μM IPTG is notated as $mtrCAB^{0.18}$. By plotting the concentration of heme *c* per $OD_{600\ nm}$ as a function of promoter activity, we observe distinct trends for the expression of MtrCAB and CymAMtrCAB (Figure 5-2B). Both strains gradually increase in cytochrome *c* production until ~0.37 relative promoter activity (arb. units, Table 5-2). At this promoter activity, *mtrCAB* and *cymAmtrCAB* express 140 ± 14 and 109 ± 9 μM heme *c* $OD_{600\ nm}^{-1}$, respectively (Figure 5-2C, Table 5-3). However, at 0.72 relative promoter activity (arb. unit), the cytochrome *c* expression dramatically decreases in the *mtrCAB* strain (red triangles, Figure 5-2C). This is consistent with our previous observations that overexpression of MtrCAB in *E. coli* is damaging to the cell membrane (Appendix G), decreases cell density (Figure 3-4 and and Appendix G), and decreases holocytochrome *c* expression (Figures 2-2 and 3-4) (*92*, *148*). Conversely, expression of CymAMtrCAB plateaued between 0.37 and 0.72 relative promoter activity (arb. unit) (blue circles, Figure 5-2C). The heme *c* concentration per $OD_{600\ nm}$ is also shown as a function of inducer concentration in Figure 5-2D. In summary, the holocytochrome *c* synthesized per cell as the result of induction of the *mtrCAB* and *cymAmtrCAB* strains is significantly different, and this controlled expression of the pathways allows the investigation of the affect of the number of conduits per cell on iron oxide respiration.

Table 5-2: Relative promoter activity (normalized GFP expression) as a function of inducer (IPTG) concentration as measured in Goldbeck et al (*92*)**.**

[IPTG] (μM)	Rel. Promoter Activity (arb. unit)
0.0	0.0013
1.0	0.0110
10.0	0.1801
50.0	0.3725
250.0	0.7200

Table 5-3: Concentration of heme *c* per $OD_{600\ nm}$ for the *mtrCAB* and *cymAmtrCAB* strains under a range of induction conditions.

[IPTG] (μM)	Rel. Promoter Activity (arb. unit)	[heme *c*] in *mtrCAB* μM $OD_{600\ nm}^{-1}$	[heme *c*] in *cymAmtrCAB* μM $OD_{600\ nm}^{-1}$
0.0	0.0013	24 ± 8	18 ± 4
1.0	0.0110	40 ± 13	38 ± 10
10.0	0.1801	120 ± 15	90 ± 16
50.0	0.3725	140 ± 14	109 ± 9
250.0	0.7200	83 ± 16	106 ± 2
10.0 + δ-ALA	0.1801	149 ± 14	132 ± 31

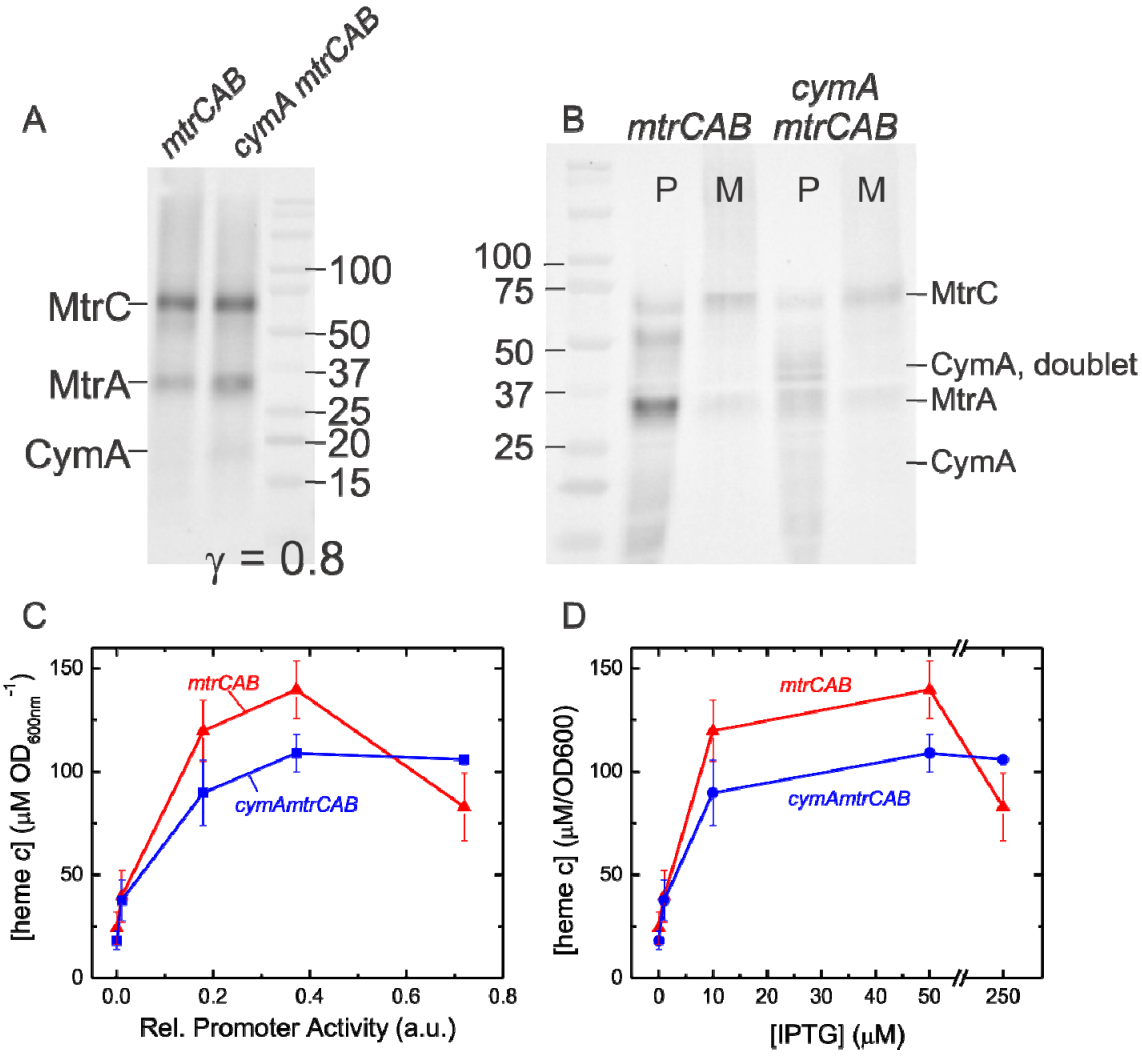

Figure 5-2. Characterization of the *mtrCAB* and *cymAmtrCAB* strains. (A) Heme *c* staining of *mtrCAB* and *cymAmtrCAB* whole cell lysates, after induction of both strains with 10 μM IPTG. Heme *c* was detected with enhanced chemiluminescence (see Methods), and equal total protein (8 μg) was loaded per lane for direct comparison of the band sizes per cell. The predominant bands correspond to CymA, MtrA and MtrC indicating simultaneous expression of the full length cytochromes *c* in the *cymAmtrCAB* strain. The image was adjusted to 0.8 gamma, but all densitometric analysis was done on the original image (γ = 1.0). (B) Heme *c* staining of periplasmic and membrane fractions of the *mtrCAB* and *cymAmtrCAB* strains show MtrA and MtrC are full length at 34 and 71 kD, respectively. The periplasmic fraction (P) of *mtrCAB* showed mostly MtrA as well as a proposed MtrA dimer. The membrane fraction (M) showed a mixture of MtrC and MtrA, with the predominant band being MtrC. The periplasmic (P) and membrane (M) fractions of *cymAmtrCAB* also show MtrA and MtrC in the same pattern. A faint, broad band of CymA is in the periplasmic fraction at 21 kD, as well as a proposed CymA dimer at 44 kD. (C) Effect of induction on concentration of heme *c* per $OD_{600\ nm}$ of *mtrCAB* and *cymAmtrCAB* cells as measured by diffuse reflectance. Total cytochrome *c*

expression in both strains increase until 0.37 rel. promoter activity (arb. unit defined in Goldbeck) (50 μM IPTG); however, the heme c concentration in the *mtrCAB* strain decreases at 0.72 rel. promoter activity (arb. unit) (250 μM IPTG). (D) The heme *c* concentration per $OD_{600\ nm}$ is also shown as a function of inducer concentration ([IPTG]) for convenience.

5.3. Increasing the concentration of the outer membrane spanning pathway, MtrCAB, does not improve reduction of solid Fe_2O_3, but improves strain survival.

The affect of the number of conduits per cell on iron oxide respiration and survival in the *mtrCAB* strain was probed by measuring the reduced iron concentration and colony forming units over a range of promoter activities. The *mtrCAB* and *cymAmtrCAB* strains were grown aerobically and subsequently transferred into anaerobic media supplemented with 40 mM D,L-lactate as the carbon source and 6.0 mg mL^{-1} Fe_2O_3 (*s*) as the sole terminal electron acceptor. The inducer, IPTG, was also added to the media where appropriate to maintain cytochrome *c* expression over the course of the experiment. Equal cell densities were resuspended in the anaerobic-Fe_2O_3 media ($OD_{600\ nm}$ = 1.0, or ~1 x10^9 cfu mL^{-1}). Under these experimental conditions, we anticipate that respiration lactate with Fe_2O_3 (*s*) as the sole terminal electron acceptor should be the only means of energy generation available to *E. coli.* A *ccm*-expressing strain was also monitored to account for any changes in basal Fe_2O_3 (*s*) reduction. The Fe(II) concentration was measured as a function of time using the ferrozine assay (*168*). We probed survival of these strains by monitoring the colony forming units (cfu), selecting for the retention of the *mtrCAB* and *cymAmtrCAB* plasmids on LB-Kanamycin plates.

The cytochrome c maturation expressing strain, *ccm*, was not able to significantly reduce iron oxide and showed significant decrease in CFUs (Figure 5-5 and Table 5-4). This demonstrates that the native *E. coli* strain is unable to respire or grow when Fe_2O_3 (*s*) is the sole terminal electron acceptor available. The *mtrCAB* strain shows statistical improvement over the *ccm* only strain in the total Fe_2O_3 (*s*) reduced over 21 days (Tables 5-4 and 5-5). However, induction of the outer membrane spanning pathway, MtrCAB, does not statistically change the total Fe_2O_3 (*s*) reduced (Figure 5-3A). This implies that the number of conduits in the *mtrCAB* strain is not a rate limiting parameter in the reduction of solid iron oxide.

Due to limitations of the ferrozine assay and the relatively slow reduction of Fe_2O_3 (*s*) by our strains, we are unable to quantitatively measure [Fe(II)] at early time points. Unlike [Fe(II)], we can observe drastic changes in colony forming units (cfu) over short time scales. We interpret relative CFUs as an indication of the impact on the survival of the strain in conditions where solid Fe_2O_3 is the only possible terminal electron acceptor. In the *mtrCAB* strain, the early survival of the strains exhibits a similar trend to [heme *c*] (blue and red triangles, respectively, Figure 5-3B). The survival of the *mtrCAB* strain increases until a relative promoter activity of 0.18, and then sharply declines. This observation is an indication that overexpression of MtrCAB in *E. coli* negatively impacts viability and *in vivo* metal reduction.

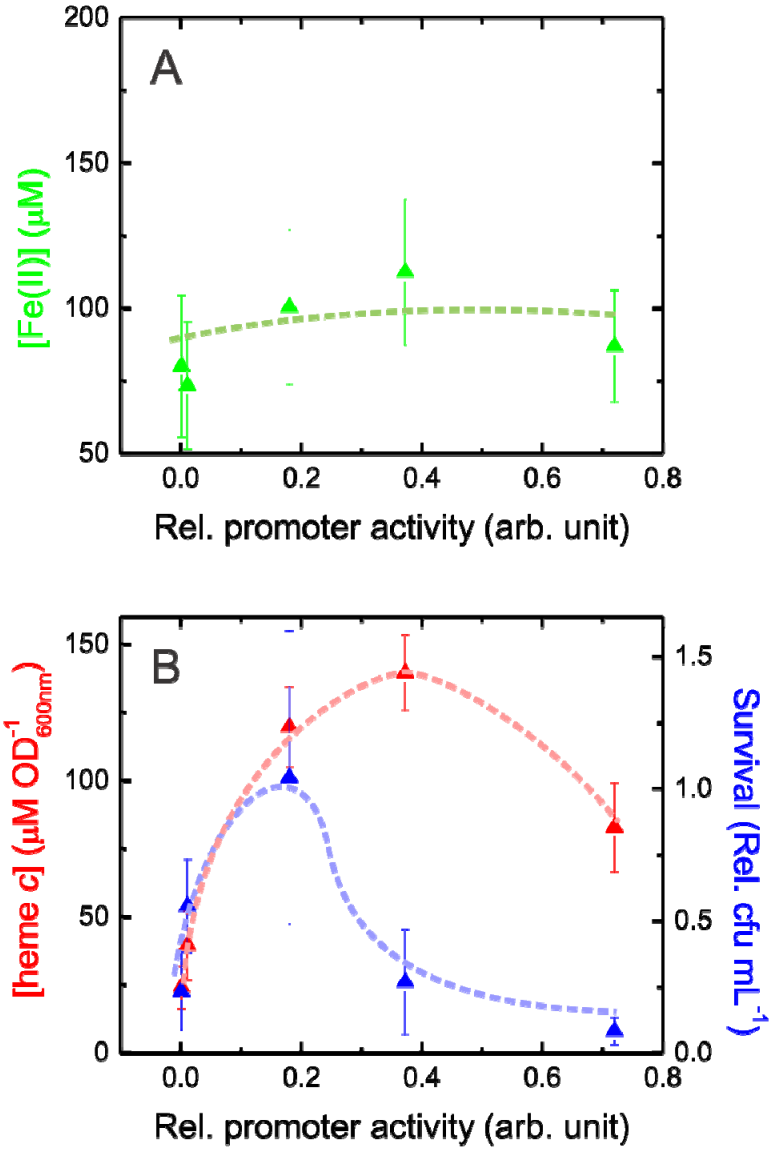

Figure 5-3. Increasing MtrC+MtrA concentration does not increase electron transfer from the *mtrCAB* strain to Fe_2O_3(*s*). (A) Total Fe_2O_3 (*s*) reduced to Fe(II) reduced by the *mtrCAB* strain after 21 days (green triangles) as a function of promoter activity. Iron oxide reduction does not significantly change with increasing induction levels, which correspond to increasing MtrC and MtrA concentration per cell. (B) Relative CFUs of the *mtrCAB* strain after 4 days (blue triangles) as a function of promoter activity. At 0.18 promoter activity or less, induction is correlated with increased cell survival. At 0.37 promoter activity and above, induction impedes survival. Lines are provided to guide the eye. The axes are scaled as in Figure 5-4 to enable direct comparison between the *mtrCAB* and *cymAmtrCAB* strains.

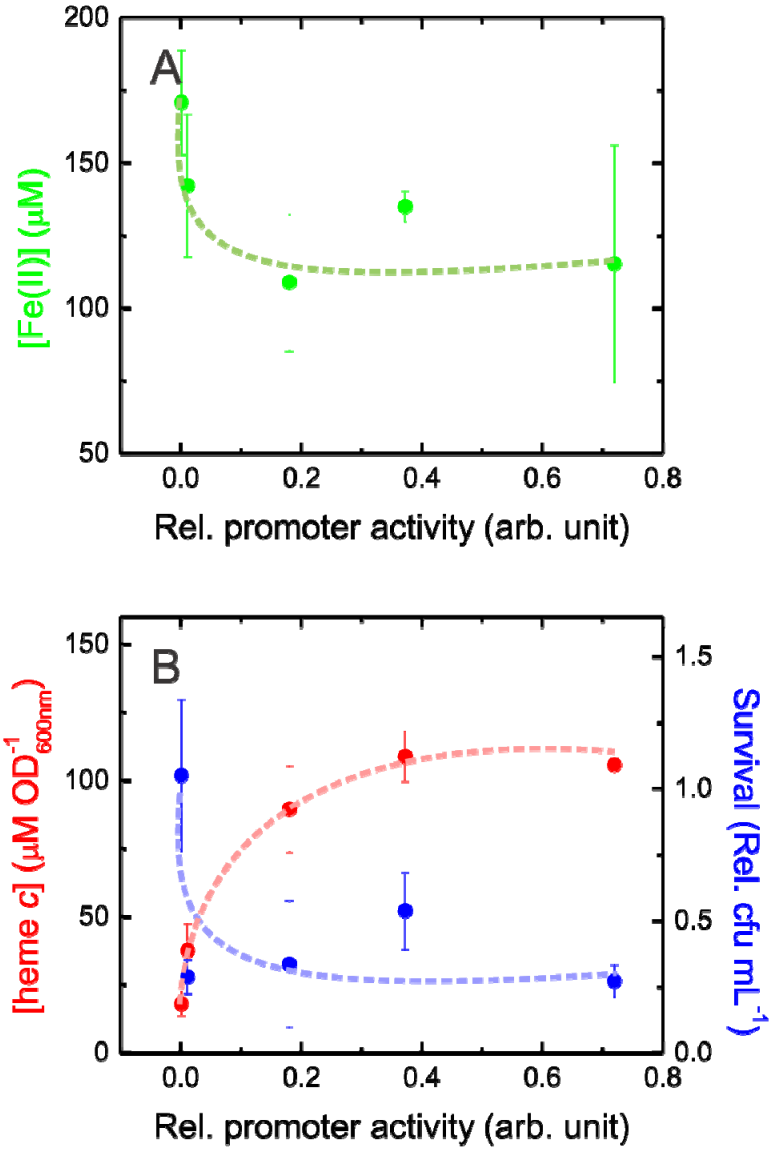

Figure 5-4. Low level expression of CymA with MtrCAB increases Fe_2O_3(*s*) reduction and *E. coli* survival. (A) Total Fe_2O_3 (*s*) reduced by the *cymAmtrCAB* strain after 21 days (green triangles) as a function of IPTG induction level. In the absence of IPTG, the *cymAmtrCAB* strain produced more Fe(II) than the *mtrCAB* strain at any induction level. (B) Relative CFUs of the *cymAmtrCAB* strain after 4 days (blue circles) as a function of IPTG concentration. In the *cymAmtrCAB* strain, the strain survival (panel B, blue) is well-correlated with Fe_2O_3 reduced (panel A, green). Lines are provided to guide the eye. The axes are scaled as in Figure 5-3 to enable direct comparison between the *mtrCAB* and *cymAmtrCAB* strains.

Table 5-4: Iron reduction and relative CFU changes by the *mtrCAB* and *cymAmtrCAB* strains under solid iron oxide reducing conditions.

Rel. Promoter Activity (arb. unit)	*mtrCAB*		*cymAmtrCAB*	
	[Fe(II)] (μM) day 21	Rel. CFU mL^{-1} day 4	[Fe(II)] (μM) day 21	Rel. CFU mL^{-1} day 4
0.0013	80 ± 24	2.3 (±1.5) $x10^{-1}$	171 ± 18	1.1 (±0.3) $x10^{0}$
0.0110	74 ± 22	5.6 (±1.8) $x10^{-1}$	142 ± 25	2.9 (±0.7) $x10^{-1}$
0.1801	100 ± 27	1.0 (±0.6) $x10^{0}$	109 ± 24	3.4 (±2.4) $x10^{-1}$
0.3725	112 ± 25	2.7 (±2.0) $x10^{-1}$	135 ± 5	5.4 (±1.5) $x10^{-1}$
0.7200	87 ± 19	8.5 (±5.1) $x10^{-2}$	115 ± 41	2.7 (±0.6) $x10^{-1}$
0.1801 + δ-ALA	137 ± 38	5.4 (±5.1) $x10^{-1}$	183 ± 28	1.8 (±0.7) $x10^{1}$
0.1801 + ribo	197 ± 51	3.7 (±1.3) $x10^{-1}$	270 ± 7	1.2 (±0.9) $x10^{1}$

Note: The *ccm* strain values are: 62 ± 19 [Fe(II)] (μM) and 6.6 (±4.9) $x10^{-2}$ relative cfu mL^{-1}

Table 5-5: Select p-values from a two-sided t-test comparing the highest iron reducing strains shown in Figure 5-5.

Sample 1	Sample 2	p-value
ccm	$mtrCAB^{0.37}$	0.049
ccm	$cymAmtrCAB^{0.001}$	0.002
$mtrCAB^{0.37}$	$cymAmtrCAB^{0.001}$	0.031

5.4. The *cymAmtrCAB* strain exhibits opposite trends between concentrations of heme *c* and solid Fe_2O_3 reduction of strain survival.

To determine the affect of the number of conduits per cell on iron oxide respiration and survival in the *cymAmtrCAB* strain, we probed the reduced iron concentration and colony forming units over a range of promoter activities. By comparing the iron reduction by the *mtrCAB* and *cymAmtrCAB* strains, we can observe the impact of expressing CymA in addition to MtrCAB. The iron reducing and survival of the *cymAmtrCAB* strain over a range of promoter activities was measured as described above and shown in Figure 5-4. The plots in Figures 5-3 and 5-4 are displayed on the same scale for ease of comparison. The *cymAmtrCAB* strain displayed a different trend from the *mtrCAB* strain in Fe_2O_3 (*s*) reduction and survival. Specifically, iron oxide reduction decreases with increasing induction of *cymAmtrCAB* and plateaus between 0.011 and 0.18 promoter activity (arb. unit) (Figure 5-4A). Interestingly, the uninduced *cymAmtrCAB* strain was the best iron reducer in the induction series and significantly reduced more Fe_2O_3 (*s*) than any of the *mtrCAB* induced strains (Figure 5-4A and Table 5-5). This implies that any induction of the *cymAmtrCAB* strain inhibits function of the electron transfer pathway. One possible explanation for this decrease in function is toxicity from protein expression; however, the *cymAmtrCAB* strain does not show dramatic decreases in overall biomass after aerobic growth like the *mtrCAB* strain (Appendix G). Thus it is necessary to further investigate why induction of the *cymAmtrCAB* strain restricts the iron oxide reducing ability.

Unlike the *mtrCAB* strain, the *cymAmtrCAB* strain survival is anticorrelated to [heme *c*] (blue and red circles, respectively, Figure 5-4B). Interestingly, the iron oxide reduced (Figure 5-4A) and the cell survival (blue circles, Figure 5-4B) both decrease and

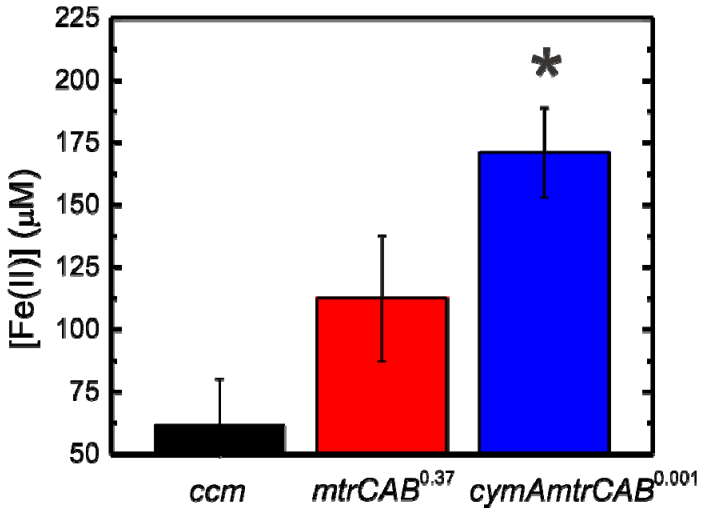

Figure 5-5. The *cymAmtrCAB* strain can reduce more Fe_2O_3 than the *mtrCAB* strain. A comparison of the *mtrCAB* and *cymAmtrCAB* strains showing the highest iron reduction shows that uninduced *cymAmtrCAB* statistically increased iron reducing function over both the *ccm* and best performer from the *mtrCAB* induction series. This suggests that the addition of CymA increases the flux of electrons to iron oxide as a terminal electron acceptor. The p-values for these cultures are in Table 5-5.

plateau with increasing promoter activity. This indicates that the use of iron oxide as a terminal electron acceptor by the *cymAmtrCAB* strain is strongly correlated with cell survival.

Overall, the addition of CymA increased the total iron oxide reduced by the engineered *E. coli* (Figure 5-5), substantiating earlier experiments that show CymA greatly increases respiration soluble Fe(III) citrate as the terminal electron acceptor (Figure 4-6). This observation indicates that CymA is increasing recycling of the quinol pool and thus feeding more electrons into the electron conduit, and thus the *cymAmtrCAB* strain is able to better utilize iron oxide as a terminal electron acceptor.

5.5. Heme biosynthesis precursor, δ-ALA, improves cytochrome *c* expression but not iron reduction.

We and others have previously observed that the addition of the heme biosynthesis precursor δ-aminolevulinic acid (δ-ALA) improved the heterologous expression of cytochromes *c* (*91*, *92*). To determine if limited heme, and thus limited holocytochrome *c* biogenesis, impacts iron oxide reduction and strain survival, the experiments described above were repeated with strains grown in the presence of δ-ALA. If the *mtrCAB* or *cymAmtrCAB* strains are limited by biogenesis of holocytochrome *c* at a given promoter activity, then increasing the number of conduits by increasing holocytochrome *c* expression could improve electron flux to solid iron oxide. δ-ALA was not added to the anaerobic cell suspension to avoid the complication of cells excreting heme *b*, which may potentially be utilized as a soluble redox carrier.

The *mtrCAB* and *cymAmtrCAB* strains showed a moderate increase in the concentration of heme *c* per cell when grown in the presence of δ-ALA (Table 5-3). The cultures grown with δ-ALA exhibited 24% and 67% increase in heme c content over *mtrCAB*$^{0.18}$ and *cymAmtrCAB*$^{0.18}$, respectively (Table 5-3). This indicates that the *cymAmtrCAB* strain is more limited by heme biosynthesis than the *mtrCAB* strain; this may be due to the expression of an additional tetraheme cytochrome *c* in the *cymAmtrCAB* strain.

The total iron reduced over 21 days was not statistically different between the samples with and without δ-ALA added to the growth medium (Figure 5-6 and Tables 5-4 and 5-6). This supports the observations made in the induction titration of the *mtrCAB* and *cymAmtrCAB* strains that showed increasing the number of electron conduits per cell does not correlate with increased iron oxide reduction (Figures 5-3 and 5-4). Additionally, this observation excludes toxicity of IPTG as a potential explanation for the decrease in function with increasing induction. Thus, simply increasing the number of conduits in our strains does not increase the function of the engineered strains.

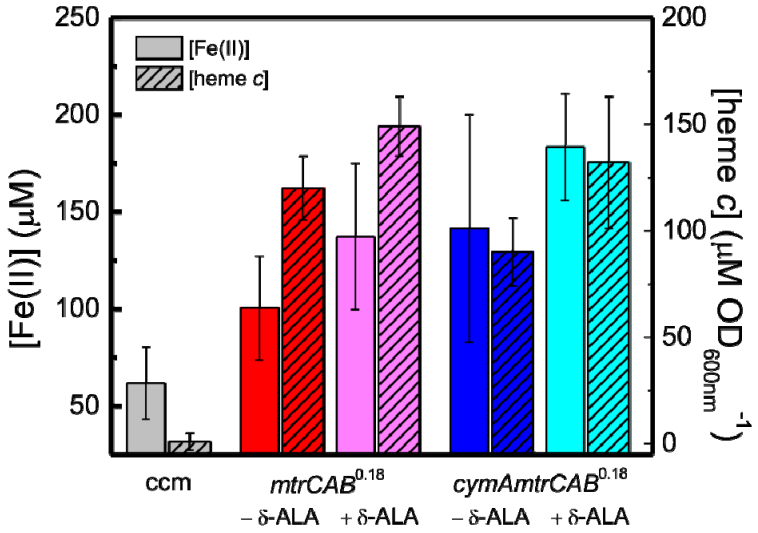

Figure 5-6. Heme biosynthesis precursor δ-ALA increases the cytochrome *c* concentration but does not improve Fe_2O_3 reduction. Fe_2O_3 reduced to Fe(II) is shown in empty columns, while concentration of heme *c* per cell is shown with hash marks. The *mtrCAB*$^{0.18}$ strain is shown in red, and the δ-ALA supplemented *mtrCAB*$^{0.18}$ strain is shown in pink. The *cymAmtrCAB*$^{0.18}$ strain is shown in blue, and the δ-ALA supplemented *cymAmtrCAB*$^{0.18}$ strain is shown in cyan. The addition of δ-ALA to the growth medium slightly increased the holocytochrome *c* concentration per cell. The total iron reduced over 21 days was not statistically different between the samples with and without δ-ALA added to the growth medium. This adds to the evidence that increasing the number of electron conduits per cell does not necessarily increase the electron flux to solid metal oxides.

Table 5-6: Select p-values from a two-sided t-test for total iron reduced for samples with and without δ-ALA added.

Sample 1	Sample 2	p-value
ccm	$mtrCAB^{0.18}$	0.108
ccm	$cymAmtrCAB^{0.18}$	0.085
ccm	$mtrCAB^{0.18}_{+\ \delta\text{-ALA}}$	0.036
ccm	$cymAmtrCAB^{0.18}_{+\ \delta\text{-ALA}}$	0.003
$mtrCAB^{0.18}$	$mtrCAB^{0.18}_{+\ \delta\text{-ALA}}$	0.240
$cymAmtrCAB^{0.18}$	$cymAmtrCAB^{0.18}_{+\ \delta\text{-ALA}}$	0.054

5.6. Riboflavin enhances both solid Fe_2O_3 reduction and strain survival.

In *S. oneidensis* MR-1, it has been hypothesized that an alternative to reducing an extracellular terminal electron acceptor by direct contact is reduction of riboflavin by MtrC, which carries electrons to the terminal electron acceptor *via* diffusion. To probe if iron reduction by the MtrC-expressing *E. coli* strains is enhanced by riboflavin, strains grown at 0.18 relative promoter activity units were supplemented with 5 μM riboflavin in the anaerobic media. We found that riboflavin significantly increases total Fe_2O_3 (*s*) reduced in both strains (Figure 5-7 and Tables 5-4 and 5-7). Overall, the addition of riboflavin increased total iron oxide reduced by 2.0x and 2.5x in the *mtrCAB* and *cymAmtrCAB* strains, respectively (Figure 5-7).

The *cymAmtrCAB* strain survival correlated with the total iron oxide reduced, in a manner similar to the correlation between iron reduced and survival over different induction strengths. Interestingly, the *cymAmtrCAB* strain supplemented with riboflavin dramatically increased the relative CFUs, growing about 10x the cell density of the original suspension (Figure 5-7A). However, this effect is linked to the addition of CymA; the addition of riboflavin did not statistically change the survival of the *mtrCAB* strain (Figure 5-7).

Table 5-7: Select p-values from a two-sided t-test for total iron reduced for samples with and without riboflavin supplemented.

Sample 1	Sample 2	p-value
ccm	$mtrCAB^{0.18}_{+\ \text{riboflavin}}$	0.013
ccm	$cymAmtrCAB^{0.18}_{+\ \text{riboflavin}}$	0.001
$mtrCAB^{0.18}$	$mtrCAB^{0.18}_{+\ \text{riboflavin}}$	0.045
$cymAmtrCAB^{0.18}$	$cymAmtrCAB^{0.18}_{+\ \text{riboflavin}}$	0.011

5.7. Discussion.

In this chapter, we sought to determine how the electron transfer rate to an extracellular terminal electron acceptor could be improved in the engineered *E. coli* strains. Specifically, the focus of these experiments was on how the quinol dehydrogenase CymA, the number of electron conduits, and the presence of riboflavin affect the iron reducing capability and survival of the strains. We found that increasing the number of electron conduits did not correlate with increased function, implying that

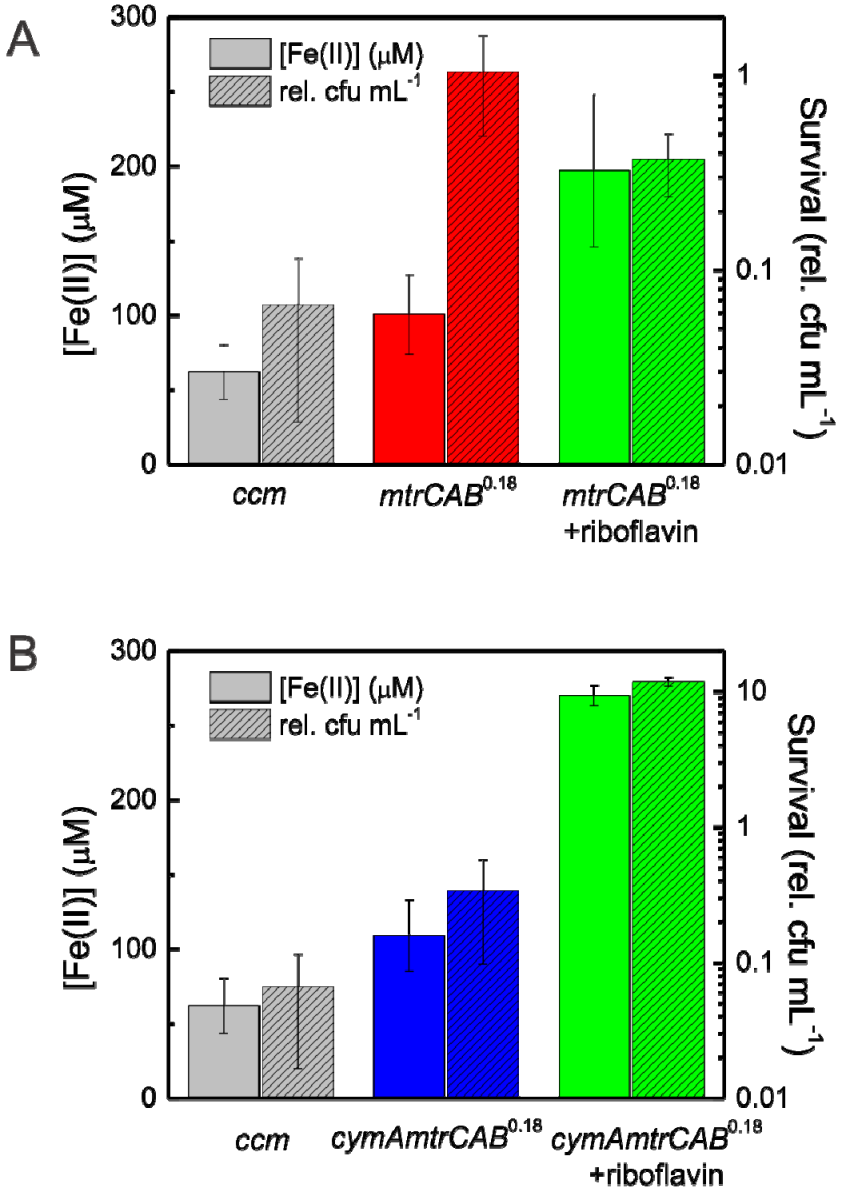

Figure 5-7. Riboflavin improves Fe_2O_3 reduction in the *mtrCAB* and *cymAmtrCAB* strains and survival in the *cymAmtrCAB* strain. Total Fe_2O_3 (*s*) reduced to Fe(II) and relative cfus by the *ccm* (grey), *mtrCAB*$^{0.18}$ (red) *cymAmtrCAB*$^{0.18}$ (blue), and strains supplemented with 5 μM riboflavin (green). (A) The addition of riboflavin to the *mtrCAB*$^{0.18}$ strain increased iron reduction by ~2-fold but did not statistically change the strain survival. (B) The addition of riboflavin enhanced iron reduction by ~2.5-fold for the *cymAmtrCAB*$^{0.18}$ strain. Additionally, the survival of the *cymAmtrCAB*$^{0.18}$ strain dramatically increased in the presence of riboflavin. Assuming direct contact contributes equally in the cultures with and without the supplementation of riboflavin, 77% of the iron oxide was reduced by riboflavin.

the system is not conduit-limited (Figures 5-3, 5-4, 5-6). The addition of CymA moderately increased the electron flux to iron oxide (Figure 5-5). Finally, riboflavin was found to dramatically increase both iron reduction and survival (Figure 5-7).

5.7.1. Expression of the *mtrCAB* and *cymAmtrCAB* pathways display fundamentally different phenotypes.

The correlation between heme c and function in the *mtrCAB* and *cymAmtrCAB* strains is complicated. The concentration of heme *c* in the *mtrCAB* strain sharply decreases after 0.37 promoter activity (arb unit) (Figure 5-2C). The sharp decline in heme *c* concentration at 0.72 promoter activity (arb unit) correlated with less total biomass after the typical 16 hour growth, signifying a toxic effect under these growth conditions. Similar trends were observed in *mtrCAB* strains in Chapters 2 and 3. The *cymAmtrCAB* strain, however, did not show a decline in heme *c* concentration over the same range of IPTG concentrations.

With the *mtrCAB* strain, the survival of the strain was well correlated with the heme *c* concentration (Figure 5-3B). At high induction activity of the *mtrCAB* plasmid, we have observed decreased cell biomass and iron reduction. These strain impairments are likely the cause of the decrease in function, thus demonstrating the importance of maintaining normal cellular processes (i.e. not going into shock) to increasing electron flux to an extracellular material. Thus, at high induction activity units, we speculate this apparent correlation between heme *c* concentration and survival is actually an affect of the general toxicity of membrane protein overexpression.

The *cymAmtrCAB* strain survival is instead correlated to iron reduced and anticorrelated to the concentration of heme *c* (Figure 5-4). This deviation from the *mtrCAB* strain indicates a few interesting features of the *cymAmtrCAB* strain. First, the expression of CymAMtrCAB does not appear to perturb viability over these promoter activity units (Figure 5-2C). Further examination of the membrane integrity by fluorescent staining or cryo-electron microscopy compared to the *mtrCAB* strains would provide important supplemental evidence. Thus, unlike the *mtrCAB* strain, the same correlation to strain survival and heme *c* is not apparent (Figure 5-4B).

At this point in time, it is unclear why the *cymAmtrCAB* strain does not show this same toxic effect. It is also unclear why the total heme *c* concentration is lower in the *cymAmtrCAB* strain. The only regulatory element that has changed on the *mtrCAB* region of the *cymAmtrCAB* plasmid is the ribosome binding site (RBS) associated with MtrC. The original *mtrCAB* plasmid design involved the use of an NdeI restriction site as the start codon (Section 2.9.1.1) and the RBS regulating MtrC translation was inherent to the modified pET30a+ vector. This RBS is traditionally used in the expression of cytosolic proteins, thus it is a strong RBS. In the *cymAmtrCAB* plasmid, the native *Shewanella* RBS regulates translation of MtrC. The Salis RBS calculator gives us an approximation of the relative translation initiation rates. The values have been re-tabulated and simplified here for convenience (Table 5-8), but can also be viewed in Table 5-1.

As discussed previously, it is yet unknown which 16S rRNA is appropriate to use for analysis in the B strain of *E. coli* (personal communication, Dr. Salis). Still, Table 5-8 points out some striking differences between the RBS strength on MtrC in the *mtrCAB* and *cymAmtrCAB* plasmids. The *mtrCAB* plasmid has a much stronger RBS on MtrC (8.3 - 87.0 $x10^3$ arb. units) as opposed to the *cymAmtrCAB* plasmid (1.4 - 1.8 $x10^3$ arb. units).

Additionally, the predicted ratio of MtrC:MtrB by calculated RBS strengths in the *S. oneidensis* MR-1 is 1:1.5 (Table 5-8), which is close to the 1:1 ratio found in the conduit. The ratio of MtrC:MtrB is 1:(0.02-0.03) in the *mtrCAB* plasmid; this ratio is 1:(0.2-1.5) in the *cymAmtrCAB* plasmid (Table 5-8). The ratio of MtrC to MtrB more closely matches the original organism in the *cymAmtrCAB*. I speculate that the high theoretical translation initiation rate of MtrC in the *mtrCAB* plasmid is the limiting factor to the biogenesis of MtrCAB in that strain.

The ratio of holo-CymA to holo-Mtr in the *cymAmtrCAB* strain has yet to be determined, but this may aid the prediction of which 16S rRNA is appropriate to use for each protein as the ratios of CymA to the Mtr proteins vary in each case. This would assume that the translation initiation rate directly correlates to the concentration of holo-cytochrome *c*; thus, to do this comparison, one would want to compare multiple induction conditions to ensure that the strain is not biogenesis limited.

Table 5-8. Calculated RBS strengths using the Salis Lab RBS Calculator (*191*).

	Translation initiation rate (AU, x10^3) *mtrCAB* plasmid (I5023)[1-2]		**Translation initiation rate (AU, x10^3) *cymAmtrCAB* plasmid (I5049)[1]**		***S. oneidensis* MR-1 (AU, x10^3)**
Gene	**A**	**B**	**A**	**B**	**B**
cymA	---	---	0.7	4.1	3.5
mtrC	8.3	87.0	1.4	1.8	1.8
mtrA	1.5	6.7	1.5	6.7	6.7
mtrB	0.2	2.7	0.2	2.7	2.7

[1]The A and B columns correspond to the 16S rRNA sequenced used in the calculation: (A) TAACCGTAG and (B) ACCTCCTTA.
[2]The *mtrCAB* has two predicted translational initiation rates. This represents the start site with the more negative ΔG_{total}. For more detail, see Table 5-1.

5.7.2. Increasing the number of electron conduits does not increase solid Fe_2O_3 reduction.

There is not a simple correlation between cytochrome *c* concentration and iron reduction across both strains (Figure 5-8,9). The *mtrCAB* strain only showed a significant increase in iron reduction when the media was supplemented with riboflavin (green half-filled triangle, Figure 5-8). There was a subtle upward trend with increasing heme *c* concentration; however, the 6x increase in heme *c* concentration only increased the iron reduced by 1.7x (red and blue triangles, Figure 5-8A). This method of plotting the data also hides the decline in heme *c* concentration at high promoter activity (red triangle, indicated "1", Figure 5-8A). The *cymAmtrCAB* correlation between heme *c* concentration and iron reduction is concave (Figure 5-8B); in other words, the iron reduced starts high with low concentration of heme *c*, then decreases with increasing heme *c* concentration, followed by an increase with the δ-ALA sample. However, the δ-ALA does not statistically change the iron reduced by the *cymAmtrCAB*$^{0.18}$ strain (Table 5-6).

Taken together, the data shows that, in our most recent strains, simply increasing in the number of conduits does not increase the function of the engineered strains. Further investigation is required to determine if this is inherent to the pathway or if other factors,

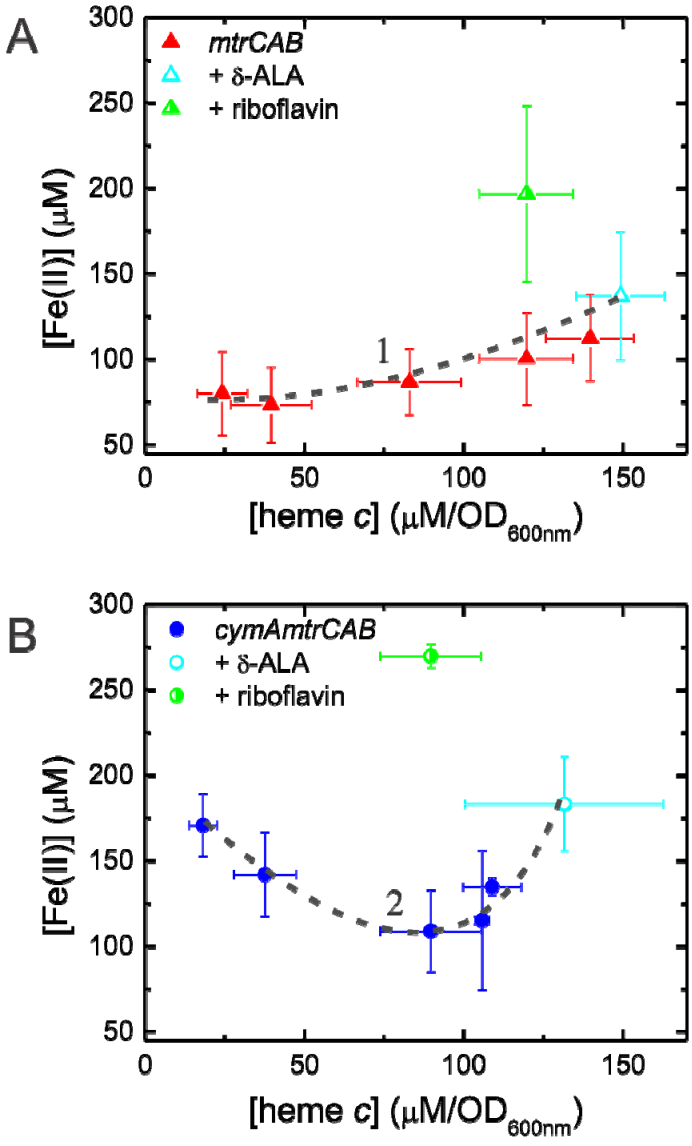

Figure 5-8. Increasing the concentration of heme *c* per cell does not simply correlate Fe_2O_3 reduced in the *mtrCAB* and *cymAmtrCAB* strains. (A) The correlation between iron reduced and number of conduits per cell in the *mtrCAB* strain is plotted. The *mtrCAB* strain only showed a significant increase in iron reduction when the media was supplemented with riboflavin (green half-filled triangle). There was a subtle upward trend with increasing heme *c* concentration; however, the 6x increase in heme *c* concentration only increased the iron reduced by 1.7x (red and cyan triangles). This method of plotting the data also hides the decline in heme *c* concentration at high promoter activity (indicated as "1"). (B) The correlation between iron reduced and number of conduits per cell in the *cymAmtrCAB* strain is plotted. The *cymAmtrCAB* correlation between heme *c* concentration and iron reduction is concave (blue and cyan circles). However, the δ-ALA (cyan) does not statistically change the iron reduced by the *cymAmtrCAB*$^{0.18}$ strain

(indicated as "2"). In both A and B, riboflavin significantly increases iron reduction without changing cytochrome *c* concentration.

---

such as protein ratios or increased carbon utilization, would create a greater dependency on electron conduit concentration.

5.7.3. Addition of CymA moderately improves reduction of solid Fe_2O_3 and has a dramatic impact on cell survival.

Iron reduction was moderately improved with the addition of CymA (Figure 5-4A), but this rate is still comparatively ~30 times slower than *Shewanella* (*173*). The more dramatic effect is seen in the survival of the strains over time. Compared to the increase in soluble iron reduction in the *cymAmtrA* strain in Chapter 4, this increase is modest. This implies that although quinol pool was a rate limiting step in the *mtrCAB* strain, but that there are other factors impeding iron oxide reduction.

The greater effect was observed in the survival of the *cymAmtrCAB* strain (Figure 5-4B). The strain with the better survival at day 4 was also the strain that reduced the most iron oxide measured at day 21 (Figure 5-4). As previously discussed, the limitations of the ferrozine assay do not allow an accurate reading of the Fe(II) concentration at earlier time points. There are three possible explanations for the observed correlation between survival and iron reduction in the *cymAmtrCAB* strain: i) more viable cells increased the amount of iron reduced; ii) the iron reduction rate per cell increased; or iii) both the reduction rate per cell and number of cells increased. A better measurement to determine which explanation is relevant would be measuring the current to an anode because all of these measurements may be made over a shorter time scale.

In summation, we speculate that the addition of CymA increases the recycling of the quinol pool during solid Fe_2O_3 reduction, but that other rate limiting steps for electron flux to extracellular metal oxide still exist.

5.7.4. Extracellular electron transfer is limited by direct contact with the extracellular terminal electron acceptor.

S. oneidensis MR-1 reduces anodes and solid inorganic oxides by both direct contact and by using diffusible redox species, such as riboflavin or flavin mononucleotide (FMN) (*5*, *29*, *47*). It is estimated that 20% of the overall reduction of extracellular inorganic material is specifically due to direct contact with the surface while about 80% is due to diffusible redox species. We sought to determine whether MtrCAB could reduce iron *via* riboflavin in the absence of additional *Shewanella* cytochromes *c*. Because there is basal iron reduction by the *ccm* strain, we use the difference between the *mtr* strains and the *ccm* strain to determine the amount of Mtr-dependent iron reduction. We assume that culture supplemented with riboflavin represents total iron reduced by both direct contact and soluble redox carriers and that the culture without riboflavin is solely direct contact. We find that the ratio of iron reduced by direct contact to redox carriers is 28%:72% and 23%:77% in the *mtrCAB* and *cymAmtrCAB* strains, respectively. These ratios closely match the ratio observed in the native organism (*5*, *29*, *47*). This indicates

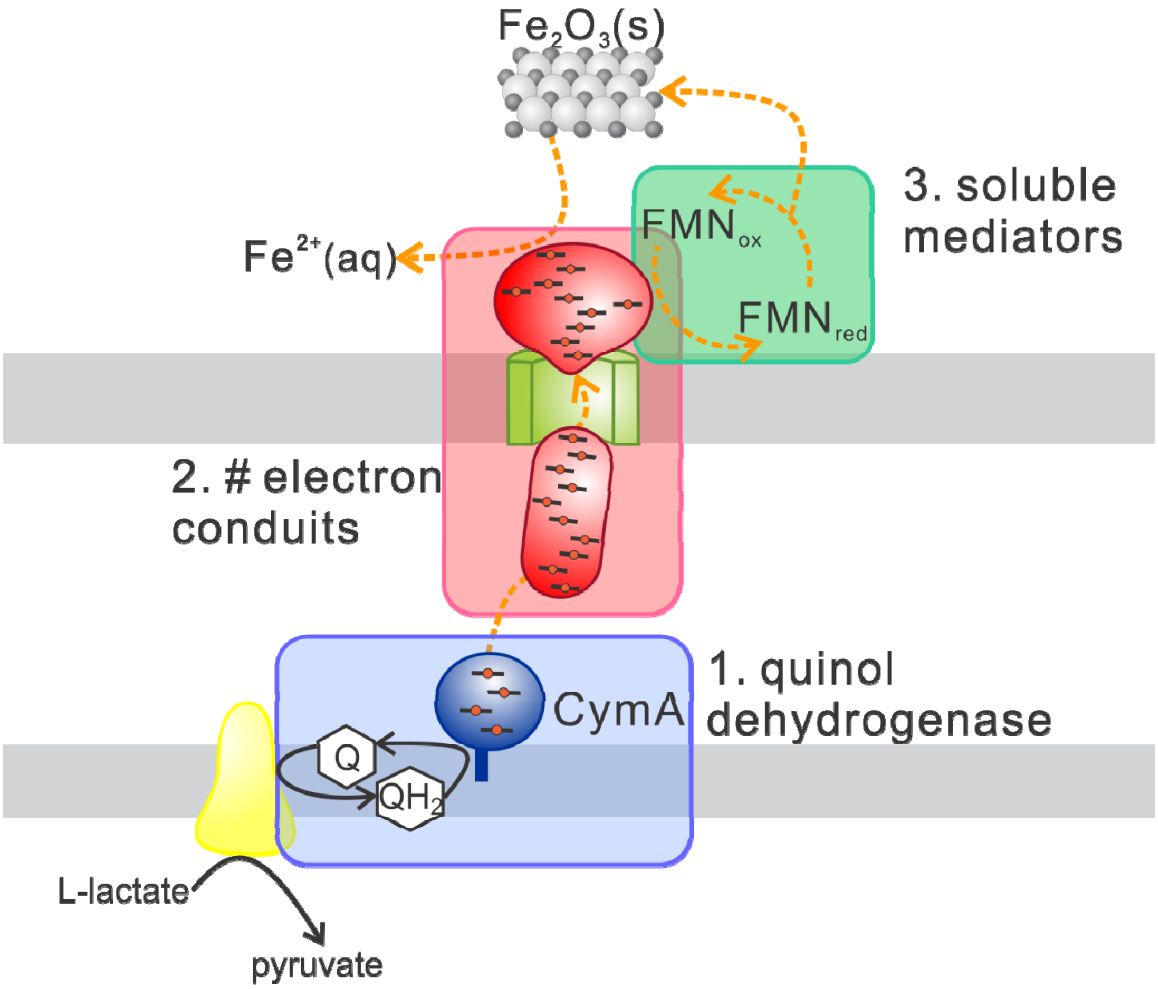

Figure 5-9. Overview of the potential rate limiting steps in the reduction of extracellular metal oxides addressed in this chapter. The first rate limiting step (blue box) of recycling at the quinol pool has been addressed by additional expression of CymA in the engineered strains. However, the ratio of CymA to the Mtr complex in the outer membrane would provide interesting insight into the logistics of the entire pathway. The second potential rate limiting step (pink box) was insufficient Mtr outer membrane complexes to transfer electrons from the quinol dehydrogenase to the extracellular metal oxide. Increasing the number of electron conduits did not improve the iron oxide reducing function of the strains, but rather negatively impacted cell viability. The third potential rate limiting step (green box) is limited surface contact of the Mtr outer membrane complex to the solid metal oxide. This was alleviated by addition of the diffusible redox carrier, riboflavin. Overall, the two limiting factors were the quinol dehydrogenase and direct contact with the metal oxide.

that, like in the native organism, MtrC is able to utilize solid metal oxides as terminal electron acceptors *via* both direct contact with the mineral and diffusible redox carriers.

The reliance on riboflavin to increase the electron flux could be viewed as beneficial or harmful. Redox shuttles would make applications requiring a spatially-defined, molecularly-defined route challenging. Additionally, chemical supplementation adds significant cost during scale-up. However, if an application simply requires the maximal current possible, then the addition of riboflavin would be a critical addition to the media.

5.7.5. Potential remaining rate limiting steps in Fe_2O_3 reduction by *E. coli*.

Enhancing electron flux to an extracellular inorganic material is vital to increase the maximal current that these engineered strains can deliver to an anode. By addressing hypothesized rate limiting steps in the engineered strains, the *mtrCAB* and *cymAmtrCAB* strains demonstrate iron oxide reduction rates 56% and 138% faster, respectively, than the initial strain described in chapter 2. Additionally, the supplementation with riboflavin increased the rates of the *mtrCAB* and *cymAmtrCAB* strains by 139% and 278%, respectively, over the original strain.

The fastest iron reduction rate in the engineered *E. coli* cultures described here is still ~1.3 times slower than *S. oneidensis* MR-1 (*173*) and unable to sustain growth for long periods of time, indicating that further work is still required in strain engineering to match the rates of the native organism. There are still other potential rate limiting steps that could reduce the flux of electrons to an extracellular metal oxide. The *E. coli* lactate dehydrogenase, *ldhA*, evolved to take acetate to lactate rather than lactate to acetate, as in *Shewanella.* Thus the ~300-fold slower activity of the *E. coli* lactate dehydrogenase compared to that in *Shewanella* (*37*) could limit the electron flow to CymAMtrCAB. This could be addressed in one of two ways, depending on the goal. The first would work towards the specific optimization in *E. coli*. One could use alternative carbon sources in the cultures. Although I have done a series of experiments to determine what carbon sources work best in this system, experiments using a mixture of these carbon sources with a fermentable sugar, such as glucose, may provide additional reducing equivalents to the quinol pool. This would likely also increase viability of the strains, which are more suited for anaerobic fermentation than anaerobic respiration; because viability has been shown to directly increase electron flux to both metal oxides and anodes, one may speculate that increasing viability with fermentable substrates may also increase electron flux. The second approach would be transferring the *Shewanella* lactate dehydrogenase to a plasmid for general use. This would be advantageous for moving into other organisms in the future that may also not be evolved for oxidation of non-fermentable carbon sources.

Another potential rate limiting step is that the ratio of CymA to the Mtr outer membrane complex may not yet be optimized. The number of MtrC proteins per cell was reported as 72,000 by Ross (*174*), however the number of CymA per cell in the *Shewanella* has yet to be determined. Once the ratio of CymA to Mtr proteins is known in the *Shewanella* organism, we may better design plasmids to match that ratio in the engineered *E. coli* strains. Then, a series of mutations in the CymA RBS to vary the translational strength associated with CymA could allow the tuning of the concentration

of CymA versus the Mtr complex. Additionally, this could potentially provide interesting insight into whether *Shewanella* expresses the optimal ratio itself.

Finally, these strains were shown to have different efficiencies at metal oxide reduction versus anode reduction. Thus performing similar experiments in an electrochemical set up, where anode reactions happen on a much shorter time scale, would allow us to more carefully evaluate the efficiency of the electron flux.

5.8. Materials and Methods.

5.8.1. Plasmids and strains.

The plasmids and strains used in this study are listed in Table 5-9 and 5-10, respectively. The *ccm* (pEC86) and *mtrCAB* (I5023) plasmids were described previously and co-transformed into the *E. coli* strain C43(DE3) (Lucigen).

Table 5-9: Plasmids used in Chapter 5.

Plasmid	Promoter	Protein coding region	Antibiotic resistance	Source
pSB1ET2 (pET30a+)	T7 *lac*	none	Kan	Jensen 2010
pEC86	tet	*ccmA-H*	Chl	Arslan 1998
I5023	T7 *lac*	*mtrCAB*	Kan	Jensen 2010
I5049	T7 *lac*	*cymAmtrCAB*	Kan	This paper

Table 5-10: Strains used in Chapter 5.

Strain	Cell Line	Plasmid(s)	Gene(s)
ccm	C43(DE3)	pEC86	*ccmA-H*
mtrCAB	C43(DE3)	pEC86, I5023	*ccmA-H, mtrCAB*
cymAmtrCAB	C43(DE3)	pEC86, I5049	*ccmA-H, cymA, mtrCAB*

The *cymAmtrCAB* (I5049) plasmid was constructed for this work. Primers containing an NdeI site and an EcoRI site (Table 5-11, Primers 1 and 2) and Pfx Platinum polymerase (Invitrogen) were used to amplify *cymA* from the *Shewanella oneidensis* MR-1 genome, including 14 base pairs upstream from the start codon. Primers containing an EcoRI site and a PstI site (Table 5-11, Primers 3 and 4) and Pfx Platinum polymerase (Invitrogen) were used to amplify *mtrCAB* from the *Shewanella oneidensis* MR-1 genome, including 116 base pairs upstream from the MtrC start codon where there is a native EcoRI site. First, the *mtrCAB* PCR fragment, digested with EcoRI and PstI (New England Biolabs), was ligated to a modified pET30a+ vector, pSB1ET2, using T4 DNA ligase (Roche). Then the *cymA* PCR fragment, digested with NdeI and EcoRI (New England Biolabs), was ligated upstream of *mtrCAB* in the pET vector. Finally, the start codon, ATG, located in the NdeI site was removed by site directed mutagenesis (QuikChange II, Agilent Technologies) to avoid premature transcription of *cymA* using primers 5 and 6 (Table 5-11). The resulting *cymAmtrCAB* plasmid (I5023) was co-transformed with pEC86 into C43(DE3) (Lucigen) to make the *cymAmtrCAB* strain.

Table 5-11: Primers used in Chapter 5.

Primer	Description	Primer Sequence (5'-3')[1-3]
1	Sense primer, PCR of *cymA* from *Shewanella oneidensis* MR-1 including 14 bp upstream	CCGCCATATGTTGGAGATAGAGT AATGAAC
2	Antisense primer, PCR of *cymA* from *Shewanella oneidensis* MR-1	CCGGGAATTCTTGCAGCGTTAAA CCTTATCCTTTTGG
3	Sense primer, PCR of *mtrCAB* from *Shewanella oneidensis* MR-1, including 116 bp upstream	CCGCGAATTCTATTTCCAGCATC CACTTAAGTCGCT
4	Antisense primer, PCR of *mtrCAB* from *Shewanella oneidensis* MR-1	CCGGTCTAGATTAGAGTTTGTAA CTCATGCTC
5	Sense primer, mutagenesis of NdeI site	AATAATTTTGTTTAACTTTAAGA AGGAGATATACAT***ATT***TTGGAGA TAGAGTAATGAAC
6	Antisense primer, mutagenesis of NdeI site	GTTCATTACTCTATCTCCAA***AAT*** ATGTATATCTCCTTCTTAAAGTT AAACAAAATTATT

[1]**Bold font**: homologous region to BL21(DE3) genome flanking gene to be knocked out
[2]Underlined: region upstream of *cymA* start codon
[3]***Bold-Italics***: mutation site

5.8.2. Growth conditions and media composition.

All strains, unless otherwise specified, were grown in 2xYT media at 30 °C with 50 μg mL^{-1} kanamycin; strains containing the *ccm* plasmid were grown with an additional 30 μg mL^{-1} chloramphenicol. Glycerol stocks were used to inoculate 5 mL 2xYT media, and cultures were grown overnight at 37 °C with 250-rpm shaking. Then 500 μL of overnight cultures were back-diluted into 50 mL 2xYT media and grown with 250-rpm shaking at 30 °C and were induced with IPTG at an $OD_{600\ nm}$ of ~0.5-0.7. After induction, the shaking was reduced to 200-rpm and the cells were grown 16 hours at 30 °C. For samples grown with the heme biosysnthesis precursor, δ-aminolevunlinic acid, 1 mM δ-ALA was added at the initial inoculation of the 50 mL 2xYT.

For periplasmic and membrane fractionations, 5 mL of overnight culture were used to inoculate 1 L media. The cultures were grown with 250-rpm shaking at 30 °C and were induced with IPTG at an $OD_{600\ nm}$ of ~0.5-0.7. After induction, the shaking was reduced to 200-rpm and the cells were grown 16 hours at 30 °C.

Cell suspensions used for $Fe_2O_3(s)$ reduction assays were resuspended in anaerobic defined M1 media supplemented with 40 mM D,L-Lactate and 0.2% casamino acids. The M1 media consists of 50 mM PIPES (piperazine-*N,N′*-bis(2-ethanesulfonic acid)), 7.5 mM NaOH (final pH 7.4), 28 mM NH_4Cl, 1.3 mM KCl, 4.3 mM $NaH_2PO_4 \cdot H_2O$, 100 mM NaCl, and 10 mL/L each of vitamin, amino acid, and trace mineral 100x stock solutions. The 100x vitamin stock solution contained: 2 mg/L D-biotin (B7), 2 mg/L folic acid (B9), 10 mg/L pyridoxine HCl (B6), 5 mg/L thiamine HCl (B1), 5 mg/L nicotinic acid (B3), 5 mg/mL D-panthothenic acid, hemicalcium salt (B5), 0.1 mg/L cobalamin (B12), 5 mg/L *p*-aminobenzoic acid (PABA), and 5 mg/L α-lipoic acid. The 100x amino acid stock solution (pH 7.0) contained: 2 g/L L-glutamic acid, 2

g/L L-arginine, and 2 g/L D,L-serine. The 100x trace mineral stock solution (pH 7.0) contained: 7.85 mM $C_6H_9NO_3Na_3$, 12.17 mM $MgSO_4 \cdot 7H_2O$, 2.96 mM $MnSO_4 \cdot H_2O$, 17.11 mM NaCl, 0.36 mM $FeSO_4 \cdot 7H_2O$, 0.68 mM $CaCl_2 \cdot 2H_2O$, 0.42 mM $CoCl_2 \cdot 6H_2O$, 0.95 mM $ZnCl_2$, 0.040 mM $CuSO_4 \cdot 5H_2O$, 0.021 mM $AlK(SO_4)_2 \cdot 12H_2O$, 0.016 mM H_3BO_3, 0.010 mM $Na_2MoO_4 \cdot 2H_2O$, 0.010 mM $NiCl_2 \cdot 6H_2O$, and 0.076 mM $Na_2WO_4 \cdot 2H_2O$.

5.8.3. Subcellular Fractionation.

Periplasmic and membrane preparations were performed as previously described (*148*).

5.8.4. Diffuse reflectance spectroscopy of whole cells for quantitative heme *c* detection.

The concentration of cytochromes *c* in intact cells were determined by diffuse reflectance as previously described in Goldbeck et. al. (*92*) and Chapter 3.

5.8.5. Enhanced chemiluminenesce (ECL) to detect *c*-type cytochromes in whole cell lysates.

A cell pellet from 1.5 mL of culture was resuspended in 0.1 mL Bacterial Protein Extraction Reagent (B-Per, ThermoScientific). The cells were frozen at -20 ºC immediately after growth and then thawed immediately before analysis. Cells were lysed for 30 minutes at room temperature with lysozyme and DNAse, along with salts necessary for optimal function, to the following final concentrations: 6 μg mL^{-1} chicken egg white lysozyme (Sigma), 1 μg mL^{-1} DNAase, 3.9 mM $MgSO_4$, 0.96 mM EDTA, and 0.98 mM phenylmethylsulfonyl fluoride (PMSF). Total protein of the cell lysates was determined by BCA Protein Assay Kit (ThermoScientific). The appropriate dilution of cells in 100 mM HEPES, pH 7.4, to load a total of 8 μg of protein of whole cell lysate was added to NuPAGE 4x Sample Buffer (Bio-Rad). Samples were heated at 95 °C for 5 minutes and run in a 4-20% Tris-HCl polyacrylamide gel (Bio-Rad) at 200 V for 1 hour. The gel was rinsed twice in water and then equilibrated in cold Pierce Western Transfer buffer (ThermoScientific) for 15 minutes. The proteins were transferred to a 0.45 μm nitrocellulose membrane (Bio-Rad) in Pierce Western Transfer buffer at 30 V for 100 minutes. Ponceau S staining was used to confirm uniform transfer across all lanes.

For the enhanced chemiluminescence staining, the blot was incubated for 5 minutes in 10 mL of Pierce Pico West Enhanced Chemiluminescence substrate (ThermoScientific), a 1: 1 mixture of Pico West Peroxide Solution and Luminol Enhancer solution. The chemiluminescent signal was detected using the ChemiDoc™ XRS system. The chemiluminescent signal and molecular weights were quantified using ImageJ.

5.8.6. Solid bulk Fe_2O_3 reduction assay.

Cells from 50-mL cultures were pelleted, washed, and resuspended in anaerobic M9 minimal media to a final $OD_{600\ nm}$ of 1.0. All subsequent steps were performed in an anaerobic chamber (Coy Laboratory Products) with an environment of 2% H_2 in N_2. For the bulk Fe_2O_3 reduction assay, 6.0 mg mL^{-1} of particulate Fe_2O_3 (Sigma) was added to anaerobic cultures. IPTG was added to the anaerobic media to maintain cytochrome

expression over the period of the experiment. δ-ALA was not added to anaerobic cultures to avoid overproduction and secretion of protoheme IX, which could act as a soluble redox carrier; rather δ-ALA was only included in aerobic growth to strictly observe the affect of increasing the number of electron conduits. Riboflavin was added to certain cultures at 5 μM concentration to observe the affect of soluble redox carriers.

The colony forming units (cfu) and Fe(II) concentration for each culture was measured over time. To determine colony forming units, dilutions of each culture were plated on LB plates supplemented with kanamycin to select for the retention of the *mtrCAB* or *cymAmtrCAB* plasmids. Plates were grown at 37 °C overnight. Colony forming units were measured within the range of 25-200 colonies to ensure a quantitative range. Error bars represent standard deviation by triplicate cultures. The Fe(II) concentration was determined with the ferrozine assay, adapted from Stookey (*168*). One aliquot of each culture was acid extracted in 0.5 M HCl for 1 h. An aliquot of each acid extracted sample was then added to the dye, ferrozine (Acros Organics) buffered in 100 mM Hepes, pH 8.0, which absorbs at 563 nm ($\varepsilon_{563\ nm}$ = 27.9 mM^{-1} cm^{-1}) when bound to Fe (II). The concentration of Fe(II) in each culture was subtracted by any abiotic iron reduction observed in sterile media-only controls at each time point. Error bars represent standard deviation by triplicate cultures.

Chapter 6

Discussion and future work on engineering extracellular electron transfer in heterologous hosts.

6.1. Discussion of the data described in this dissertation.

Both organisms and human-made technological devices use the flow of charge as the basic currency of information and energy. The soft materials properties and waxy cell membranes generally do not interface electrically with solid materials. Creating an interface that permits electrical communication between living and non-living systems would enable new opportunities in fields such as biosensing, bioenergy conversion, and biocomputing. Thus my dissertation focuses on creating a blueprint for the bidirectional flow of electrons between living and non-living systems that is transferrable to a multitude of cell lines. I take a biologically-focused approach to connect the living and non-living worlds: use synthetic biology to introduce a new electron transfer pathway into *E. coli*.

This strategy takes advantage of the respiratory capability of the dissimilatory metal reducing bacterium *Shewanella oneidensis* MR-1. *Shewanella* uses a network of multiheme cytochromes that are able to transfer charge across the inner and outer membranes of the bacteria *via* the heme moiety in the cytochromes. This pathway enables *Shewanella* to route electrons along a well-defined path from the cell interior to an extracellular inorganic material acting as a terminal electron acceptor during anaerobic respiration. By genetically engineering the cell to build and maintain the bioelectronic connections, the cells can autonomously assemble and repair these connections.

This work describes the first time the outer membrane spanning and double membrane spanning *Shewanella* electron transfer pathway was heterologously expressed in *Escherichia coli*. Additionally, these engineered *E. coli* strains are shown to reduce soluble iron, solid iron oxide, and anodes. This work not only serves as a landmark for the expression of complex membrane associated pathways, but it also demonstrates proof of concept that this pathway could be transferrable to other cell lines. This dissertation represents the first step towards engineering bidirectional communications with electrodes, and it opens up an array of opportunities for studying the biochemical and enzymatic properties of these unique proteins as well as the potential for novel hybrid technologies. Here, I will discuss the overall findings described in the previous chapters.

6.1.1. A sweet spot of maximal expression of cytochromes *c* in *E. coli* is achieved *via* tight regulation of *mtr* and *ccm* synthesis.

At the beginning of this project, I primarily worked with the *E. coli* strain BL21(DE3) because of the literature precedence for MtrA expression, as well as its complete T2SS (compared to K-strains). Additionally, the system required T7 RNA polymerase encoded on the genome such that a plasmid regulated by the T7 *lac* promoter was usable. Although the BL21(DE3) strain was able to express *mtrCAB* and demonstrated solid iron reduction (Figures 2-4, 2-6, and 2-7; Pgs 33, 36, and 38), I

observed that induction of the *Shewanella* cytochrome *c* genes in these strains led to a number of cell stress symptoms. These observations included decrease in holocytochrome *c* synthesis (Figures 2-2, 3-4, 3-10, and 5-2; Pgs 29, 54, 64, and 100), slowed growth (Figure 3-3; Pg 49), less biomass from overnight growth (Figure 3-4, Pg 54; Appendix G-1), fewer colony forming units per $OD_{600\ nm}$, increased forward and side scatter in flow cytometry (Figures 3-2 and 3-11, Pgs 49 and 66), damaged membranes (Appendix G-2), and elongated cells (Appendix G-2). These phenotypes suggested that even minimal induction of the *mtr* operon in the original strain was negatively impacting normal cell health. Additionally, since the uninduced conditions gave the highest cytochrome c levels in the original BL21(DE3) strains, we were unable to tune the levels of cytochrome expressed.

In order to gain greater control over the rate of *mtr* synthesis, strains evolved to express membrane proteins, C41(DE3) and C43(DE3) (*84*, *85*), were tested for their ability to express the *mtr* proteins. These so-called Walker strains control the synthesis of the T7 RNA polymerase more tightly, leading to less basal expression in the absence of the IPTG inducer; these strains also produce less T7 RNA polymerase at maximal IPTG induction. Additionally, a library of constitutive promoters was used to tightly control *ccm* synthesis. Screening 16 strains and 12 IPTG concentrations (192 possible conditions) helped to discover a "sweet spot" of maximal expression of the Mtr proteins (Figure 3-4, Pg 54). With the expression profile of these conditions, a phase diagram of how these controls impact holocytochrome *c* production in *E. coli* was proposed (Figure 3-12, Pg 68). When the transcription of *ccm* and *mtr* were too low, there was not enough polypeptide synthesized. When *ccm* transcription was too high, the secretion limited the amount of Ccm available in the inner membrane to attach the hemes; when *mtr* transcription was too high, the system was maturation limited (Figure 3-12, Pg 68). Thus, cytochrome *c* expression requires gentle tuning of the various components to achieve maximal holocytochrome *c* expression. These observations may be applied to other membrane protein expression systems.

6.1.2. Function of the electron conduit in *E. coli* is correlated with cell fitness rather than the number of electron conduits per cell.

Originally, I hypothesized that increasing the number of electron conduits per cell would increase the electron flux to an extracellular metal or an anode. The reasoning specifically is that increasing the number of conduits would increase the specific possible contact sites between the cell and the electrode, as well as increase the total number of routes that metabolic electrons could traverse across the membranes. An analogy to this hypothesis is that by adding additional lanes (conduits) to a highway, there are more potential paths for cars (electrons) to navigate.

However, I observed across many different strains and experiments that the maximum expression of the electron conduit per cell does not correlate with maximal reduction of extracellular acceptors (Figures 3-11, 5-3, 5-4, and 5-8; Pgs 66, 102, 103, and 111). In fact, usually strains with fewer electron conduits per cell and better overall cell health demonstrated the greatest electron flux to an extracellular terminal electron acceptor (Figures 3-11, 4-8, 5-3, 5-4, and 5-7; Pgs 66, 89, 102, 103, and 108). There are a number of possibilities that could explain this counterintuitive observation. For example, if there are limited electrons being delivered to the conduit, then it would be

inherently true that increasing the number of conduits per cell will not increase electron flux. Thus, in this case, the rate of electrons flowing into and out of all the conduits in a cell is not limiting. Another possibility is that there may be additional proteins or carriers that are as yet unidentified that enhance the rate of transport across the periplasm. Thus, it is imperative that future researchers keep an open mind about the number of conduits per cell in the engineered strains and reevaluate this conclusion as factors like coulombic efficiency are improved in the engineered strain.

To summarize these findings, one may again apply the highway analogy. It was anticipated that adding more lanes to the highway would increase the number of potential paths for cars. However, if there are few cars (i.e. electrons), then increasing the number of lanes (i.e. conduits per cell) will not increase flow. Thus there are still many avenues that must be investigated to improve the heterologous electron transfer pathway such that it performs at the maximum potential. Additionally, knowing that cell growth confers a selective advantage in function allows for a simple phenotype for screening adaptive evolution of anode reduction.

6.1.3. Matching the inner membrane quinol dehydrogenase to the electron conduit increases electron flux to both soluble and insoluble terminal electron acceptors.

In the original design of this project, the strains were designed such that the electron transfer to MtrA relied upon *E. coli* inner membrane cytochromes *c*, like NapC (Figure 2-6, Pg 36). This approach was taken because the expression of the partial pathway, MtrCAB, was already an ambitious challenge in functional expression. Although this was a necessary first step, this approach undercut one of the goals of making this system a transferrable pathway: a molecularly defined route for electron transfer. Without a specific electron transfer partner connecting metabolic electron stores at the quinol pool and MtrA, there is an undefined step in the pathway.

Based upon sequence homology, it was predicted that NapC could functionally replace CymA in the heterologous system (*64*). Additionally, the homologue for SirCD, NrfCD, was proposed to act as a separate quinol dehydrogenase capable of replacing CymA (*71*). In addition to these proteins, there were two other inner membrane cytochromes *c*, TorY and TorC, with high sequence homology to CymA (Table 4-1, Pg 75; Appendix C-2). To test whether any or all of these proteins could donate electrons to MtrA, a series of knockouts were developed using the Datsenko and Wanner λ-red knockout method (*170*). By testing these strains for their ability to respire Fe(III) citrate in the presence and absence of MtrA, we were able to infer their relative ability to donate electrons to MtrA in iron citrate reducing conditions. This data suggests that NapC (Figure 2-6, Pg 36) and NrfCD (Figure 4-3, Pg 79) are the primary electron donors to MtrA, while TorY and TorC do not participate significantly (Figure 4-4, Pg 81).

To increase the flux of electrons to an extracellular terminal electron acceptor, new strains were developed to express the first half of the pathway, CymA MtrA, as well as the complete pathway, CymA MtrCAB. The addition of CymA as the inner membrane quinol dehydrogenase was predicted to be an important addition to the heterologous pathway because it is theoretically better matched for electron transfer to MtrA based on the fact that these proteins co-evolved together in the same organism. As predicted, CymA was shown to increase both iron reduction and fitness in the case of Fe(III) citrate respiration (Figures 4-6 and 4-7; Pgs 86-87) and solid Fe_2O_3 respiration (Figures 5-4,

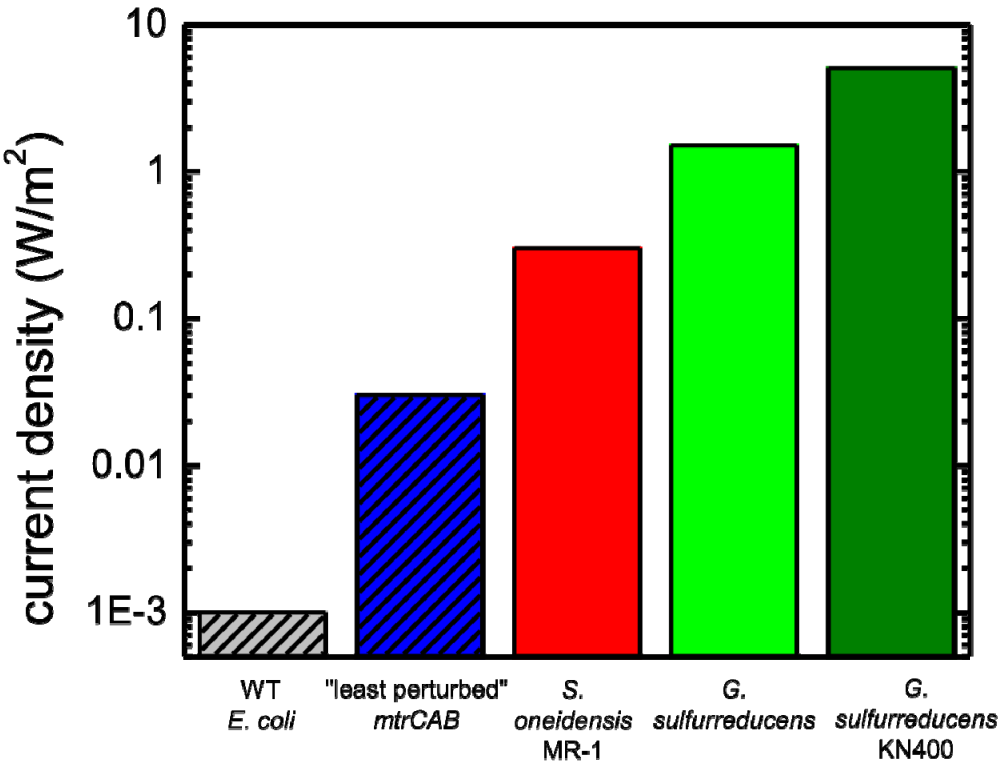

Figure 6-1. The current density of the "least perturbed" engineered strain has drastically improved over the background current, but still shows that there is much room for improvement. *E. coli* strains are showed in hashed columns. The current density measured from the "least perturbed" *mtrCAB* strain shows a 30x increase in current density measured from the "least perturbed" strain (blue) over the baseline current (grey). This signifies a marked improvement conferred by the careful tuning of both the *mtr* and *ccm* operons in the engineered *E. coli*. Although the current density of this particular strain is much higher than the background, it is still an order of magnitude less than the native *Shewanella oneidensis* MR-1 current density (red). Current densities of *Geobacter sulfurreducens* (light green) and *Geobacter sulfurreducens* KN400 (dark green) have current densities 50x and 160x greater than the least perturbed *E. coli* strain, respectively.

5-5, and 5-8; Pgs 103, 105, and 111). Additionally, the expression of CymA confers the selective advantage of growth or greater survival in the iron citrate (Figure 4-6, Pg 86) and iron oxide respiration (Figures 5-4 and 5-7; Pgs 103 and 108). Thus, the expression of the full pathway now allows us to further control the pathway modularity, potentially creating more opportunities for creating an electron transfer toggle switch.

6.1.4. How do these engineered *E. coli* strains compare to *Shewanella*?

The performance of the engineered strains must be compared to the native strains in order to know how the function of the strains may be improved. The current density measured from the "least perturbed" strain in Chapter 3 (Figure 3-11, Pg 66) is displayed with current densities of *Shewanella* and *Geobacter* strains in Figure 6-1. This shows a 30x increase in current density measured from the "least perturbed" strain (blue, Figure 6-1) over the baseline current (grey, Figure 6-1). This signifies a marked improvement conferred by the careful tuning of both the *mtr* and *ccm* operons in the engineered *E. coli*. Although the current density of this particular strain is much higher than the background, it is still an order of magnitude less than the native *Shewanella oneidensis* MR-1 current density (red, Figure 6-1). Current densities of *Geobacter sulfurreducens* (light green, Figure 6-1) and *Geobacter sulfurreducens* KN400 (dark green, Figure 6-1) have current densities 50x and 160x greater than the least perturbed *E. coli* strain, respectively. It is generally observed that *Geobacter* strains can reach higher current densities than *Shewanella*; however, the *Geobacter* electron transfer pathway is not yet fully characterized. Thus, the enhanced function of *Geobacter* cannot be paired with other interesting pathways, such as carbon fixation pathways, which severely limits biotechnological applications that one could imagine possible with *Geobacter*-level current densities.

These observations suggest that there are still ways to improve current density in the engineered *E. coli* strains. I believe that optimizing the coulombic efficiency of the strain and the ratios of the proteins expressed are imperative to enhance the function of the engineered *E. coli* strains such that they match that of *Shewanella*.

6.2. Suggested future work.

In this section, I will describe unanswered questions from the work described above and suggest possible ways that they may be addressed.

6.2.1. How can the coulombic efficiency be improved in the engineered strains?

One of the unexplored hypotheses discussed in minor detail above is the problem of coulombic efficiency. Coulombic efficiency is the number of electrons that were delivered to the anode compared to the total number of electrons possible based on the amount of carbon source added. If one assumes that all of the current energy output by the strains is from lactate oxidation, then the coulombic efficiency of the BL21(DE3) *mtrCAB* strain is ~0.1% (Appendix F-4, Figure F-7), and the coulombic efficiency of the BL21(DE3) *cymAmtrCAB* strain is ~1% (Appendix F-4, Figure F-8). To compare to the native organism, *Shewanella oneidensis* MR-1 has been shown to have a coulombic efficiency of up to 18%, while other *Shewanella* strains have been reported to have coulombic efficiencies of up to 35% (*196*). This is an important factor that must be

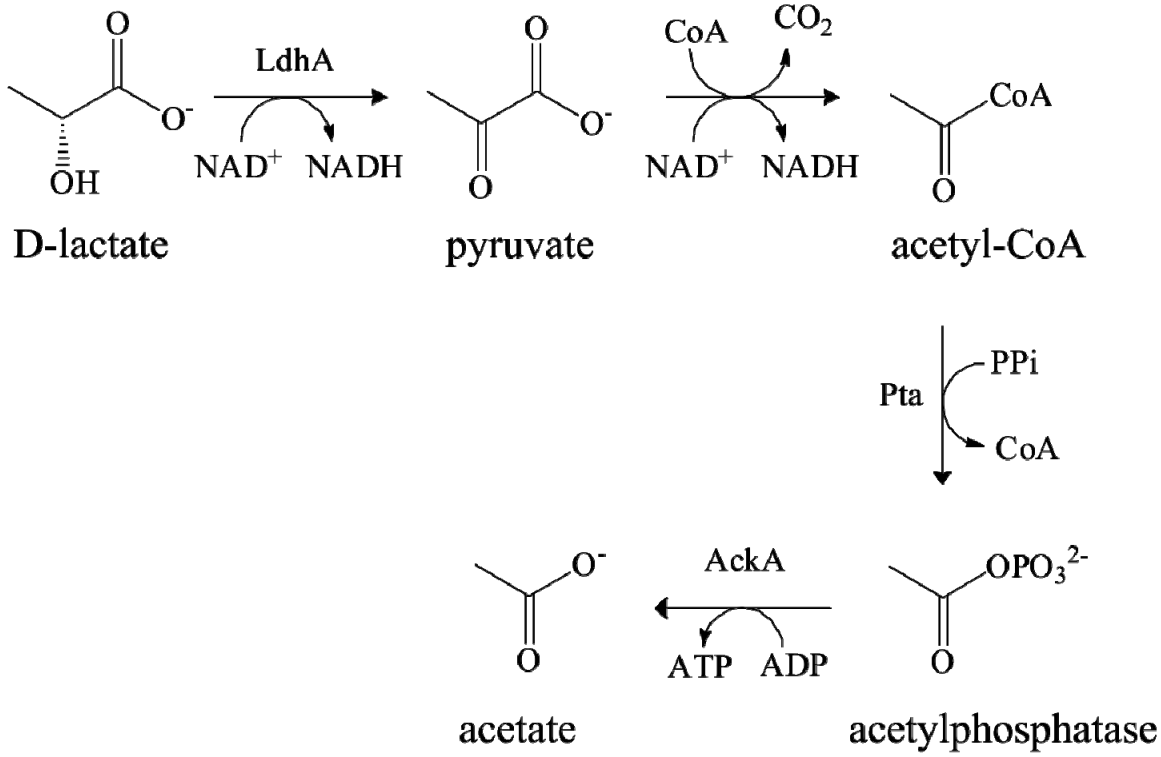

Net reaction:

$$ADP + Pi + 2\ NAD^+ + C_3H_6O_3^- \longrightarrow C_2H_3O_2^- + CO_2 + 2\ NADH + ATP$$

Thus, 4 e^- per 1 molecule lactate

Figure 6-2. The respiration scheme of lactate in *E. coli* results in 4 electrons per molecule of lactate. Lactate is broken down in several steps to acetate, and the chemical energy is stored in the form of NADH. Each NADH stores two electrons, and these electrons are transferred to the quinol pool by the proton pumping NADH dehydrogenase, NDH-1. For every lactate molecule, 4 electrons may be delivered to the quinol pool and 8 protons are pumped across the inner membrane.

improved to reach the power density required for applications because, by improving coulombic efficiency, it is predicted that the current, or electron flux, to an anode would also increase.

6.2.1.1. Specifically improving lactate utilization by heterologous expression of lactate dehydrogenase.

Because the coulombic efficiency is basically a measure of how many possible electrons are received at the electrode, this property can be attributed to how well the carbon source is utilized by the strain. In our system, the carbon source used is lactate. Chemical energy from lactate is obtained in the form of NADH from the breakdown of lactate to acetate. The proposed scheme is shown in Figure 6-2. The respiration of D-lactate results in the formation of two NADH molecules, which store 2 electrons each. The proton pumping NADH dehydrogenase, NDH-1, transfers the electrons from NADH to menaquinol in the inner membrane. The proton motive force for NDH-1 is estimated to be 2 H^+/e^-, or 4 protons per NADH (*77*). Overall, for every lactate molecule, a maximum of 4 electrons may be delivered to the quinol pool and 8 protons are pumped across the inner membrane.

It was shown that the lactate dehydrogenase activity in *E. coli* was 10-fold lower at oxidizing lactate than the *Shewanella* D-lactate dehydrogenase (38 ± 3 vs. 835 ± 89 nmol mg^{-1} min^{-1}) (*37*). This relative difference could contribute for the 18-fold difference in coulombic efficiency discussed in the previous section. Thus, I hypothesize that expressing the lactate dehydrogenase from *Shewanella oneidensis* MR-1 in the engineered *E. coli* strain would confer the ability to oxidize lactate at a rate closer to *Shewanella* and generate a greater metabolic electron store at the quinol pool.

The challenge to express yet another set of proteins must be addressed. Because this system is already a 2-plasmid expression system, it quite limits the ability to add yet another plasmid. For each plasmid introduced, each must have its own origin of replication, antibiotic resistance marker, and induction system. Designing a three-plasmid system in *E. coli* is challenging on its own, which would make moving into broad-host plasmids an even greater challenge. Thus a solution that may be broadly applicable to other strains must be devised. In other words, proposing to make changes on the genome would be a low-throughput solution because these changes may become necessary when moving into new organisms. Thus I suggest that our system necessitates the creation of a plasmid that has two separate expression operons under the control of tightly tunable promoters. It is essential that these promoters use different inducers such that each could be controlled separately.

Adding a second operon in one plasmid of a 2-plasmid system would allow us to expand the potential of this system. For instance, it would allow us to use the artificial amino acid system to study protein dynamics (*197–200*). Another potential example would be expressing additional protein systems proposed to be of importance in power density output, such as a biofilm protein. Yet another application one can imagine in the long-term would be the addition of proteins necessary for electrosynthesis of complex molecules. Thus, by re-designing the plasmids to allow for additional protein expression, the application set of this system expands drastically.

It is important to note that the anaerobic media is also supplemented with hydrolyzed casein as a source of amino acids and that these amino acids may also be

utilized as carbon sources. To make a more careful measure of the coulombic efficiency of the strains, I suggest using media not supplemented with hydrolyzed casein. This could possibly further decrease the observed coulombic efficiency, but by carefully controlling the carbon sources available to the strain, we will gain a more detailed understanding of the electron transfer mechanism in *E. coli*.

6.2.1.2. Screening anode respiration with a series of carbon sources and variable dissolved oxygen concentrations could maximize current density in the engineered *E. coli* strains.

An alternative way to address low coulombic efficiency without additional genetic engineering is to screen existing strains for the best possible set of conditions for anode respiration. I consistently observe that increased cell viability is correlated with increased iron oxide and anode reduction. If this correlation between function and viability is generally true, then one could also argue that providing conditions in which the cells may better thrive would also increase function. For example, it was previously assumed that avoiding fermentable substrates, such as glucose, would force the strain to only anaerobically respire the solid substrates as a terminal electron acceptor. However, as discussed above, lactate dehydrogenase is a poor enzyme in *E. coli*. By providing a substrate that *E. coli* is evolved to metabolize, like glucose, perhaps the viability would increase and thus current output would increase. In addition, oxygen had to be completely absent from the iron citrate and iron oxide reduction assays because O_2(g) will immediately re-oxidize Fe(II) to Fe(III) in the presence of O_2 under neutral pH, which would distort iron reduction results. However, anodes are not oxygen sensitive in this way, which makes electrochemical cells an ideal way to investigate if low oxygen conditions enhance current output. Additionally, it was observed by TerAvest et al. that low oxygen presence (i.e. not detectable by a dissolved oxygen sensor) by passive diffusion increased current output in *Shewanella* (personal communication).

Thus, I hypothesize that current density and coulombic efficiency could be improved by screening different carbon sources and dissolved oxygen concentrations without additional genetic modifications. This is a fairly simple but labor intensive theory to test. In *E. coli*, non-fermentable carbon sources include lactate, glycerol, and formate; and the typical fermentable substrate of *E. coli* is glucose. As a first step, I would suggest testing the *cymAmtrCAB*$^{0.001}$ culture in a three-electrode electrochemical cell with 40 mM of the individual non-fermentable carbon sources in parallel with cells that have mixed 50/50 non-fermentable carbon sources and glucose. An additional sub-set of these experiments would be repeated with low dissolved oxygen by passive diffusion. Ideally, the essential data collected in these experiments would include current output over time, cell density, media pH, and media analyte concentrations by HPLC (for accurate coulombic efficiency calculations). It would also be interesting to collect spectroscopic data to see how the cytochrome *c* concentration is changing over time in these strains.

Although these experiments are relatively straightforward, the data will require careful analysis to get the full story of how viability and current output are related. Specifically, the data will need to be presented as coulombic efficiency, total current output, as well as current per cell. The coulombic efficiency is a testament to how well the carbon source is being utilized; these data would be vital for scale-up applications in which economical use of the carbon source is required. The total current output, likewise,

would be a testament to what conditions are overall the most "economical," or generate the most current overall. However, the overall current does not indicate whether the greater current density is the result of better conditions for cell growth or better conditions for electron transfer; i.e. it does not address whether the current is increased just because there is an increase in the number of cells. Thus, the performance of the cells should also be presented as current density per cell. Strains and conditions that increase current density per cell would represent the conditions in which the cells are the best "catalyst" or electron donors to the anode. It is expected that this should correlate with enhanced carbon source utilization and coulombic efficiency.

Screening for the best carbon source utilization is an attractive option because it does not involve the additional work of developing new plasmid systems or the complications inherent to additional membrane protein expression; however, it would require "brute force" experimentation up-front to screen many different carbon sources and combinations of carbon sources. Both approaches have their own merit, and I would suggest trying both in tandem to see which provides the best results.

6.2.2. How does the relative ratio of CymA to Mtr change the efficiency of the pathway and quinol pool turnover?

In Chapter 5, I discussed that another potential rate limiting step in electron transfer to the extracellular iron oxide was that the ratio of CymA to the Mtr outer membrane complex is not optimized in the current strain. The relative concentration of CymA to Mtr per cell is not yet reported for *Shewanella*, and one can imagine that this ratio might change based upon the needs of the cell and respiration conditions. Thus having a way to tune the concentration of CymA relative to the Mtr proteins may provide interesting insight into how these proteins interact in the native system. Additionally, the only CymAMtrCAB strain tested to-date has only allowed testing of one CymA concentration in metal oxide reducing conditions; this strain does not allow us to determine if we are limited by CymA concentration in the cell because any inducer concentration decreased the iron reducing capability.

Thus, I hypothesize that additional control on CymA expression relative to that of the Mtr proteins could maximize electron flux to an extracellular inorganic surface. I propose making a series of plasmids with variable ribosome binding site sequences such that we have a large range of RBS strengths relative to the Mtr proteins. This would be a way to tightly control the ratio, while the inducer IPTG controls the overall amount of cytochromes *c* expressed.

To address this question, first the ratio of CymA to Mtr proteins should be determined in *Shewanella*. This would help guide plasmid design with the Salis RBS calculator. Currently, Matt Hepler in the Ajo-Franklin lab is working towards a technique to determine relative concentrations of cytochromes *c* in the engineered strains *via* diffuse reflectance and quantitative enhanced chemiluminescence staining. Once the relative staining activities of MtrC, MtrA, and CymA are known, this technique could potentially be applied to *Shewanella* samples grown under different conditions. This would be fairly difficult to determine compared to the engineered *E. coli* strains because there are 42 *c*-type cytochromes encoded on the *Shewanella* genome, thus adding additional background not present in the *E. coli* strains. Thus, I suggest also pursuing this ratio by

quantitative immunoblotting, although the Ajo-Franklin lab currently does not have access to antibodies for these proteins.

A series of mutations in the RBS sequence preceding CymA would then create a library of variable translational rate of CymA. Translational rate is predicted with the Salis RBS calculator. Currently there are two 16S rRNA sequences known in the BL21(DE3) strain, each of which give strikingly different predicted translational rates especially in regard to the relative predicted ratio of CymA to MtrC/A (Tables 5-1 and 5-8; Pgs 97 and 109). This complicates the predictive nature of the RBS strengths; however, close examination of the data in Salis et al. shows that the relative RBS strengths are more meaningful on a log scale (*191*). Thus, I suggest randomly designating one of the 16S rRNAs as the predictor and making a library of RBS strengths in two stages. First, create a library over a large range of RBS strengths. For example, RBS strengths increasing by an order of magnitude over the range of 0.1 to 100,000 would enable large-range screening. These strains should be analyzed for their concentration of CymA per cell, as well as MtrCAB per cell. Lastly, the strains would be screened for their effect on iron oxide respiration or electron flux to an anode. If a particular range of RBS strengths showed improved function, then a second series of mutations could be constructed to fine tune the RBS of CymA further.

Another approach would be developing a plasmid with CymA on one inducible promoter and MtrCAB on another inducible promoter. However, as discussed in the previous section, because we also have to contend with expressing the *ccm* operon on a separate plasmid, we are limited by expression systems. This idea is similar to the pCDFDuet plasmid system (*201*). This plasmid has two coding regions under the same inducible promoter (T7 lac), thus it would not be able to separately control the CymA and MtrCAB operons. In order to proceed with this method, a new plasmid with two coding regions under separate inducible promoters would be necessary. As discussed earlier, creating such a plasmid would be beneficial to this system because it would allow additional expression of other operons; however, by choosing to express CymA off of the 3rd coding region, it would take away that freedom. One interesting aspect of this approach is that it would allow us to test if separate transcription of CymA provides a toggle switch to electron flow to an anode. Thus I suggest that the first approach of tuning the RBS strength would provide a better long-term solution to engineering the CymA/Mtr ratio.

Tuning the RBS associated with CymA would allow the tuning of the concentration of CymA versus the Mtr complex. These experiments would determine a catalytic amount of CymA in the heterologous electron conduit.

6.2.3. How do lipoproteins get localized to the outer leaflet of the outer membrane in *E. coli*?

It is as yet unclear how MtrC is localized to the outer leaflet of the outer membrane in either Shewanella or *E. coli*. The T2SS is fairly well described for the secretion of polypeptides across the inner membrane and the outer membrane. The chaperoning and mechanism of insertion of integral β-barrel proteins in the outer membrane is starting to become clear. In addition, the lipidation of lipoproteins is well characterized as well as their chaperoning to the inner leaflet of the outer membrane. However, the literature fails to discuss how the Lol pathway and Gsp pathway work

together to chaperone lipoproteins to the outer leaflet of the outer membrane. It has been shown GspD and GspG are essential in *Shewanella* for dissimilatory metal reduction as well as the localization of some outer membrane lipoprotein cytochromes *c* (*74*, *75*). It is currently unclear how the lipidation of MtrC and localization to the inner leaflet of the outer membrane by Lol may interplay with Gsp localization to the outer leaflet of the outer membrane.

Furthermore, *E. coli* does not have any major cell surface exposed lipoproteins. The most abundant lipoprotein in *E. coli* is Braun's (murein) lipoprotein, or Lpp (*134*). Braun's lipoprotein is a trimer that forms an alanine-zipper structure, spanning approximately 8 nm in length (*202*). Lpp is involved in the stability of the membrane and tethering the peptidoglycan layer to the outer membrane. One unique feature of Lpp is that it is found in two orientations in the membrane: tethered to the peptidoglycan layer (periplasmic) and integral to the outer membrane (surface exposed); the ratio of periplasmic to surface exposed Lpp is 2:1 (*203*, *204*). The lipoprotein TraT was demonstrated to be surface exposed by enzymatic isotope labeling in whole cells (*205*). However, research on TraT seems to have dropped off significantly since the mid 1990's, leaving relatively little information available on the structure. Both of these proteins were used as display systems for small peptides on the surface of the cell (*206*, *207*). Again, however, neither of these proteins – or other *E. coli* lipoproteins – is proposed to be almost completely surface exposed as MtrC; they even may have variable localization in the membrane.

The physical orientation of the electron conduit is vital to its function, and thus begs for additional investigation of the specific localization of MtrC in *E. coli*. This is especially important because, as discussed above, there are no known native *E. coli* lipoproteins that are proposed to be solvent exposed to this degree. It has been assumed in our system that at least some portion of MtrC is correctly localized to the outer leaflet of the outer membrane because of the strain functionality. However, one can imagine that if only a small percentage of MtrC exposed is properly localized, then the additional MtrC expression and periplasmic face localization would be a significant and unnecessary burden on the cell.

Thus, I propose that a series of experiments must be performed to identify the precise localization of MtrC in the heterologous system. If there is a significant sub-set of MtrC that is not surface exposed, the relatively unstudied localization must be studied in the native host. Additionally, it would be quite informative to follow the expression of and discover the targeting sequence of MtrC because it could potentially open the door to an entirely new method of programmed surface exposed expression of targets for whole cell applications without the need of fusion proteins.

In all of the fractionation data reported in this dissertation, MtrC was observed in the membrane portion of subcellular fractionations (Figures 2-3 and 5-2; Pgs 31 and 100). However, this does not distinguish between inner or outer membrane. There are methods to separate the inner and outer membrane, such as density gradient separations, however this still would not differentiate between the different periplasmic and outer leaflets of the outer membrane. To determine whether MtrC was surface exposed, Shi et al. used a proteinase K assay in wild type *Shewanella* as well as *gspD* and *gspG* knockouts (*75*). Shi and coworkers found that the membrane impermeable serine protease decreased MtrC in the wild type strain, observed by western blotting, but not in the T2SS knockouts

(*75*). This suggests that proteinase K is a viable candidate for screening cell surface exposure of MtrC.

Previously, I had worked with Cheryl Goldbeck in the Ajo-Franklin lab briefly on using proteinase K to detect changes in the cytochrome *c* peaks in whole cells; however, this did not show a visible change in peaks. In addition, these experiments were performed before the diffuse reflectance technique for detecting cytochromes *c* was developed. Detecting changes in the cytochrome *c* concentration in whole cells by dual-beam visible spectroscopy is a qualitative measure complicated by cell scattering; additionally complicating this measurement was the presence of MtrA which also contributes to these peaks. Thus I propose that the proteinase K treatments should be revisited. In the next round of experiments, I propose that both diffuse reflectance and enhanced chemiluminescent staining of the cytochromes in whole cell lysates be analyzed for changes in overall cytochrome *c* concentrations per cell and specific changes to the amount of MtrC per cell, respectively. I suggest that this method be done on the *mtrA*, *mtrCAB*, and *cymAmtrCAB* strains, where the *mtrA* strain could act as a negative control. It would also be worth doing this same procedure with *Shewanella* as a positive control for the method. Additionally, *gsp* mutants are available in the Keio strain collection (*208*), so a similar test as performed by Shi et al. to determine Gsp dependence on MtrC localization could be performed in the heterologous system. Note that the Keio strains are K-12 derivatives without the T7 RNA polymerase, so they cannot directly be used for this test; however, these strains demonstrate that the *gsp* genes are not essential genes and thus are capable of being knocked out in the strain of our choosing.

Specifically, equal number of cells from each strain should be resuspended in buffer with 0.5 mg/mL proteinase K added. The manufacturer (New England Biolabs) suggests using Tris buffer, pH 7.4, for maximal activity, but I would recommend also trying the buffers HEPES or PIPES if Tris is observed to affect cell viability or membrane porosity. Additionally, sodium chloride should be added to prevent cell lysis (~100-150 mM NaCl), and calcium chloride should be added for proteinase K activity (1 mM $CaCl_2$). Shi et al. also added 50 μM $MgSO_4$ to the protease buffer. It is important that the cells must not be lysed and the outer membrane must not be permeabilized; the *mtrA* strain can be used as a control for these affects because normally the periplasmic MtrA protein should not be proteolyzed by proteinase K in intact cells. Incubation times should be tested between 1-3 hours at room temperature. After incubation with proteinase K, the enzyme should be inactivated by phenylmethylsulfonyl fluoride (PMSF). The treated cells should be spun down and washed to remove trace proteinase K. Then whole cell lysates may be prepared as reported previously in Chapters 4 and 5. These lysates may be run by SDS-PAGE and stained by enhanced chemiluminescence to test for changes in the MtrC band; equal number of cells should be loaded for direct comparison of the MtrC band per cell.

If it is found that a large fraction of MtrC is not localized on the cell surface in comparison to the *Shewanella* positive control, one must address the localization mechanism of MtrC. It is altogether possible that *E. coli* does not recognize the signal for localizing this lipoprotein to the cell surface *via* Gsp. Because there is still no known consensus sequence for chaperoning proteins to Gsp secretin, it is currently not possible to engineer or optimize the signal sequence specifically for *E. coli*. Because the Ajo-Franklin lab's expertise is cytochrome *c* expression, it would be wise to collaborate with

type 2 secretion system experts to discover what portions of the Lol and Gsp systems are required for proper MtrC expression.

6.3. Emerging applications and movements to come in the field of heterologous electron conduit expression.

There are three important directions that are wide open in this field for serious advancement: (1) testing inward electron transfer for electrosynthesis; (2) expressing electron conduits from other genera; and (3) moving the *Shewanella* conduit into other organisms that perform unique tasks.

Gralnick and coworkers recently reported that *Shewanella* could utilize the same pathway to oxidize a cathode, essentially injecting electrons into the cells and allowing the synthesis of succinate (*26*). Additionally, the Lovley lab has shown the same injection of electrons into acetogens to convert carbon dioxide into water and complex carbon organic compounds (*27*, *28*). Reversing the electron flow in the heterologous pathway allows us to expand the applications to synthesis of complex molecules and carbon fixation in a wide variety of microbial genera.

It is worth continually asking ourselves if we are expressing the "right" pathway. In other words, is there another pathway in the dissimilatory metal reducing bacteria subset that will perform better than the *Shewanella* pathway? This is an open-ended question that does not have a straightforward answer. *Geobacter* and *Geothrix* are additional genera discussed in the literature for their ability to reduce anodes, and each genus has its own set of advantages and disadvantages. The *Geobacter* pathway is not well characterized, inherently making it difficult to reengineer in another strain. However, this pathway is unique from *Shewanella* in that it only performs electron transfer in direct contact with an electrode (*11*, *30*). So if an application cannot rely on soluble redox factors, perhaps the *Geobacter* pathway would be better suited than the *Shewanella* pathway. Additionally, the *Geobacter* strain is capable of producing much higher power densities than *Shewanella*, making it a very attractive option for re-engineering into a heterologous organism (Figure 6-1).

Geothrix fermentans is another emerging DMRB with its own unique properties (*31*). *Geothrix* displayed optimal current density at +0.55 V vs SHE, which is unusually high compared to typical 0 V vs SHE of other bacteria (*31*). Like *Shewanella*, *Geothrix* secretes soluble redox mediators. However, the mediators secreted by *Geothrix* are unique because they have two radically different midpoint potentials: riboflavin at -0.2 V and an unidentified mediator with UV-absorbance at +0.3 V (*31*). Although the electron conduit in *Geothrix* is also not yet characterized, this genus provides the potential for a heterologous strain to operate at a large range of redox potentials. As more microbes and pathways are characterized and add to our understanding of dissimilatory metal reduction, we may be able to utilize the different pathways to specifically tune the redox potentials necessary for different types of anode or cathode reactions.

This dissertation has broadened our understanding of the expression of these complex pathways in heterologous organisms. While expressing the *Shewanella* pathway in *E. coli* was a necessary step for proof-of-principle, *E. coli* is not well-suited for high-impact, breakthrough applications. With the lessons we have learned in cytochrome *c* expression, it is now possible for us to explore moving the pathway into other organisms with interesting biotechnological applications. Our system allows us to combine the

electron conduit with complex pathways, like carbon fixation and photosynthesis. These unnatural pathway combinations would drastically expand the applications in energy conversion, biosynthesis, and biosensing applications. When moving forward into more diverse strains, it will be important to consider the anaerobic metabolism and the post-translational modification efficiency, as discussed in Section 1.3.5. To transfer the system to a different prokaryote would simply require the choice of an appropriate promoter and origin of replication, use of a host-specific signal sequence to ensure proper localization, and modification of the ccm genes to achieve their expression under aerobic conditions.

6.4. The first step towards engineering bidirectional communications with electrodes has demonstrated proof-of-concept and opens the door to new hybrid technologies.

Engineering an efficient means of bi-directional electronic communication between living and nonliving systems has the potential to create hybrid applications in bioenergy, biosensing, and biocomputing. My dissertation was demonstrated the feasibility of a wholly biological approach that meets this challenge and provides a novel blueprint for cellular-electronic connections. Through the addition of novel genetic information, we have engineered electronic communication between living cells and inorganic materials. The genetic nature of this approach makes it applicable to many cell types and specifies the route of electron transfer. The cell directs the assembly of the electron conduit, requiring no experimenter assembly or intervention. Finally, based on the natural system's respiratory versatility, we anticipate that our engineered system should be able to reduce multiple types of inorganic electrodes.

At the onset of this project, it was uncertain if the expression of this pathway in *E. coli* would be possible, let alone functional. It is rather easy for one to assume that the expression of a pathway would automatically confer the function of this pathway; but as we have learned, the expression of this system is complex and can negatively impact cell viability if not tuned properly. Many other labs had been attempting to express this pathway in *E. coli* at the same time, but we were the only lab able to express and demonstrate function. Additionally, after the initial publication in *PNAS*, the original *mtrCAB* strain was sent out to several of those labs to see if the strain could produce current. Even with several labs having access to the strain, we were still the only lab with the proper synthetic biology tools to re-tune the pathway for current production.

This dissertation represents the first step towards engineering bidirectional communications with electrodes, and it opens up an array of opportunities for studying the biochemical and enzymatic properties of these unique proteins as well as the potential for novel hybrid technologies.

References

(1) Patolsky, F.; Timko, B. P.; Yu, G.; Fang, Y.; Greytak, A. B.; Zheng, G.; Lieber, C. M. Detection, Stimulation, and Inhibition of Neuronal Signals with High-Density Nanowire Transistor Arrays. *Science* **2006**, *313*, 1100–1104.

(2) Ionescu-Zanetti, C.; Shaw, R. M.; Seo, J.; Jan, Y.-N.; Jan, L. Y.; Lee, L. P. Mammalian electrophysiology on a microfluidic platform. *Proceedings of the National Academy of Sciences* **2005**, *102*, 9112–9117.

(3) Alferov, S.; Coman, V.; Gustavsson, T.; Reshetilov, A.; von Wachenfeldt, C.; Hägerhäll, C.; Gorton, L. Electrical communication of cytochrome enriched *Escherichia coli* JM109 cells with graphite electrodes. *Electrochimica Acta* **2009**, *54*, 4979–4984.

(4) Coman, V.; Gustavsson, T.; Finkelsteinas, A.; von Wachenfeldt, C.; Hägerhäll, C.; Gorton, L. Electrical Wiring of Live, Metabolically Enhanced *Bacillus subtilis* Cells with Flexible Osmium-Redox Polymers. *Journal of the American Chemical Society* **2009**, *131*, 16171–16176.

(5) Marsili, E.; Baron, D. B.; Shikhare, I. D.; Coursolle, D.; Gralnick, J. A.; Bond, D. R. Shewanella secretes flavins that mediate extracellular electron transfer. *Proceedings of the National Academy of Sciences* **2008**, *105*, 3968–3973.

(6) Park, D. H.; Zeikus, J. G. Electricity Generation in Microbial Fuel Cells Using Neutral Red as an Electronophore. *Appl. Environ. Microbiol.* **2000**, *66*, 1292–1297.

(7) Gunawardena, A.; Fernando, S.; To, F. Performance of a Yeast-mediated Biological Fuel Cell. *Int J Mol Sci* **2008**, *9*, 1893–1907.

(8) Rabinowitz, J. D.; Vacchino, J. F.; Beeson, C.; McConnell, H. M. Potentiometric Measurement of Intracellular Redox Activity. *Journal of the American Chemical Society* **1998**, *120*, 2464–2473.

(9) Collier, J. H.; Mrksich, M. Engineering a biospecific communication pathway between cells and electrodes. *Proceedings of the National Academy of Sciences of the United States of America* **2006**, *103*, 2021–2025.

(10) Kim, H. J.; Park, H. S.; Hyun, M. S.; Chang, I. S.; Kim, M.; Kim, B. H. A mediator-less microbial fuel cell using a metal reducing bacterium, *Shewanella putrefaciens*. *Enzyme and Microbial Technology* **2002**, *30*, 145–152.

(11) Bond, D. R.; Lovley, D. R. Electricity Production by *Geobacter sulfurreducens* Attached to Electrodes. *Appl. Environ. Microbiol.* **2003**, *69*, 1548–1555.

(12) Rabaey, K.; Boon, N.; Siciliano, S. D.; Verhaege, M.; Verstraete, W. Biofuel Cells Select for Microbial Consortia That Self-Mediate Electron Transfer. *Appl. Environ. Microbiol.* **2004**, *70*, 5373–5382.

(13) Rabaey, K.; Rozendal, R. A. Microbial electrosynthesis - revisiting the electrical route for microbial production. *Nat. Rev. Microbiol.* **2010**, *8*, 706–716.

(14) Lovley, D. R.; Nevin, K. P. A shift in the current: New applications and concepts for microbe-electrode electron exchange. *Current Opinion in Biotechnology* **2011**, *22*, 441–448.

(15) Rosenbaum, M.; Angenent, L. T. Genetically modified microorganisms for bioelectrochemical systems. In *Bioelectrochemical Systems: From Extracellular Electron Transfer to Biotechnological Application*; Rabaey, K.; Angenent, L. T.;

Schroder, U.; Keller, J., Eds.; International Water Association: London, 2010; pp. 101–117.
(16) Su, L.; Jia, W.; Hou, C.; Lei, Y. Microbial biosensors: a review. *Biosens Bioelectron* **2011**, *26*, 1788–1799.
(17) Benenson, Y. Biomolecular computing systems: principles, progress and potential. *Nat. Rev. Genet.* **2012**, *13*, 455–468.
(18) TerAvest, M. A.; Li, Z.; Angenent, L. T. Bacteria-based biocomputing with Cellular Computing Circuits to sense, decide, signal, and act. *Energy & Environmental Science* **2011**, *4*, 4907.
(19) Gralnick, J. A.; Newman, D. K. Extracellular respiration. *Mol Microbiol* **2007**, *65*, 1–11.
(20) Shi, L.; Squier, T. C.; Zachara, J. M.; Fredrickson, J. K. Respiration of metal (hydr)oxides by *Shewanella* and *Geobacter*: a key role for multihaem c-type cytochromes. *Mol Microbiol* **2007**, *65*, 12–20.
(21) Myers, C. R.; Nealson, K. H. Bacterial Manganese Reduction and Growth with Manganese Oxide as the Sole Electron Acceptor. *Science* **1988**, *240*, 1319–1321.
(22) Lovley, D. R.; Phillips, E. J. P. Novel Mode of Microbial Energy Metabolism: Organic Carbon Oxidation Coupled to Dissimilatory Reduction of Iron or Manganese. *Appl Environ Microbiol* **1988**, *54*, 1472–1480.
(23) Hedrick, D. B.; Peacock, A. D.; Lovley, D. R.; Woodard, T. L.; Nevin, K. P.; Long, P. E.; White, D. C. Polar lipid fatty acids, LPS-hydroxy fatty acids, and respiratory quinones of three *Geobacter* strains, and variation with electron acceptor. *J. Ind. Microbiol. Biotechnol.* **2009**, *36*, 205–209.
(24) Davis, J. B.; Yarbrough, H. F., Jr Preliminary Experiments on a Microbial Fuel Cell. *Science* **1962**, *137*, 615–616.
(25) Ringeisen, B. R.; Henderson, E.; Wu, P. K.; Pietron, J.; Ray, R.; Little, B.; Biffinger, J. C.; Jones-Meehan, J. M. High power density from a miniature microbial fuel cell using *Shewanella oneidensis* DSP10. *Environ. Sci. Technol.* **2006**, *40*, 2629–2634.
(26) Ross, D. E.; Flynn, J. M.; Baron, D. B.; Gralnick, J. A.; Bond, D. R. Towards electrosynthesis in shewanella: energetics of reversing the mtr pathway for reductive metabolism. *PLoS ONE* **2011**, *6*, e16649.
(27) Nevin, K. P.; Hensley, S. A.; Franks, A. E.; Summers, Z. M.; Ou, J.; Woodard, T. L.; Snoeyenbos-West, O. L.; Lovley, D. R. Electrosynthesis of Organic Compounds from Carbon Dioxide Is Catalyzed by a Diversity of Acetogenic Microorganisms▽. *Appl Environ Microbiol* **2011**, *77*, 2882–2886.
(28) Nevin, K. P.; Woodard, T. L.; Franks, A. E.; Summers, Z. M.; Lovley, D. R. Microbial Electrosynthesis: Feeding Microbes Electricity To Convert Carbon Dioxide and Water to Multicarbon Extracellular Organic Compounds. *mBio* **2010**, *1*.
(29) Brutinel, E. D.; Gralnick, J. A. Shuttling happens: soluble flavin mediators of extracellular electron transfer in *Shewanella*. *Appl. Microbiol. Biotechnol.* **2012**, *93*, 41–48.
(30) Richter, H.; McCarthy, K.; Nevin, K. P.; Johnson, J. P.; Rotello, V. M.; Lovley, D. R. Electricity Generation by *Geobacter sulfurreducens* Attached to Gold Electrodes. *Langmuir* **2008**, *24*, 4376–4379.

(31) Mehta-Kolte, M. G.; Bond, D. R. *Geothrix fermentans* secretes two different redox-active compounds to utilize electron acceptors across a wide range of redox potentials. *Appl. Environ. Microbiol.* **2012**, *78*, 6987–6995.
(32) Shi, L.; Richardson, D. J.; Wang, Z.; Kerisit, S. N.; Rosso, K. M.; Zachara, J. M.; Fredrickson, J. K. The roles of outer membrane cytochromes of *Shewanella* and *Geobacter* in extracellular electron transfer. *Environmental Microbiology Reports* **2009**, *1*, 220–227.
(33) Myers, C. R.; Myers, J. M. The outer membrane cytochromes of *Shewanella oneidensis* MR-1 are lipoproteins. *Letters in Applied Microbiology* **2004**, *39*, 466–470.
(34) Hartshorne, R.; Jepson, B.; Clarke, T.; Field, S.; Fredrickson, J.; Zachara, J.; Shi, L.; Butt, J.; Richardson, D. Characterization of *Shewanella oneidensis* MtrC: a cell-surface decaheme cytochrome involved in respiratory electron transport to extracellular electron acceptors. *Journal of Biological Inorganic Chemistry* **2007**, *12*, 1083–1094.
(35) Ross, D. E.; Ruebush, S. S.; Brantley, S. L.; Hartshorne, R. S.; Clarke, T. A.; Richardson, D. J.; Tien, M. Characterization of Protein-Protein Interactions Involved in Iron Reduction by *Shewanella oneidensis* MR-1. *Appl. Environ. Microbiol.* **2007**, *73*, 5797–5808.
(36) Reardon, C. L.; Dohnalkova, A. C.; Nachimuthu, P.; Kennedy, D. W.; Saffarini, D. A.; Arey, B. W.; Shi, L.; Wang, Z.; Moore, D.; McLean, J. S.; Moyles, D.; Marshall, M. J.; Zachara, J. M.; Fredrickson, J. K.; Beliaev, A. S. Role of outer-membrane cytochromes MtrC and OmcA in the biomineralization of ferrihydrite by *Shewanella oneidensis* MR-1. *Geobiology* **2010**, *8*, 56–68.
(37) Pinchuk, G. E.; Rodionov, D. A.; Yang, C.; Li, X.; Osterman, A. L.; Dervyn, E.; Geydebrekht, O. V.; Reed, S. B.; Romine, M. F.; Collart, F. R.; Scott, J. H.; Fredrickson, J. K.; Beliaev, A. S. Genomic reconstruction of *Shewanella oneidensis* MR-1 metabolism reveals a previously uncharacterized machinery for lactate utilization. *Proc. Natl. Acad. Sci. U.S.A.* **2009**, *106*, 2874–2879.
(38) Brutinel, E. D.; Gralnick, J. A. Anomalies of the anaerobic tricarboxylic acid cycle in *Shewanella oneidensis* revealed by Tn-seq. *Mol. Microbiol.* **2012**, *86*, 273–283.
(39) Scott, J. H.; Nealson, K. H. A biochemical study of the intermediary carbon metabolism of *Shewanella putrefaciens*. *J. Bacteriol.* **1994**, *176*, 3408–3411.
(40) McMillan, D. G. G.; Marritt, S. J.; Butt, J. N.; Jeuken, L. J. C. Menaquinone-7 is specific cofactor in tetraheme quinol dehydrogenase CymA. *J. Biol. Chem.* **2012**, *287*, 14215–14225.
(41) Firer-Sherwood, M. A.; Bewley, K. D.; Mock, J.-Y.; Elliott, S. J. Tools for resolving complexity in the electron transfer networks of multiheme cytochromes c. *Metallomics* **2011**, *3*, 344–348.
(42) Myers, C. R.; Myers, J. M. Cloning and sequence of *cymA*, a gene encoding a tetraheme cytochrome c required for reduction of iron(III), fumarate, and nitrate by *Shewanella putrefaciens* MR-1. *J. Bacteriol.* **1997**, *179*, 1143–1152.
(43) Bretschger, O.; Obraztsova, A.; Sturm, C. A.; Chang, I. S.; Gorby, Y. A.; Reed, S. B.; Culley, D. E.; Reardon, C. L.; Barua, S.; Romine, M. F.; Zhou, J.; Beliaev, A. S.; Bouhenni, R.; Saffarini, D.; Mansfeld, F.; Kim, B.-H.; Fredrickson, J. K.;

Nealson, K. H. Current Production and Metal Oxide Reduction by *Shewanella oneidensis* MR-1 Wild Type and Mutants. *Appl Environ Microbiol* **2007**, *73*, 7003–7012.

(44) Hartshorne, R. S.; Reardon, C. L.; Ross, D.; Nuester, J.; Clarke, T. A.; Gates, A. J.; Mills, P. C.; Fredrickson, J. K.; Zachara, J. M.; Shi, L.; Beliaev, A. S.; Marshall, M. J.; Tien, M.; Brantley, S.; Butt, J. N.; Richardson, D. J. Characterization of an electron conduit between bacteria and the extracellular environment. *Proceedings of the National Academy of Sciences* **2009**, *106*, 22169–22174.

(45) Clarke, T. A.; Edwards, M. J.; Gates, A. J.; Hall, A.; White, G. F.; Bradley, J.; Reardon, C. L.; Shi, L.; Beliaev, A. S.; Marshall, M. J.; Wang, Z.; Watmough, N. J.; Fredrickson, J. K.; Zachara, J. M.; Butt, J. N.; Richardson, D. J. Structure of a bacterial cell surface decaheme electron conduit. *Proc. Natl. Acad. Sci. U.S.A.* **2011**, *108*, 9384–9389.

(46) Coursolle, D.; Baron, D. B.; Bond, D. R.; Gralnick, J. A. The Mtr Respiratory Pathway Is Essential for Reducing Flavins and Electrodes in *Shewanella oneidensis*. *J. Bacteriol.* **2010**, *192*, 467–474.

(47) Von Canstein, H.; Ogawa, J.; Shimizu, S.; Lloyd, J. R. Secretion of flavins by *Shewanella* species and their role in extracellular electron transfer. *Appl. Environ. Microbiol.* **2008**, *74*, 615–623.

(48) Jiang, X.; Hu, J.; Fitzgerald, L. A.; Biffinger, J. C.; Xie, P.; Ringeisen, B. R.; Lieber, C. M. Probing electron transfer mechanisms in *Shewanella oneidensis* MR-1 using a nanoelectrode platform and single-cell imaging. *Proc. Natl. Acad. Sci. U.S.A.* **2010**, *107*, 16806–16810.

(49) Gorby, Y. A.; Yanina, S.; McLean, J. S.; Rosso, K. M.; Moyles, D.; Dohnalkova, A.; Beveridge, T. J.; Chang, I. S.; Kim, B. H.; Kim, K. S.; Culley, D. E.; Reed, S. B.; Romine, M. F.; Saffarini, D. A.; Hill, E. A.; Shi, L.; Elias, D. A.; Kennedy, D. W.; Pinchuk, G.; Watanabe, K.; Ishii, S.; Logan, B.; Nealson, K. H.; Fredrickson, J. K. Electrically conductive bacterial nanowires produced by *Shewanella oneidensis* strain MR-1 and other microorganisms. *Proceedings of the National Academy of Sciences* **2006**, *103*, 11358–11363.

(50) El-Naggar, M. Y.; Wanger, G.; Leung, K. M.; Yuzvinsky, T. D.; Southam, G.; Yang, J.; Lau, W. M.; Nealson, K. H.; Gorby, Y. A. Electrical transport along bacterial nanowires from *Shewanella oneidensis* MR-1. *PNAS* **2010**.

(51) Pitts, K. E.; Dobbin, P. S.; Reyes-Ramirez, F.; Thomson, A. J.; Richardson, D. J.; Seward, H. E. Characterization of the *Shewanella oneidensis* MR-1 Decaheme Cytochrome MtrA. *Journal of Biological Chemistry* **2003**, *278*, 27758–27765.

(52) Myers, C. R.; Myers, J. M. Cell surface exposure of the outer membrane cytochromes of *Shewanella oneidensis* MR-1. *Lett. Appl. Microbiol.* **2003**, *37*, 254–258.

(53) Beliaev, A. S.; Saffarini, D. A.; McLaughlin, J. L.; Hunnicutt, D. MtrC, an outer membrane decahaem *c* cytochrome required for metal reduction in *Shewanella putrefaciens* MR-1. *Mol Microbiol* **2001**, *39*, 722–730.

(54) Myers, C. R.; Myers, J. M. MtrB is required for proper incorporation of the cytochromes OmcA and OmcB into the outer membrane of *Shewanella putrefaciens* MR-1. *Appl. Environ. Microbiol* **2002**, *68*, 5585–5594.

(55) Bagos, P. G.; Liakopoulos, T. D.; Spyropoulos, I. C.; Hamodrakas, S. J. PRED-TMBB: a web server for predicting the topology of β-barrel outer membrane proteins. *Nucleic Acids Res* **2004**, *32*, W400–W404.

(56) Schicklberger, M.; Bücking, C.; Schuetz, B.; Heide, H.; Gescher, J. Involvement of the *Shewanella oneidensis* decaheme cytochrome MtrA in the periplasmic stability of the beta-barrel protein MtrB. *Appl. Environ. Microbiol.* **2011**, *77*, 1520–1523.

(57) Edwards, M. J.; Hall, A.; Shi, L.; Fredrickson, J. K.; Zachara, J. M.; Butt, J. N.; Richardson, D. J.; Clarke, T. A. The Crystal Structure of the Extracellular 11-heme Cytochrome UndA Reveals a Conserved 10-heme Motif and Defined Binding Site for Soluble Iron Chelates. *Structure* **2012**, *20*, 1275–1284.

(58) Rodrigues, M. L.; Oliveira, T. F.; Pereira, I. A. C.; Archer, M. X-ray structure of the membrane-bound cytochrome *c* quinol dehydrogenase NrfH reveals novel haem coordination. *EMBO J* **2006**, *25*, 5951–5960.

(59) Firer-Sherwood, M. A.; Ando, N.; Drennan, C. L.; Elliott, S. J. Solution-based structural analysis of the decaheme cytochrome, MtrA, by small-angle X-ray scattering and analytical ultracentrifugation. *J Phys Chem B* **2011**, *115*, 11208–11214.

(60) Clarke, T. A.; Cole, J. A.; Richardson, D. J.; Hemmings, A. M. The crystal structure of the pentahaem *c*-type cytochrome NrfB and characterization of its solution-state interaction with the pentahaem nitrite reductase NrfA. *Biochem. J.* **2007**, *406*, 19–30.

(61) Breuer, M.; Zarzycki, P.; Blumberger, J.; Rosso, K. M. Thermodynamics of Electron Flow in the Bacterial Deca-heme Cytochrome MtrF. *J. Am. Chem. Soc.* **2012**, *134*, 9868–9871.

(62) Marritt, S. J.; Lowe, T. G.; Bye, J.; McMillan, D. G. G.; Shi, L.; Fredrickson, J.; Zachara, J.; Richardson, D. J.; Cheesman, M. R.; Jeuken, L. J. C.; Butt, J. N. A functional description of CymA, an electron-transfer hub supporting anaerobic respiratory flexibility in *Shewanella*. *Biochemical Journal* **2012**, *444*, 465–474.

(63) Marritt, S. J.; McMillan, D. G. G.; Shi, L.; Fredrickson, J. K.; Zachara, J. M.; Richardson, D. J.; Jeuken, L. J. C.; Butt, J. N. The roles of CymA in support of the respiratory flexibility of *Shewanella oneidensis* MR-1. *Biochem. Soc. Trans.* **2012**, *40*, 1217–1221.

(64) Gescher, J. S.; Cordova, C. D.; Spormann, A. M. Dissimilatory iron reduction in *Escherichia coli*: identification of CymA of *Shewanella oneidensis* and NapC of *E. coli* as ferric reductases. *Mol. Microbiol* **2008**, *68*, 706–719.

(65) Arslan, E.; Schulz, H.; Zufferey, R.; Künzler, P.; Thöny-Meyer, L. Overproduction of theBradyrhizobium japonicum *c*-Type Cytochrome Subunits of the cbb3 Oxidase in *Escherichia coli*. *Biochemical and Biophysical Research Communications* **1998**, *251*, 744–747.

(66) Fernandes, A. P.; Couto, I.; Morgado, L.; Londer, Y. Y.; Salgueiro, C. A. Isotopic labeling of c-type multiheme cytochromes overexpressed in *E. coli*. *Protein Expr. Purif.* **2008**, *59*, 182–188.

(67) Londer, Y. Y.; Giuliani, S. E.; Peppler, T.; Collart, F. R. Addressing Shewanella oneidensis “cytochromome”: the first step towards high-throughput expression of cytochromes *c*. *Protein Expr. Purif* **2008**, *62*, 128–137.

(68) Londer, Y. Y. Expression of recombinant cytochromes *c* in *E. coli*. *Methods Mol. Biol.* **2011**, *705*, 123–150.
(69) Londer, Y. Y.; Pokkuluri, P. R.; Orshonsky, V.; Orshonsky, L.; Schiffer, M. Heterologous expression of dodecaheme "nanowire" cytochromes *c* from *Geobacter sulfurreducens*. *Protein Expr. Purif.* **2006**, *47*, 241–248.
(70) Londer, Y. Y.; Pokkuluri, P. R.; Erickson, J.; Orshonsky, V.; Schiffer, M. Heterologous expression of hexaheme fragments of a multidomain cytochrome from *Geobacter sulfurreducens* representing a novel class of cytochromes *c*. *Protein Expr. Purif.* **2005**, *39*, 254–260.
(71) Cordova, C. D.; Schicklberger, M. F. R.; Yu, Y.; Spormann, A. M. Partial functional replacement of CymA by SirCD in *Shewanella oneidensis* MR-1. *J. Bacteriol.* **2011**, *193*, 2312–2321.
(72) Schuetz, B.; Schicklberger, M.; Kuermann, J.; Spormann, A. M.; Gescher, J. Periplasmic Electron Transfer via the *c*-Type Cytochromes MtrA and FccA of *Shewanella oneidensis* MR-1. *Appl. Environ. Microbiol.* **2009**, *75*, 7789–7796.
(73) Donald, J. W.; Hicks, M. G.; Richardson, D. J.; Palmer, T. The *c*-Type Cytochrome OmcA Localizes to the Outer Membrane upon Heterologous Expression in *Escherichia coli*. *J Bacteriol* **2008**, *190*, 5127–5131.
(74) Gralnick, J. A.; Vali, H.; Lies, D. P.; Newman, D. K. Extracellular respiration of dimethyl sulfoxide by *Shewanella oneidensis* strain MR-1. *Proc. Natl. Acad. Sci. U.S.A.* **2006**, *103*, 4669–4674.
(75) Shi, L.; Deng, S.; Marshall, M. J.; Wang, Z.; Kennedy, D. W.; Dohnalkova, A. C.; Mottaz, H. M.; Hill, E. A.; Gorby, Y. A.; Beliaev, A. S.; Richardson, D. J.; Zachara, J. M.; Fredrickson, J. K. Direct Involvement of Type II Secretion System in Extracellular Translocation of *Shewanella oneidensis* Outer Membrane Cytochromes MtrC and OmcA. *J Bacteriol* **2008**, *190*, 5512–5516.
(76) Prats, R.; de Pedro, M. A. Normal growth and division of *Escherichia coli* with a reduced amount of murein. *J Bacteriol* **1989**, *171*, 3740–3745.
(77) *Escherichia coli and Salmonella: Cellular and Molecular Biology*; Neidhardt, F. C., Ed.; 2nd ed.; ASM Press, 1996.
(78) Kalwarczyk, T.; Tabaka, M.; Holyst, R. Biologistics--diffusion coefficients for complete proteome of *Escherichia coli*. *Bioinformatics* **2012**, *28*, 2971–2978.
(79) Molenaar, D.; van Berlo, R.; de Ridder, D.; Teusink, B. Shifts in growth strategies reflect tradeoffs in cellular economics. *Mol. Syst. Biol.* **2009**, *5*, 323.
(80) Zhuang, K.; Vemuri, G. N.; Mahadevan, R. Economics of membrane occupancy and respiro-fermentation. *Mol Syst Biol* **2011**, *7*, 500.
(81) Gram, H. "{U}ber die isolierte F"{a}rbung der Schizomyceten in Schnitt- und Trockenpr"{a}paraten. *Fortschritte der Medizin* **1884**, *2*, 185–89.
(82) Wickström, D.; Wagner, S.; Baars, L.; Ytterberg, A. J.; Klepsch, M.; van Wijk, K. J.; Luirink, J.; de Gier, J.-W. Consequences of depletion of the signal recognition particle in *Escherichia coli*. *J. Biol. Chem.* **2011**, *286*, 4598–4609.
(83) Bürk, J.; Weiche, B.; Wenk, M.; Boy, D.; Nestel, S.; Heimrich, B.; Koch, H.-G. Depletion of the signal recognition particle receptor inactivates ribosomes in *Escherichia coli*. *J. Bacteriol.* **2009**, *191*, 7017–7026.
(84) Wagner, S.; Baars, L.; Ytterberg, A. J.; Klussmeier, A.; Wagner, C. S.; Nord, O.; Nygren, P.-Å.; van Wijk, K. J.; de Gier, J.-W. Consequences of Membrane

Protein Overexpression in *Escherichia coli*. *Molecular & Cellular Proteomics* **2007**, *6*, 1527–1550.

(85) Wagner, S.; Klepsch, M. M.; Schlegel, S.; Appel, A.; Draheim, R.; Tarry, M.; Högbom, M.; van Wijk, K. J.; Slotboom, D. J.; Persson, J. O.; de Gier, J.-W. Tuning *Escherichia coli* for membrane protein overexpression. *Proc. Natl. Acad. Sci. U.S.A.* **2008**, *105*, 14371–14376.

(86) Hoober, J. K.; Kahn, A.; Ash, D. E.; Gough, S.; Kannangara, C. G. Biosynthesis of delta-aminolevulinate in greening barley leaves. IX. Structure of the substrate, mode of gabaculine inhibition, and the catalytic mechanism of glutamate 1-semialdehyde aminotransferase. *Carlsberg Res. Commun.* **1988**, *53*, 11–25.

(87) Jordan, P. M.; Cheung, K.-M.; Sharma, R. P.; Warren, M. J. 5-Amino-6-hydroxy 3,4,5,6-tetrahydropyran-2-one (HAT): A stable, cyclic form of glutamate 1-semialdehyde, the natural precursor for tetrapyrroles. *Tetrahedron Letters* **1993**, *34*, 1177–1180.

(88) Frankenberg, N.; Moser, J.; Jahn, D. Bacterial heme biosynthesis and its biotechnological application. *Appl. Microbiol. Biotechnol.* **2003**, *63*, 115–127.

(89) Panek, H.; O'Brian, M. R. A whole genome view of prokaryotic haem biosynthesis. *Microbiology* **2002**, *148*, 2273–2282.

(90) Layer, G.; Reichelt, J.; Jahn, D.; Heinz, D. W. Structure and function of enzymes in heme biosynthesis. *Protein Sci.* **2010**, *19*, 1137–1161.

(91) Philipp-Dormston, W. K.; Doss, M. Over-production of porphyrins and heme in heterotrophic bacteria. *Z. Naturforsch., C, Biosci.* **1975**, *30*, 425–426.

(92) Goldbeck, C. P.; Jensen, H. M.; TerAvest, M. A.; Beedle, N.; Appling, Y.; Hepler, M.; Cambray, G.; Mutalik, V.; Angenent, L. T.; Ajo-Franklin, C. M. Tuning Promoter Strengths for Improved Synthesis and Function of Electron Conduits in *Escherichia coli*. *ACS Synth. Biol.* **2013**, *2*, 150–159.

(93) Fekkes, P.; Driessen, A. J. Protein targeting to the bacterial cytoplasmic membrane. *Microbiol. Mol. Biol. Rev.* **1999**, *63*, 161–173.

(94) De Keyzer, J.; van der Does, C.; Driessen, A. J. M. The bacterial translocase: a dynamic protein channel complex. *Cell. Mol. Life Sci.* **2003**, *60*, 2034–2052.

(95) Rusch, S. L.; Kendall, D. A. Oligomeric states of the SecA and SecYEG core components of the bacterial Sec translocon. *Biochim. Biophys. Acta* **2007**, *1768*, 5–12.

(96) Segers, K.; Anné, J. Traffic jam at the bacterial sec translocase: targeting the SecA nanomotor by small-molecule inhibitors. *Chem. Biol.* **2011**, *18*, 685–698.

(97) Solov'eva, T. F.; Novikova, O. D.; Portnyagina, O. Y. Biogenesis of β-barrel integral proteins of bacterial outer membrane. *Biochemistry Mosc.* **2012**, *77*, 1221–1236.

(98) Hagan, C. L.; Silhavy, T. J.; Kahne, D. β-Barrel Membrane Protein Assembly by the Bam Complex. *Annual Review of Biochemistry* **2011**, *80*, 189–210.

(99) Maier, R.; Eckert, B.; Scholz, C.; Lilie, H.; Schmid, F.-X. Interaction of trigger factor with the ribosome. *J. Mol. Biol.* **2003**, *326*, 585–592.

(100) Nannenga, B. L.; Baneyx, F. Reprogramming chaperone pathways to improve membrane protein expression in *Escherichia coli*. *Protein Sci.* **2011**, *20*, 1411–1420.

(101) Choi, J. H.; Lee, S. Y. Secretory and extracellular production of recombinant proteins using *Escherichia coli*. *Appl. Microbiol. Biotechnol.* **2004**, *64*, 625–635.
(102) Liang, F.-C.; Bageshwar, U. K.; Musser, S. M. Position-dependent effects of polylysine on Sec protein transport. *J. Biol. Chem.* **2012**, *287*, 12703–12714.
(103) Wang, L.; Miller, A.; Kendall, D. A. Signal peptide determinants of SecA binding and stimulation of ATPase activity. *J. Biol. Chem.* **2000**, *275*, 10154–10159.
(104) Bechtluft, P.; Nouwen, N.; Tans, S. J.; Driessen, A. J. M. SecB--a chaperone dedicated to protein translocation. *Mol Biosyst* **2010**, *6*, 620–627.
(105) Crane, J. M.; Mao, C.; Lilly, A. A.; Smith, V. F.; Suo, Y.; Hubbell, W. L.; Randall, L. L. Mapping of the docking of SecA onto the chaperone SecB by site-directed spin labeling: insight into the mechanism of ligand transfer during protein export. *J. Mol. Biol.* **2005**, *353*, 295–307.
(106) Randall, L. L.; Henzl, M. T. Direct identification of the site of binding on the chaperone SecB for the amino terminus of the translocon motor SecA. *Protein Sci.* **2010**, *19*, 1173–1179.
(107) Suo, Y.; Hardy, S. J. S.; Randall, L. L. Orientation of SecA and SecB in complex, derived from disulfide cross-linking. *J. Bacteriol.* **2011**, *193*, 190–196.
(108) Mergulhão, F. J. M.; Summers, D. K.; Monteiro, G. A. Recombinant protein secretion in *Escherichia coli*. *Biotechnology Advances* **2005**, *23*, 177–202.
(109) Hsieh, Y.; Zhang, H.; Lin, B.; Cui, N.; Na, B.; Yang, H.; Jiang, C.; Sui, S.; Tai, P. C. SecA alone can promote protein translocation and ion channel activity: SecYEG increases efficiency and signal peptide specificity. *J. Biol. Chem.* **2011**, *286*, 44702–44709.
(110) Driessen, A. J. M.; Nouwen, N. Protein translocation across the bacterial cytoplasmic membrane. *Annu. Rev. Biochem.* **2008**, *77*, 643–667.
(111) Welte, T.; Kudva, R.; Kuhn, P.; Sturm, L.; Braig, D.; Müller, M.; Warscheid, B.; Drepper, F.; Koch, H.-G. Promiscuous targeting of polytopic membrane proteins to SecYEG or YidC by the *Escherichia coli* signal recognition particle. *Mol. Biol. Cell* **2012**, *23*, 464–479.
(112) Luirink, J.; Yu, Z.; Wagner, S.; de Gier, J.-W. Biogenesis of inner membrane proteins in *Escherichia coli*. *Biochimica et Biophysica Acta (BBA) - Bioenergetics* **2012**, *1817*, 965–976.
(113) Luirink, J.; von Heijne, G.; Houben, E.; de Gier, J.-W. Biogenesis of inner membrane proteins in *Escherichia coli*. *Annu. Rev. Microbiol.* **2005**, *59*, 329–355.
(114) Ullers, R. S.; Houben, E. N. G.; Raine, A.; ten Hagen-Jongman, C. M.; Ehrenberg, M.; Brunner, J.; Oudega, B.; Harms, N.; Luirink, J. Interplay of signal recognition particle and trigger factor at L23 near the nascent chain exit site on the *Escherichia coli* ribosome. *J. Cell Biol.* **2003**, *161*, 679–684.
(115) Berks, B. C. A common export pathway for proteins binding complex redox cofactors. *Molecular Microbiology* **1996**, *22*, 393–404.
(116) Lee, P. A.; Tullman-Ercek, D.; Georgiou, G. The bacterial twin-arginine translocation pathway. *Annu. Rev. Microbiol.* **2006**, *60*, 373–395.
(117) Fröbel, J.; Rose, P.; Müller, M. Twin-arginine-dependent translocation of folded proteins. *Philos. Trans. R. Soc. Lond., B, Biol. Sci.* **2012**, *367*, 1029–1046.

(118) Petersen, T. N.; Brunak, S.; von Heijne, G.; Nielsen, H. SignalP 4.0: discriminating signal peptides from transmembrane regions. *Nat Meth* **2011**, *8*, 785–786.
(119) Juncker, A. S.; Willenbrock, H.; Von Heijne, G.; Brunak, S.; Nielsen, H.; Krogh, A. Prediction of lipoprotein signal peptides in Gram-negative bacteria. *Protein Sci.* **2003**, *12*, 1652–1662.
(120) Sanders, C.; Turkarslan, S.; Lee, D.-W.; Daldal, F. Cytochrome *c* biogenesis: the Ccm system. *Trends Microbiol.* **2010**, *18*, 266–274.
(121) Allen, J. W. A.; Leach, N.; Ferguson, S. J. The histidine of the *c*-type cytochrome CXXCH haem-binding motif is essential for haem attachment by the *Escherichia coli* cytochrome *c* maturation (Ccm) apparatus. *Biochem. J.* **2005**, *389*, 587–592.
(122) Thony-Meyer, L.; Fischer, F.; Kunzler, P.; Ritz, D.; Hennecke, H. *Escherichia coli* genes required for cytochrome c maturation. *J. Bacteriol.* **1995**, *177*, 4321–4326.
(123) Christensen, O.; Harvat, E. M.; Thöny-Meyer, L.; Ferguson, S. J.; Stevens, J. M. Loss of ATP hydrolysis activity by CcmAB results in loss of *c*-type cytochrome synthesis and incomplete processing of CcmE. *FEBS J.* **2007**, *274*, 2322–2332.
(124) Feissner, R. E.; Richard-Fogal, C. L.; Frawley, E. R.; Kranz, R. G. ABC transporter-mediated release of a haem chaperone allows cytochrome *c* biogenesis. *Mol. Microbiol.* **2006**, *61*, 219–231.
(125) Schulz, H.; Hennecke, H.; Thöny-Meyer, L. Prototype of a heme chaperone essential for cytochrome *c* maturation. *Science* **1998**, *281*, 1197–1200.
(126) Stevens, J. M.; Mavridou, D. A. I.; Hamer, R.; Kritsiligkou, P.; Goddard, A. D.; Ferguson, S. J. Cytochrome *c* biogenesis System I. *FEBS J* **2011**, *278*, 4170–4178.
(127) Grove, J.; Tanapongpipat, S.; Thomas, G.; Griffiths, L.; Crooke, H.; Cole, J. *Escherichia coli* K-12 genes essential for the synthesis of *c*-type cytochromes and a third nitrate reductase located in the periplasm. *Mol. Microbiol.* **1996**, *19*, 467–481.
(128) Thöny-Meyer, L.; Künzler, P.; Hennecke, H. Requirements for maturation of Bradyrhizobium japonicum cytochrome *c*550 in *Escherichia coli*. *Eur. J. Biochem.* **1996**, *235*, 754–761.
(129) Tokuda, H. Biogenesis of outer membranes in Gram-negative bacteria. *Biosci. Biotechnol. Biochem.* **2009**, *73*, 465–473.
(130) Narita, S. ABC transporters involved in the biogenesis of the outer membrane in gram-negative bacteria. *Biosci. Biotechnol. Biochem.* **2011**, *75*, 1044–1054.
(131) Oudega, B.; Clark, D.; Stegehuis, F.; Majoor, M. J.; Luirink, J. A lipoprotein signal peptide plus a cysteine residue at the amino-terminal end of the periplasmic protein beta-lactamase is sufficient for its lipid modification, processing and membrane localization in *Escherichia coli*. *FEMS Microbiol. Lett.* **1993**, *108*, 353–359.
(132) Kamalakkannan, S.; Murugan, V.; Jagannadham, M. V.; Nagaraj, R.; Sankaran, K. Bacterial lipid modification of proteins for novel protein engineering applications. *Protein Eng. Des. Sel.* **2004**, *17*, 721–729.

(133) Denham, E. L.; Ward, P. N.; Leigh, J. A. Lipoprotein Signal Peptides Are Processed by Lsp and Eep of Streptococcus uberis. *J. Bacteriol.* **2008**, *190*, 4641–4647.
(134) Kovacs-Simon, A.; Titball, R. W.; Michell, S. L. Lipoproteins of bacterial pathogens. *Infect. Immun.* **2011**, *79*, 548–561.
(135) Hutchings, M. I.; Palmer, T.; Harrington, D. J.; Sutcliffe, I. C. Lipoprotein biogenesis in Gram-positive bacteria: knowing when to hold 'em, knowing when to fold 'em. *Trends Microbiol.* **2009**, *17*, 13–21.
(136) Korotkov, K. V.; Sandkvist, M.; Hol, W. G. J. The type II secretion system: biogenesis, molecular architecture and mechanism. *Nat Rev Micro* **2012**, *10*, 336–351.
(137) Douzi, B.; Filloux, A.; Voulhoux, R. On the path to uncover the bacterial type II secretion system. *Phil. Trans. R. Soc. B* **2012**, *367*, 1059–1072.
(138) Reichow, S. L.; Korotkov, K. V.; Hol, W. G. J.; Gonen, T. Structure of the cholera toxin secretion channel in its closed state. *Nat. Struct. Mol. Biol.* **2010**, *17*, 1226–1232.
(139) Schulze, R. J.; Zückert, W. R. *Borrelia burgdorferi* lipoproteins are secreted to the outer surface by default. *Molecular Microbiology* **2006**, *59*, 1473–1484.
(140) Nakayama, H.; Kurokawa, K.; Lee, B. L. Lipoproteins in bacteria: structures and biosynthetic pathways. *FEBS Journal* **2012**, *279*, 4247–4268.
(141) Sklar, J. G.; Wu, T.; Kahne, D.; Silhavy, T. J. Defining the roles of the periplasmic chaperones SurA, Skp, and DegP in *Escherichia coli*. *Genes Dev.* **2007**, *21*, 2473–2484.
(142) Rizzitello, A. E.; Harper, J. R.; Silhavy, T. J. Genetic evidence for parallel pathways of chaperone activity in the periplasm of *Escherichia coli*. *J. Bacteriol.* **2001**, *183*, 6794–6800.
(143) Wu, S.; Ge, X.; Lv, Z.; Zhi, Z.; Chang, Z.; Zhao, X. S. Interaction between bacterial outer membrane proteins and periplasmic quality control factors: a kinetic partitioning mechanism. *Biochem. J.* **2011**, *438*, 505–511.
(144) Knowles, T. J.; Scott-Tucker, A.; Overduin, M.; Henderson, I. R. Membrane protein architects: the role of the BAM complex in outer membrane protein assembly. *Nat Rev Micro* **2009**, *7*, 206–214.
(145) Sánchez-Pulido, L.; Devos, D.; Genevrois, S.; Vicente, M.; Valencia, A. POTRA: a conserved domain in the FtsQ family and a class of beta-barrel outer membrane proteins. *Trends Biochem. Sci.* **2003**, *28*, 523–526.
(146) Knowles, T. J.; Jeeves, M.; Bobat, S.; Dancea, F.; McClelland, D.; Palmer, T.; Overduin, M.; Henderson, I. R. Fold and function of polypeptide transport-associated domains responsible for delivering unfolded proteins to membranes. *Mol. Microbiol.* **2008**, *68*, 1216–1227.
(147) Francetic, O.; Belin, D.; Badaut, C.; Pugsley, A. P. Expression of the endogenous type II secretion pathway in *Escherichia coli* leads to chitinase secretion. *The EMBO Journal* **2000**, *19*, 6697–6703.
(148) Jensen, H. M.; Albers, A. E.; Malley, K. R.; Londer, Y. Y.; Cohen, B. E.; Helms, B. A.; Weigele, P.; Groves, J. T.; Ajo-Franklin, C. M. Engineering of a synthetic electron conduit in living cells. *Proceedings of the National Academy of Sciences* **2010**, *107*, 19213–19218.

(149) Schembri, M. A.; Kjaergaard, K.; Klemm, P. Global gene expression in *Escherichia coli* biofilms. *Mol. Microbiol.* **2003**, *48*, 253–267.
(150) Jeong, H.; Barbe, V.; Lee, C. H.; Vallenet, D.; Yu, D. S.; Choi, S.-H.; Couloux, A.; Lee, S.-W.; Yoon, S. H.; Cattolico, L.; Hur, C.-G.; Park, H.-S.; Ségurens, B.; Kim, S. C.; Oh, T. K.; Lenski, R. E.; Studier, F. W.; Daegelen, P.; Kim, J. F. Genome sequences of *Escherichia coli* B strains REL606 and BL21(DE3). *J. Mol. Biol.* **2009**, *394*, 644–652.
(151) Brenner, K.; Arnold, F. H. Self-Organization, Layered Structure, and Aggregation Enhance Persistence of a Synthetic Biofilm Consortium. *PLoS ONE* **2011**, *6*, e16791.
(152) Twite, A. A.; Hsiao, S. C.; Onoe, H.; Mathies, R. A.; Francis, M. B. DNA Hybridization: Direct Attachment of Microbial Organisms to Material Surfaces Through Sequence-Specific DNA Hybridization. *Advanced Materials* **2012**, *24*, 2365–2365.
(153) Daraselia, N.; Dernovoy, D.; Tian, Y.; Borodovsky, M.; Tatusov, R.; Tatusova, T. Reannotation of *Shewanella oneidensis* Genome. *omics* **2003**, *7*, 171–175.
(154) Genome sequencing and analysis of the model grass *Brachypodium distachyon*. *Nature* **2010**, *463*, 763–768.
(155) Benner, S. A.; Sismour, A. M. Synthetic biology. *Nat Rev Genet* **2005**, *6*, 533–543.
(156) Gardner, T. S.; Cantor, C. R.; Collins, J. J. Construction of a genetic toggle switch in *Escherichia coli*. *Nature* **2000**, *403*, 339–342.
(157) Andrianantoandro, E.; Basu, S.; Karig, D. K.; Weiss, R. Synthetic biology: new engineering rules for an emerging discipline. *Mol Syst Biol* **2006**, *2*, 2006.0028.
(158) Serrano, L. Synthetic biology: promises and challenges. *Mol Syst Biol* **2007**, *3*, 158.
(159) Lu, T. K.; Khalil, A. S.; Collins, J. J. Next-generation synthetic gene networks. *Nat Biotech* **2009**, *27*, 1139–1150.
(160) Khalil, A. S.; Collins, J. J. Synthetic biology: applications come of age. *Nat Rev Genet* **2010**, *11*, 367–379.
(161) Ro, D.-K.; Paradise, E. M.; Ouellet, M.; Fisher, K. J.; Newman, K. L.; Ndungu, J. M.; Ho, K. A.; Eachus, R. A.; Ham, T. S.; Kirby, J.; Chang, M. C. Y.; Withers, S. T.; Shiba, Y.; Sarpong, R.; Keasling, J. D. Production of the antimalarial drug precursor artemisinic acid in engineered yeast. *Nature* **2006**, *440*, 940–943.
(162) Gibson, D. G.; Glass, J. I.; Lartigue, C.; Noskov, V. N.; Chuang, R.-Y.; Algire, M. A.; Benders, G. A.; Montague, M. G.; Ma, L.; Moodie, M. M.; Merryman, C.; Vashee, S.; Krishnakumar, R.; Assad-Garcia, N.; Andrews-Pfannkoch, C.; Denisova, E. A.; Young, L.; Qi, Z.-Q.; Segall-Shapiro, T. H.; Calvey, C. H.; Parmar, P. P.; Hutchison, C. A.; Smith, H. O.; Venter, J. C. Creation of a Bacterial Cell Controlled by a Chemically Synthesized Genome. *Science* **2010**, science.1190719.
(163) Beliaev, A. S.; Saffarini, D. A. *Shewanella putrefaciens mtrB* Encodes an Outer Membrane Protein Required for Fe(III) and Mn(IV) Reduction. *J Bacteriol* **1998**, *180*, 6292–6297.

(164) Dubendorf, J. W.; Studier, F. W. Controlling basal expression in an inducible T7 expression system by blocking the target T7 promoter with lac repressor. *Journal of Molecular Biology* **1991**, *219*, 45–59.
(165) Studier, F. W.; Rosenberg, A. H.; Dunn, J. J.; Dubendorff, J. W. Use of T7 RNA polymerase to direct expression of cloned genes. *Meth. Enzymol* **1990**, *185*, 60–89.
(166) Thomas, P. E.; Ryan, D.; Levin, W. An improved staining procedure for the detection of the peroxidase activity of cytochrome P-450 on sodium dodecyl sulfate polyacrylamide gels. *Analytical Biochemistry* **1976**, *75*, 168–176.
(167) Myers, C. R.; Myers, J. M. Localization of cytochromes to the outer membrane of anaerobically grown *Shewanella putrefaciens* MR-1. *J. Bacteriol.* **1992**, *174*, 3429–3438.
(168) Stookey, L. L. Ferrozine---a new spectrophotometric reagent for iron. *Analytical Chemistry* **1970**, *42*, 779–781.
(169) Williams, H. D.; Poole, R. K. Reduction of iron(III) by *Escherichia coli* K12: Lack of involvement of the respiratory chains. *Current Microbiology* **1987**, *15*, 319–324.
(170) Datsenko, K. A.; Wanner, B. L. One-step inactivation of chromosomal genes in *Escherichia coli* K-12 using PCR products. *Proc. Natl. Acad. Sci. U.S.A* **2000**, *97*, 6640–6645.
(171) Wigginton, N. S.; Rosso, K. M.; Stack, A. G.; Hochella, J. Long-Range Electron Transfer across Cytochrome−Hematite (α-Fe_2O_3) Interfaces. *The Journal of Physical Chemistry C* **2009**, *113*, 2096–2103.
(172) Jones, M. E.; Fennessey, C. M.; DiChristina, T. J.; Taillefert, M. *Shewanella oneidensis* MR-1 mutants selected for their inability to produce soluble organic-Fe(III) complexes are unable to respire Fe(III) as anaerobic electron acceptor. *Environmental Microbiology* **2010**, *12*, 938–950.
(173) Bose, S.; Hochella Jr., M. F.; Gorby, Y. A.; Kennedy, D. W.; McCready, D. E.; Madden, A. S.; Lower, B. H. Bioreduction of hematite nanoparticles by the dissimilatory iron reducing bacterium *Shewanella oneidensis* MR-1. *Geochimica et Cosmochimica Acta* **2009**, *73*, 962–976.
(174) Ross, D. E.; Brantley, S. L.; Tien, M. Kinetic Characterization of OmcA and MtrC, Terminal Reductases Involved in Respiratory Electron Transfer for Dissimilatory Iron Reduction in *Shewanella oneidensis* MR-1. *Appl Environ Microbiol* **2009**, *75*, 5218–5226.
(175) Wang, Z.; Liu, C.; Wang, X.; Marshall, M. J.; Zachara, J. M.; Rosso, K. M.; Dupuis, M.; Fredrickson, J. K.; Heald, S.; Shi, L. Kinetics of Reduction of Fe(III) Complexes by Outer Membrane Cytochromes MtrC and OmcA of *Shewanella oneidensis* MR-1. *Appl. Environ. Microbiol.* **2008**, *74*, 6746–6755.
(176) Nikaido, H. Isolation of outer membranes. In *Bacterial Pathogenesis Part A: Identification and Regulation of Virulence Factors*; Academic Press, 1994; Vol. Volume 235, pp. 225–234.
(177) Wang, S.-B.; Min, Y.-L.; Yu, S.-H. Synthesis and Magnetic Properties of Uniform Hematite Nanocubes. *The Journal of Physical Chemistry C* **2007**, *111*, 3551–3554.

(178) Gao, T.; O'Brian, M. R. Control of DegP-dependent degradation of *c*-type cytochromes by heme and the cytochrome *c* maturation system in *Escherichia coli*. *J. Bacteriol.* **2007**, *189*, 6253–6259.
(179) Narayanan, A.; Ridilla, M.; Yernool, D. A. Restrained expression, a method to overproduce toxic membrane proteins by exploiting operator-repressor interactions. *Protein Sci.* **2011**, *20*, 51–61.
(180) Kelly, J. R.; Rubin, A. J.; Davis, J. H.; Ajo-Franklin, C. M.; Cumbers, J.; Czar, M. J.; de Mora, K.; Glieberman, A. L.; Monie, D. D.; Endy, D. Measuring the activity of BioBrick promoters using an in vivo reference standard. *J Biol Eng* **2009**, *3*, 4.
(181) Engler, C.; Gruetzner, R.; Kandzia, R.; Marillonnet, S. Golden gate shuffling: a one-pot DNA shuffling method based on type II restriction enzymes. *PLoS ONE* **2009**, *4*, e5553.
(182) Scott, M.; Gunderson, C. W.; Mateescu, E. M.; Zhang, Z.; Hwa, T. Interdependence of cell growth and gene expression: origins and consequences. *Science* **2010**, *330*, 1099–1102.
(183) Venkataraman, A.; Rosenbaum, M. A.; Perkins, S. D.; Werner, J. J.; Angenent, L. T. Metabolite-based mutualism between *Pseudomonas aeruginosa* PA14 and *Enterobacter aerogenes* enhances current generation in bioelectrochemical systems. *Energy & Environmental Science* **2011**, *4*, 4550.
(184) McGuirl, M. A.; Lee, J. C.; Lyubovitsky, J. G.; Thanyakoop, C.; Richards, J. H.; Gray, H. B.; Winkler, J. R. Cloning, heterologous expression, and characterization of recombinant class II cytochromes *c* from *Rhodopseudomonas palustris*. *Biochim. Biophys. Acta* **2003**, *1619*, 23–28.
(185) Xiong, Y.; Chen, B.; Shi, L.; Fredrickson, J. K.; Bigelow, D. J.; Squier, T. C. Targeted protein degradation of outer membrane decaheme cytochrome MtrC metal reductase in *Shewanella oneidensis* MR-1 measured using biarsenical probe CrAsH-EDT(2). *Biochemistry* **2011**, *50*, 9738–9751.
(186) Louro, R. O.; Paquete, C. M. The quest to achieve the detailed structural and functional characterization of CymA. *Biochem. Soc. Trans.* **2012**, *40*, 1291–1294.
(187) Méjean, V.; Iobbi-Nivol, C.; Lepelletier, M.; Giordano, G.; Chippaux, M.; Pascal, M. C. TMAO anaerobic respiration in *Escherichia coli*: involvement of the tor operon. *Mol. Microbiol.* **1994**, *11*, 1169–1179.
(188) Barrett, E. L.; Kwan, H. S. Bacterial reduction of trimethylamine oxide. *Annu. Rev. Microbiol.* **1985**, *39*, 131–149.
(189) Silvestro, A.; Pommier, J.; Pascal, M. C.; Giordano, G. The inducible trimethylamine N-oxide reductase of *Escherichia coli* K12: its localization and inducers. *Biochim. Biophys. Acta* **1989**, *999*, 208–216.
(190) Gon, S.; Patte, J. C.; Méjean, V.; Iobbi-Nivol, C. The torYZ (yecK bisZ) operon encodes a third respiratory trimethylamine N-oxide reductase in *Escherichia coli*. *J. Bacteriol.* **2000**, *182*, 5779–5786.
(191) Salis, H. M.; Mirsky, E. A.; Voigt, C. A. Automated design of synthetic ribosome binding sites to control protein expression. *Nat Biotech* **2009**, *27*, 946–950.
(192) Hussain, H.; Grove, J.; Griffiths, L.; Busby, S.; Cole, J. A seven-gene operon essential for formate-dependent nitrite reduction to ammonia by enteric bacteria. *Mol. Microbiol.* **1994**, *12*, 153–163.

(193) Einsle, O. Structure and function of formate-dependent cytochrome *c* nitrite reductase, NrfA. *Meth. Enzymol.* **2011**, *496*, 399–422.
(194) Gon, S.; Giudici-Orticoni, M. T.; Méjean, V.; Iobbi-Nivol, C. Electron transfer and binding of the *c*-type cytochrome TorC to the trimethylamine N-oxide reductase in *Escherichia coli*. *J. Biol. Chem.* **2001**, *276*, 11545–11551.
(195) Baron, D.; LaBelle, E.; Coursolle, D.; Gralnick, J. A.; Bond, D. R. Electrochemical Measurement of Electron Transfer Kinetics by *Shewanella oneidensis* MR-1. *J. Biol. Chem.* **2009**, *284*, 28865–28873.
(196) Bretschger, O.; Cheung, A. C. M.; Mansfeld, F.; Nealson, K. H. Comparative Microbial Fuel Cell Evaluations of *Shewanella* spp. *Electroanalysis* **2010**, *22*, 883–894.
(197) De Graaf, A. J.; Kooijman, M.; Hennink, W. E.; Mastrobattista, E. Nonnatural Amino Acids for Site-Specific Protein Conjugation. *Bioconjugate Chem.* **2009**, *20*, 1281–1295.
(198) Hendrickson, T. L.; Crécy-Lagard, V. de; Schimmel, P. Incorporation of Nonnatural Amino Acids into Proteins. *Annual Review of Biochemistry* **2004**, *73*, 147–176.
(199) Noren, C. J.; Anthony-Cahill, S. J.; Griffith, M. C.; Schultz, P. G. A general method for site-specific incorporation of unnatural amino acids into proteins. *Science* **1989**, *244*, 182–188.
(200) Winter, M. B.; McLaurin, E. J.; Reece, S. Y.; Olea, C.; Nocera, D. G.; Marletta, M. A. Ru-Porphyrin Protein Scaffolds for Sensing O2. *J. Am. Chem. Soc.* **2010**, *132*, 5582–5583.
(201) Tolia, N. H.; Joshua-Tor, L. Strategies for protein coexpression in *Escherichia coli*. *Nat. Methods* **2006**, *3*, 55–64.
(202) Shu, W.; Liu, J.; Ji, H.; Lu, M. Core structure of the outer membrane lipoprotein from *Escherichia coli* at 1.9 å resolution. *Journal of Molecular Biology* **2000**, *299*, 1101–1112.
(203) Inouye, M.; Shaw, J.; Shen, C. The assembly of a structural lipoprotein in the envelope of *Escherichia coli*. *J. Biol. Chem.* **1972**, *247*, 8154–8159.
(204) Cowles, C. E.; Li, Y.; Semmelhack, M. F.; Cristea, I. M.; Silhavy, T. J. The free and bound forms of Lpp occupy distinct subcellular locations in *Escherichia coli*. *Mol. Microbiol.* **2011**, *79*, 1168–1181.
(205) Sukupolvi, S.; O'Connor, C. D. TraT lipoprotein, a plasmid-specified mediator of interactions between gram-negative bacteria and their environment. *Microbiol. Rev.* **1990**, *54*, 331–341.
(206) Van Bloois, E.; Winter, R. T.; Kolmar, H.; Fraaije, M. W. Decorating microbes: surface display of proteins on *Escherichia coli*. *Trends in Biotechnology* **2011**, *29*, 79–86.
(207) Yang, C.; Zhu, Y.; Yang, J.; Liu, Z.; Qiao, C.; Mulchandani, A.; Chen, W. Development of an Autofluorescent Whole-Cell Biocatalyst by Displaying Dual Functional Moieties on *Escherichia coli* Cell Surfaces and Construction of a Coculture with Organophosphate-Mineralizing Activity. *Appl Environ Microbiol* **2008**, *74*, 7733–7739.
(208) Baba, T.; Ara, T.; Hasegawa, M.; Takai, Y.; Okumura, Y.; Baba, M.; Datsenko, K. A.; Tomita, M.; Wanner, B. L.; Mori, H. Construction of *Escherichia coli* K-

12 in-frame, single-gene knockout mutants: the Keio collection. *Mol Syst Biol* **2006**, *2*, 2006.0008.

(209) Cao, Z.; Qi, Z.; Sprencel, C.; Newton, S. M.; Klebba, P. E. Aromatic components of two ferric enterobactin binding sites in *Escherichia coli* FepA. *Mol. Microbiol.* **2000**, *37*, 1306–1317.

(210) Tullman-Ercek, D.; DeLisa, M. P.; Kawarasaki, Y.; Iranpour, P.; Ribnicky, B.; Palmer, T.; Georgiou, G. Export pathway selectivity of *Escherichia coli* twin arginine translocation signal peptides. *J. Biol. Chem.* **2007**, *282*, 8309–8316.

(211) Mitra, K.; Ubarretxena-Belandia, I.; Taguchi, T.; Warren, G.; Engelman, D. M. Modulation of the bilayer thickness of exocytic pathway membranes by membrane proteins rather than cholesterol. *Proc. Natl. Acad. Sci. U.S.A.* **2004**, *101*, 4083–4088.

(212) Matias, V. R. F.; Al-Amoudi, A.; Dubochet, J.; Beveridge, T. J. Cryo-Transmission Electron Microscopy of Frozen-Hydrated Sections of *Escherichia coli* and *Pseudomonas aeruginosa*. *J. Bacteriol.* **2003**, *185*, 6112–6118.

(213) Graham, L. L.; Beveridge, T. J.; Nanninga, N. Periplasmic space and the concept of the periplasm. *Trends Biochem. Sci.* **1991**, *16*, 328–329.

(214) Vollmer, W.; Seligman, S. J. Architecture of peptidoglycan: more data and more models. *Trends Microbiol.* **2010**, *18*, 59–66.

Appendix A: Primers, Plasmids, and Strains

Table A-1: Primer and oligo sequences used in this dissertation.

Primer Name	Chapter – Primer Number	Sequence (5'-3')
AF121	2-1	GGCCGAATTCAAGAACTGCCTAAAAATGAA
AF122	2-2	AACCTCTAGATTAGCGCTGTAATAGCTTGCCA
AF123	2-3	CCGCGAATTCATGAACGCACAAAAATCAAAAATCGC
AF124	2-4	CCGGTCTAGATTAGAGTTTGTAACTCATGCTC
AF184	2-5	CGCTCACAAAGTAACTCTCTGGCTTCAAGCATACCCACGCA ATAACCCTGGTGTAGGCTGGAGCTGCTTC
AF188	2-6	TGGGGAATACCTTTACCCCATCAAAAGGTTACGGGAAATAA GAGGTTATTATGGGAATTAGCCATGGTCC
AF207	2-7	CGCTCACAAAGTAACTCTCTGGCTT
AF189	2-8	TGGGGAATACCTTTACCCCATCAAA
AF419	3-1	TAACTTGACAATTAATCATCCGGCTCATAAAATTTGTGGA
AF420	3-2	CAAGTCCACAAATTTTATGAGCCGGATGATTAATTGTCAA
AF421	3-3	TAACTTGACAATTAATCATCCGGCTCGTAATGTTTGTGGA
AF422	3-4	CAAGTCCACAAACATTACGAGCCGGATGATTAATTGTCAA
AF423	3-5	TAACTTGACAATTAATCATCCGGCTCGTAGTGTTTGTGGA
AF424	3-6	CAAGTCCACAAACACTACGAGCCGGATGATTAATTGTCAA
AF425	3-7	TAACTTTCAATTTAATCATCCGGCTCGTATAATGTGTGGA
AF426	3-8	CAAGTCCACACATTATACGAGCCGGATGATTAAATTGAAA
AF427	3-9	TAACTTCAAATTTAATCATCCGGCTCGTATAATGTGTGGA
AF428	3-10	CAAGTCCACACATTATACGAGCCGGATGATTAAATTTGAA
AF429	3-11	TAACTTTGCGGTTAATCATCCGGCTCGTATAATGTGTGGA
AF430	3-12	CAAGTCCACACATTATACGAGCCGGATGATTAACCGCAAA
AF431	3-13	TAACTTGACAATTAATCATCCGGCTCTTAGGTTCTGTGGA
AF432	3-14	CAAGTCCACAGAACCTAAGAGCCGGATGATTAATTGTCAA
AF433	3-15	TAACTTGACAATTAATCATCGGCTCGTAGATTTTGTGGA
AF434	3-16	CAAGTCCACAAAATCTACGAGCCGATGATTAATTGTCAA
AF435	3-17	TAACTTGTGCTTTAATCATCCGGCTCGTAGAGTGTGTGGA
AF436	3-18	CAAGTCCACACACTCTACGAGCCGGATGATTAAAGCACAA
AF437	3-19	TAACTTCCTCCTTAATCATCCGGCTCGTATAATGTGTGGA
AF438	3-20	CAAGTCCACACATTATACGAGCCGGATGATTAAGGAGGAA
AF439	3-21	TAACTTATAAATTAATATCCGGCTCGTATAATGTGTGGA
AF440	3-22	CAAGTCCACACATTATACGAGCCGGATATTAATTTATAA
AF441	3-23	TAACTTTCAGGTTAATCATCGGCTCGTATAATGTGTGGA
AF442	3-24	CAAGTCCACACATTATACGAGCCGATGATTAACCTGAAA
AF443	3-25	TAACTTAGCCCTTAATCATCCGGCTCGTATAATGTGTGGA
AF444	3-26	CAAGTCCACACATTATACGAGCCGGATGATTAAGGGCTAA
AF445	3-27	TAACTTATTCCTTAATCATCGGCTCGTATAATGTGTGGA
AF446	3-28	CAAGTCCACACATTATACGAGCCGATGATTAAGGAATAA
AF447	3-29	TAACTTCCTGGTTAATCATCCGGCTCATAAAATTTGTGGA
AF448	3-30	CAAGTCCACAAATTTTATGAGCCGGATGATTAACCAGGAA
AF470	3-31	TAACTTGACAATTAATCATCCGGCTCTTAGGGTGTGTGGA
AF471	3-32	CAAGTCCACACACCCTAAGAGCCGGATGATTAATTGTCAA
AF472	3-33	TAACTTGTTCTTTAATCATCGGCTCGTATAATGTGTGGA
AF473	3-34	CAAGTCCACACATTATACGAGCCGATGATTAAAGAACAA
AF476	3-35	TAACTTGCCGCTTAATCATCCGGCTCGTATAATGTGTGGA
AF477	3-36	CAAGTCCACACATTATACGAGCCGGATGATTAAGCGGCAA
AF478	3-37	TAACTTGACAATTAATCATCCGGCTCGTAGGTTATGTGGA

AF479	3-38	CAAGTCCACATAACCTACGAGCCGGATGATTAATTGTCAA
AF480	3-39	TAACTTGACAATTAATCATCCGGCTCATATCGTTTGTGGA
AF481	3-40	CAAGTCCACAAACGATATGAGCCGGATGATTAATTGTCAA
AF324	4-1	ATTTAATTATACAATGATTTCGGTGTCCAGTAATTTAATTA GAGGAATCTGTGTAGGCTGGAGCTGCTTC
AF328	4-2	ATTTGCTCATTAAGATCGCTTCACTAAACCATAATTCTACA GGGGTTATTGTGTAGGCTGGAGCTGCTTC
AF465	4-3	CAATAACCCCGTTCCGCCTCGCAAGGGGCGGAAAACACAAT GGAGTGAATGTGTAGGCTGGAGCTGCTTC
AF325	4-4	ATAAATTCACGTCTTGTTAATGTCATAACTTCCTCCCTGAT CAACGAGGAATGGGAATTAGCCATGGTCC
AF329	4-4	TTGTGCCAGAAAACGCCGACGTGATGCCTGAAAGAGATCGT TATTGTTCAATGGGAATTAGCCATGGTCC
AF466	4-5	GAAAACCGACTTCAGGAAGGAATACGTCCAGAAACCACCTC TTTTCTGGCATGGGAATTAGCCATGGTCC
AF326	4-6	ATTTAATTATACAATGATTTCGGTG
AF330	4-7	ATTTGCTCATTAAGATCGCTTCACT
AF467	4-8	CAATAACCCCGTTCCGCCTCGCAAG
AF327	4-9	ATAAATTCACGTCTTGTTAATGTCA
AF331	4-10	TTGTGCCAGAAAACGCCGACGTGAT
AF468	4-11	GAAAACCGACTTCAGGAAGGAATAC
AF353	4-12	CCGCCATATGAACTGGCGTGCACTATTTAAACCCAG
AF356	4-13	CCGCCATATGTTGGAGATAGAGTAATGAAC
AF354	4-14	CCGGGAATTCTTGCAGCGTTAAACCTTATCCTTTTGG
AF449	4-15	AATAATTTTGTTTAACTTTAAGAAGGAGATATACATATTTT GGAGATAGAGTAATGAAC
AF450	4-16	GTTCATTACTCTATCTCCAAAATATGTATATCTCCTTCTTA AAGTTAAACAAAATTATT
AF474	4-17	ATATGAATTCTTTGCCCAAGCAGGGGGAGCTCGCTCC
AF475	4-18	CCGGTCTAGATTAGCGCTGTAATAGCTTGC
AF356	5-1	CCGCCATATGTTGGAGATAGAGTAATGAAC
AF354	5-2	CCGGGAATTCTTGCAGCGTTAAACCTTATCCTTTTGG
AF355	5-3	CCGCGAATTCTATTTCCAGCATCCACTTAAGTCGCT
AF124	5-4	CCGGTCTAGATTAGAGTTTGTAACTCATGCTC
AF449	5-5	AATAATTTTGTTTAACTTTAAGAAGGAGATATACATATTTT GGAGATAGAGTAATGAAC
AF450	5-6	GTTCATTACTCTATCTCCAAAATATGTATATCTCCTTCTTA AAGTTAAACAAAATTATT

Table A-2: Plasmids used and developed in this dissertation.

Plasmid Name	Promoter	Protein Coding Regions(s)	Antibiotic Resistance(s)	Source/Chapter
pSB1ET2 (pET30a+)	T7 lac	n/a	Kan	Chapter 1
I5023	T7 lac	*mtrA*	Kan	Chapter 1
I5024	T7 lac	*mtrCAB*	Kan	Chapter 1
pEC86	Tet	*ccmA-H*	Chl	Dr. Steve Singer (*65*)
pKD46	P_{araB}	λ-red recombinase	Amp	Coli Genetic Stock (*170*)
pKD3	n/a	n/a	Amp, Chl	Coli Genetic Stock (*170*)
pKD4	n/a	n/a	Amp, Kan	Coli Genetic Stock (*170*)
pCP20	n/a	FLP	Amp	Coli Genetic Stock (*170*)
I5040	T7 lac	*cymA*	Kan	Chapter 4
I5052	T7 lac	*cymAmtrA*	Kan	Chapter 4
I5049	T7 *lac*	*cymAmtrCAB*	Kan	Chapter 5

Table A-3: Strains and cell lines developed in this dissertation.

MFe#	Strain Knickname	Cell Line	Plasmids	Gene(s) Expressed	Chapter used
MFe207	wt	BL21(DE3)	pSB1ET2	None	2,3,4
MFe208	*ccm*	BL21(DE3)	pSB1ET2; pEC86	*ccmA-H*	2,3,4
MFe291	*mtrA*	BL21(DE3)	I5023; pEC86	*mtrA, ccmA-H*	2,4
MFe290	*mtrCAB*	BL21(DE3)	I5024; pEC86	*mtrCAB, ccmA-H*	2,3
MFe254	Δ*napC*	BL21(DE3)Δ*napC*	pSB1ET2	None	2
MFe255	Δ*napC ccm*	BL21(DE3)Δ*napC*	pSB1ET2; pEC86	*ccmA-H*	2
MFe292	Δ*napC mtrA*	BL21(DE3)Δ*napC*	I5023; pEC86	*mtrA, ccmA-H*	2
MFe291	Δ*napC mtrCAB*	BL21(DE3)Δ*napC*	I5024; pEC86	*mtrCAB, ccmA-H*	2
MFe513	BioFAB p550	C43(DE3)	G550	*gfp*	3
MFe514	BioFAB p554	C43(DE3)	G554	*gfp*	3
MFe515	BioFAB p557	C43(DE3)	G577	*gfp*	3
MFe516	BioFAB p586	C43(DE3)	G586	*gfp*	3
MFe517	BioFAB p589	C43(DE3)	G589	*gfp*	3
MFe518	BioFAB p598	C43(DE3)	G598	*gfp*	3
MFe519	BioFAB p611	C43(DE3)	G611	*gfp*	3
MFe520	BioFAB p613	C43(DE3)	G613	*gfp*	3
MFe521	BioFAB p635	C43(DE3)	G635	*gfp*	3
MFe522	BioFAB p640	C43(DE3)	G640	*gfp*	3
MFe523	BioFAB p656	C43(DE3)	G656	*gfp*	3
MFe524	BioFAB p661	C43(DE3)	G661	*gfp*	3
MFe525	BioFAB p668	C43(DE3)	G668	*gfp*	3
MFe526	BioFAB p704	C43(DE3)	G704	*gfp*	3
MFe527	BioFAB p708	C43(DE3)	G708	*gfp*	3
MFe504	pET30a GFP	C43(DE3)	pET30a+ GFP	*gfp*	3
MFe447	$ccm^{0.099}$	Mach1	M635	*ccmA-H*	3
MFe448	$ccm^{0.028}$	Mach1	M613	*ccmA-H*	3
MFe449	$ccm^{0.027}$	Mach1	M611	*ccmA-H*	3
MFe450	$ccm^{0.015}$	Mach1	M586	*ccmA-H*	3
MFe451	$ccm^{0.006}$	Mach1	M589	*ccmA-H*	3
MFe452	$ccm^{0.002}$	Mach1	M554	*ccmA-H*	3

MFe453	*ccm*$^{0.000}$	Mach1	M656	*ccmA-H*	3
MFe454	*ccm*$^{0.033}$	Mach1	M640	*ccmA-H*	3
MFe455	*ccm*$^{0.003}$	Mach1	M698	*ccmA-H*	3
MFe456	*ccm*$^{0.0??}$	Mach1	M597	*ccmA-H*	3
MFe457	*ccm*$^{0.001}$	Mach1	M550	*ccmA-H*	3
MFe458	*ccm*$^{0.210}$	Mach1	M661	*ccmA-H*	3
MFe459	*ccm*$^{1.0}$	Mach1	M704	*ccmA-H*	3
MFe543	Least perturbed *ccm*	C43(DE3)	M640	*ccmA-H*	3
MFe499	Most cytochrome *ccm*	C43(DE3)	M635	*ccmA-H*	3
MFe464	*ccm*$^{0.099}$ *mtrCAB*$^{\#}$ or 'most cytochrome'	C43(DE3)	I5024; M635	*mtrCAB, ccmA-H*	3
MFe465	*ccm*$^{0.028}$ *mtrCAB*$^{\#}$	C43(DE3)	I5024; M613	*mtrCAB, ccmA-H*	3
MFe466	*ccm*$^{0.027}$ *mtrCAB*$^{\#}$	C43(DE3)	I5024; M611	*mtrCAB, ccmA-H*	3
MFe467	*ccm*$^{0.015}$ *mtrCAB*$^{\#}$	C43(DE3)	I5024; M586	*mtrCAB, ccmA-H*	3
MFe468	*ccm*$^{0.006}$ *mtrCAB*$^{\#}$	C43(DE3)	I5024; M589	*mtrCAB, ccmA-H*	3
MFe469	*ccm*$^{0.002}$ *mtrCAB*$^{\#}$	C43(DE3)	I5024; M554	*mtrCAB, ccmA-H*	3
MFe470	*ccm*$^{0.000}$ *mtrCAB*$^{\#}$	C43(DE3)	I5024; M656	*mtrCAB, ccmA-H*	3
MFe471	*ccm*$^{0.033}$ *mtrCAB*$^{\#}$ or 'least perturbed'	C43(DE3)	I5024; M640	*mtrCAB, ccmA-H*	3
MFe472	*ccm*$^{0.003}$ *mtrCAB*$^{\#}$	C43(DE3)	I5024; M698	*mtrCAB, ccmA-H*	3
MFe473	*ccm*$^{0.0??}$ *mtrCAB*$^{\#}$	C43(DE3)	I5024; M597	*mtrCAB, ccmA-H*	3
MFe474	*ccm*$^{0.001}$ *mtrCAB*$^{\#}$	C43(DE3)	I5024; M550	*mtrCAB, ccmA-H*	3
MFe477	*ccm*$^{0.210}$ *mtrCAB*$^{\#}$	C43(DE3)	I5024; M661	*mtrCAB, ccmA-H*	3
MFe431	*ccm*$^{1.0}$ *mtrCAB*$^{\#}$	BL21(DE3)	pEC86, I5040	*ccmA-H, cymA*	4
MFe536	*cymAmtrA*	BL21(DE3)	pEC86, I5052	*ccmA-H, cymAmtrA*	4
MFe372	Δ*torY-ccm*	BL21(DE3)Δ*torY*	pSB1ET2; pEC86	*ccmA-H*	4
MFe366	Δ*torY-mtrA*	BL21(DE3)Δ*torY*	pEC86, I5023	*ccmA-H, mtrA*	4
MFe344	Δ*torC-ccm*	BL21(DE3)Δ*torC*	pSB1ET2; pEC86	*ccmA-H*	4
MFe345	Δ*torC-mtrA*	BL21(DE3)Δ*torC*	pEC86, I5023	*ccmA-H, mtrA*	4
MFe506	Δ*nrfBCD-ccm*	BL21(DE3)Δ*nrfBCD*	pSB1ET2; pEC86	*ccmA-H*	4
MFe507	Δ*nrfBCD-mtrA*	BL21(DE3)Δ*nrfBCD*	pEC86, I5023	*ccmA-H, mtrA*	4
MFe408	*ccm*	C43(DE3)	pSB1ET2; pEC86	*ccmA-H*	5
MFe409	*mtrCAB*	C43(DE3)	pEC86, I5023	*ccmA-H, mtrCAB*	3,5
MFe444	*cymAmtrCAB*	C43(DE3)	pEC86, I5049	*ccmA-H, cymAmtrCAB*	5

Appendix B: Media and Buffer Compositions

Table B-1: Media and Buffer Compositions.

Name	Purpose	Composition
2xYT	Aerobic growth media	5 g L^{-1} NaCl 10 g L^{-1} yeast extract 16 g L^{-1} tryptone
M9 minimal media	*E. coli* minimal growth media	12.8 g L^{-1} $Na_2HPO_4 \cdot 7H_2O$ 3.0 g L^{-1} KH_2PO_4 0.50 g L^{-1} NaCl 1.0 g L^{-1} NH_4Cl) 0.4% lactate 1 mM thiamine HCl 0.2% casamino acids 2.0 mM $MgSO_4$ 0.1 mM $CaCl_2$
M1 minimal media	*Shewanella* minimal media for iron reduction assays in Chapters 4 and 5 as well as electrochemistry in Appendix F.	40 mM D,L-Lactate 0.2% casamino acids 50 mM PIPES 7.5 mM NaOH (final pH 7.4) 28 mM NH_4Cl 1.3 mM KCl 4.3 mM $NaH_2PO_4 \cdot H_2O$ 100 mM NaCl <u>10 mL L^{-1} 100x vitamin mix:</u> 2 mg L^{-1} D-biotin (B7) 2 mg L^{-1} folic acid (B9) 10 mg L^{-1} pyridoxine HCl (B6) 5 mg L^{-1} thiamine HCl (B1) 5 mg L^{-1} nicotinic acid (B3) 5 mg L^{-1} D-panthothenic acid hemicalcium salt (B5) 0.1 mg L^{-1} cobalamin (B12) 5 mg L^{-1} *p*-aminobenzoic acid (PABA) 5 mg L^{-1} α-lipoic acid. <u>10 mL L^{-1} 100x amino acid mix (pH 7):</u> 2 g L^{-1} L-glutamic acid 2 g L^{-1} L-arginine 2 g L^{-1} D,L-serine. <u>10 mL L^{-1} 100x trace mineral mix (pH 7):</u> 7.85 mM $C_6H_9NO_3Na_3$

		12.17 mM $MgSO_4 \cdot 7H_2O$ 2.96 mM $MnSO_4 \cdot H_2O$ 17.11 mM NaCl 0.36 mM $FeSO_4 \cdot 7H_2O$ 0.68 mM $CaCl_2 \cdot 2H_2O$ 0.42 mM $CoCl_2 \cdot 6H_2O$ 0.95 mM $ZnCl_2$ 0.040 mM $CuSO_4 \cdot 5H_2O$ 0.021 mM $AlK(SO_4)_2 \cdot 12H_2O$ 0.016 mM H_3BO_3 0.010 mM $Na_2MoO_4 \cdot 2H_2O$ 0.010 mM $NiCl_2 \cdot 6H_2O$ 0.076 mM $Na_2WO_4 \cdot 2H_2O$
M4 minimal media	*Shewanella* minimal media for electrochemistry in Chapter 3	0.221 g L^{-1} K_2HPO_4 0.099 g L^{-1} KH_2PO_4 0.168 g L^{-1} $NaHCO_3$ 1.189 g L^{-1} NH_4SO_4 7.305 g L^{-1} NaCl 1.192 g L^{-1} HEPES 40 mM L-lactate <u>10 mL L^{-1} $CaCl_2$ stock solution:</u> 7.13 g L^{-1} $CaCl_2 \cdot 2H_2O$ <u>10 mL L^{-1} trace mineral solution:</u> 2.26 g L^{-1} Na_2EDTA 24.89 g L^{-1} $MgSO_4 \cdot 7H_2O$ 0.029 g L^{-1} $MnSO_4 \cdot 4H_2O$ 0.058 g L^{-1} NaCl 0.068 g L^{-1} $FeCl_2$ 0.065 g L^{-1} $CoCl_2$ 0.029 g L^{-1} $ZnSO_4 \cdot 7H_2O$ 0.005 g L^{-1} $CuSO_4 \cdot 5H_2O$ 0.350 g L^{-1} H_3BO_3 0.080 g L^{-1} Na_2MoO_4 0.119 g L^{-1} $NiCl_2 \cdot 6H_2O$ 0.028 g L^{-1} Na_2SeO_4
Ferrozine	Measuring [Fe(II)]	100 mM HEPES, pH 8.0 0.5 g L^{-1} Ferrozine (Acros organics)
TXHN	Membrane protein suspension buffer	5% (w/v) Triton X-100 50 mM HEPES pH 7.4 200 mM NaCl

Appendix C: Homology between *Shewanella* and *E. coli* proteins

Appendix C-1. BLAST of MtrA against *E. coli.*

The primary sequence of MtrA before processing by Sec is as follows with the 10 heme binding motifs, CXXCH, shown in bold.

MKNCLKMKNLLPALTITMAMSAVMALVVTPNAYASKWDEKMTP
EQVEATLDKKFAEGNYSPKGADS**CLMCH**KKSEKVMDLFKGVHG
AIDSSKSPMAGLQ**CEACH**GPLGQHNKGGNEPMITFGKQSTLSADK
QNSV**CMSCH**QDDKRMSWNGGHHDNADVA**CASCH**QVHVAKDP
VLSKNTEMEV**CTSCH**TKQKADMNKRSSHPLKWAQMT**CSDCH**NP
HGSMTDSDLNKPSVNDT**CYSCH**AEKRGPKLWEHAPVTEN**CVTC**
HNPHGSVNDGMLKTRAPQL**CQQCH**ASDGHASNAYLGNTGLGSN
VGDNAFTGGRS**CLNCH**SQVHGSNHPSGKLLQR

The primary sequence of MtrA after processing by Sec is as follows with the 10 heme binding motifs, CXXCH, shown in bold. The prediction software SignalP4.0 was used for this prediction. (http://www.cbs.dtu.dk/services/SignalP/)

SKWDEKMTPEQVEATLDKKFAEGNYSPKGADS**CLMCH**KKSEKV
MDLFKGVHGAIDSSKSPMAGLQ**CEACH**GPLGQHNKGGNEPMITF
GKQSTLSADKQNSV**CMSCH**QDDKRMSWNGGHHDNADVA**CASC**
HQVHVAKDPVLSKNTEMEV**CTSCH**TKQKADMNKRSSHPLKWAQ
MT**CSDCH**NPHGSMTDSDLNKPSVNDT**CYSCH**AEKRGPKLWEHA
PVTEN**CVTCH**NPHGSVNDGMLKTRAPQL**CQQCH**ASDGHASNAY
LGNTGLGSNVGDNAFTGGRS**CLNCH**SQVHGSNHPSGKLLQR

When the cleaved sequence of MtrA was put into BLAST software (http://blast.ncbi.nlm.nih.gov/Blast.cgi) against *E. coli*, the following sequence similarities were determined.

Table C-1: MtrA homology to *E. coli* proteins.

Gene #	Short Name	Function	Score (bits)	E value
EG11945	NrfB	Pentaheme cytochrome c nitrite reductase	72	6E-14
EG13277	TorY	Pentaheme cytochrome c TMAO reducatase	35	0.008
EG12060	NapC	Tetraheme cytochrome c quinol dehydrogenase	34	0.010
EG11781	NrfA	Pentaheme cytochrome c552 nitrite reductase	32	0.067
EG11815	TorC	Pentaheme cytochrome c TMAO reducatase	26	2.8
EG13520	YgaQ	Pseudogene alpha-amylase	25	4.8

These BLAST results indicate that there is one protein with similar sequence to MtrA: NrfB. If you examine the homology results carefully, NrfB is most similar to the first half of the MtrA primary structure, overlapping with the first 5 heme binding motifs.

>Eg11945 NrfB: periplasmic pentaheme cytochrome c nitrite reductase

Length = 188, Score = 71.6 bits (174), Expect = 6e-14

Identities = 48/141 (34%), Positives = 70/141 (49%), Gaps = 24/141 (17%)

```
Query: 32  SCLMCHKKSEKVMDLFKGVHGAIDSSKSPMAGLQCEACHG-PLGQHNKGG------NEPM 84
           +CL CHK   + M    G H ++ +  + +  + C  CHG P  QH +G       NEPM
Sbjct: 48  ACLDCHKPDTEGMH---GKHASVINPNNKLP-VTCTNCHGQPSPQHREGVKDVMRFNEPM 103

Query: 85  ITFGKQSTLSADKQNSVCMSCHQDD--KRMSWNGGHHDNADVACASCHQVHVAKDPV--L 140
              G+Q        NSVCMSCH  +  ++  W    H    VACASCH +H  +D +  L
Sbjct: 104 YKVGEQ--------NSVCMSCHLPEQLQKAFWPHDVH-VTKVACASCHSLHPQQDTMQTL 154

Query: 141 SKNTEMEVCTSCHTKQKADMN 161
           S    +++C  CH+ Q+ + N
Sbjct: 155 SDKGRIKICVDCHSDQRTNPN 175
```

Appendix C-2. BLAST of CymA against *E. coli.*

The primary sequence of CymA before processing by Sec is as follows with the 4 heme binding motifs, CXXCH, shown in bold.

MNWRALFKPSAKYSILALLVVGIVIGVVGYFATQQTLHATSTDAF
CMSCHSNHSLKNEVLASAHGGGKAGVTVQ**CQDCH**LPHGPVDYL
IKKIIVSKDLYGFLTIDGFNTQAWLDENRKEQADKALAYFRGNDS
AN**CQHCH**TRIYENQPETMKPMAVRMHTNNFKKDPETRKT**CVDC**
HKGVAHPYPKG

The primary sequence of CymA after processing by Sec is as follows with the 4 heme binding motifs, CXXCH, shown in bold. The prediction software SignalP4.0 was used for this prediction. (http://www.cbs.dtu.dk/services/SignalP/)

TSTDAF**CMSCH**SNHSLKNEVLASAHGGGKAGVTVQ**CQDCH**LPH
GPVDYLIKKIIVSKDLYGFLTIDGFNTQAWLDENRKEQADKALAYF
RGNDSAN**CQHCH**TRIYENQPETMKPMAVRMHTNNFKKDPETRK
T**CVDCH**KGVAHPYPKG

When the cleaved sequence of CymA was put into BLAST software (http://blast.ncbi.nlm.nih.gov/Blast.cgi) against *E. coli*, the following sequence similarities were determined.

Table C-2: CymA homology to *E. coli* proteins.

Gene #	Short Name	Function	Score (bits)	E value
EG13277	TorY	Pentaheme cytochrome c TMAO reducatase	98	3E-22
EG12060	NapC	Tetraheme cytochrome c quinol dehydrogenase	94	5E-21
EG11815	TorC	Pentaheme cytochrome c TMAO reducatase	90	7E-20
EG11119	YceD	Function unknown, DUF177 family	30	0.088
EG12473	YjeK	Weak lysine 2,3-aminomutase	29	0.15
EG10547	lrp	Global regulatory protein, Leu responsive	26	0.97

These BLAST results indicate that the first three proteins, TorY, NapC, and TorC, have high sequence similarity to CymA. All of these proteins are multiheme cytochromes c that act as quinol dehydrogenases in different anaerobic metabolic processes. One striking difference in the group is the number of heme binding motifs: the Tor proteins have 5 heme binding motifs whereas NapC and CymA both have four heme binding motifs. The literature normally reports NapC most similar to CymA because of this distinction.

>Eg13277 TorY: Pentaheme cytochrome c TMAO reducatase

Score = 97.8 bits (242), Expect = 3e-22
Identities = 51/147 (34%), Positives = 75/147 (51%), Gaps = 5/147 (3%)

```
Query: 1   TSTDAFCMSCHSNHSLKNEVLASAHGGGKAGVTVQCQDCHLPHGPVDYLIKKIIVSKDLY 60
           TS  AFC+SCHS      E   + H   + G+  +C DCH+P   +DYL  K+  SKD+Y
Sbjct: 33  TSDTAFCLSCHSMSKPFEEYQGTVHFSNQKGIRAECADCHIPKSGMDYLFAKLKASKDIY 92

Query: 61  GFLTIDGFNTQAWLDENRKEQADKALAYFRGNDSANCQHCHTRIYENQPETMKPMAVRMH 120
                 ++    + +R+E A+      +  DSA C+ CH+         +    A +MH
Sbjct: 93  HEFVSGKIDSDDKFEAHRQEMAETVWKELKATDSATCRSCHS-FDAMDIASQSESAQKMH 151

Query: 121 TNNFKKDPETRKTCVDCHKGVAHPYPK 147
            N  +KD E   TC+DCHKG+AH  P+
Sbjct: 152 -NKAQKDSE---TCIDCHKGIAHFPPE 174
```

>EG12060 NapC: Tetraheme cytochrome c quinol dehydrogenase

Score = 93.6 bits (231), Expect = 5e-21
Identities = 52/148 (35%), Positives = 78/148 (52%), Gaps = 11/148 (7%)

```
Query: 2   STDAFCMSCHS-NHSLKNEVLASAHGGGKAGVTVQCQDCHLPHGPVDYLIKKIIVSKDLY 60
           +T+ FC+SCH   +++  E + S H   ++GV   C DCH+PH  V  +I+K+  SK+LY
Sbjct: 52  NTEEFCISCHEMRNTVYQEYMDSVHYNNRSGVRATCPDCHVPHEFVPKMIRKLKASKELY 111

Query: 61  G--FLTIDGFNTQAWLDENRKEQADKALAYFRGNDSANCQHCHTRIYENQPETMKPMAVR 118
           G  F  ID   T    + +R   A       + N+S  C++CH   Y +     K +A +
Sbjct: 112 GKIFGVID---TPQKFEAHRLTMAQNEWRRMKDNNSQECRNCHNFEYMD-TTAQKSVAAK 167

Query: 119 MHTNNFKKDPETRKTCVDCHKGVAHPYP 146
           MH    K      +TC+DCHKG+AH  P
Sbjct: 168 MHDQAVKDG----QTCIDCHKGIAHKLP 191
```

>EG11815 TorC: Pentaheme cytochrome c TMAO reducatase

Score = 89.7 bits (221), Expect = 7e-20
Identities = 48/150 (32%), Positives = 70/150 (46%), Gaps = 13/150 (8%)

```
Query: 1   TSTDAFCMSCHSNHSLKNEVLASAHGGGKAGVTVQCQDCHLPHGPVDYLIKKIIVSKDLY 60
           TST  FC+SCHS   +  E   S H    +GV  +C DCH+P      + +K+  S D+Y
Sbjct: 42  TSTTEFCVSCHSMQPVYEEYKQSVHFQNASGVRAECHDCHIPPDIPGMVKRKLEASNDIY 101

Query: 61  GFLTIDGFNTQAWLDENRKEQADKALAYFRGNDSANCQHCHT----RIYENQPETMKPMA 116
                 +T    +  R E A++  A  + N+SA C+ CH          +  PE  + M
Sbjct: 102 QTFIAHSIDTPEKFEAKRAELAEREWARMKENNSATCRSCHNYDAMDHAKQHPEAARQMK 161

Query: 117 VRMHTNNFKKDPETRKTCVDCHKGVAHPYP 146
           V    N         ++C+DCHKG+AH  P
Sbjct: 162 VAAKDN---------QSCIDCHKGIAHQLP 182
```

Appendix C-3. BLAST of MtrB against *E. coli.*

The primary sequence of MtrB before processing by Sec is as follows.

MKFKLNLITLALLANTGLAVAADGYGLANANTEKVKLSAWSCKG
CVVETGTSGTVGVGVGYNSEEDIRSANAFGTSNEVAGKFDADLNF
KGEKGYRASVDAYQLGMDGGRLDVNAGKQGQYNVNVNYRQIA
TYDSNSALSPYAGIGGNNLTLPDNWITAGSSNQMPLLMDSLNALE
LSLKRERTGLGFEYQGESLWSTYVNYMREEKTGLKQASGSFFNQS
MMLAEPVDYTTDTIEAGVKLKGDRWFTALSYNGSIFKNEYNQLDF
ENAFNPTFGAQTQGTMALDPDNQSHTVSLMGQYNDGSNALSGRI
LTGQMSQDQALVTDNYRYANQLNTDAVDAKVDLLGMNLKVVSK
VSNDLRLTGSYDYYDRDNNTQVEEWTQISINNVNGKVAYNTPYD
NRTQRFKVAADYRITRDIKLDGGYDFKRDQRDYQDRETTDENTV
WARLRVNSFDTWDMWVKGSYGNRDGSQYQASEWTSSETNSLLR
KYNLADRDRTQVEARITHSPLESLTIDVGARYALDDYTDTVIGLTE
SKDTSYDANISYMITADLLATAFYNYQTIESEQAGSSNYSTPTWTG
FIEDQVDVVGAGISYNNLLENKLRLGLDYTYSNSDSNTQVRQGITG
DYGDYFAKVHNINLYAQYQATEKLALRFDYKIENYKDNDAANDI
AVDGIWNVVGFGSNSHDYTAQMLMLSMSYKL

The primary sequence of MtrB after processing by Sec is as follows. The prediction software SignalP4.0 was used for this prediction. (http://www.cbs.dtu.dk/services/SignalP/)

ADGYGLANANTEKVKLSAWSCKGCVVETGTSGTVGVGVGYNSE
EDIRSANAFGTSNEVAGKFDADLNFKGEKGYRASVDAYQLGMDG
GRLDVNAGKQGQYNVNVNYRQIATYDSNSALSPYAGIGGNNLTL
PDNWITAGSSNQMPLLMDSLNALELSLKRERTGLGFEYQGESLWS
TYVNYMREEKTGLKQASGSFFNQSMMLAEPVDYTTDTIEAGVKL
KGDRWFTALSYNGSIFKNEYNQLDFENAFNPTFGAQTQGTMALDP
DNQSHTVSLMGQYNDGSNALSGRILTGQMSQDQALVTDNYRYA
NQLNTDAVDAKVDLLGMNLKVVSKVSNDLRLTGSYDYYDRDNN
TQVEEWTQISINNVNGKVAYNTPYDNRTQRFKVAADYRITRDIKL
DGGYDFKRDQRDYQDRETTDENTVWARLRVNSFDTWDMWVKG
SYGNRDGSQYQASEWTSSETNSLLRKYNLADRDRTQVEARITHSP
LESLTIDVGARYALDDYTDTVIGLTESKDTSYDANISYMITADLLA
TAFYNYQTIESEQAGSSNYSTPTWTGFIEDQVDVVGAGISYNNLLE
NKLRLGLDYTYSNSDSNTQVRQGITGDYGDYFAKVHNINLYAQY
QATEKLALRFDYKIENYKDNDAANDIAVDGIWNVVGFGSNSHDY
TAQMLMLSMSYKL

When the cleaved sequence of MtB was put into BLAST software (http://blast.ncbi.nlm.nih.gov/Blast.cgi) against *E. coli*, the following sequence similarities were determined.

Table C-3: MtrB homology to *E. coli* proteins.

Gene #	Short Name	Function	Score (bits)	E value
EG13605	YaiT	Pseudogene reconstruction, autotransporter family	44	4E-5
EG13297	YaiO	Outer membrane protein, function unknown	31	0.31
EG10293	FepA	Ferrienterobactein outer membrane receptor	30	0.70
EG10018	CsrD	Targets csrBC sRNAs for degradation by RNAseE	28	2.0
EG10827	RecE	RecET recombinase, exonuclease VIII	28	2.6
EG13378	YeeJ	Overexpression increases adhesion and biofilm formation	27	4.5

These BLAST results indicate that there are not any genes very close in primary structure to MtrB. Nothing is known about YaiT except that it is similar in sequence to outer membrane porins.

```
>Eg13605 YaiT: Pseudogene reconstruction, autotransporter family
 Score = 43.9 bits (102), Expect = 4e-05
 Identities = 99/471 (21%), Positives = 169/471 (35%), Gaps = 84/471 (17%)

Query: 4   KLNLITLALLANTGLAVAADGYGLANANTEKVKLSAWSCKGCVVETG------------- 50
           KL   T+ L   + L +  DGY     +T+ + ++++S       TG
Sbjct: 440 KLTSDTIDLTNGSSLNIGEDGY----VDTDHLTINSYSTVALTESTGWGADDYNLYANTI 495

Query: 51  ---TSGTVGVGVGYNSEEDIRSANAFGTS--------NEVAGKFDA-------DLNFKGE 92
                G + V V     E  R+     TS         N V+G FD         + +   +
Sbjct: 496 TVTNGGVLDVNVDQFDTEAFRTDKLELTSGNIADHNGNVVSGVFDIHSSDYVLNADLVND 555

Query: 93  KGYRASVDAYQLGMDGGRLDVNAGKQGQYNVNVNYR-QIATYDSNSALSPYAGIGGNNLT 151
           + +  S   Y  G+      V     G   +N N      T   NS++       GN
Sbjct: 556 RTWDTSKSNYGYGI------VAMNSDGHLTINGNGDVDNGTELDNSSVDNVVAATGNYKV 609

Query: 152 LPDNWITAGS----SNQMPLLMDSLNALELSLKRERTGLG-FEYQGESLWSTYVNYMRE- 205
             DN   AG+     ++  + ++ +N+        +  LG + YQ E   +T V    E
Sbjct: 610 RIDNATGAGAIADYKDKEIIYVNDVNSNATFSAANKADLGAYTYQAEQRGNTVVLQQMEL 669

Query: 206 -----EKTGLKQASGSFFNQSMMLAEPVDYTTDTIEAGVKLKGDRWFTALSYNGSIFKNE 260
                +  A+ + +N      + V         G+   G  W   +SY G  F  +
Sbjct: 670 TDYANMALSIPSANTNIWNLEQ---DTVGTRLTNSRHGLADNGGAW---VSYFGGNFNGD 723

Query: 261 YNQLDFENAFNPTFGAQTQGTMALDPDNQSHTVSLMGQYNDGSNALSGRILTGQMSQDQ- 319
              ++++   N   G        +D +N    V     +  G   ++ R  +GQ+ QD
Sbjct: 724 NGTINYDQDVN---GIMVGVDTKIDGNNAKWIVGAAAGFAKGD--MNDR--SGQVDQDSQ 776

Query: 320 -ALVTDNYRYANQLNTDAVDAKVDLLGMNLKVVSKVSNDLRLTGSYDYYDRDNNTQVEEW 378
            A +  +  +AN +  D   +            S  +NDL  T S   Y  D +T  + W
Sbjct: 777 TAYIYSSAHFANNVFVDGSLS-----------YSHFNNDLSATMSNGTYV-DGSTNSDAW 824

Query: 379 ---TQISINNVNGKVAYNTPYDNRTQRFKVAADYRITRDIKLDG-GYDFKR 425
              +   +   G   Y TPY + +  F+   DY+++ D+K+DG  YD  R
Sbjct: 825 GFGLKAGYDFKLGDAGYVTPYGSVSGLFQSGDDYQLSNDMKVDGQSYDSMR 875
```

One of the interesting results was sequence similarity to FepA, an enterobactin binder and transporter. However, the region of FebA responsible for transportation and binding of enterobactin (Y260, Y272, R316, F329) is not within the similar sequence region. So the only similarity to FepA appears to be the basic outer membrane porin structure (*209*).

>FepA: enterobactin transporter

Score = 24.6 bits (52), Expect = 0.015, Method: Compositional matrix adjust.
Identities = 48/258 (19%), Positives = 106/258 (41%), Gaps = 40/258 (16%)

```
Query  162  RTGLGFEYQGESLWSTYVNYMREEK-TGLKQASGSFFNQSM--MLAEPVDYTTDTIEAGV  218
            + G+   Y+  SL+ T  NY+   K  G   ++G  + Q    + AE    T+   E G+
Sbjct  459  KMGIARAYKAPSLYQTNPNYILYSKGQGCYASAGGCYLQGNDDLKAE----TSINKEIGL  514

Query  219  KLKGDRWFTALSYNGSIFKNEYNQLDFENAFNPTFGAQTQGTMALDPDNQSHTVSLMGQY  278
            + K D W   +++    F+N     D+ N     + A  Q  +  D          + Q+
Sbjct  515  EFKRDGWLAGVTW----FRN-----DYRNKIEAGYVAVGQNAVGTD----------LYQW  555

Query  279  NDGSNALSGRILTGQMS---QDQALVTDNYRYANQLNTDAVDAKVDLLG---MNLKVVSK  332
            ++   A+    L G ++    +  + T+N  Y  +        ++ ++    +N  +  +
Sbjct  556  DNVPKAVV-EGLEGSLNVPVSETVMWTNNITYMLKSENKTTGDRLSIIPEYTLNSTLSWQ  614

Query  333  VSNDLRLTGSYDYYDRDNNTQVEEWTQISINNVNGKVAYNTPYDNRTQRFKVAADYRITR  392
               DL +  ++ +Y +    +     Q ++     +++   PY        ++A + +T+
Sbjct  615  AREDLSMQTTFTWYGKQQPKKYNYKGQPAVGPETKEIS---PY----SIVGLSATWDVTK  667

Query  393  DIKLDGGYDFKRDQRDYQ  410
            ++ L GG D   D+R ++
Sbjct  668  NVSLTGGVDNLFDKRLWR  685
```

Appendix C-4. BLAST of MtrC against *E. coli.*

The sequence of MtrC before cleavage is as follows with the lipobox sequence underlined.

MMNAQKSKIALLLAASAVTMALTGCGGSDGNNGNDGSDGGEPA
GSIQTLNLDITKVSYENGAPMVTVFATNEADMPVIGLANLEIKKAL
QLIPEGATGPGNSANWQGLGSSKSYVDNKNGSYTFKFDAFDSNKV
FNAQLTQRFNVVSAAGKLADGTTVPVAEMVEDFDGQGNAPQYT
KNIVSHEVCASCHVEGEKIYHQATEVETCISCHTQEFADGRGKPHV
AFSHLIHNVHNANKAWGKDNKIPTVAQNIVQDNCQVCHVESDML
TEAKNWSRIPTMEVCSSCHVDIDFAAGKGHSQQLDNSNCIACHNS
DWTAELHTAKTTATKNLINQYGIETTSTINTETKAATISVQVVDAN
GTAVDLKTILPKVQRLEIITNVGPNNATLGYSGKDSIFAIKNGALDP
KATINDAGKLVYTTTKDLKLGQNGADSDTAFSFVGWSMCSSEGK
FVDCADPAFDGVDVTKYTGMKADLAFATLSGKAPSTRHVDSVN
MTACANCHTAEFEIHKGKQHAGFVMTEQLSHTQDANGKAIVGLD
ACVTCHTPDGTYSFANRGALELKLHKKHVEDAYGLIGGNCASCH
SDFNLESFKKKGALNTAAAADKTGLYSTPITATCTTCHTVGSQYM
VHTKETLESFGAVVDGTKDDATSAAQSETCFYCHTPTVADHTKV
KM

The primary sequence of MtrC after the signal sequence is cleaved at the lipobox is as follows.

CGGSDGNNGNDGSDGGEPAGSIQTLNLDITKVSYENGAPMVTVFA
TNEADMPVIGLANLEIKKALQLIPEGATGPGNSANWQGLGSSKSY
VDNKNGSYTFKFDAFDSNKVFNAQLTQRFNVVSAAGKLADGTTV
PVAEMVEDFDGQGNAPQYTKNIVSHEVCASCHVEGEKIYHQATE
VETCISCHTQEFADGRGKPHVAFSHLIHNVHNANKAWGKDNKIPT
VAQNIVQDNCQVCHVESDMLTEAKNWSRIPTMEVCSSCHVDIDFA
AGKGHSQQLDNSNCIACHNSDWTAELHTAKTTATKNLINQYGIET
TSTINTETKAATISVQVVDANGTAVDLKTILPKVQRLEIITNVGPNN
ATLGYSGKDSIFAIKNGALDPKATINDAGKLVYTTTKDLKLGQNG
ADSDTAFSFVGWSMCSSEGKFVDCADPAFDGVDVTKYTGMKAD
LAFATLSGKAPSTRHVDSVNMTACANCHTAEFEIHKGKQHAGFV
MTEQLSHTQDANGKAIVGLDACVTCHTPDGTYSFANRGALELKL
HKKHVEDAYGLIGGNCASCHSDFNLESFKKKGALNTAAAADKTG
LYSTPITATCTTCHTVGSQYMVHTKETLESFGAVVDGTKDDATSA
AQSETCFYCHTPTVADHTKVKM

When the cleaved sequence of MtrC was entered into BLAST software (http://blast.ncbi.nlm.nih.gov/Blast.cgi) against *E. coli*, no sequence came back with a high sequence similarity. This demonstrates how unique the protein MtrC is for *E. coli* to express. Because none of these alignments span more than 46 amino acid residues, I do not display them here.

Appendix C-5. BLAST of SirCD against *E. coli.*

Note that the *Shewanella oneidensis* MR-1 genome is not annotated with SirC or SirD; rather the genome is annotated as NrfC and NrfD. The locus identifiers for these proteins are SO0483 and SO0484 for SirC and SirD, respectively. However, I call them SirCD here to avoid confusion with the present literature on the functional replacement of CymA with the so-called SirCD (*71*). Note that the *Shewanella oneidensis* MR-1 genome is not annotated with SirC or SirD; rather the genome is annotated as NrfC and NrfD. The locus identifiers for these proteins are SO0483 and SO0484 for SirC and SirD, respectively.

First I will cover SirC. SirC/NrfC is an iron sulfur protein with the following primary amino acid sequence.

MSENIERRRFLKSAGMCSLILTPLAGCSVKEDADSAHKPHYVMVF
DQNKCVGCGDCKTACNQANNLPAGVSRVILEQQSGRVEGQACPH
CGKMVCDCERKFVRVSCQQCKNAPCVTVCPTGAAHRDAKTGIVT
MDASKCAGCKYCIGACPYNARLINNNTDVADNCDFCLHSKLSKG
ELPACVQSCKYDALIFGDANDPQSYVSKLLAVKDSVRIKPQFGTEP
SLRYIPIVKLGV

SirC has a signal sequence for the TAT secretion system, leaving the following primary sequence after cleavage. The signal sequence is reported as 27 amino acid residues long (*210*).

SVKEDADSAHKPHYVMVFDQNKCVGCGDCKTACNQANNLPAGV
SRVILEQQSGRVEGQACPHCGKMVCDCERKFVRVSCQQCKNAPC
VTVCPTGAAHRDAKTGIVTMDASKCAGCKYCIGACPYNARLINN
NTDVADNCDFCLHSKLSKGELPACVQSCKYDALIFGDANDPQSYV
SKLLAVKDSVRIKPQFGTEPSLRYIPIVKLGV

When the cleaved sequence of SirC was entered into BLAST software (http://blast.ncbi.nlm.nih.gov/Blast.cgi) against *E. coli*, the following sequence similarities were determined.

Table C-4: SirC homology to *E. coli* proteins.

Gene #	Short Name	Function	Score (bits)	E value
EG11946	*nrfC*	Formate-dependent nitrite reduction	180	8e-47
EG13958	*ydhX*	Ferredoxin-like protein	150	7e-38
EG11799	*hybA*	Hydrogenase subunit	105	3e-24
EG10233	*dmsB*	DMSO reductase subunit	100	7e-23
EG13845	*ynfG*	S- and N-oxide reductase	100	1e-22

The top hit, NrfC, is a formate-dependent nitrate reductase with four [4Fe-4S] clusters. The alignment is as follows. This alignment is particularly high, with only 5% gaps (highlighted in green).

```
>EG11946 nrfC Formate-dependent nitrite reduction
          Length = 223

 Score =  180 bits (456), Expect = 8e-47
 Identities = 93/223 (41%), Positives = 130/223 (58%), Gaps = 12/223 (5%)

Query: 7   RRRFLKSAGMCSLILTPLAGCSVKEDADSAHKPHYVMVFDQNKCVGCGDCKTACNQANNL 66
           RR+FL   G+ + + +  AG  V +  +  +   Y MV D++ C+GC  C  AC + N +
Sbjct: 5   RRQFLTGVGVLAAV-SGTAGRVVAKTLN-INGVRYGMVHDESLCIGCTACMDACREVNKV 62

Query: 67  PAGVSRVILEQQSGRVEGQACPHCGKMVCDCERKFVRVSCQQCKNAPCVTVCPTGAAHRD 126
           P GVSR+ + +   + E           D + +F R SCQ C +APCV VCPTGA+ RD
Sbjct: 63  PEGVSRLTIIRSEPQGEFP----------DVKYRFFRKSCQHCDHAPCVDVCPTGASFRD 112

Query: 127 AKTGIVTMDASKCAGCKYCIGACPYNARLINNNTDVADNCDFCLHSKLSKGELPACVQSC 186
           A +GIV ++   C GC+YCI ACPY  R I+  T  AD CDFC  + L  G+LPACV++C
Sbjct: 113 AASGIVDVNPDLCVGCQYCIAACPYRVRFIHPVTKTADKCDFCRKTNLQAGKLPACVEAC 172

Query: 187 KYDALIFGDANDPQSYVSKLLAVKDSVRIKPQFGTEPSLRYIP 229
              AL FG+ +DP S +S+LL  K + R K   GT+P L  +P
Sbjct: 173 PTKALTFGNLDDPNSEISQLLRQKPTYRYKLALGTKPKLYRVP 215
```

Next I will cover SirD. SirD is a predicted integral membrane protein with eight conserved hydrophobic regions. The primary sequence is as follows. There was no identified signal sequence by the SignalP server, but I would speculate the signal sequence is much shorter than average. The first predicted transmembrane region begins at the residue 17, whereas most signal cleavage sites are approximately located 20-30 residues into the sequence.

MDFTLGLSQGVAWPWPIAVYLFFAGISGGALTIALALRFYLGQVE
NTAFLKAATLLSFVTISLGMLCLVLDLTNPLFFWRILVFYNLNSVM
SIGVIALSVYIPLVAVVALLALEKELMAIPQLKFLAPIIAKLKGFRRP
MEALALVLALSVCAYTGFLISALIRFPLINTSVLPALFIASGLSAGG
ASAKMLAVWLFKEPLHSGEMKILHGAEWPIMFAEAMFIFMIATAL
LTGNAGGQFAFAAFHEGVWASVFWIGVVGIGFAAPLLLNFATGK
HFSHSAKAFYMSGMCAVVGMMCLRLFILLAGQNYAI

When the SirD was entered into BLAST software (http://blast.ncbi.nlm.nih.gov/Blast.cgi) against *E. coli*, only two sequences were shown to have any similarity. Thus it is worth noting that NrfD/SirD are unique sequences in both the *E. coli* and *Shewanella* genomes.

Table C-5: SirD homology to *E. coli* proteins.

Gene #	Short Name	Function	Score (bits)	E value
EG11947	*nrfD*	Formate-dependent nitrate reduction	181	4e-47
ET11800	*hybB*	Hydrogenase subunit, cytochrome b	35	8e-3

The top hit, NrfD, is a formate-dependent nitrate reductase with four [4Fe-4S] clusters. The alignment is as follows. This alignment is particularly high, with only 3% gaps (highlighted in green). It is also fairly interesting that the hydrogenase subunits HybA and HybB both appeared in the sequence alignments for SirC and SirD, respectively. This may suggest that the hydrogenase functions similarly to the Nrf/Sir proteins.

```
>EG11947 nrfD Formate-dependent nitrite reduction
          Length = 318

 Score =  181 bits (460), Expect = 4e-47
 Identities = 106/307 (34%), Positives = 167/307 (54%), Gaps = 10/307 (3%)

Query: 9   QGVAWPWPIAVYLFFAGISGGALTIALALRFYLGQV--ENTAFLKAATLLSFVTISLGML 66
           + + W WPIA+YLF  GIS G +T+A+ LR +  Q    ++  L+   ++    + LG+L
Sbjct: 10  ESLVWDWPIAIYLFLIGISAGLVTLAVLLRRFYPQAGGADSTLLRTTLIVGPGAVILGLL 69

Query: 67  CLVLDLTNPLFFWRILVFYNLNSVMSIGVIALSVYIPLVAVVALLALEKELMAI-----P 121
            LV  LT P  FW+++  Y+  SVMS+GV+   +Y+ ++ +      E +L+A+     P
Sbjct: 70  ILVFHLTRPWTFWKLMFHYSFTSVMSMGVMLFQLYMVVLVLWLAKIFEHDLLALQQRWLP 129

Query: 122 QLKFLAPIIAKLKGFRRPMEALALVLALSVCAYTGFLISALIRFPLINTSVLPALFIASG 181
           +L  +  +++ L    R +E L LVLA+ + AYTGFL+SAL  +P +N  +LP LF+ SG
Sbjct: 130 KLGIVQKVLSLLTPVHRGLETLMLVLAVLLGAYTGFLLSALKSYPFLNNPILPVLFLFSG 189

Query: 182 LSAGGASAKMLAVWLFKEPLHSGEMKILHGAEWPIMFAEAMFIFMIATALLTGNAGGQFA 241
           +S+G A A +      +   HS E + +H  E P+++ E   +      L  G+ G   A
Sbjct: 190 ISSGAAVALIAMAIRQRSNPHSTEAQFVHRMEIPVVWGEIFLLVAFFVGLALGDDGKVRA 249

Query: 242 F-AAFHEGVWASVFWIGVVGIGFAAPLLLNFATGKHFSHSAKAFYMSGMCAVVGMMCLRL 300
             AA   G W   FW+GV G+G   P+LL     +  S    A   +   ++VG++ LR
Sbjct: 250 LVAALGGGFWTWWFWLGVAGLGLIVPMLLKPWVNR--SSGIPAVLAACGASLVGVLMLRF 307

Query: 301 FILLAGQ 307
           FIL AGQ
Sbjct: 308 FILYAGQ 314
```

Appendix C-6. BLAST of the Lol proteins against *E. coli.*

In this section, I will cover the alignment of the LolABCDE proteins between *E. coli* and *Shewanella*. To start, here is an overview of the set of proteins and how they align with one another.

Table C-6: *Shewanella* Lol protein homology to *E. coli* Lol proteins.

***E. coli* protein**	***Shewie* protein**	**Score (bits)**	**e-value**
LolA	LolA	129	2e-37
LolB	LolB	45	8e-7
LolC	LolC	183	1e-53
LolC	LolE	273	5e-88
LolD	LolD	265	1e-89
LolE	LolE	211	7e-64
LolE	LolC	354	4e-119

One oddity about this alignment is that LolC and LolE have mismatched alignments (ie LolC is more like LolE and vice versa). Additionally, LolB is the least "alike" the *E. coli* version of the Lol system, with the e-value for alignment between the two LolB proteins being less only 8e-7. LolB plays the role of inserting the lipoproteins into the outer membrane. Closer inspection of the LolB sequences show a lipobox signal sequence in both proteins (underlined), but that there is a large portion of the protein that does not align well (bold).

LolB in Shewie:

MNNLKRFTKSIFSCIALSGLLFLGGC**ETLPPMTDLSPITVDNAAQA**
KAWELQGKLAIRTPEDKLSANLYWRHSEERDELTLTTMLGTTVLT
LEATPNSAHLHIDGKDFRDTNAQALLERVSGWSIPINDLPLWITGQI
GSLDRVIAVDSAGQAKQLQNMQTPPPWLVTFLSWQSQSGAKVPY
QLTLERGDLQLKLQLNQWQALGKPSILLGEKP

LolB in BL21:

MPLPDFRLIRLLPLAALVLTAC**SVTTPKGPGKSPDSPQWRQHQQ**
DVRNLNQYQTRGAFAYISDQQKVYARFFWQQTGQDRYRLLLTNP
LGSTELELNAQPGNVQLVDNKGQRYTADDAEEMIGKLTGMPIPLN
SLRQWILGLPGDATDYKLDDQYRLSEITYSQNGKNWKVVYGGYD
TKTQPAMPANMELTDGGQRIKLKMDNWIVK

Next, I will show the alignments of each *Shewanella* protein with its counterpart in *E. coli*.

LolA:

Score	Expect	Method	Identities	Positives	Gaps
129 bits(323)	2e-37	Compositional matrix adjust.	69/203(34%)	103/203(50%)	2/203(0%)

```
Query  2    MKKIAITCALLSSLVASSVWADAASDLKSRLDKVSSFHASFTQKVTDGSGAAVQEGQGDL  61
            MKK+     L   L +++V AD A  L+  L    S  A F Q VTD +   +Q G G
Sbjct  1    MKKLLCAVLLSPLLYSNAVLADDAKQLRETLTGTESLKADFKQTVTDVNKKVIQSGAGVF  60

Query  62   WVKRPNLFNWHMTQPDESILVSDGKTLWFYNPFVEQATATWLKDATGNTPFMLIARNQSS  121
             +  PN F WH+T PDES +V+DGK LW YNPF E+         A   +P  L+     +
Sbjct  61   ALAHPNQFYWHLTAPDESKIVADGKDLWIYNPFAEEVVIMDFTQAITASPIALLVHRDDA  120

Query  122  DWQQYNIKQNGDDFVLTPKASNGNLKQFTINVGRDGTIHQFSAVEQDDQRSSYQLKSQQN  181
             W QY + +  D + + PKA++  +    +   + GT+++F+ ++     S + L +Q +
Sbjct  121  TWSQYAVTKKQDCYEIKPKATDAGISAVNVCFNK-GTLNKFNVLDDKGNLSQFDLSNQHS  179

Query  182  GAV-DAAKFTFTPPQGVTVDDQR  203
              +  D A F F   P  V VDDQR
Sbjct  180  ISTGDKALFKFVLPDNVDVDDQR  202
```

LolB:

Score	Expect	Method	Identities	Positives	Gaps
45.1 bits(105)	8e-07	Compositional matrix adjust.	41/155(26%)	79/155(50%)	5/155(3%)

```
Query  52   YQTRGAFAYISDQQKVYARFFWQQTGQDRYRLLLTNPLGSTELELNAQPGNVQL-VDNKG  110
            ++ +G  A  + + K+ A  +W+ + ++R  L LT  LG+T L L A P +  L +D K
Sbjct  49   WELQGKLAIRTPEDKLSANLYWRHS-EERDELTLTTMLGTTVLTLEATPNSAHLHIDGKD  107

Query  111  QRYTADDAEEMIGKLTGMPIPLNSLRQWILGLPGDATDY-KLDDQYRLSEITYSQNGKNW  169
              R T  +A+ ++ +++G  IP+N L  WI G  G       +D   +  ++   Q    W
Sbjct  108  FRDT--NAQALLERVSGWSIPINDLPLWITGQIGSLDRVIAVDSAGQAKQLQNMQTPPPW  165

Query  170  KVVYGGYDTKTQPAMPANMELTDGGQRIKLKMDNW  204
             V +  + +++   +P  + L  G  ++KL+++ W
Sbjct  166  LVTFLSWQSQSGAKVPYQLTLERGDLQLKLQLNQW  200
```

LolC:

Score	Expect	Method	Identities	Positives	Gaps
183 bits(464)	1e-53	Compositional matrix adjust.	127/415(31%)	217/415(52%)	21/415(5%)

```
Query  1    MYQPVALFIGLRYMRGRAADRFGRFVSWLSTIGITLGVMALVTVLSVMNGFERELQNNIL  60
            M  P+AL IG R+ R R ++ F  F+S+ ST GI LGV  L+ VLS MNGFEREL+  +L
Sbjct  1    MKGPLALSIGWRFYRARQSNSFISFISFASTAGIALGVAVLIIVLSAMNGFERELEQRLL  60

Query  61   GLMPQA-ILSSEHGSLNPQQLPETAVKLDGVNRVAPITTGDVVLQSARSVAVGVMLGIDP  119
            G++ QA ++       + + + +TA++++G+   AP      ++Q          ++GIDP
Sbjct  61   GVISQADVVGVNEPIADWRAVEQTALQIEGITAAAPFIRMQGLVQKPGGFQGLAVVGIDP  120

Query  120  AQK---DPLTPYLVNVKQTDLEPGKYNVILGEQLASQLGVNRGDQIRVMVPSAS-QFTPM  175
             Q+     L+ ++       L     +++LGE L  +LG+  GD + + V     +
Sbjct  121  EQEAKVSTLSQFMSPETWQSLSEDDNHIVLGESLLKKLGLEVGDTLALYVQDLDPEHAGS  180

Query  176  GRIPSQRLFNVIGTFAANSEVDGYEMLVNIEDASRLMRYPAGNITGWRLW----LDEPLK  231
             R      F V G +    E++     + +  A+ ++    G +TG R+       + P K
Sbjct  181  LRAAKSHRFVVSGVYRLGGELELTTAYIPMRYAANILNLHQG-VTGVRISVTQVFEAPAK  239

Query  232  VDSLSQQKLPEGSKWQDWRDRKGELFQAVRMEKNMMGLLLSLIVAVAAFNIITSLGLMVM  291
            +  L    L +     DW   +G L+Q +++ + +M L+L L++ VA FNI++++L + V
Sbjct  240  IRELGY-ALNQSVYISDWTRTQGHLYQDIQLVRTIMYLVLVLVIGVACFNIVSTLVMAVR  298

Query  292  EKQGEVAILQTQGLTPRQIMMVFMVQGASAGIIGAILGAALGALLASQLN----NLMPII  347
            +K  E+AIL T GL+   +M +FMVQGA  G++G  LG  +G   A  L+    ++  ++
Sbjct  299  DKASEIAILMTMGLSRLSVMGIFMVQGALNGLVGCALGGVIGIATAINLSAIARDIEQLL  358

Query  348  GVLLDGAA------LPVAIEPLQVIVIALVAMAIALLSTLYPSWRAAATQPAEAL  396
            G+ L  A       LP  +    V ++   A  ++L++TLYP+W+A+   PA+AL
Sbjct  359  GIQLLSADVYFVDFLPSELHMADVSLVIATAFVMSLIATLYPAWKASRIGPAQAL  413
```

LolD:

Score	Expect	Method	Identities	Positives	Gaps
265 bits(678)	1e-89	Compositional matrix adjust.	129/223(58%)	168/223(75%)	0/223(0%)

```
Query  1    MNKILLQCDNLCKRYQEGSVQTDVLHNVSFSVGEGEMMAIVGSSGSGKSTLLHLLGGLDT  60
            M  +LLQ   + K Y +G V T VL +V   V +GE +AIVG+SGSGKSTLLH++G LD
Sbjct  16   MQDVLLQVQAVSKSYHDGDVTTQVLSDVDLQVFKGEQLAIVGTSGSGKSTLLHIMGTLDK  75

Query  61   PTSGDVIFNGQPMSKLSSAAKAELRNQKLGFIYQFHHLLPDFTALENVAMPLLIGKKKPA  120
            P+SG V+  G+ + ++SSA +A++RNQ LGFIYQFHHLLP+FTALENVAMP  I  +
Sbjct  76   PSSGKVLLAGEDLYQVSSARQAQIRNQDLGFIYQFHHLLPEFTALENVAMPAFIQGRDRT  135

Query  121  EINSRALEMLKAVGLDHRANHRPSELSGGERQRVAIARALVNNPRLVLADEPTGNLDARN  180
               + A  +L+ VGL HR  +H P+ELSGGERQRVAIARAL+N P+LVLADEPTGNLDA++
Sbjct  136  LAQADAKVLLERVGLGHRMSHIPAELSGGERQRVAIARALINKPKLVLADEPTGNLDAKS  195

Query  181  ADSIFQLLGELNRLQGTAFLVVTHDLQLAKRMSRQLEMRDGRL  223
             +++++L+ EL    GTAF+VVTHD +LA RM RQL M++G L
Sbjct  196  GEAVYELIRELANQLGTAFVVVTHDPKLAARMDRQLTMKNGYL  238
```

LolE:

Score	Expect	Method	Identities	Positives	Gaps
211 bits(536)	7e-64	Compositional matrix adjust.	130/416(31%)	221/416(53%)	14/416(3%)

```
Query  1    MAMPLSLLIGLRFSRGRRRGGMVSLISVISTIGIALGVAVLIVGLSAMNGFERELNNRIL  60
            M +   L +G R+ R R+     S I++ +  GI LGVA LIV  S MNG E +L  RIL
Sbjct  1    MDLRFPLYVGYRYWRARKANAFASFITLFAVSGIFLGVAALIVVSSVMNGLEGQLKQRIL  60

Query  61   AVVPHGEIEAVDQPWTNWQEALDHVQKVPGIAAAAPYINFTGLVESGANLRAIQVKGVNP  120
              VP   +     P ++W  A + +  +PG+    P ++   +V+S AN+RA+QV GV P
Sbjct  61   GAVPQLTVY-TKAPLSDWTIAAEKLTMLPGVQGVTPSVSTQAMVQSAANIRAVQVFGVFP  119

Query  121  QQEQRLSALPSFVQGDAWRNFKAGEQQIIIGKGVADALKVKQGDWVSIMIPNSNPEHKLM  180
            +  ++LSA+       A+    +G+ Q+I+G  +A  LKV  GD V ++  +       L
Sbjct  120  ELAEKLSAVAQHTYSGAFSELTSGQYQVILGSELARQLKVSPGDTVRLLSGDGVVYSPLG  179

Query  181  Q-PKRVRLHVAGILQLSGQLDHSFAMIPLADAQQYLDMGS-SVSGIALKMTDVFNANKLV  238
              P + +  V+ + ++  Q+D   A +   DA++ +   S  ++ + L + D F A  L
Sbjct  180  PVPSQRKFLVSAVFEMGSQVDAGVAYVHYQDAKRLMRQPSDEINQLRLYLNDPFTAPALA  239

Query  239  RDAGEVTNSY---VYIKSWIGTYGYMYRDIQMIRAIMYLAMVLVIGVACFNIVSTLVMAV  295
            +D  ++  +         W  TYG+++  ++M + +M L + L++ VA FNIVS LVM V
Sbjct  240  KDVQQILTAQGIEATTSDWRDTYGHLFSAVKMEKNMMSLMLSLIVAVAAFNIVSALVMMV  299

Query  296  KDKSGDIAVLRTLGAKDGLIRAIFVWYGLLAGLFGSLCGVIIGVVVSLQLTPIIEWIEKL  355
             DK+ D+AVL+T G +   +  IFV  GLL  + G   G+++G++++L L  ++
Sbjct  300  VDKTTDVAVLKTQGLRTSAVMGIFVVQGLLNAVLGLALGLVVGILITLNLNGLMAT----  355

Query  356  IGHQFLSSDIYFIDFLPSELHWLDVFYVLVTALLLSLLASWYPARRASNIDPARVL  411
            +G   L +       LP +L    +  ++V  L+++L+A+ YPA RA+ + PA  L
Sbjct  356  LGISILGAG----QMLPVKLALGQLSLIIVGTLVVTLVATLYPALRAARVQPATAL  407
```

Appendix D. Additional structural and spatial information about the *Shewanella* electron conduit.

Appendix D-1. MtrB is predicted to be a 28 β-strand β-barrel protein.

Using the PRED-TMBB software (http://biophysics.biol.uoa.gr/PRED-TMBB/), the secondary structure of MtrB can be predicted. Using the n-best fit model, it is predicted that MtrB has 28 β–strands. MtrB is proposed to act as a porin that allows MtrA to traverse the outer membrane, enabling heme-heme distance between MtrA and MtrC to be small enough for tunneling from MtrA to MtrC.

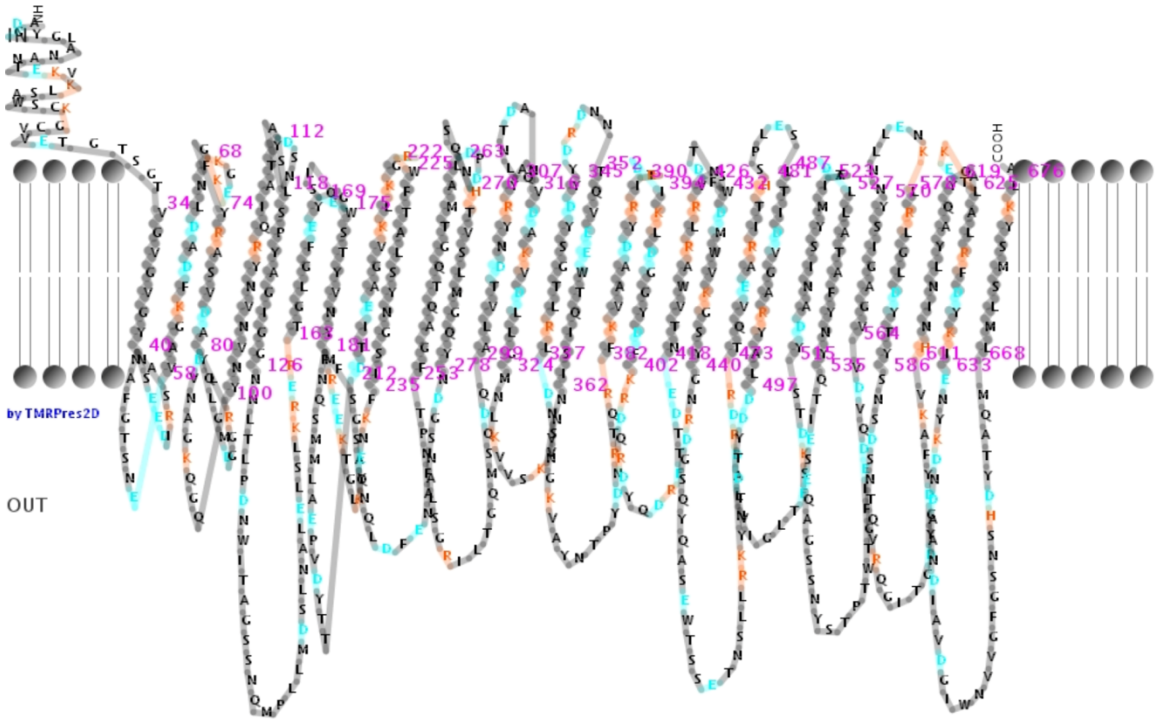

Figure D-1. The predicted secondary structure of MtrB is a 28 β-strand β-barrel integral outer membrane protein. MtrB is predicted to form a porin like structure in the outer membrane.

Appendix D-2. Spatial and dimensional data about the gram negative double membrane and Mtr pathway.

The spatial arrangement of the electron conduit in the membrane is vital to its function. The gram negative double membrane dictates the arrangement of the conduit, and there have been several measurements on the dimensions of the membrane structure in *E. coli* and a few in *Shewanella.* Additionally, there have been recent publications on the dimensions and structure of the conduit proteins or their homologues. I have collected this spatial information here (*45*, *58–60*, *211–214*).

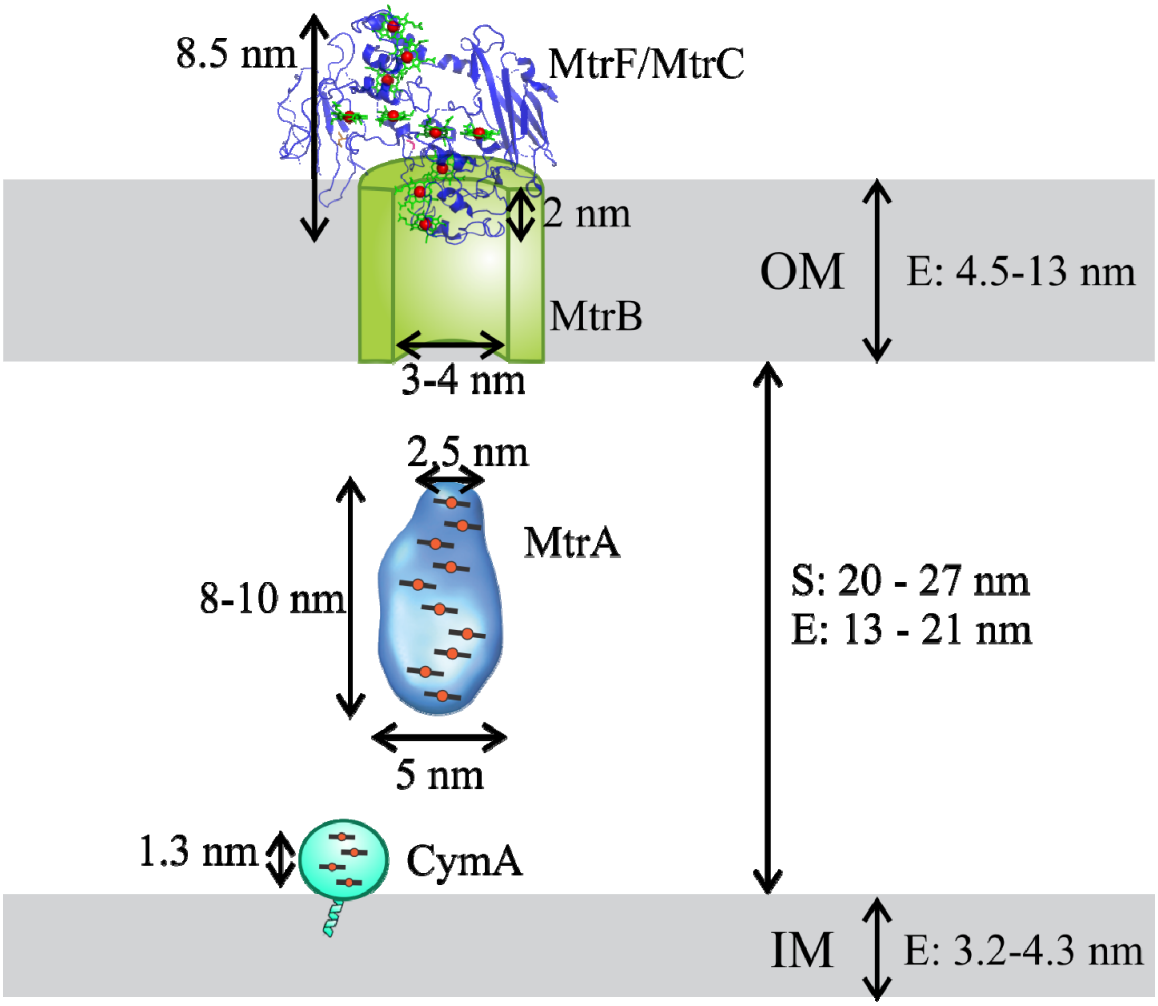

Figure D-2. A scaled schematic of the electron conduit. The CymA dimension is based off of NrfH. The MtrA dimensions are based on SAXS data. The MtrC dimensions are based on the MtrF crystal structure. "S" stands for *Shewanella* dimensions; "E" stands for *E. coli* dimensions. Note that the average OM thickness is 7 nm.

Appendix E: Electronic transitions in cytochromes *c* and how they are reflected in the visible spectra of the proteins.

One of the major breakthroughs in the high throughput screening of holocytochrome *c* expression was utilizing the characteristic electronic absorption spectra to measure the amount of protein per cell. Here I will summarize the electron transitions and spin states that dictate these spectroscopic peaks.

Appendix E-1. Crystal field theory and spin states.

Although there are a number of ways to describe bonding interactions, the relatively simplistic crystal field theory accounts for and describes much of the behavior observed in cytochromes *c*. Crystal field theory is similar to molecular orbital theory in the patterns of splitting electronic energy levels, and it serves as a first approximation of magneto-optical spectra.

The d-orbital of the iron ion is split into two energy levels in an octahedral six-coordinate field: e_g and t_{2g}. The orbitals within the e_g energy level are $d_{x^2-y^2}$ and d_{z^2}; the orbitals in the t_{2g} energy level are d_{xy}, d_{xz}, and d_{yz}. The energy difference between the e_g and t_{2g} levels is annotated Δ_o and is dictated by the ligand coordinating the ion (Figure E-1).

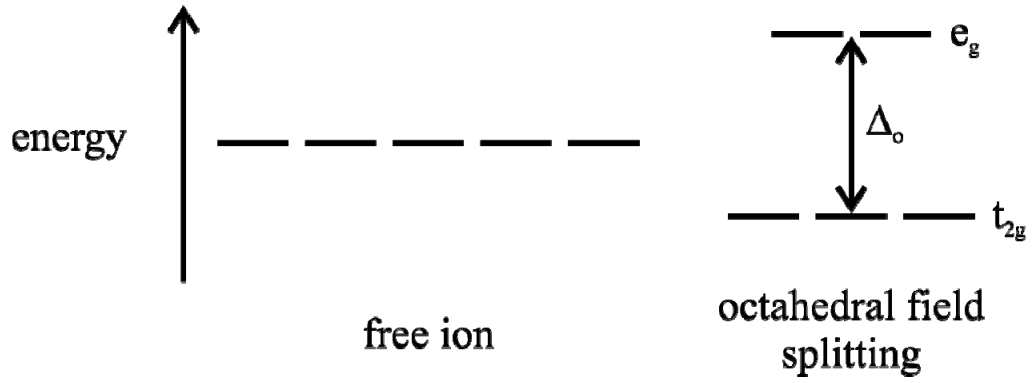

Figure E-1. Octahedral crystal field d-orbital splitting. The strength of the d-orbital splitting is Δ_o. This energy difference is dependent on the electrostatic field dictated by the ligands. The orbitals within the e_g energy level are $d_{x^2-y^2}$ and d_{z^2}; the orbitals in the t_{2g} energy level are d_{xy}, d_{xz}, and d_{yz}.

The spin state, or the way the electrons fill the split d-orbitals, depends on the relative magnitudes of the field splitting (Δ_o) and the energy required to pair electrons (P). In the presence of a weak crystal field, the field splitting energy is relatively low. In this case, the energy to pair electrons is greater than the field splitting energy, thus the electrons will fill in the higher energy state, e_g ("high spin," Figure G-2). Conversely, in the presence of a strong crystal field, the field splitting energy is relatively high. In this case, the energy to pair electrons is less than the field splitting energy, thus the electrons pair in the lower energy state, t_{2g} ("low spin," Figure G-2).

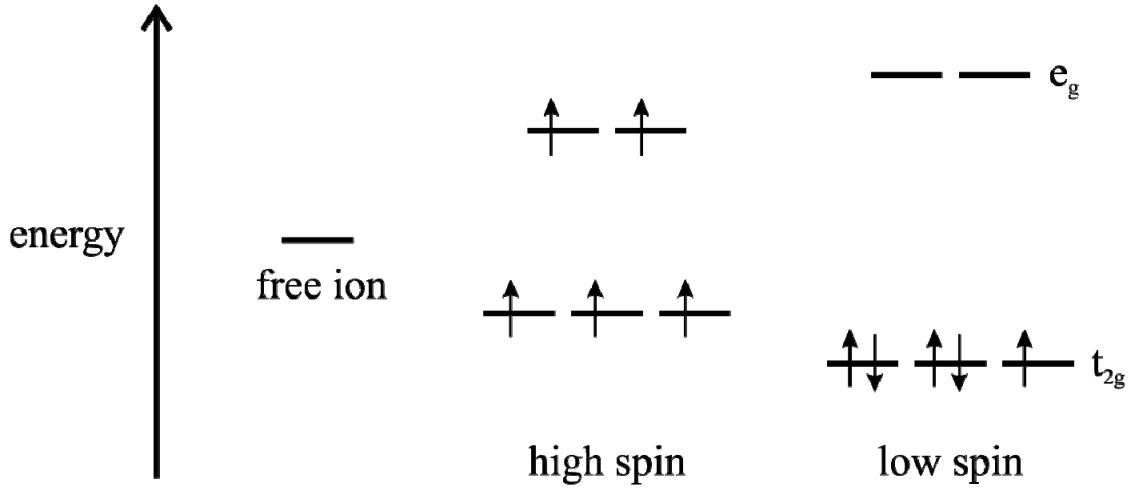

Figure E-2. High spin and low spin octahedral ferric iron. The filling of the electrons within the octahedral spin Fe(III) ion depends on the relative magnitude of the field splitting energy (Δ_o) and the energy required to pair electrons (P). The high spin state represents a weak crystal field and $\Delta_o < P$. The low spin state represents a strong crystal field and $\Delta_o > P$.

The degeneracy of the e_g orbitals may be disrupted if the crystal field is weak (Figure E-3). Porphyrin is generally considered to be a strong-field ligand, thus any weakness of the crystal field in heme is attributed to a reduction in the axial ligand component, usually the result of lengthening the Fe-axial ligand bond length. The result is that $d_{x^2-y^2}$remains at a high energy level, as it is more strongly affected by the porphyrin, while the d_{z^2} energy level decreases. In this case, the degeneracy of the t2g orbital set is partially split. Thus, quantum mechanically mixed spin states are possible when the axial ligand component of the heme weakens the overall crystal field (Figure E-3).

The affect from rhombic distortion, or in-plane distortion, of the iron ion is not shown here. Rhombic distortion along with axial distortion would cause the splitting of the d_{xy} and d_{yz} orbitals, with the d_{yz} orbital being the higher energy state.

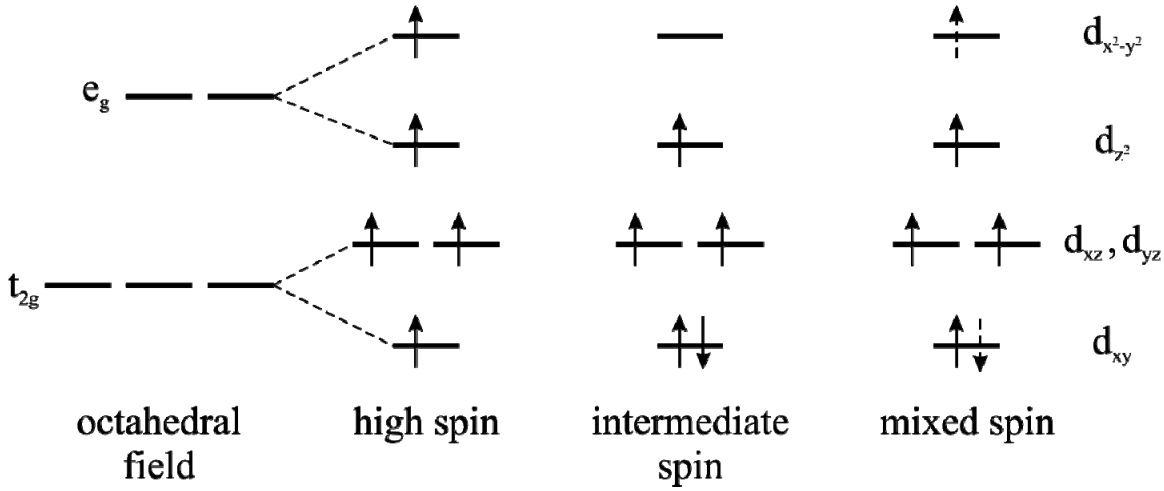

Figure E-3. Tetragonal (axial) distortion can cause intermediate and quantum mechanically mixed spin states. When the axial ligand weakens the crystal field, the degeneracy of the e_g and t_{2g} orbial sets is disrupted, allowing for intermediate and quantum mechanically mixed spin states. The low spin state of the tetragonal distorted splitting is not shown in Figure E-3, but it has two electrons in the d_{xy} orbital and the remaining three electrons in the d_{xz} and d_{yz} orbitals.

Appendix E-2. Electronic transitions in cytochromes *c* determine spectral peaks.

The electronic absorbance of cytochromes *c* is determined by the interaction between the orbitals in the porphyrin, iron, and the axial ligand (Figure E-4). There are three basic types of transitions, and thus bands in optical spectra, that are characteristic of cytochromes *c*: (i) π to π*; (ii) charge transfer; and (iii) d-d.

The π to π* transitions are notated in Figure E-4 with the transfers 1 and 2. These transitions are the excitation of the electrons from the bonding to antibonding orbitals in the porphyrin. They contribute to the major spectra bands observed in cytochromes *c*. Both transitions 1 and 2 are allowed and are observed in the Soret band and α/β bands (Figure E-5).

The charge transfer transitions are notated in Figure E-4 with the transfers 3-9. These are the result of electron transfer between the orbitals of the porphyrin and iron or the axial ligand and iron. Of these transitions, numbers 3-5 are allowed. These transitions display bands in ferricytochromes (Fe(III)) at 600 nm in high spin cytochromes *c* or 1200-1500 nm in low spin cytochromes *c*. Transitions 4 and 5 are not allowed in ferrocytochromes (Fe(II)) because the d_{xz} and d_{yz} orbitals would be completely filled. Transition 9 is strictly forbidden while the transitions 6-8 depend on the ligand.

The d to d transitions are notated in Figure E-4 with the transfers 10 and 11. These transitions are formally forbidden by selection rules. However, bands at 800-860 nm were proposed to result from transition 11 in horse ferrocytochrome *c* (Fe(II)).

There are specific diagnostic bands worth noting. A charge transfer band at 695 nm is diagnostic of a Met axial ligand. This band is observed in ferrocytochromes *c* and is pH sensitive. Another diagnostic band is for high spin ferricytochromes (Fe(III)) at 600-640 nm. This band was once attributed to water axial ligation, but has since been refuted. This band is also a charge transfer band instead between the porphyrin and the Fe(III) ion.

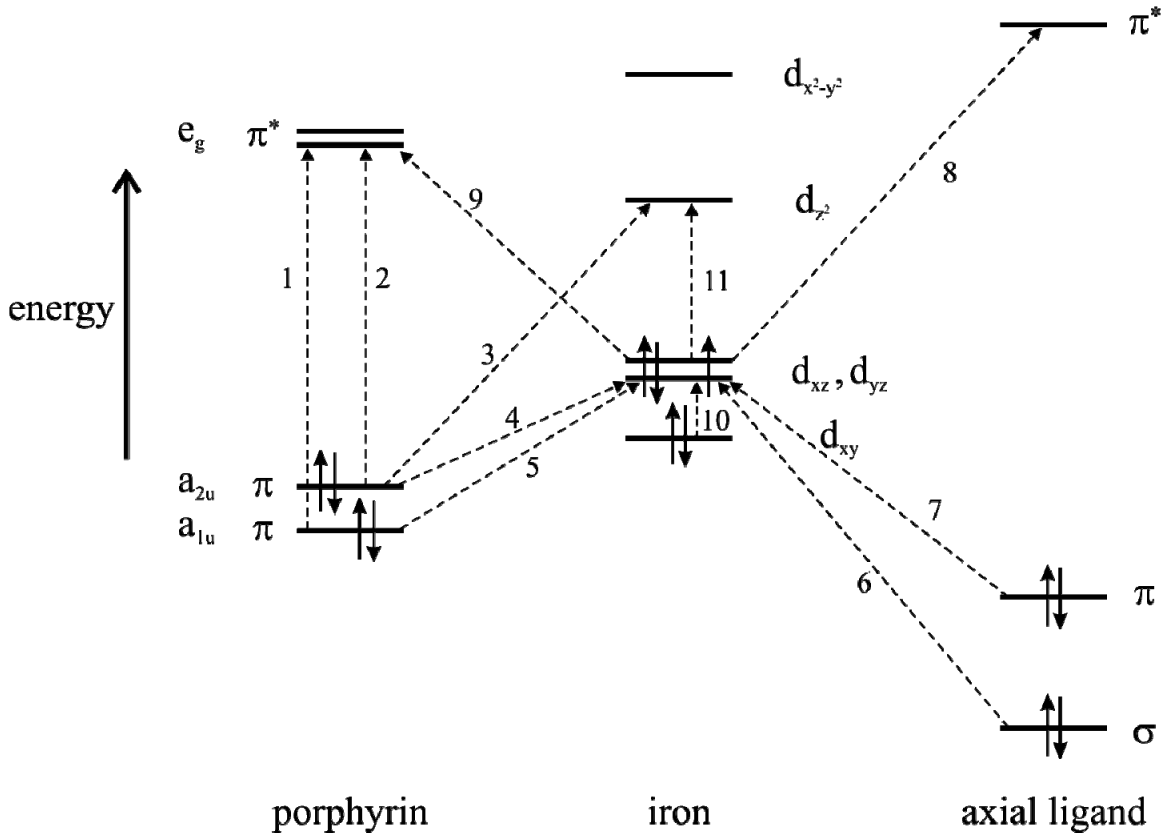

Figure E-4. Energy level diagram of the electronic transitions in ferricytochromes *c*. All transitions are annotated by dashed lines. Transitions 1 and 2 are allowed π to π* transitions. Transitions 3-9 are charge transfer transitions; 3-5 are allowed while 9 is strictly forbidden. Finally, transitions 10-11 are d-d transitions.

Appendix F: A brief overview on microbial fuel cells and electrochemical cells developed for this work.

Appendix F-1. Microbial fuel cells.

Microbial fuel cells are traditionally an electrochemical cell with two chambers: the anode and the cathode chambers. In this bioelectrochemical system, the cells act as the catalyst; the cells donate metabolic electrons by either direct contact or diffusible redox species to the anode. The anode and cathode chambers are separated by a proton exchange membrane, such as Nafion. Protons generated from the metabolism of the cell diffuse to the cathode, where they react with oxygen and the electrons and the cathode to form water. The cathodic side is oxygenic, by necessity, while the anodic side is typically anoxic to promote the utilization of the anode as the terminal electron acceptor.

The electrode materials vary, but a favorite anode material is graphite; graphite is chose both on the basis of low cost and its availability in many forms, such as rods or porous felt. The cathode material varies greatly, both in material and in type. Platinum serves as a good cathode material but is not cost effective on a larger scale.

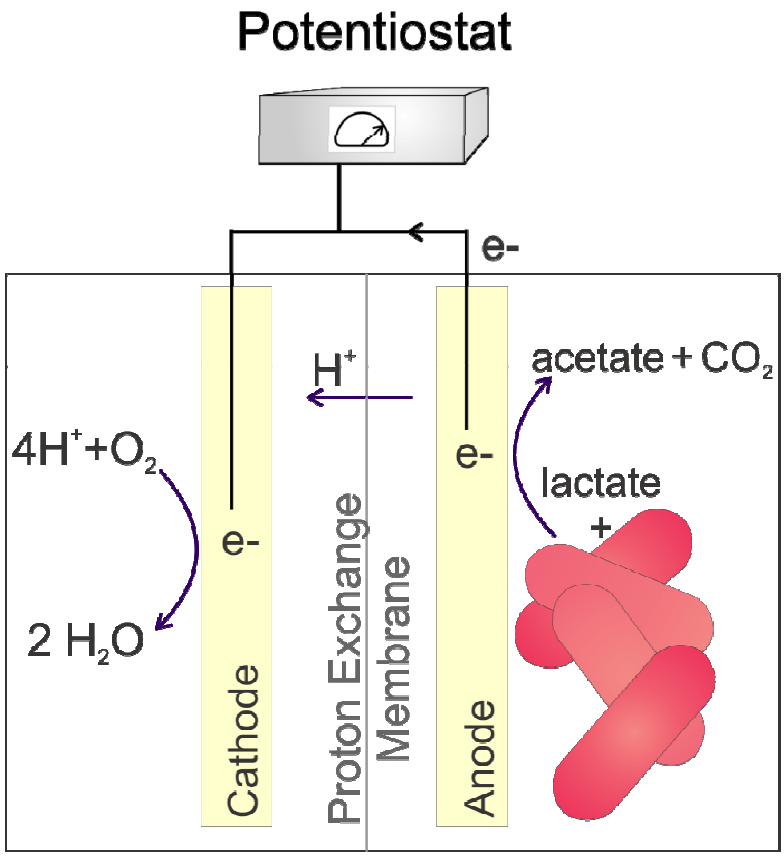

Figure F-1. A schematic of a microbial fuel cell. The anode side contains culture that respires a carbon source, generally forming CO_2, protons, and electrons. The electrons are deposited on the anode, generating a current measured by a potentiostat. The protons diffuse across a proton exchange membrane where they react with electrons and oxygen on the cathode to form water, thus completing the circuit.

Appendix F-2. Glass three electrochemical cell for controlled potential i-t curves.

Microbial fuel cells rely on the potentials of the materials to thermodynamically drive the electron transfer. This process may not produce the highest possible current density as the native materials properties may not maximally drive electron transfer. Rather resistors are generally used to control electron flow. An alternative electrochemical system is a three electrode electrochemical cell in which a reference electrode, controlled by a potentiostat, sets the anode at a bias potential. This allows the user to tune the anode material to the optimal potential for cell anode reduction. For *Shewanella* and *Geobacter*, the typically used bias potential is +0.24 V vs SHE (0.04 V vs Ag/AgCl).

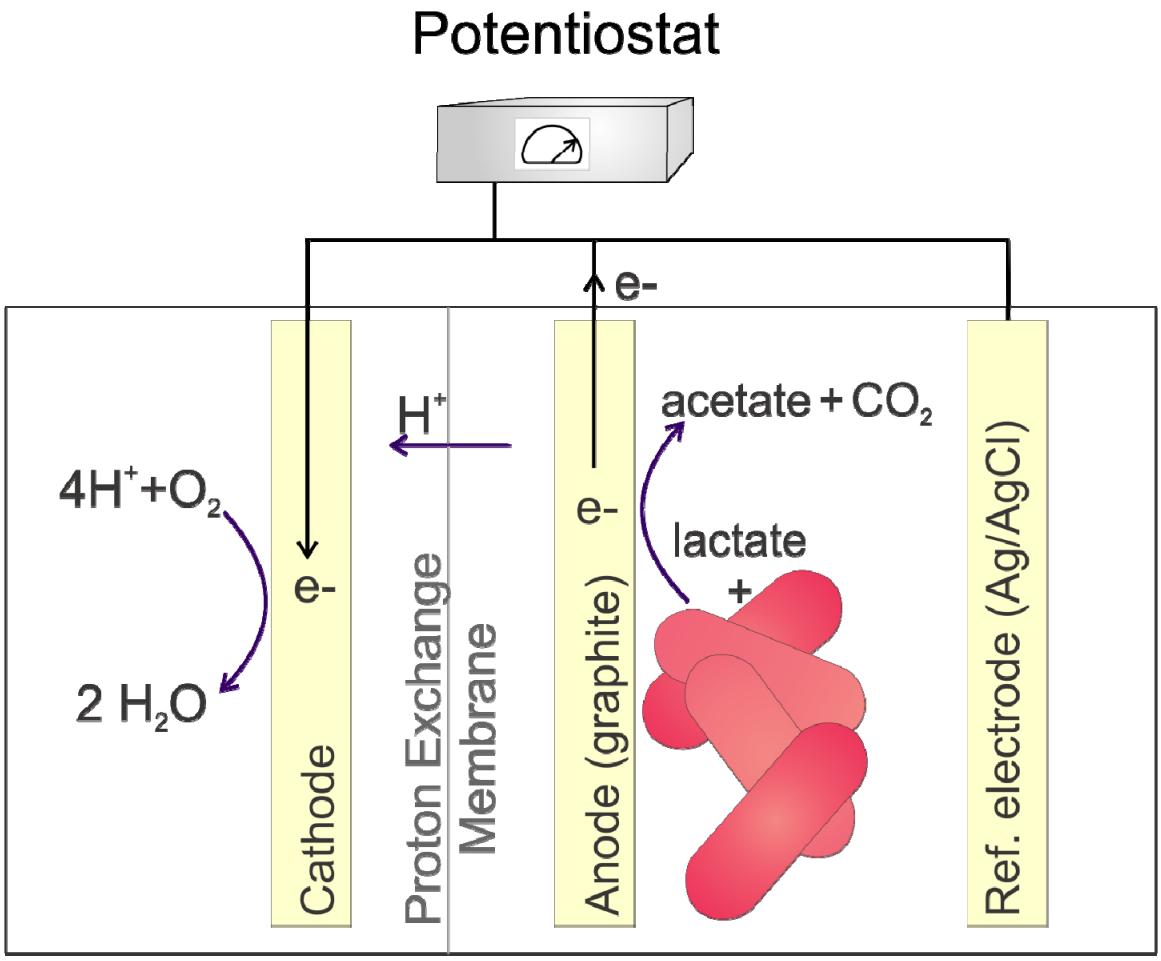

Figure F-2. A schematic of a three electrode electrochemical cell for controlled potential coulometry. The anode side contains both an anode material and reference electrode that sets a bias potential at the anode. The anodic chamber contains culture that respires a carbon source, forming CO_2, protons, and electrons. The electrons are deposited on the anode, generating a current measured by a potentiostat. The protons diffuse across a proton exchange membrane where they react with electrons and oxygen on the cathode to form water, thus completing the circuit.

In our original design for the two-chamber three-electrode system, we consulted Adams and Chittenden in Berkeley, CA. They constructed the glass design in Figure F-3. The unique gasket designed between the two chambers clamps the proton exchange membrane, Nafion, in place. This set-up may be autoclaved completely assembled. The anode side is filled with defined media and the cathode side is filled with the same buffer of the defined media, and the two solutions are separated by Nafion. Graphite electrodes may also be autoclaved, so this system is overall a very simple cell to set up and keep sterile. The reference electrode is immersed into the anode chamber through one of the side ports. All that one needs to do is inject the cells and a defined amount of carbon source to initiate the current system.

The anode side is bubbled continuously with nitrogen to maintain anoxic atmosphere. The inlet/outlets may be located at either side port or in the top-cap's septum. Similarly, the cathode side is bubbled with air to ensure oxygen is available for the cathode reaction. The Nafion proton exchange membrane does not exchange gases, so each side is able to maintain separate atmospheric conditions.

In future designs, I would advise making the anodic side port for the reference electrode upright (i.e. not on a slant). This would make it easier to maintain proper media levels to have the electrode immersed fully.

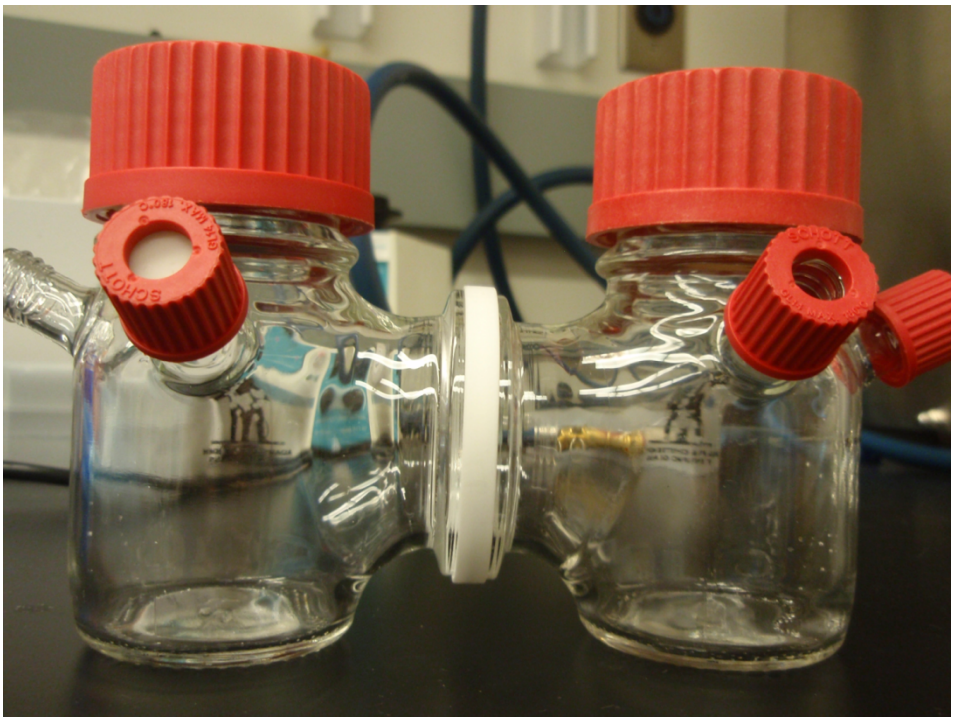

Figure F-3. The glass electrochemical cell designed with and made by Adams and Chittenden. One advantage to using the glass cells is that one can visually inspect the liquid level, electrode immersion, cell density, and if cell settling is preventing contact with the anode.

Appendix F-3. PEEK three electrode electrochemical cell for use with ITO slide anode.

An additional three electrode cell was devolved with Mark Alper at LBL specifically designed for current density measurements of cells chemically attached to ITO coated glass slides. The schematic is shown in Figure F-4.

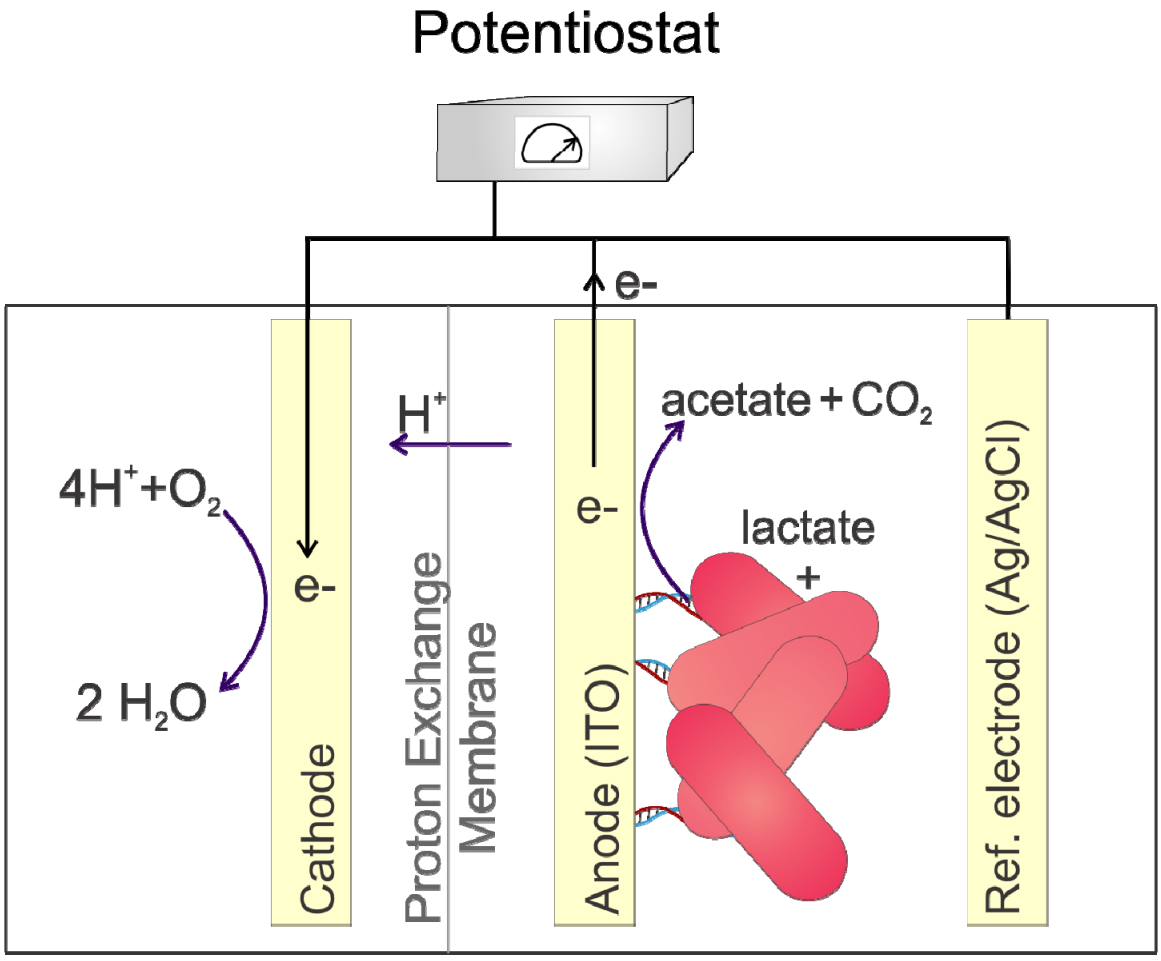

Figure F-4. A schematic of a PEEK electrochemical cell specifically for current density measurements of cells chemically attached to ITO coated glass slides. The anode chamber contains both the ITO anode and reference electrode that sets a bias potential at the anode. The cells are covalently linked to the ITO slide by programmed DNA attachment. The electrons are deposited on the anode, generating a current measured by a potentiostat. The protons diffuse across a proton exchange membrane where they react with electrons and oxygen on the cathode to form water, thus completing the circuit.

This cell was specifically designed to hold two glass slides coated with electrode material close to one another such that the system is not diffusion limited (Figure F-5). The material PEEK was chosen for its inability to exchange oxygen through. This cell works similarly to the glass set up in the previous section. The main difference is in assembly. Because the electrode in this system is coated with cells, it cannot be included in the autoclave process. And because of the way the cells are assembled, you cannot autoclave the assembled cell with media already inside. Rather, all of the materials are dry-autoclaved and assembled in a sterile hood.

One disadvantage to using an opaque plastic material as the housing for the electrochemical cell is that you may not see what is occurring inside the cell. Thus it is difficult to observe if there is significant evaporation of the liquid from bubbling. This issue can be slowed by humidifying the gases used in purging, but does not completely eliminate evaporation.

Because B strains of *E. coli* do not form biofilms, we sought to engineer an artificial surface coating of the engineered strains on an electrode surface. By programming cell adhesion to the electrode surface, we hypothesized that the mechanism of direct contact of MtrC to the electrode would be greatly enhanced over planktonic cells in solution (Figure F-5).

The Francis lab at UC Berkeley developed chemistry to attach DNA oligos to free amines on the cell surface and the complementary strand to a glass surface, which then directs cell-surface adhesion by hybridization of the DNA oligos (*74*). We used the same technique to anchor our strains to an electrode surface, specifically indium tin oxide (ITO), with nanoscale control (Figure F-6). ITO is advantageous because it is transparent, permitting both electrochemical and microscopy techniques to be carried out with the same sample. Examples of patterned cells on ITO coated glass slides are shown in Figure F-6. The patterning was done by Amy Twite of the Francis lab at UC Berkeley. The cells were stained with Texas red for viewing by fluorescence microscopy (Figure F-6).

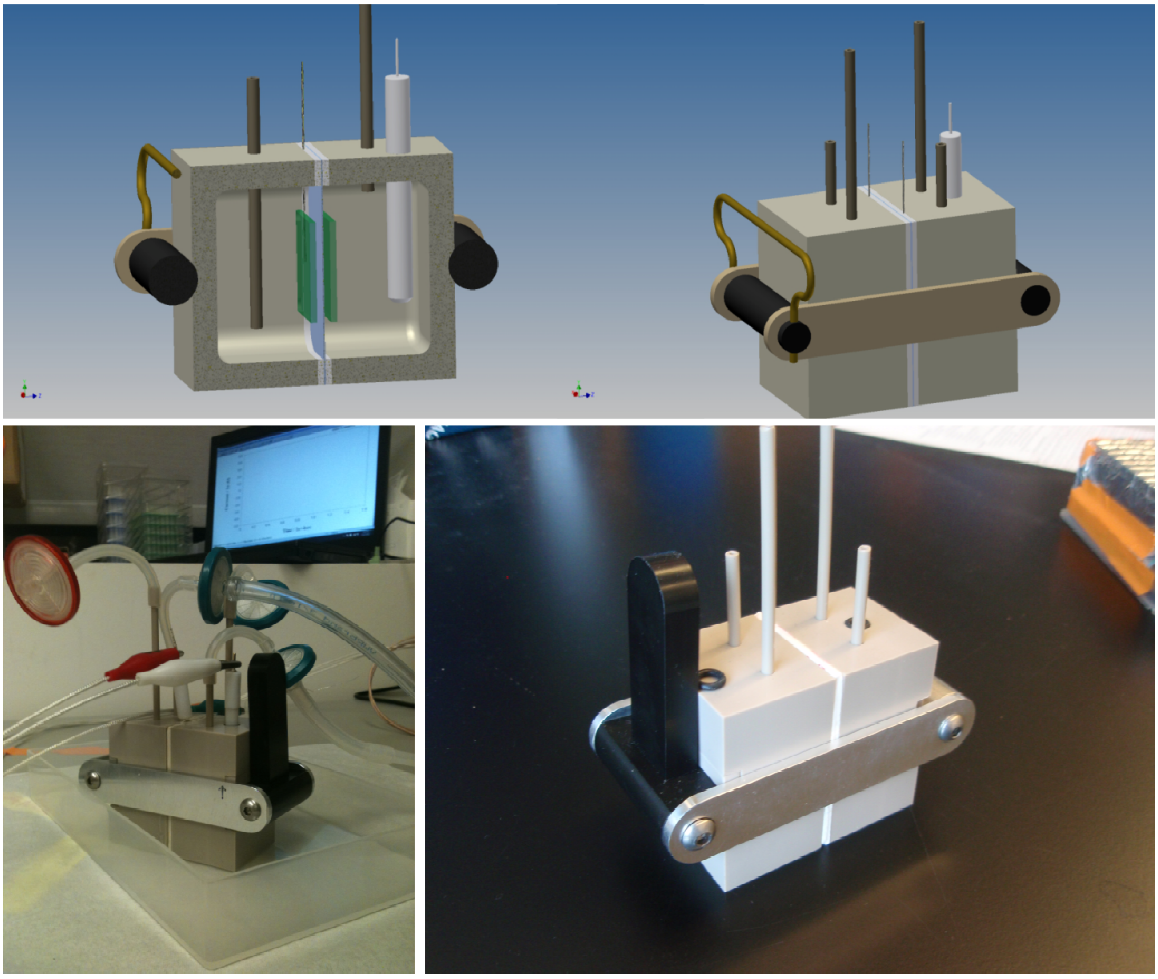

Figure F-5. Design and prototype of the PEEK 3-electrode electrochemical cell. This electrochemical set-up was specifically designed to hold two glass slides coated with electrode material close to one another such that the system is not diffusion limited.

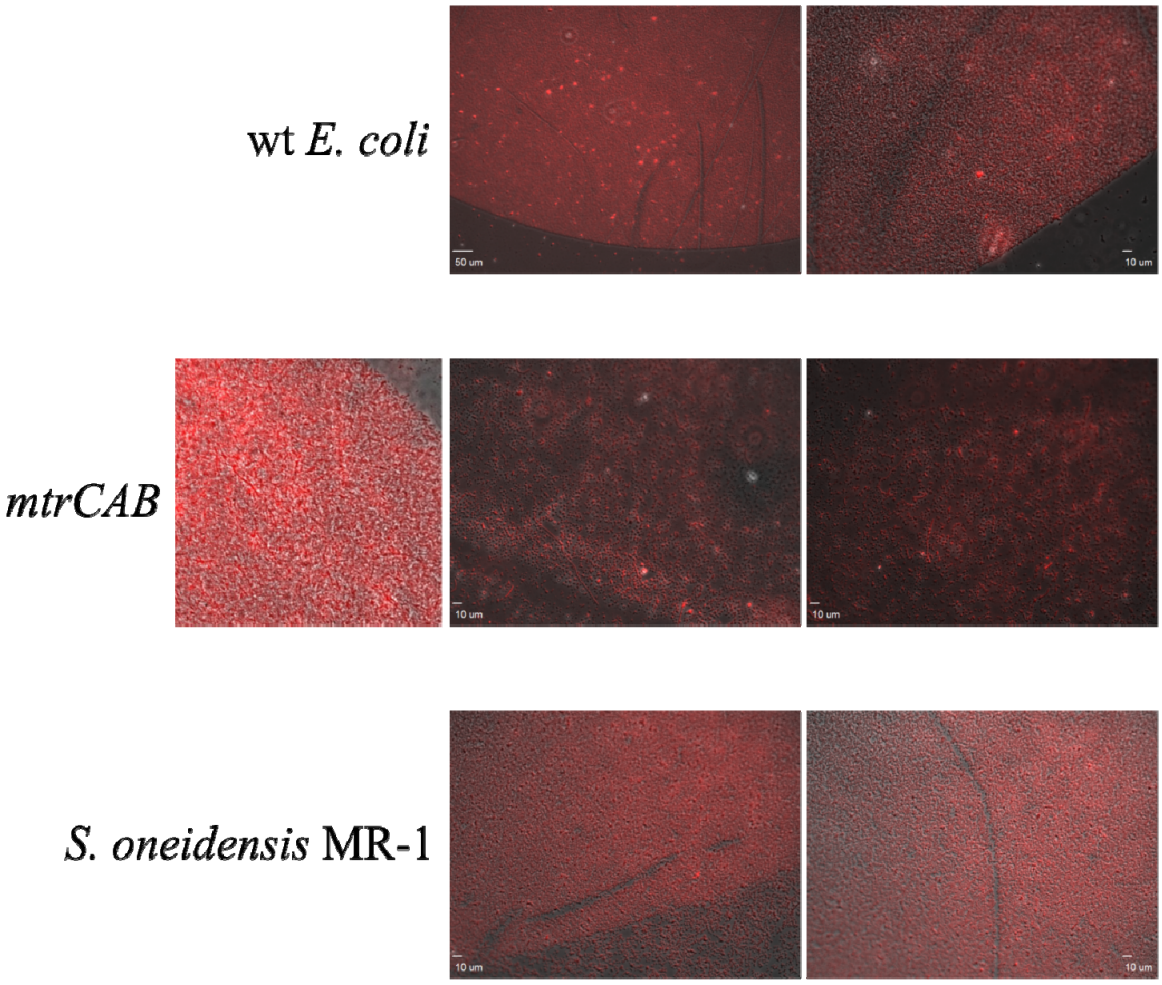

Figure F-6. Patterned cells on ITO coated glass slides. The cells were stained with Texas red for fluorescence microscopy. The coverage of the patterning was variable, as seen in the BL21(DE3) *mtrCAB* strain. The left-most image shows good coverage from one experiment whereas the right two images show poor coverage from another experiment. Interestingly, the *Shewanella* strain did not have a defined edge to the patterning, unlike the other strains.

Appendix F-4. Examples of microbial fuel cell and controlled coulometry experiments with the engineered strains demonstrate current.

To summarize this appendix, I have included a few examples of current generation from the engineered strains. First (Figure F-7) is a collaboration with Ben Gross of the El-Naggar lab at USC. The BL21(DE3) *mtrCAB* strain was tested in a microbial fuel cell with a graphite anode and plantinized graphite cathode. The fuel cell set up is shown on the left, and the sample i-t curve is shown on the right. The chamber on the left is the cathodic chamber, filled with PIPES buffer. The chamber on the right is the anodic chamber in which the cells were suspended in M9 media. The blue arrows indicate injection of lactate into the anodic chamber.

The shape of the curve is quite unusual: the increase in current is slow before the plateau. This suggests that the engineered *E. coli* were not able to attach or "swim" towards the anode, but rather relied upon diffusion to associate with the anode. The observed current is ~3 orders of magnitude less than that observed in *Shewanella*. Additionally, the coulombic efficiency observed by this system of this strain is 0.1%, instead of the 18% observed in *Shewanella*.

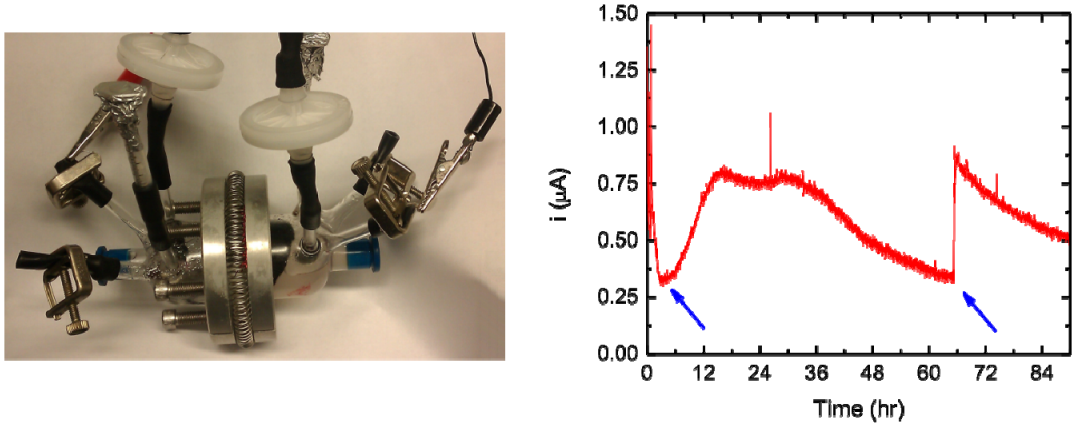

Figure F-7. Microbial fuel cell current measured from the BL21(DE3) *mtrCAB* strain. The picture shows the MFC set-up developed and used by the El-Naggar lab at USC. The chamber on the left is the cathodic chamber, filled with PIPES buffer. The chamber on the right is the anodic chamber in which the cells were suspended in M9 media. The blue arrows indicate injection of lactate into the anodic chamber. The coulombic efficiency observed by this system of this strain is 0.1%.

This next example of current being measured from the engineered strains is with the PEEK 2-chamber 3-electrode cell. The anode material was an ITO-coated slide adhered to an external Pt wire with copper tape. This overall anode material had a higher resistance than the graphite anode used in the previous i-t curve. The cathode was a Pt wire. The cells used in this example were BL21(DE3) *cymAmtrCAB*. This strain was not described elsewhere in the dissertation; it relied upon leaky expression of the electron conduit genes and thus is uninduced. The anode was biased to 0.02V vs Ag/AgCl. The peak current density observed in this system is much greater than the previous microbial fuel cell and strain, and the coulombic efficiency observed was ~1%.

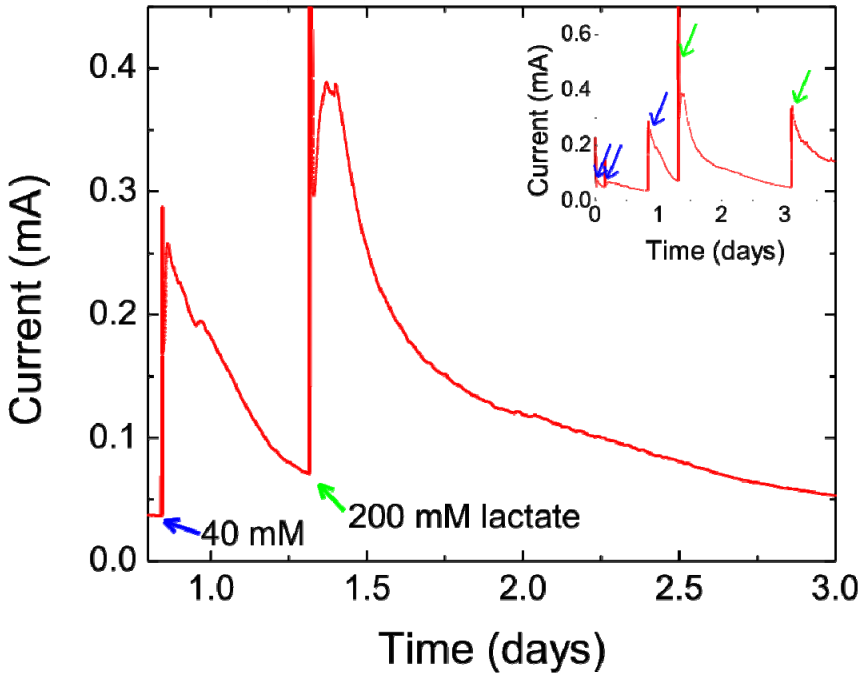

Figure F-8. Current measured from the BL21(DE3) *cymAmtrCAB* strain. The anode chamber had an ITO slide as the anode materials and the *cymAmtrCAB* strain suspended in M1 media. The blue arrows indicate injection of 40 mM lactate into the anodic chamber and the green arrows indicate 200 mM lactate injection. The coulombic efficiency observed by this system of this strain is ~1%.

Appendix G: Supplemental data on how induction of the *mtrCAB* operon impacts the cell membrane and overall biomass

One of the overarching problems mentioned throughout this dissertation is how the overexpression of the *mtrCAB* operon negatively impacted the cell viability and membranes. The majority of the data presented in the text of the dissertation was growth curves, cell pellet size, and changes observed by flow cytometry. Here, I supply supplemental data to support this claim. The data includes overnight biomass versus induction levels and cryo electron microscopy.

Appendix G-1. Changes in biomass from overnight growth is related to both the induction of the strains and the strain.

The OD_{600nm} of the *mtrCAB* and *cymAmtrCAB* strains studied in Chapter 5 were plotted versus the promoter activity (i.e. induction) in Figure G-1. The *E. coli* strain used to express the proteins here are the C43(DE3) strain. For both the *mtrCAB* (red circles) and *cymAmtrCAB* (blue triangles) strains, the non-induced cells show the same final biomass as the *ccm* strain (black square). Adding δ-ALA to the media during aerobic growth did not change the final biomass (hollow data points at promoter activity ~0.18).

Finally, it is interesting that the *mtrCAB* strain is more affected than the *cymAmtrCAB* strain by induction. Originally, we had hypothesized that MtrB could be toxic to the cell because it is essentially creating large "holes" in the outer membrane. Thus one can imagine that if the expression of MtrB is too high, then one would begin to observe toxic effects, such as lower biomass and viability. Additionally, we hypothesized that the cell would show even more dramatic phenotypes when expressing an additional cytochrome, CymA. However, this was not the case; the *cymAmtrCAB* strain actually appears to the "healthier" strain.

Besides the addition of *cymA*, the only regulatory information that was changed between the *mtrCAB* and *cymAmtrCAB* plasmids was the RBS of *mtrC* (Tables 5-1 and 5-8; Pgs 97 and 109). Thus I speculate that the first and foremost problem with the *mtrCAB* strain is that the translational balance of MtrC:MtrA:MtrB is not optimized; it is in fact predicted by the Salis RBS calculator that the translation of MtrC is much too high. However, after this problem was solved in the *cymAmtrCAB* strain, there is still a ~1.5x decrease in biomass after high induction levels. Thus there are additional problems with the expression of the total operon besides the relative ratios of MtrC:MtrA:MtrB.

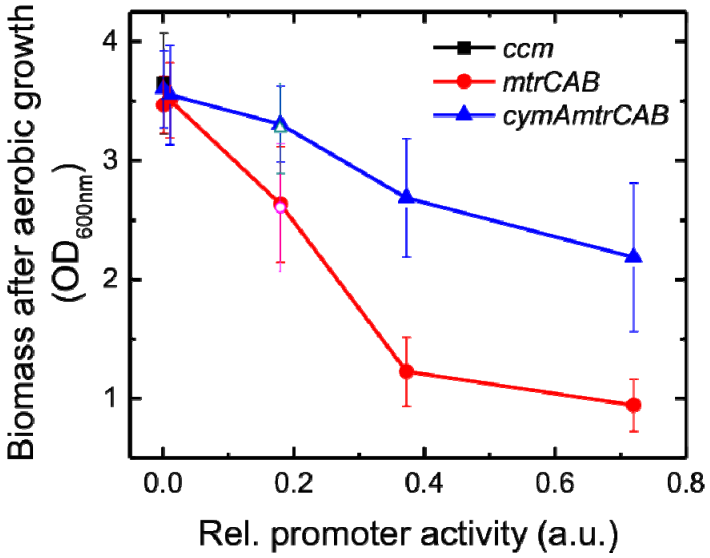

Figure G-1. The final biomass after aerobic growth decreases in strains that were heavily induced. The *mtrCAB* strain demonstrates a greater effect in the decrease of biomass than the *cymAmtrCAB* strain. The OD_{600nm} of the *mtrCAB* (red circles) and *cymAmtrCAB* (blue triangles) strains studied in Chapter 5 were plotted versus the promoter activity. Adding δ-ALA to the media during aerobic growth did not change the final biomass (hollow data points at promoter activity ~0.18).

Appendix G-2. Cryo electron microscopy of the BL21(DE3) *mtrCAB* strain shows changes in cell morphology and severely impacted membrane structure.

Cryo electron microscopy of the BL21(DE3) *mtrCAB* strain discussed in Chapter 2 was done in collaboration with Roseann Csencsits at the Donnor Lab of UC Berkeley. These images show that there are significant changes in the cell membrane at high levels of IPTG (100 μM). The morphological changes in the membrane and cell size are indicators of cells in shock.

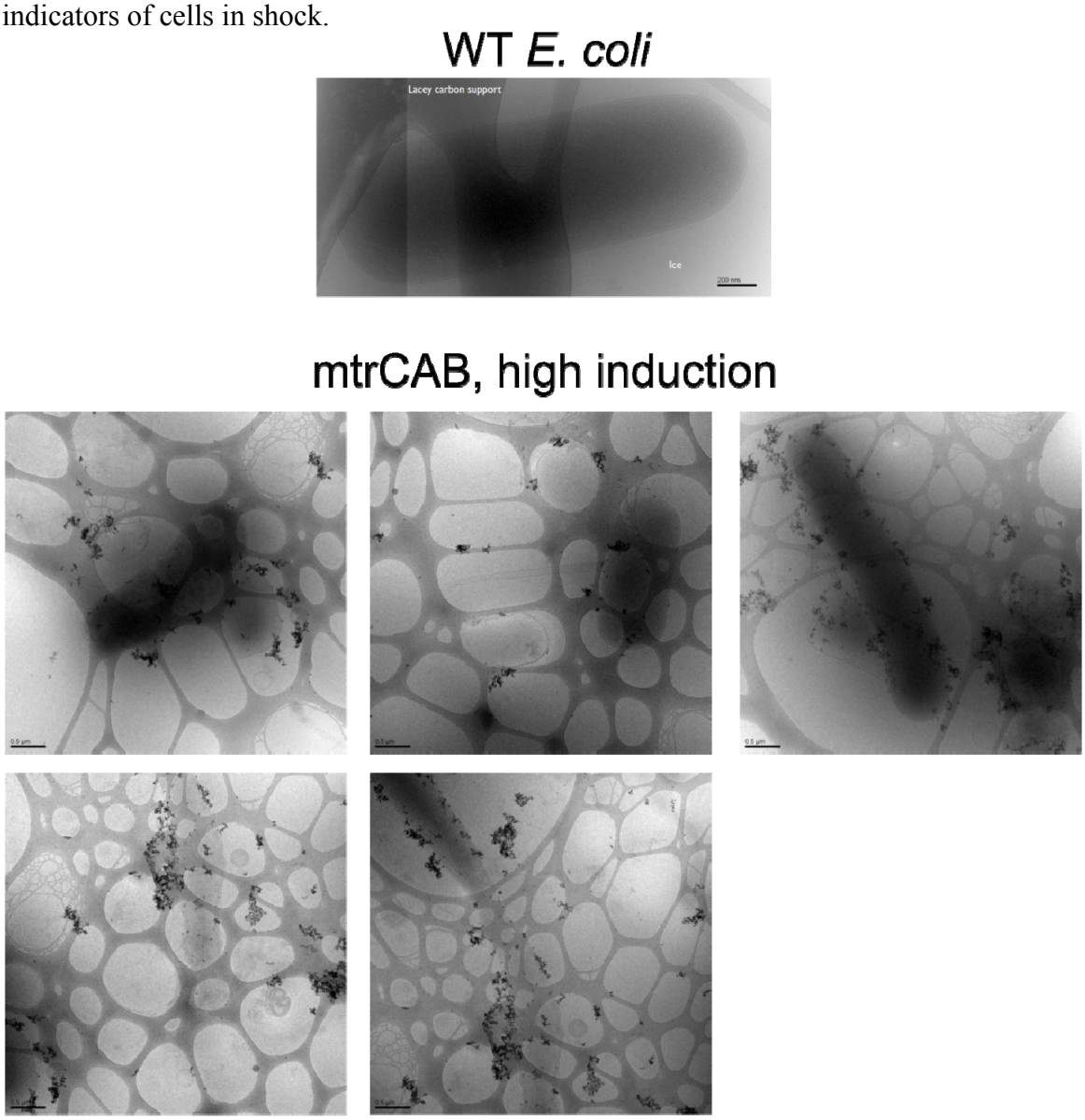

Figure G-2. The induction of the *mtrCAB* operon shows defective cell membranes and elongated cells. The top image is the BL21(DE3) strain with an empty pET vector. The lacey carbon support and ice in the image top is labeled. This image shows typical *E. coli* cell morphology and unimpaired membranes. The sample images of highly induced *mtrCAB* strains (100 μM IPTG) show unusual membrane appendages, ripples, blebs, holes, and elongation. The small black aggregates are gold nanoparticles used for 3-d image processing.

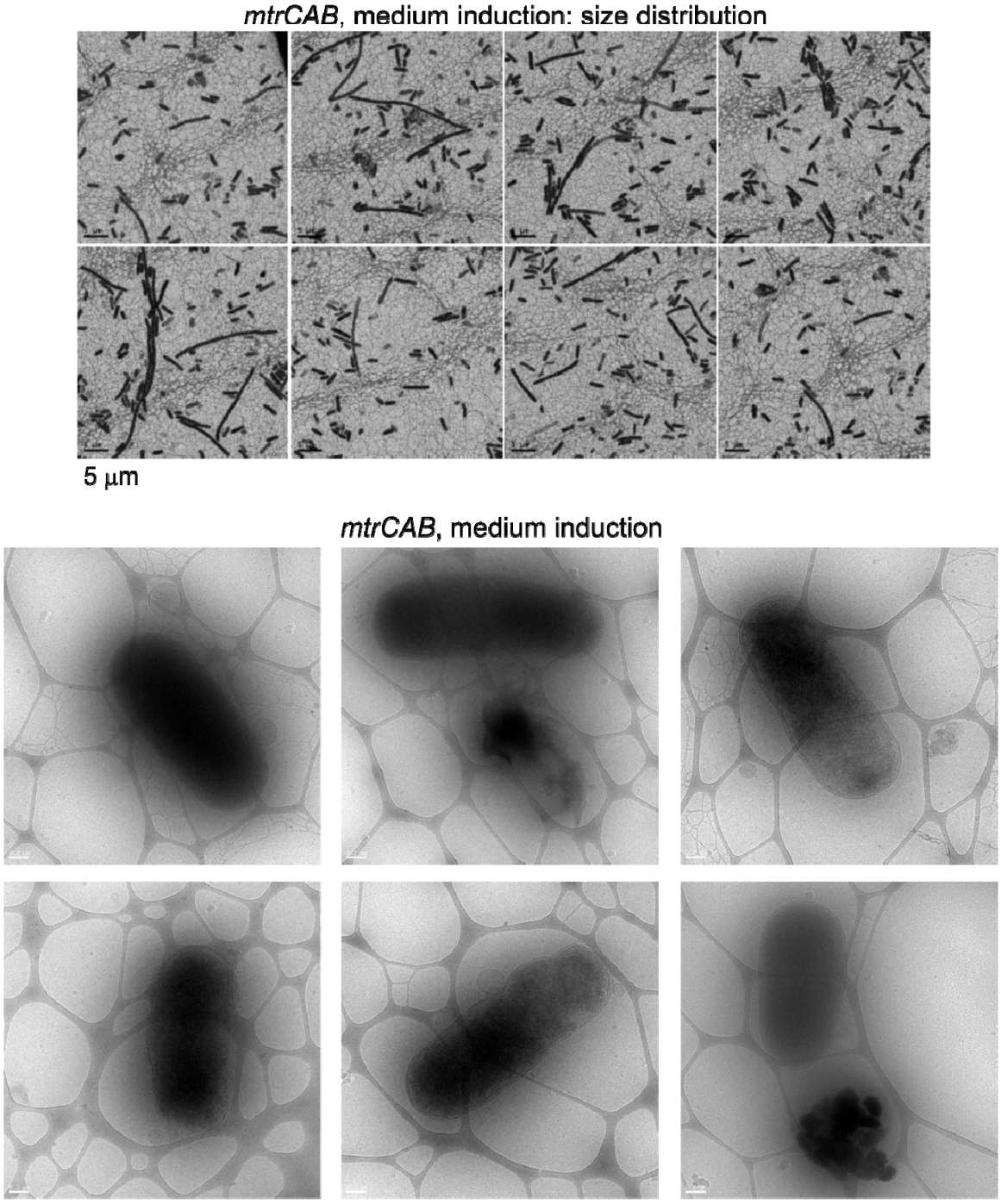

Figure G-3. Moderate induction of the *mtrCAB* operon showed impaired membranes and overall changes in cell size. The top panel shows a representative sampling of the cell sizes of the BL21(DE3) *mtrCAB* strain induced with 10 μM IPTG. A similar image of wild type *E. coli* would show less than 5% elongated cells, whereas this strain shows a much higher percentage of filamentous cells. The bottom panel shows a

few cells at higher magnification. These cells also demonstrate membrane ripples, blebs, and holes.